GRAN SASSO SCIENCE INSTITUTE

PhD thesis

in

Astroparticle Physics

On the origin of high energy neutrinos detected by IceCube

Advisor:
Francesco Vissani

Candidate:
Andrea Palladino

XXX PhD Cycle

To my wife,
the positive energy
of my life

CONTENTS

INTRODUCTION

CONTEXT The discovery of a diffuse flux of high energy neutrinos made by IceCube, a neutrino telescope of 1 km^3 located in the South Pole, has opened a new era for neutrino astronomy. The observations of IceCube are compatible with the theoretical expectations related to the astrophysical neutrinos. However many important questions, raised by these findings, are still unresolved: what is the source and the mechanism of production of the astrophysical neutrinos seen by IceCube? Is it an astrophysical mechanism? Is their origin extragalactic or is there also a galactic population? How to use high energy neutrino events within multi-messenger physics?

AIMS In this thesis we describe the mechanisms of cosmic neutrino production and the sources in which these processes can occur. After the production we follow the path of neutrinos, i.e. their propagation till the Earth and their interaction with the detectors. We give an interpretation of the flux of high energy neutrinos and we analyze them in a context of multi-messenger physics, searching for spatial correlation with γ-rays or other known radiation fields.

LAYOUT OF THE THESIS In the first chapter we describe the mechanisms of production, focusing especially on the standard case of neutrinos produced by the pions decay and briefly discussing other hypotheses.

In the second chapter we discuss the most plausible sources of high energy neutrinos, giving a brief review of possible extragalactic and Galactic sources.

In the third chapter we begin the exposition of the original results obtained in this PhD project. We discuss the neutrino oscillations using the so called "natural parametrization", that is an analytical method that permits to compute the oscillations and their uncertainties without using a Montecarlo simulation [1]. In the same chapter we briefly describe the exotic possibility that neutrinos decay before reaching the Earth [2]. In the fourth chapter we provide a theoretical description of the interactions between high energy neutrinos and nucleons. Then we describe and discuss the effective areas of the IceCube telescope [3].

The first four chapters collect the background knowledge necessary to understand chapter five, in which we analyze:

1. the flavor composition of the measured high energy neutrinos, using two complementary representations, namely the track-to-shower ratio [4] and the " triangle representation" [1];

2. the neutrino decay, comparing the theoretical scenario with the present data [2];

3. the very high energy events, still missing in the IceCube telescope: double pulses and resonant events due to the Glashow resonance [3, 5]

Chapter six is dedicated to the interpretation of the fluxes detected by IceCube. The null hypothesis, adopted in most experimental analyses of the data, is that the flux of high energy neutrinos can be explained using a power law flux, isotropically distributed. Historically it was expected that the flux of astrophysical neutrinos was distributed as E^{-2} and the renowned bound of Waxman and Bahcall concerns just the normalization of this flux.

We argue that there is some tension with the previous theoretical models and with the single power law interpretation, as we deeply analyze in this chapter. We propose a model in which different populations of neutrinos contribute to the observed flux [6, 7]. This is in better agreement with the present observations but more data are required to firmly constrain (or rule out) this interpretation or the single power law model.

The last chapter is dedicated to the connection between neutrinos and other observable radiation, considering specific astrophysical assumptions. We analyze the potential of the Galactic center to produce high energy neutrinos [8], basing our inference on the observations in the γ-rays sky. After that we focus on two extragalactic sources, i.e. BL Lacs [9, 10] and Starburst Galaxies. In this case the connection with neutrinos is realized looking at γ-rays (for BL Lacs) and infrared or x-rays (for starburst).

RESULTS The main original results presented in the thesis are the following ones:

1. The flavor composition of the cosmic neutrinos detected by IceCube is compatible with any plausible mechanism of production of neutrinos, namely pions decay, neutrons decay and decay of heavy mesons containing the quark charm. Due to the low statistics it is not possible to rule out any of these mechanisms [1, 4].

2. Based on the flavor, the scenario of full neutrino decay is disfavored by the present data; particularly the normal hierarchy shows a tension of 2 sigma whereas the inverted hierarchy shows a tension of 3 sigma [2].

3. Up to now no double pulses (tau) or resonant events (Glashow) have been observed. We found that it is not surprising, since we expect no more than 0.15 double pulses per year [3] and no more than 0.5 resonant events per year [3, 5] in the most promising scenarios.

4. We provide an estimation of the Galactic component, finding that Galactic neutrinos from disk could exist and could be distributed as $E^{-2.4}$ [7]. The contribution of the Galactic component to the diffuse flux should be of 10%-15% [6, 7], with a null Galactic component disfavored at 2σ. We also analyzed the role of atmospheric prompt neutrinos, expected from a theoretical point of view but not yet detected.

5. On the multi-messenger point of view, we found that the Galactic center cannot produce events with a flux at a level detectable in IceCube [8], although the Galactic center is very interesting for the γ-rays astronomy.

6. Considering extragalactic sources, we found that the BL Lacs show a tension of 3.7σ in the hypothesis that they are the main emitters of high energy neutrinos above 200 TeV [9]. On the other side, starburst galaxies seem to have the necessary budget to explain IceCube neutrinos, but more observations are required to constrain the scenario.

SUMMARY Neutrino astronomy is a new and interesting field of astroparticle physics. Unfortunately, due to the properties of neutrinos that weakly interact with the matter, it is extremely hard to detect high energy neutrinos. Even with a km^3 detector no more than ~ 10 neutrinos per year are expected.

We have seen that some features, such as the flavor composition and the neutrino decay scenario, can be significantly constrained also by the existing experimental samples. However, in order to give a correct interpretation to cosmic neutrinos, a bigger exposure is required.

Up to now we have some hints of different aspects, such as the evidence of a quasi-isotropic diffuse flux, that seems to favor the extragalactic origin. On the other side there is a tension between what is observed from North and South and a Galactic flux of neutrinos can reconcile the observations.

There is no evidence of point sources and this is a very unpleasant situation, but it is quite difficult to give a definitive answer with only 29 throughgoing muons, taking into account that 1/3 of them could be of atmospheric origin. The upcoming IceCube generation 2, with an exposure of 6-7 times greater, will help to progress in the study of the origin of high energy neutrinos.

Summarizing there are several ideas "on the origin of high energy neutrinos"and some of them have been proposed or discussed in this thesis. There is also a firm point though: high energy cosmic neutrinos have been observed, with a significance greater than 6σ ! We are in the beginning of a new era of neutrino astronomy and in the next years we will put a lot of effort in discussing the question: *where do high energy neutrinos come from?*

NOTATION

- The flux of neutrinos is generally indicated with ϕ_ℓ, where $\ell = e, \mu, \tau$ denotes the neutrino flavor. When it is necessary to distinguish between neutrino and antineutrinos the flux is indicated with ϕ_{ν_ℓ} or $\phi_{\bar{\nu}_\ell}$ (see chapter 1);
- the notation $(\nu_e : \nu_\mu : \nu_\tau) = (1 : 1 : 1)$ denotes the "flavor composition", whereas the notation $(\xi_e : \xi_\mu : \xi_\tau) = (1/3 : 1/3 : 1/3)$ denotes the "flavor ratio"(see chapter 1 and 3);
- the differential flux of flavor ℓ, $\frac{d\phi_\ell}{dE}$, in units of $\mathrm{GeV}^{-1}\mathrm{cm}^{-2}\mathrm{sec}^{-1}\mathrm{sr}^{-1}$, is often used when experimental measurements are discussed. When a power law flux is used, $\frac{d\phi_\ell}{dE} = F_\ell E^{-\alpha}$, F_ℓ represents the normalization and α the spectral index (see chapter 2, 5 and 6);
- the differential flux $\frac{d\phi}{dE}$, without any subscript, denotes the all-flavor flux. In this case the normalization is indicated with F and the spectral index again with α;
- the effective areas are indicated by A_ℓ, where $\ell = e, \mu, \tau$ denotes the neutrino flavor. When specific effective areas are used, such as in case of Glashow resonance or double pulses, they are indicated with an apex (see chapter 4);
- when a different flux is used, such as the flux of γ-rays, it is explicitly indicated as ϕ_γ (see chapter 7);

ACRONYMS

- HESE = High Energy Starting Events
- AGN = Active Galactic Nuclei
- BL Lacs = AGN of the BL Lacertae type
- SFG = Star Forming Galaxy
- SBG = Starburst Galaxy
- GRB = Gamma Ray Burst

1 MECHANISMS OF COSMIC NEUTRINO PRODUCTION

The fact that we observe cosmic rays on Earth and in a very wide range of energies motivates the idea of *cosmic accelerators* present in the Milky Way and outside of it. Thus, proceeding in the analogy, neutrinos are expected to be produced as results of *cosmic beam dumps*, namely, collisions of the cosmic rays in the vicinity of the source or elsewhere, very similarly to the corresponding type of experiments conducted at accelerators using fixed targets. The fact that we do not know for sure the origin of cosmic rays makes even more important and interesting the investigation of high energy neutrinos, that are stable and neutral particles and that point directly to the source. The main aspects of neutrino-cosmic ray connection are summarized in Sec. 1.1.

It is interesting to note that the earlier motivations to study high energy neutrinos were slightly different (e.g. the investigation of the neutrino cross sections). At present the motivations concern the neutrino astrophysics, particle physics and the possibility to uncover new physics phenomena, such as sterile neutrinos, neutrino decay, exotic production mechanisms. In this chapter we describe the conventional astrophysical scenarios for the production of observable high energy neutrinos. More precisely, we will give in Sec. 1.2 an overview of neutrinos produced in pion decays. In Sec. 1.3 and 1.4, respectively, we will discuss the proton-proton and the proton-gamma interaction, that are the most plausible mechanisms of production of high energy neutrinos. In the Sec. 1.5 we briefly discuss other production mechanisms. A review that examines the neutrino-cosmic ray connection is [11].

1.1 THE NEUTRINO–COSMIC RAY CONNECTION

The source of high energy neutrinos and their mechanism of production are still unknown. However several hypotheses have been proposed. The most reasonable hypothesis has an astrophysical character and postulates a connection between cosmic rays (CR) and neutrinos. A seminal paper on this connection has been written by Waxman and Bahcall in 1998 [12]; this paper will be examined in details in Sec.6.1.3. As already mentioned the cosmic rays can collide with a target producing unstable mesons, that decay giving neutrinos and gamma rays. It is not precisely known which environment offers the ideal condition to realize the collisions that lead to the neutrinos observed at the Earth. Certainly, a large number of cosmic rays, time of confinement and targets are all required, in order to produce large fluxes of neutrinos. Let us remark that not all the cosmic rays are protons, but different chemical compositions of the CR have been detected at the Earth, especially at very high energy, although one refers frequently to CR as "protons". Anyway it is expected that nuclei give a smaller contribution to the neutrino flux when compared to protons, considering that neutrinos have been detected up to PeV energies.

As it is discussed later the two most plausible neutrino production mechanisms are the collision between accelerated protons and target protons (pp interaction) and the collision between accelerated protons and target photons ($p\gamma$ interaction). The relevance of one mechanism, with respect to the other, depends upon the environment and upon the density of gas and radiation. In our Galaxy it is possible to have pp interactions in the disk or in the halo, where the density of gas is respectively 1 nucleon/cm^3 and $10^{-3} \div 10^{-2}$ nucleons/cm^3; on the other hand in an extragalactic source, such as an AGN or an GRB, that are rich of radiation, it is plausibly easier to realize a $p\gamma$ interaction. Another possibility is the $p\gamma$ interaction between protons and the cosmic microwave background (CMB), that produces the so-called cosmogenic neutrinos (see Sec.2.3).

We begin by analyzing how neutrinos are produced and what is the relationship between their energy and the energy of cosmic rays. The scenario is that pions (mesons) are created in the collision between accelerated protons and the target and they subsequently decay into other particles. The decay of charged pions produces neutrinos and electrons (positrons), whereas the decay of neutral pions produces gamma rays. For these reasons we focus first on the pion decay and then on the difference between pp and $p\gamma$ interaction. Moreover we will discuss the contribution to the neutrino flux given by the decay of heavier mesons.

1.2 PION DECAY

Neutrinos are produced by the decay of charged pions and we are interested to know the spectrum of these neutrinos and their connection with the primary cosmic ray spectrum. Let us study the case of π^+; the same expressions apply for π^-, where it is sufficient to replace $\nu_e \to \bar{\nu}_e$, $\nu_\mu \to \bar{\nu}_\mu$ and $\bar{\nu}_\mu \to \nu_\mu$.

DECAY IN THE REST FRAME The first step of pion decay is represented by:

$$\pi^+ \to \mu^+ \nu_\mu \tag{1}$$

and the energy taken by μ^+ and ν_μ in the rest frame is given by:

$$\begin{aligned} \frac{E^0_{\nu_\mu}}{m_\pi} &\simeq \frac{1}{2}\left[1 - \left(\frac{m_\mu}{m_\pi}\right)^2\right] = 0.21 \\ \frac{E^0_{\mu}}{m_\pi} &\simeq \frac{1}{2}\left[1 + \left(\frac{m_\mu}{m_\pi}\right)^2\right] = 0.79 \end{aligned}$$

The second step of decay is represented by:

$$\mu^+ \to e^+ \bar{\nu}_\mu \nu_e$$

Since $m_\mu \gg m_e \gg m_\nu$ the energy taken by the secondary particles is about $1/3$ in the rest frame. Recalling that a muon takes about $3/4$ of the pion's energy it is a good approximation to say that:

Each neutrino from pion decay takes, an average, 1/4 of the pion's energy.

We will clarify this assumption later, using the energy distribution of the secondary particles. At the end of the chain of decay of π^+ and π^- the flavor composition of neutrinos, obtained counting the number of neutrinos of a certain flavor[1], is equal to

$$(\nu_e : \nu_\mu : \nu_\tau) = (1 : 2 : 0)$$

LABORATORY FRAME The calculation of the spectrum of neutrinos, produced by a a generic spectrum of pions, has been done in [13]. A similar approach can be also found in [11, 14, 15]; in the following of this chapter we will follow the last reference, in which an exhaustive treatment of the pp interaction is presented.

In order to evaluate the spectrum of neutrinos, produced by a generic spectrum of pions $J_\pi(E_\pi)$, we use the following formula:

$$\phi_{\nu_\ell}(E_{\nu_\ell}) = \int_0^1 f_{\nu_\ell}(x) J_\pi\left(\frac{E_{\nu_\ell}}{x}\right)\frac{dx}{x} \tag{2}$$

where $f_{\nu_\ell}(x)$ represents the distribution of the energy carried by a neutrino with respect to the energy of pion in the laboratory frame, with

$$x = \frac{E_{\nu_\ell}}{E_\pi}$$

The functions $f_{\nu_\ell}(x)$ are probability functions density, taken from [15]. In the case of the first neutrino, that comes from the two body decay of the pion (see Eq.1), the expression is trivial and it is given by a flat probability density function:

$$f_{\nu_\mu}(x) = \frac{1}{\ell}\theta(\ell - x) \tag{3}$$

where the parameter ℓ is defined as:

$$\ell = 1 - \left(\frac{m_\mu}{m_\pi}\right)^2$$

This value is 2 times greater than the fraction of energy taken by the neutrino in the rest frame. The numerical factor 2 is due to the Lorentz transformation in the hypothesis $E_\pi \gg m_\pi$, as follows:

$$E_{\nu,\max} = \frac{1}{m_\pi}(E_\pi E_\nu^0 + p_\pi p_\nu^0) \simeq E_\pi\left(\frac{\ell}{2} + \frac{\ell}{2}\right) \simeq \ell\, E_\pi$$

The expressions for the neutrinos from three body decay are more complicated. The full calculations are reported in [15]; here we report only the functions, that are equal to:

$$f_{\bar{\nu}_\mu}(x) = g_\mu(x)\theta(x - r) + [h_{\mu,1}(x) + h_{\mu,2}(x)]\theta(r - x) \tag{4}$$

$$f_{\nu_e}(x) = g_e(x)\theta(x - r) + [h_{e,1}(x) + h_{e,2}(x)]\theta(r - x) \tag{5}$$

[1] For the moment we do not distinguish between ν and $\bar{\nu}$ talking about the flavor composition; the difference between ν and $\bar{\nu}$ will be explicitly discussed in Sec.1.4 and in the following of the thesis.

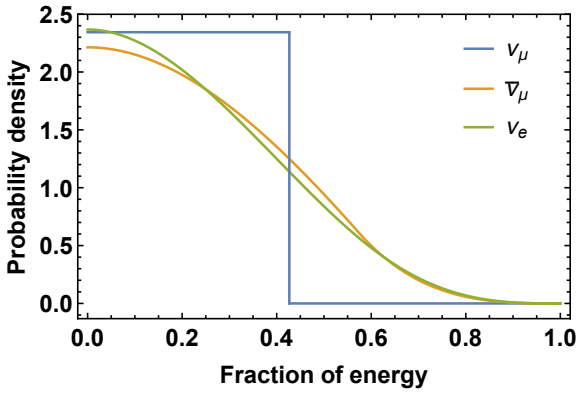

Figure 1: *Energy distribution of neutrinos from the decay of* π^+

where $r = (m_\mu/m_\pi)^2 \simeq 0.57$ and $\ell = 1 - r$. The functions $g_\mu(x)$, $h_{\mu,1}(x)$, $h_{\mu,2}(x)$, $g_e(x)$, $h_{e,1}(x)$, $h_{e,2}(x)$ written explicitly are:

$$
\begin{aligned}
g_\mu(x) &= \frac{3-2r}{9(1-r)^2}[9x^2 - 6\log(x) - 4x^2 - 5] \\
h_{\mu,1}(x) &= \frac{3-2r}{9(1-r)^2}[9r^2 - 6\log(r) - 4r^2 - 5] \\
h_{\mu,2}(x) &= \frac{(1+2r)(r-x)}{9r^2}[9(r+x) - 4(r^2 + rx + x^2)] \\
g_e(x) &= \frac{2}{3(1-r)^2}\{(1-x)[6(1-x)^2 + r(5+5x-4x^2)] + 6r\log(x)\} \\
h_{e,1}(x) &= \frac{2}{3(1-r)^2}[(1-r)(6-7r+11r^2-4r^3) + 6r\log(r)] \\
h_{e,2}(x) &= \frac{2(r-x)}{3r^2}(7r^2 - 4r^3 + 7rx - 4r^2x - 2x^2 - 4rx^2)
\end{aligned}
$$

The three functions f_{ν_μ}, $f_{\bar{\nu}_\mu}$ and f_{ν_e} are illustrated in Fig. 1.

1.3 *pp* MECHANISM

In pp interaction mostly π^+, π^- and π^0 are created, with a smaller contribution of kaons. The precise calculations of neutrino spectra use quite heavy numerical calculations. Presently three well developed codes of simulations of pp interactions are public available – Pythia [16], SIBYLL [17], QGSJET [18]. The last two as well as some other models are combined in the more general CORSIKA code [19] designed for simulations of interactions of cosmic rays with the Earth atmosphere. These codes are based on phenomenological models of p-p interactions incorporated with comprehensive experimental data obtained at particle accelerators.

While these codes can be directly used for calculations of gamma-ray spectra for any distribution of primary protons, it is quite useful to have in mind the following simply considerations:

- in the interaction between relativistic protons and proton targets π^+, π^- and π^0 are created in about equal amount, due to the isospin symmetry;

- after the decay of charged pions both ν_e (from π^+) and $\bar{\nu}_e$ (from π^-) are created. This aspect will become relevant in the following of the thesis, particularly in sections dedicated to the Glashow resonance, that is discussed in Sec.3.1.4 and Sec.4.5.4;
- the mean energy of neutrinos is about $1/4$ of the energy of pions. Since the leading pion produced in pp collisions has $1/5$ of the energy of the initial proton, we can say that generally to produce a neutrino of energy E_ν a proton with energy

$$E_p \simeq 20 E_\nu$$

  is required.
- the shape of the neutrino spectra is, generally, the same of the accelerated protons spectrum. This statement becomes not true when an energy cutoff is present in the spectrum of primary particles.

Let us analyze the case in which protons have a power law distribution for the energy spectrum. This is a simple case but it is also a very important one, since it usually occurs in astrophysical environments, for example in the Fermi mechanism of acceleration. Therefore this case is extremely important for neutrino astronomy and it is largely used in the literature.

1.3.1 The power law case

In the case of power law spectrum of accelerated protons also pions will be power law distributed. Let us consider a spectrum of pions with a normalization A and a spectral index α:

$$J_\pi(E_\pi) = A\ E_\pi^{-\alpha}$$

Using the general expression of Eq.2, we find that the spectrum of neutrinos has the same shape of the pion's spectrum with an extra numerical factor:

$$\phi_{\nu_\ell}(E_{\nu_\ell}) = A\ E_{\nu_\ell}^{-\alpha}\ \zeta_{\nu_\ell}(\alpha) \tag{6}$$

where $\zeta_{\nu_\ell}(\alpha)$ depends on the spectral index α in the following manner [14]:

$$\zeta_{\nu_\ell}(\alpha) = \int_0^1 f_{\nu_\ell}(x)\ x^{\alpha-1}\ dx \tag{7}$$

In the case of $\alpha = 2$, the $\zeta(\alpha)$ corresponds to the average fraction of energy carried by neutrinos. In Tab.1 there are some values of $\zeta(\alpha)$ for the three neutrinos from π^+ decay and for different values of α. Let us notice that the average fraction of energy taken by the neutrino from two body decay is a bit smaller (about 80%) than the energy taken by neutrinos from three body decay.

1.3.2 Flavor composition

The ζ factors are important to correctly evaluate the flavor composition at the source. Since neutrinos that come from pion decay have different spectra, generally it is not correct to simply count the number of neutrinos of a certain flavor produced at the end of the chain of decays. This procedure would be only correct for an E^{-1} spectrum, that does not occur in realistic

Table 1: *Table of ζ factor of neutrinos from π^+ decay. In case of π^- decay the first row of the table hast to be read α, $\zeta_{\bar{\nu}_\mu}$, ζ_{ν_μ}, $\zeta_{\bar{\nu}_e}$.*

α	ζ_{ν_μ}	$\zeta_{\bar{\nu}_\mu}$	ζ_{ν_e}
2.0	0.213	0.265	0.257
2.3	0.144	0.194	0.188
2.6	0.098	0.146	0.141

scenarios. Assuming a power law spectrum $E^{-\alpha}$ for the accelerated protons and the pp scenario, the ratio between the flux of muon neutrinos and electron neutrinos, in the production point, is given by:

$$r_{\mu e} \equiv \frac{2[\phi_{\nu_\mu}(E_\nu) + \phi_{\bar{\nu}_\mu}(E_\nu)]}{\phi_{\nu_e}(E_\nu) + \phi_{\bar{\nu}_e}}$$

under the assumption that the amount of π^+ is about equal to the amount of π^-, as discussed before.

Taking into account that $\zeta_{\nu_e} = \zeta_{\bar{\nu}_e}$, it follows from Eq.6 that the ratio $r_{\mu e}$ can be expressed only in terms of ζ factors, obtaining:

$$r_{\mu e}(\alpha) = \frac{\zeta_{\nu_\mu}(\alpha) + \zeta_{\bar{\nu}_\mu}(\alpha)}{\zeta_{\nu_e}(\alpha)} \simeq 1.86 - 0.20(\alpha - 2) - 0.02(\alpha - 2)^2 \tag{8}$$

The polynomial approximation is valid for $1.5 \leq \alpha \leq 3$. The function $r_{\mu e}(\alpha)$ differs from 2 especially at high values of α, as it can be noticed in the left panel of Fig.2. On the contrary for $\alpha = 2$ the ratio is not so different from 2; therefore it is safe to use the well accepted approximation $(\nu_e : \nu_\mu : \nu_\tau) = (1 : 2 : 0)$ talking about astrophysical neutrinos, in which the spectral index is expected to be not far from $\alpha = 2$, as we will see in details in the following.

1.3.3 Relation with γ-rays

The same calculation of the previous section can be done to evaluate the correlation between γ-rays and neutrinos in the hypothesis of common hadronic origin. Indeed in pp interaction, together with charged pions, also neutral pions are created; they decay in two photons ($\pi^0 \to \gamma\gamma$). The energy distribution of γ-rays, in the laboratory frame, is simply given by $f_\gamma(x) = 1$; therefore the average energy for each γ-ray is half of the pion's energy. Using Eq.7 we found that the ζ factor of γ-rays is equal to:

$$\zeta_\gamma(\alpha) = \frac{1}{\alpha}$$

In order to calculate the ratio between the flux of all neutrinos and the flux of γ-rays we use the same approach of Eq.8. Taking into account that at the end of the pions decay 2 γ-rays and 6 neutrinos are produced (2 ν_e, 2 ν_μ, 2 $\bar{\nu}_\mu$), we obtain:

$$r_{\nu\gamma} \equiv \frac{2(\phi_{\nu_\mu} + \phi_{\bar{\nu}_\mu} + \phi_{\nu_e})}{2\phi_\gamma} = \alpha(\zeta_{\nu_\mu} + \zeta_{\bar{\nu}_\mu} + \zeta_{\nu_e}) \tag{9}$$

The result is represented on the right panel of Fig.2 with an orange line.

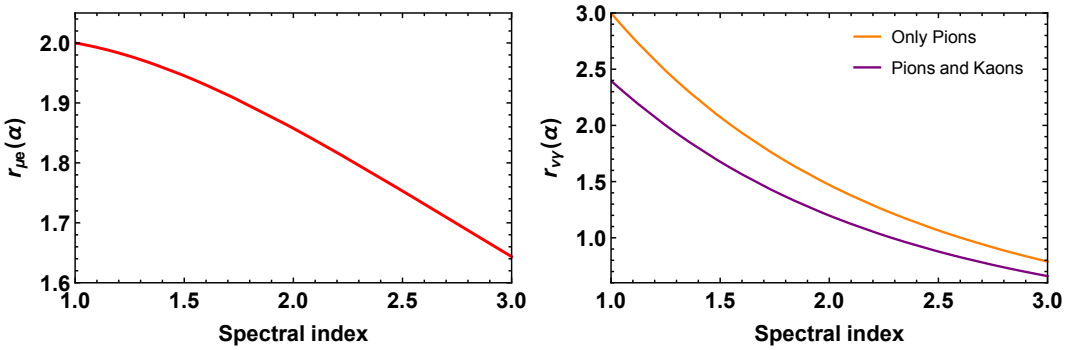

Figure 2: *On the left panel: ratio, at the source, between the flux of muon neutrinos and electron neutrinos, as a function of the spectral index α in the power law hypothesis (pp scenario). On the right panel: ratio between the flux of ν and γ in the hypothesis of common hadronic origin.*

1.3.4 The role of kaons

In the previous sections we have considered only the contribution of pions to the neutrino flux. Therefore the calculations are not very accurate, since we did not take into account the contribution to γ-rays and neutrinos that comes from heavier mesons, especially kaons. Indeed they are produced in pp interaction, although the amount of kaons is much smaller than the amount of pions. Neutrinos are produced by the decay of kaons; for example, in the case of K^+ decay, neutrinos are produced as follows [20]:

$$K \to \mu^+ \bar{\nu}_\mu \quad \text{B.R.} \simeq 64\% \tag{10}$$

$$K \to \pi^0 e^+ \bar{\nu}_e \quad \text{B.R.} \simeq 5\%$$

We denote the ζ factors of these processes with $\zeta_{K\nu_\ell}$. Another possibility is the following decay:

$$K \to \pi^+ \pi^0$$

with a $B.R. \simeq 21\%$ [20]. In this case neutrinos come from the pions decay, in the same manner already described in the previous sections.

Moreover neutrinos come also from the decay of muons, produced in the process of Eq.10:

$$\mu^+ \to e^+ \bar{\nu}_\mu \nu_e$$

We denote the ζ factors of these process with $\zeta_{K\mu\nu_\ell}$. In Tab.2 are reported the ζ factors of kaons, obtained with the same procedure used for pions (see [14] for a complete treatment).

The amount of kaons produced in the pp mechanism is 10%-20% of the amount of pions [14, 5]; therefore the contribution is small but not negligible. The modification of the flavor composition, due to the contribution of kaons in a realistic pp interaction, has been estimated in [5]. The result, obtained using a Montecarlo simulation of the pp mechanism, is that kaons affect the flavor composition by about 10% for $2.0 \leq \alpha \leq 2.6$. Particularly the presence of kaons slightly increases the fraction of muon neutrinos (antineutrinos). As a consequence the approximation $(\nu_e : \nu_\mu : \nu_\tau) = (1 : 2 : 0)$ results to be more precise when also kaons are taken into account (see left panel of Fig. 2 for comparison with the only pion scenario).

Table 2: *Table of ζ factor of neutrinos from K^+ decay.*

α	$\zeta_{K\nu_\mu}$	$\zeta_{K\nu_e}$	$\zeta_{K\mu\bar{\nu}_\mu}$	$\zeta_{K\mu\nu_e}$
2.0	0.48	0.27	0.16	0.21
2.3	0.42	0.21	0.12	0.16
2.6	0.36	0.15	0.08	0.11

GENERAL CALCULATION A general procedure, that does not require the hypothesis of power law spectrum for primary protons, has been adopted by Vissani and Villante in [21]. The contribution of kaons is considered in that work. It is interesting to illustrate the ratio between the flux of neutrinos and the flux of gamma obtained with this realistic approach, since it is useful to use this ratio in a context of multi-messenger astronomy. We denote with $r^K_{\nu\gamma}$ this ratio that is valid in the range $1.5 \leq \alpha \leq 3$. The function is well represented by the following polynomial expression:

$$r^K_{\nu\gamma}(\alpha) = 1.20 - 0.79(\alpha - 2) + 0.26(\alpha - 2)^2 \tag{11}$$

We represent the function $r^K_{\nu\gamma}$ in Fig.2 with a purple line, comparing it with the one of Eq.11, obtained using only pions and the ζ factors. Considering spectral indices between $2 \leq \alpha \leq 3$ we notice that the flux of γ is equivalent to the total flux of neutrinos in pp scenario, within an accuracy of 20-30%. It is important to underline that the production of neutrinos is always accompanied by the production of γ-rays, whereas γ-rays can be also produced by leptonic mechanisms in which neutrinos are absent. For these reasons if we observe γ-rays, their measured intensity sets an upper bound on the neutrino flux. This scenario corresponds to γ-rays produced completely by hadronic emission, i.e. by the decay of neutral pions. Anyway we will see in the following that this kind of multi-messengers approach is not always easy to implement. E.g. extragalactic γ-rays of few TeV are absorbed due to the interaction with the EBL. Moreover, in some cases, it could happen that the source is opaque to γ-rays and only neutrinos are able to escape from that region, nullifying the possibility to observe spatial correlations between γ-rays and cosmic neutrinos [22].

1.4 $p\gamma$ MECHANISM

In the case of $p\gamma$ interaction at the source the situation is very different respect to the pp interaction. In this scenario the power law spectrum of accelerated protons is not expected to be replicated by the spectra of secondary particles. On the contrary, the characteristics of target photons spectrum are relevant to obtain the neutrino spectra.

1.4.1 Delta approximation

A useful preliminary analysis of this kind of interaction can be done using the so called "δ-approximation", in which only the resonant baryon Δ^+ is produced. We refer to this scenario

also with the name "ideal $p\gamma$". After the production $p\gamma \to \Delta^+$, the resonant baryon quickly decays into:

$$p\gamma \to \begin{cases} \Delta^+ \to \pi^+ n & 1/3 \text{ of cases} \\ \Delta^+ \to \pi^0 p & 2/3 \text{ of cases} \end{cases}$$

giving π^+ and π^0, without pions with negative charge. This represents an important difference with respect to the pp interaction. The branching ratios are determined by the isospin conservation.[2]

The energy of the two final state particles in the center of mass frame is given by:

$$\begin{aligned} \frac{E_\pi}{m_\Delta} &= \frac{1}{2}\left[1 + \left(\frac{m_\pi}{m_\Delta}\right) - \left(\frac{m_n}{m_\Delta}\right)^2\right] \simeq 0.22 \\ \frac{E_n}{m_\Delta} &= \frac{1}{2}\left[1 - \left(\frac{m_\pi}{m_\Delta}\right) + \left(\frac{m_n}{m_\Delta}\right)^2\right] \simeq 0.78 \end{aligned} \tag{12}$$

The pion takes about $1/5$ of the total energy and the neutron (or proton if we consider π^0 instead of π^+) about $4/5$ of it. Later on the pion decays as just discussed in Sec.1.2 and also in this case the average energy for each neutrino turns out to be about the 5% of the primary proton's energy. Moreover the flavor composition in the δ-approximation of $p\gamma$ interaction is approximately the same of the pp interaction, i.e. $(\nu_e : \nu_\mu : \nu_\tau) = (1 : 2 : 0)$.

Anyway, there are also important differences between $p\gamma$ and pp interaction:

- the spectrum of target photons is relevant for the calculation of neutrino spectra;
- the spectrum of neutrinos produced by $p\gamma$ interaction is not power law distributed, even if the spectrum of the primary protons is a power law. On the contrary the spectrum of neutrinos is characterized by a typical bump, due to the peak in the cross section when the energy of CM is sufficient to create a Δ baryon;
- the connection between neutrinos and γ-rays from common hadronic origin is more complicated. Since the spectra of neutrinos are not power law distributed it is not possible to simply use the ζ factors. Anyway, assuming that γ-rays are not absorbed, we expect that the ratio between the flux of neutrinos and the flux of photons is smaller than the pp case. Indeed in pp scenario 2 charged pions each 1 neutral pion are produced, whereas in $p\gamma$ scenario the situation is the opposite one, i.e. 1 charged pion each 2 neutral pions. Therefore there are more photons than neutrinos;
- no $\bar{\nu}_e$ are created in the simplest treatment of this interaction. This consideration will become crucial in Sec.3.1.4, talking about the possibility to discriminate between the different mechanisms of production of high energy neutrinos.

[2] The branching ratios of the Δ^+ decay can be calculated using the ClebschGordan coefficients, for the decomposition of a state $|j, m>$ in terms of $|j_1, m_1>$ and $|j_2, m_2>$. The Δ^+ corresponds to a state $|3/2, 1/2>$, whereas π^+ and n correspond the the states $|1, 1>$ and $|1/2, -1/2>$; the ClebschGordan coefficient is $1/\sqrt{3}$ in this case. In the second process π^0 and p correspond to the states $|1, 0>$ and $|1/2, 1/2>$; the ClebschGordan coefficient is $2/\sqrt{3}$ in this case. The branching ratios are simply given by the square of these coefficients.

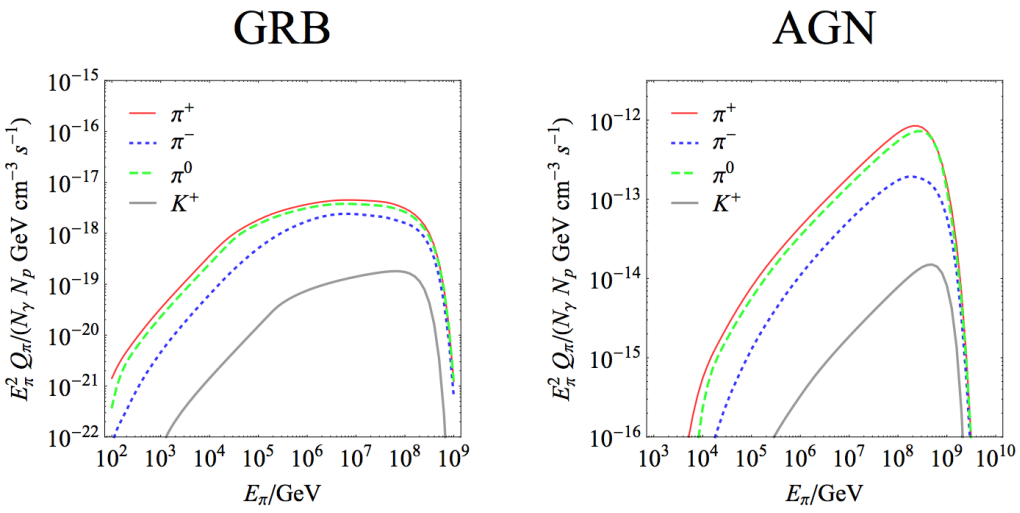

Figure 3: *Comparison among the π^+ (upper curve), π^0 (middle curve), and π^- (lower curve) spectra for GRB and AGN benchmark. The grey curve shows in addition the K^+ spectrum. Note the presence of π^- in these realistic $p\gamma$ scenarios, that are not expected in the ideal $p\gamma$. The figure is taken from [23].*

1.4.2 Realistic scenarios

In [24, 23, 25] the $p\gamma$ interaction is treated in an exhaustive manner. In Fig.3, taken from [23], the production rate $Q(E)$ of pions from a realistic $p\gamma$ interaction are illustrated. The production rate $Q(E)$ is proportional to the quantity $J(E)$ defined in Sec.1.2. In this figure the typical spectra of secondary particles, that can be produced in a realistic $p\gamma$ scenario, are represented. This mechanism usually occurs in Gamma Ray Burst, Active Galactic Nuclei and Blazars. For details see the Ref.[23]. We will talk about these astrophysical environments in Chapter 2, that is dedicated to the sources of cosmic neutrinos.

On the other side it is important to focus on some specific characteristics, that can be noticed from Fig.3. As in the δ-approximation scenario, the spectra represented in Fig.3 are not power law distributed. They are characterized by a typical bump of the $p\gamma$ interaction, very different with respect to the spectra obtained in the pp scenario. An important difference with respect to the δ-approximation case is that the flux of π^- is different from zero in realistic scenarios. This point is relevant because in some cases the flux of π^- can be very large and similar to the π^+ flux. Therefore the ratio between the flux of π^- and π^+ is not always a good indicator of the type of interaction at the source, as suggested by the oversimplified scenario. Fig.4 illustrates a case when the contribution of π^- reaches about 25% at PeV energy.

The PeV energy is a huge energy but it is relevant for the neutrino astronomy, because at this energy the contamination from the atmospheric background is absent. The first two PeV events have been observed by the IceCube experiment in the years 2010-2012 [26]. We will dedicate Chapters 5 and 6 to the interpretation of neutrino events detected by IceCube up to now.

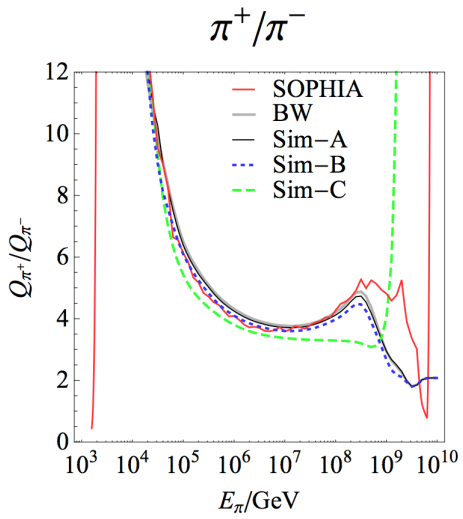

Figure 4: *Pion ratios obtained from a $p\gamma$ interaction in a GRB benchmark. Figure from [23]*

1.5 OTHER MECHANISMS OF NEUTRINO PRODUCTION

Although the standard case of complete pion decay is the most probable mechanism of production, it is not the only possibility. We discuss here a couple of interesting possibilities.

1.5.1 Damped muons

In a source with very high density or an high magnetic field it could happen that muons interact before decaying, loosing their energy. In this case only the muon neutrinos (antineutrinos) from the two body decay (see Eq.1) contribute to the high energy neutrino flux; this scenario can be called "damped muons" and it produces a totally different flavor ratio at the source with respect to the previous cases, i.e.

$$(\nu_e : \nu_\mu : \nu_\tau) = (0 : 1 : 0)$$

as discussed in [25, 4, 27]. Let us notice that also in this case the amount of electron antineutrinos is zero at the source.

1.5.2 Neutrons decay

A speculative hypothesis is that high energy neutrinos are produced by the decay of neutrons, in the well known process:

$$n \to p\, e^-\, \bar{\nu}_e$$

In this case only $\bar{\nu}_e$ are produced, but we have to take into account that, considering the same energy of the primary particle, these neutrinos are less energetic with respect to the neutrinos

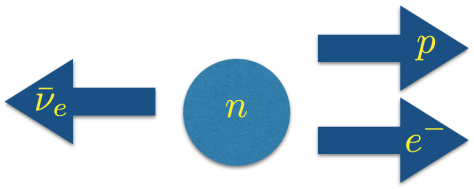

Figure 5: *The configuration in which a $\bar{\nu}_e$ from neutron decay takes the maximum energy.*

Table 3: *Table of flavor ratio. The sum of the flavor fractions is normalized to 6.*

Mechanism	ν_e	ν_μ	ν_τ	$\bar{\nu}_e$	$\bar{\nu}_\mu$	$\bar{\nu}_\tau$
ideal $p\gamma$	2	2	0	0	2	0
pp	1	2	0	1	2	0
damped muon pp	0	3	0	0	3	0
damped muon $p\gamma$	0	6	0	0	0	0
neutrons decay	0	0	0	6	0	0

from the standard pion decay, since $m_n \simeq m_p$. It can be easily understood by analyzing the process. In the rest frame the available energy is equal to:

$$Q = M_n - M_p - M_e \simeq 1.3 \text{ MeV}$$

An $\bar{\nu}_e$ takes the maximum energy, equal to $Q/2$, in the configuration represented in Fig.5. In the relativistic frame, under the condition $E_n \gg M_n$, the neutrino's maximum energy becomes equal to

$$E_\nu^{\text{lab,max}} = \gamma(1+\beta)\frac{Q}{2} \simeq E_n \times \frac{Q}{M_n}$$

Therefore an $\bar{\nu}_e$ from neutron decay has about 0.1% of the energy of the primary particle. On the other side we have seen that a neutrino from pions decay has about 5% of the energy of the primary particle. For this reason the hypothesis of neutrinos from neutron decay does not seem realistic, but this case is occasionally discussed in the literature [4, 28]. In Tab.3 is reported a summary of the flavor composition expected in the different scenarios analyzed in this chapter. From the table we immediately notice that no ν_τ are produced in the standard mechanisms of neutrino production.

2 SOURCES OF HIGH ENERGY NEUTRINOS

There are a lot of potential astrophysical sources of high energy neutrinos and in this chapter we provide a brief summary of them. In the first part of the chapter we discuss the Galactic sources. First of all we examine in which way a Galactic flux can be produced. After that we focus on point sources, as Supernova Remnant, Pulsar Wind Nebulae, Galactic center, Fermi bubbles and Microquasars. The second part of the chapter is dedicated to the extragalactic sources, where we examine Gamma-Ray Bursts, AGNs, Blazars and Starburst Galaxies. We close the chapter with the cosmogenic neutrinos, i.e. neutrinos with huge energy (> 100 PeV) that are produced by the interaction of very energetic cosmic rays with the CMB.

2.1 GALACTIC SOURCES

In our Galaxy there are several processes that could generate high energy neutrinos. Before analyzing specific objects as possible sources, we briefly describe our Galaxy.

2.1.1 The Milky Way

The Milky Way is the galaxy that contains our Solar System. The descriptive term "milky" is derived from the appearance of the galaxy from Earth. The Milky Way is one of the largest galaxy in the Local Group, with its stellar disk approximately 30 kpc in diameter. The thin disk of the Galaxy, composed of stars, gas and dust, extends vertically for about 0.3 kpc. On the other hand the thick disk, mainly populated by stars, extends about $1 \div 5$ kpc. In Fig.6 a schematic profile of the Milky Way is represented, using light years instead of parsec as unit. Let us recall that 1 ly $\simeq 0.307$ pc. At the center of our Galaxy a super massive black hole is present; it could be an interesting source of high energy neutrinos. We will dedicate Sec.7.2 to this topic.

Another important component is represented by the "galactic halo". It is an extended, roughly spherical component of the Galaxy which extends beyond the main, visible component. Several distinct components of galaxies comprise the halo:

- the galactic spheroid (stars);
- the galactic corona (hot gas, i.e. a plasma);
- the dark matter halo.

The distinction between the halo and the main body of the galaxy is clearest in spiral galaxies, where the spherical shape of the halo contrasts with the flat disc. In an elliptical galaxy, there is no sharp transition between the body of the galaxy and the halo.

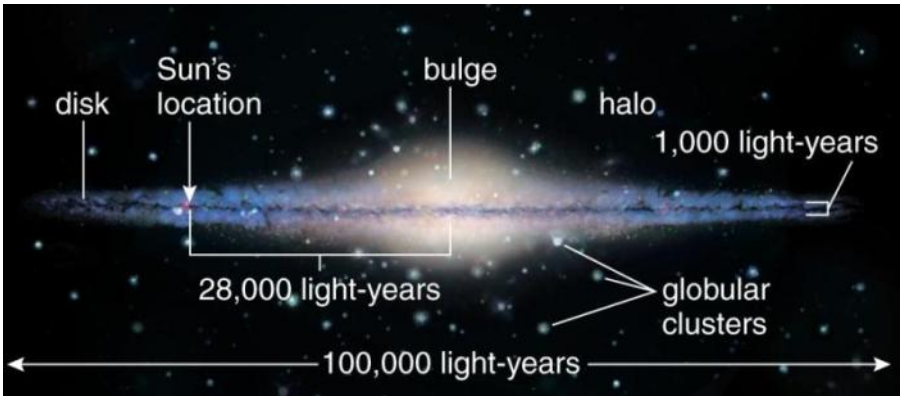

Figure 6: *Illustration of the Milky Way. Credit: wikipedia*

The total mass of all the stars in the Milky Way is estimated to be between $4.6 \times 10^{10} M_{\odot}$ and $6.43 \times 10^{10} M_{\odot}$ [29]. In addition to the stars, there is also interstellar gas, comprising 90% hydrogen and 10% helium by mass, with 2/3 of the hydrogen found in atomic form and the remaining 1/3 in molecular form. The mass of this gas amounts to a fraction from 10% to 15% of the total mass of the galaxy's stars. Interstellar dust accounts for an additional 1% of the total mass of the gas. Due the velocity of stars at the outer edge of the Milky Way, it is believed that the Milky Way is more massive than its baryonic mass and most of the mass of the Milky Way appears to be dark matter [30].

2.1.2 Disk and halo

As remarked in Sec.1.3 neutrinos can be created by the interaction between accelerated protons and the baryonic matter.

The Galactic disk, where the matter density is 1 nucleon/cm^3, offers the proton target to realize the pp interaction. Moreover it is important to notice that also the interaction between accelerated protons and the matter contained into the halo of the Galaxy can produce a non negligible amount of neutrinos. Indeed, although the density in the halo is 2-3 orders of magnitude less than in the disk, the dimension of the halo is much greater and there is a compensation between these two quantities. It is possible to understand this fact making a rough estimation of the efficiency ξ of disk and halo to produce neutrinos, that depends from the confinement time of cosmic rays (due to magnetic fields) and the cooling time due to the proton-proton interaction. The confinement time depends upon the dimension of the considered region R and the diffusion coefficient D, as follows:

$$t_{esc} \propto \frac{R^2}{D}$$

The cooling time depends upon the matter density n and the cross section of proton-proton interaction σ_{pp}, namely

$$t_{pp} \propto \frac{1}{\sigma_{pp} \times n}$$

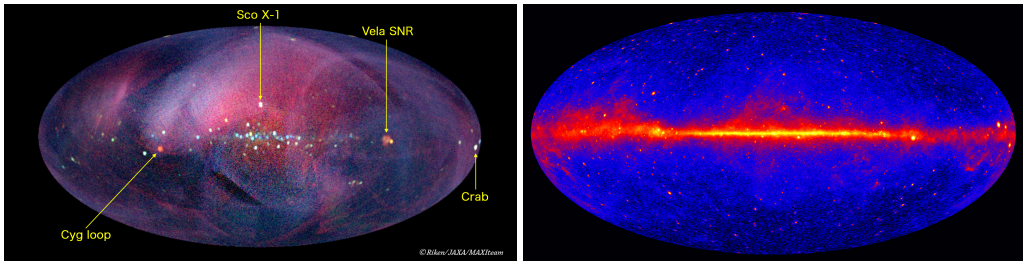

Figure 7: *Representation of the sky using x-rays [31] and γ-rays [32].*

The inelastic part of the total cross-section of pp interactions can be presented in the following form:

$$\sigma_{pp}(E_p) = 34.3 + 1.88\ L + 0.25\ L^2,\ \text{mb}$$

where $L = \ln(E_p/1\ \text{TeV})$. This approximation is taken from [15] and it has been obtained using the SIBYLL code.

Therefore the efficiency ξ of neutrino production can be generally written in the following manner:

$$\xi = \frac{t_{esc}}{t_{pp}} \propto \frac{n\ R^2}{D} \tag{13}$$

Using typical values for the disk

$$n_d = 1\ \frac{\text{nucleon}}{\text{cm}^3},\ \text{R}_\text{d} = 1\ \text{kpc}$$

and for the halo

$$n_h = 10^{-3}\ \frac{\text{nucleon}}{\text{cm}^3},\ \text{R}_\text{h} = 30\ \text{kpc}$$

we obtain the ratio between the efficiencies, that is equal to:

$$\frac{\xi_d}{\xi_h} \simeq 1\frac{D_h}{D_d} \tag{14}$$

From last equation we notice that, although the density of halo is much smaller than the density of disk, the efficiencies of neutrino production can be similar, whether the diffusion coefficients in these two regions are comparable.

Now we consider various objects in our Galaxy, that are candidate sources of high energy neutrinos.

2.1.3 Supernova Remnants

A supernova is an astronomical event that occurs during the last stellar evolutionary stages of a massive star's life, whose dramatic and catastrophic destruction is marked by one final titanic explosion. This causes the sudden appearance of a "new" bright star, before slowly fading from sight over several weeks or months.

A supernova remnant (SNR) is the structure resulting from the explosion of a star in a supernova. The supernova remnant is bounded by an expanding shock wave, and consists of

ejected material expanding from the explosion, and the interstellar material it sweeps up and shocks along the way.

The connection between Supernovae and cosmic rays was first proposed by Baade and Zwicky in 1934 [33]. The main theoretical reason why Supernova Remnants (SNR) are considered as possible sources of neutrinos has been proposed by Ginzburg and Syrovatskii [34], based on energetic considerations. They observed that the Milky Way radiates cosmic rays (CR) at a rate

$$L_{\rm CR} = V_{\rm CR}\rho_{\rm CR}/\tau_{\rm CR} \sim 10^{41}{\rm erg/s} \tag{15}$$

where the volume, the lifetime and the average density of CR are all rather uncertain. The order of magnitude of this quantities is such that $V_{\rm CR} = \pi\ h\ r^2$, with $h = 3.5$ kpc and $r = 15$ kpc. The energy density of CR is equal to $\rho_{\rm CR} \sim 1\ \frac{\rm eV}{\rm cm^3}$ and the confinement time of cosmic rays into the galaxy is order of 3×10^7 years.

The energy loss $L_{\rm CR}$ is compensated if any 30 years a new SNR (of any type) converts 10% of its kinetic energy into CR. The typical energy of a SNR can be estimated considering the kinetic energy of 10 solar masses that are ejected with a velocity of 3000 km/s, obtaining:

$$E_k = \frac{1}{2} \times 2 \cdot 10^{33}{\rm g} \times \left(3 \cdot 10^8\ \frac{\rm cm}{\rm sec}\right)^2 \simeq 10^{51}\ {\rm erg}$$

that is often expressed by a unity of energy called foe, with 1 foe = 10^{51} erg. Dividing by 30 years (i.e. $\sim 30\ \pi\ 10^7$ sec $\simeq 10^9$ sec) and multiplying by 10%, we have the injection rate of cosmic rays, which equates the loss rate of Eq.15.

The expanding clouds of gas and magnetic fields remnant of SN explosions can last for thousands of years. Theoretical models show that a maximum energy $E_{\rm max} \sim 100$ TeV can be achieved, and there are active discussions if non linear amplifications of the magnetic fields allow to reach the knee energy, around 1-10 PeV. Reaching the "ankle", with SNR, is considered unlikely. The associations between SNR and molecular clouds (MC) provide the optimal conditions to produce intense neutrino and γ-ray fluxes [35].

The best hope to detect high energy neutrinos produced by hadronic interactions is connected to young SNR, i.e. of age less than 2000 years. In fact, these are expected to contain the highest energy cosmic rays that can produce high energy neutrinos interacting with the targets. In order to be detectable the flux of neutrinos produced by SNR must exceed the flux of atmospheric neutrinos. In other words we are interested in special types of SNR's as potential neutrino sources: the closest and the youngest, among those associated to molecular clouds [36]. It should however be observed that core collapse supernovae, being connected to short living stars, are pretty naturally associated with sites of intense star formation, i.e. molecular clouds.

One can expect, a priori, that the closest SNR should be at about 1 kpc, because we have 1 new SN each many tens or years and the size of the Galaxy is several tens of kpc. A more precise estimation can be done using the spatial distribution of the SNR density into the Milky Way, that is approximately given by:

$$\frac{d\rho(r)}{dr} = \frac{r}{a^2}\ \exp\left(-\frac{r}{a}\right),\ \text{with } a \sim 3\ \text{kpc}$$

and r is the distance from the Galactic center. We are interested to know this distribution as a function of the distance from the Earth, therefore a change of coordinates is required. Using the distance L from the Earth the previous expression becomes:

$$\frac{d\rho}{dL} = \frac{L}{a^2}\int_0^{2\pi} \exp\left(-\frac{r(L,\theta)}{a}\right)\frac{d\theta}{2\pi}$$

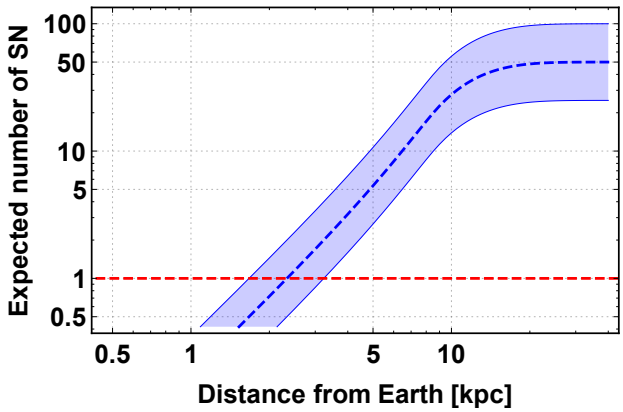

Figure 8: *Cumulative distribution of SNR as a function of the distance L from the Earth. We are assuming a new explosion every 40 years, with a factor 2 of uncertainty.*

with $r(L,\theta) = \sqrt{(L^2 + R^2 - 2LR\cos\theta)}$ and $R = 8.5$ kpc, i.e. the distance between the Earth and the Galactic center [37]. This is a probability density function. Therefore, multiplying it for the total number of Supernovae, we can estimate what is the distance L^* at which the cumulative function becomes equal to 1, i.e. the minimum distance to have at least 1 SNR. Assuming that the number of young SNR is equal to 50 (i.e. an explosion every 40 years in the last 2000 years) with an uncertainty of a factor 2, we obtain the cumulative function represented in Fig.8. We found that the minimum distance to detect at least 1 young SNR is between 1.5 and 3 kpc.

Nowadays, only two powerful SNRs have enough γ-ray luminosity to have an associated flux of neutrinos that is potentially detectable by telescopes of neutrinos. These are SNRs RXJ1713.7-3946 [38, 39, 40] and RXJ0852.0-4622 which have been extensively discussed as potential sources of high energy neutrinos. Different estimations show that in principle some events per year can be detected using a 1 km^3 detector, if the produced γ-rays have hadronic origin (see [36] and references quoted therein). However up to now the leptonic origin of the γ-rays cannot be excluded. The location of these two SNRs is not ideal to be probed by IceCube, since they are located at negative declination on the Galactic plane (respectively $-39.46°$ and $-46.22°$) and they can be observed only using the contained events that, as we will see in chapter 4, do not have the sufficient angular resolution to point the source. On the other side these two objects are perfect targets for future planned KM3NeT instrument. Therefore the hypothesis that the CR originate from SNR is still a viable hypothesis that will be tested in the next years by neutrino telescopes.

2.1.4 Pulsar wind nebulae

A pulsar wind nebula (PWN, plural PWNe), sometimes called a plerion, is a type of nebula found inside the shells of supernova remnants, that is powered by pulsar winds generated by its central pulsar. These nebulae were discovered in 1976 as small depressions at radio wavelengths near the centre of supernova remnants [41]. They have since been found to be x-ray emitters[42] and are possibly γ-ray sources [43].

PWNe are another class of galactic sources which are supposed to accelerate particles up to very high energy (100 TeV - 1 PeV). If a fraction of accelerated particles are protons, then

from the inelastic interactions between them and the ambient gas (pp interaction), high energy γ-rays and neutrinos can be produced. The presence of a proton component in the pulsar winds is still an open question but it is not excluded and it remains attractive to explain the γ-ray emission from PWNe [44]. The leptonic scenario would explain them as synchrotron emission of accelerated electrons/positrons. The number of PWNe detected in TeV band and presented in TeVCat[1] is 35 but for 7 sources no data are available. Only two sources have enough luminosity in γ-rays to produce a detectable flux of high energy neutrinos: they are the Crab nebula and Vela X.

The Crab nebula is a very well studied object at all wavelengths. It emits γ-rays up to TeV band, which are most likely produced from inverse Compton scattering of soft photons fields inside the nebula. If γ-rays are also produced by hadronic process, from this source high energy neutrinos can be detected but, presently, it seems to be a less plausible scenario with respect to the leptonic one [45].

Vela X PWN, an active pulsar associated with nebula, is a promising source of high energy neutrinos, thanks to a total luminosity equal to 112 $L_\odot$, where $L_\odot = 3.83 \times 10^{33}$ erg/s is the luminosity of the Sun. In the nebula there are the right conditions to realize the pp interaction. The origin of TeV γ-rays from Vela is under debate but, in this case, the hadronic scenario seems plausible [46]. For this reason the Vela region is a prime candidate as a galactic neutrinos source, to be detected with KM3NeT, because it is located at the negative declination of $-40^\circ\ 33^{'}\ 16.91^{''}$.

2.1.5 Galactic center

The central region of our Galaxy is of special interest. It was investigated by various experiments measuring photons at different energies. This region has the highest density of matter in the Galaxy and it includes the central Black Hole as well as several TeV γ-ray sources. The central Black Hole has a mass of about $4 \times 10^6\ M_\odot$ and it is classified as Super Massive Black Hole but no evidence of jets has been observed. Our Black Hole is not an "active galactic nucleus".

The experiment HESS has provided us with evidence of a first PeVatron located in the Galactic center [47]. An expectation for the neutrino flux has been derived from the measured γ-ray flux in [8] and it will be discussed in details in Sec.7.2.

In addition, there are three other γ-ray sources seen by HESS within 2° distance from the center of the Galaxy:

- the source J1747-281 is at the same position with the supernova remnant G 0.9+0.1;
- the source J1745-303 has no clear counterpart but is observed with a very hard energy spectrum $\alpha \simeq 1.8$ and no energy cutoff;
- the third one J1741-302 is a very faint source, at the lower edge of the HESS sensitivity.

The unidentified source (J1745-303) could produce a large neutrino flux compared to the atmospheric expectation at neutrino energies above 5 TeV, because of the hard spectrum. See [48] for a discussion of the hadronic scenario in this source. From the supernova remnant G 0.9+0.1, instead, a neutrino flux lower than the flux from the atmosphere is expected in the whole energy range.
The region of the Galactic Center seems to be a good candidate to search for neutrino emission [49], in particular because of the existence of at least three different source candidates.

[1] http://tevcat.uchicago.edu/

2.1.6 Fermi bubbles

The analysis of data collected by the Fermi-LAT experiment revealed two large extended structures near the Galactic centre, above and below the galactic plane. They are called Fermi bubbles [50] and an illustration of them is provided in the Fig.9. These structures are characterized by GeV γ-ray emission with an hard spectrum E^{-2} and a constant intensity over the whole spatial emission region. Several models [51, 52, 53, 54] explain the emission with an hadronic scenario, in which gamma rays and neutrinos are produced by the collisions of cosmic-ray protons with the interstellar matter. On the other hand, there are models that prefer leptonic mechanisms or even dark matter decay [55, 56]: in these scenarios a lower flux of neutrinos (or none at all) is expected. For these reasons the observation of a neutrino signal from the Fermi bubble would play a unique role to discriminate between different models and to understand better this astrophysical environment. Nowadays the photon flux in the energy range 1-100 GeV covered by the Fermi-LAT detector [57] from the Fermi bubble regions is:

$$E^2 \frac{d\phi_\gamma}{dE} \sim 3 \div 6 \times 10^{-7} \text{ GeV cm}^{-2}\text{s}^{-1}\text{sr}^{-1}$$

Since in the pp mechanism the flux of gamma rays and the all flavor flux of neutrinos are equal within 25-30% (see section 1.3.3), the flux of muon neutrinos, that can be measured by ANTARES, is about $1/3$ of it in the pion decay scenario:

$$E^2 \frac{d\phi_\mu}{dE} \sim 1.2 \div 2.4 \times 10^{-7} \text{ GeV cm}^{-2}\text{s}^{-1}\text{sr}^{-1}$$

This limit comes from a purely hadronic scenario and it is an upper limit. In the case of mixed scenario (leptonic plus hadronic) for the production of γ-rays, the flux of neutrinos would be less than the flux of gamma. A cutoff is expected to be present between 50 and 500 TeV for the neutrino spectrum, because a cutoff in the primary protons spectrum is expected from 1 PeV to 10 PeV. The analysis of 2008-2011 ANTARES data [58] give a 1.2σ excess of events in the Fermi bubble regions, compatible with the no-signal hypothesis. For the optimistic case of no energy cutoff in the flux, the present upper limit is a factor three larger than what is expected by the purely hadronic model based on the measured gamma-ray flux. The next generation of neutrino telescope, such as KM3NeT, will provide an improvement in sensitivity, by more than an order of magnitude.

2.1.7 Microquasars

A microquasar (or radio emitting X-ray binary system) is the little sibling of a quasar. Microquasars are named after quasars, as they have some common characteristics: strong and variable radio emission, often resolvable as a pair of radio jets, and an accretion disk surrounding system of compact objects which are either black holes or neutron stars. In quasars, the black hole is supermassive (millions of solar masses); in microquasars, the mass of the compact object is, typically, few solar masses. In microquasars, the accreted mass comes from a normal star, and the accretion disk is very luminous in the optical and X-ray regions. Microquasars are sometimes called radio-jet X-ray binaries to distinguish them from other X-ray binaries.
The composition of the jets, particularly their baryonic content, is still an open issue and it is the key issue for the expectations on the flux of neutrinos. Evidence for a baryonic content has been found only in the jets of the microquasar SS433 [59] and 4U 1630-47 [60]. The synchrotron

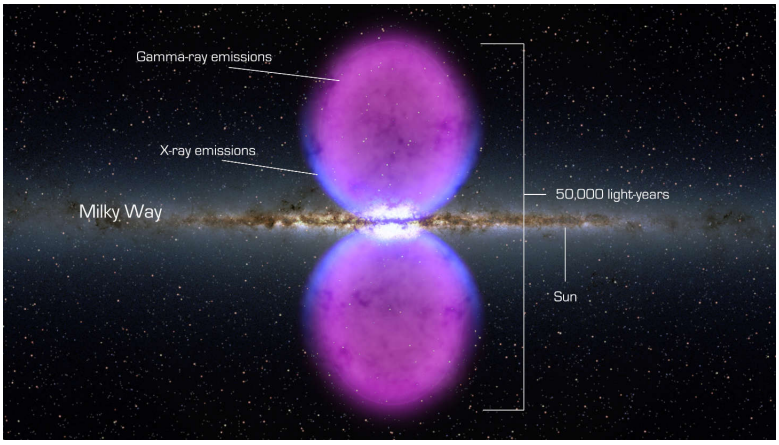

Figure 9: *Pictorial illustration of Fermi bubble. The vertical extension is about 10 kpc. Credit: wikipedia*

emission from the electrons may provide the required opacity to photo-meson production and high energy neutrino may be produced ($p\gamma$ scenario) if:

- baryons are contained in microquasar jets;
- dissipation mechanism allows them to be accelerated to very high energies, e.g. through diffusive shock acceleration.

In microquasars harbouring an early type, massive ($\geq 10 M_{\odot}$) companion star, neutrinos may be generated by the interaction of the relativistic baryons in the jets with the ions from the stellar wind (pp scenario) [61, 62]. The detection of high energy neutrinos from microquasars would give important hints about the composition of microquasar jets and about the physics that occurs in these extreme environments close to black holes or neutron stars.
The search of high energy neutrinos from microquasars has been performed by ANTARES telescope between 2007 and 2010 [63]. Different microquasars were considered and the searches did not result in a statistically significant excess above the expected background. A 90% C.L. upper limits on the neutrino fluxes, expected from different microquasars, have been calculated by the ANTARES collaboration and the constraint is:

$$E^2 \frac{d\phi}{dE} < 0.6 \div 25 \times 10^{-6} \text{ GeV cm}^{-2}\text{s}^{-1}$$

for the different sources analyzed. The motivations to search high energy neutrino emission from microquasars with additional ANTARES data or, in the longer term, by the forthcoming KM3NeT neutrino telescope remains excellent.

2.2 EXTRAGALACTIC SOURCES

For several extragalactic neutrino sources the $p\gamma$ mechanism is considered to be more important than the pp one. In this section we present the most plausible sources of high energy neutrinos, i.e. Gamma-Ray Burst, Active Galactic Nuclei, Blazars and Starburst Galaxies.

2.2.1 Gamma-Ray Bursts

GRBs are intense and rapid flashes of gamma radiation, characterized by a typical energy release of 10^{51} erg, which allows to classify them among the most energetic phenomena in the Universe. Such events have been discovered through gamma satellites, detecting isotropic high photon fluxes. It has been hypothesized that these sources are able to accelerate protons up to ultra-high energies: therefore GRBs are also promising sources of PeV neutrinos, as discussed in the literature [64, 65, 66, 67, 68]. Indeed, neutrinos emerge in a natural way from the interaction of a power law protons spectrum with the dense radiation field ($p\gamma$ interaction): in particular, 10-100 PeV protons over MeV target photons (all energies in the laboratory frame) produce neutrinos with energy around the PeV.

The original computation of neutrino flux from GRBs was done by Waxman and Bahcall [65], in the context of the internal shock fireball scenario, starting from the assumption of Fermi-accelerated protons in the relativistic ejecta of the burst that interact with the observed photon field. The interaction proceeds through the resonant production of the Δ^+, whose decay can give charged pions and therefore high energy neutrinos, as discussed in chapter 1.

In Fig.10 the expected spectrum of neutrinos from GRBs, multiplied by E^2, is illustrated. We notice that the typical spectrum of neutrinos, produced by GRBs, is expected to follow an E^{-1} spectrum until some 100 TeV and then an E^{-2} spectrum at higher energy. Above 10 PeV the spectrum becomes as soft as E^{-3}, because a loss term proportional to E^{-1} must be included, due to synchrotron radiation losses of secondaries, like pions and muons [65]. In the region where the spectrum of neutrinos is expected to be E^{-2} distributed, the calculations of Waxman and Bahcall suggest that the flux of muon neutrinos from GRBs is equal to:

$$E^2 \frac{d\phi_\mu}{dE} \simeq 4 \times 10^{-9} \text{ GeV cm}^{-2}\text{s}^{-1}\text{sr}^{-1}$$

The expected rate of GRB is about 1000 per year over 4π sr [70, 71, 72]. The most recent analysis done by the IceCube Collaboration [73] was performed searching for neutrinos of all flavors emitted by 807 GRBs during three years of data taking. Because GRBs are transient sources, it is possible to include in the analyses both the temporal and directional information about the detected events: in the IceCube data sample, five events were found in space-time coincidence with GRBs, resulting compatible with background expectations. Due to the absence of a significant excess of neutrinos associated to GRBs, it is possible to constrain the parameters space on which the theoretical model is based; in particular the bulk Lorentz factor and the baryonic load of the jet. A more detailed Monte Carlo simulation[2] of neutrino production in the GRB jet was recently performed and the new evaluation reduces the expected neutrino flux by an order of magnitude with respect to the analytic computations and therefore weakens the obtained limit. The present limit on the contribution of the GRBs to high energy neutrinos is of the order of [73]

$$E^2 \frac{d\phi_\mu}{dE} \sim 10^{-9} \text{ GeV cm}^{-2} \text{ s}^{-1} \text{ sr}^{-1}$$

This implies that the simple scenario for high-luminosity GBRs cannot explain the entire IceCube signal [73].

[2] Numerical NEUCOSMA model.

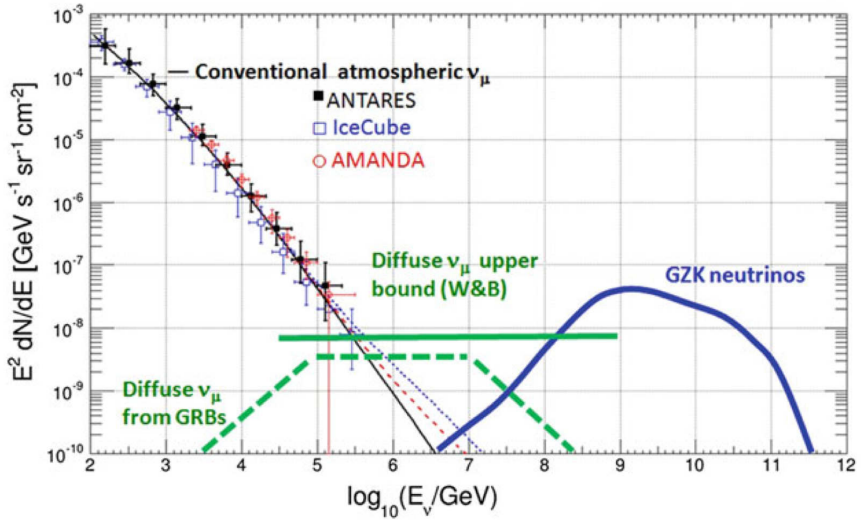

Figure 10: *Expected neutrino fluxes from different diffuse cosmic models and the atmospheric neutrino background [69].*

2.2.2 Active Galactic Nuclei

An active galactic nucleus (AGN) is a compact region at the center of a galaxy whose luminosity is much higher than the normal one over some portion of the electromagnetic spectrum, with characteristics indicating that the excess luminosity is not produced by stars. Such an excess in the non-stellar emission has been observed in the radio, microwaves, infrared, optical, ultraviolet, X-ray and gamma ray wavebands. A galaxy hosting an AGN is called an active galaxy. The radiation from an AGN is believed to be a result of accretion of matter by a supermassive black hole at the center of the host galaxy [74, 75, 76]. The central engine can accelerate protons up to very high energies, while the accretion disc is an emitter of hot thermal radiation, which gives prominent feature in the observed AGN spectra, usually refereed to as a "Big Blue Bump". Accelerated particles move along two jets perpendicular to the accretion disc and crossing this radiation field. See Fig.11 for illustration.

AGNs are considered potential sites for the high energy neutrino production [77, 78, 79, 80, 81]. High energy neutrino appear in charged pion decays created in $p\gamma \to n\pi^+$ reactions, due to the collision between protons and the blue bump photons. Protons accelerated up to 100 PeV and absorbed in the radiation field contained into the disk, with a temperature of about 15 eV and a black hole mass of $10^8 M_\odot$, can give a neutrino spectrum between 100 TeV and 10 PeV with the same spectral shape of the primary protons and compatible with the observations. Anyway the previous argument should be considered a test of plausibility; the study of the correlation between neutrino arrival directions and various AGNs position is necessary to falsify or to constraint better this type of model. This will be possible in the nearest future, when more data will be accumulated, especially using the track-like events, that are more closely linked to the source. Nowadays it is not possible to exclude (or confirm) the AGNs as potential sources of a part of the IceCube signal. An analysis of this argument has been proposed in [82].

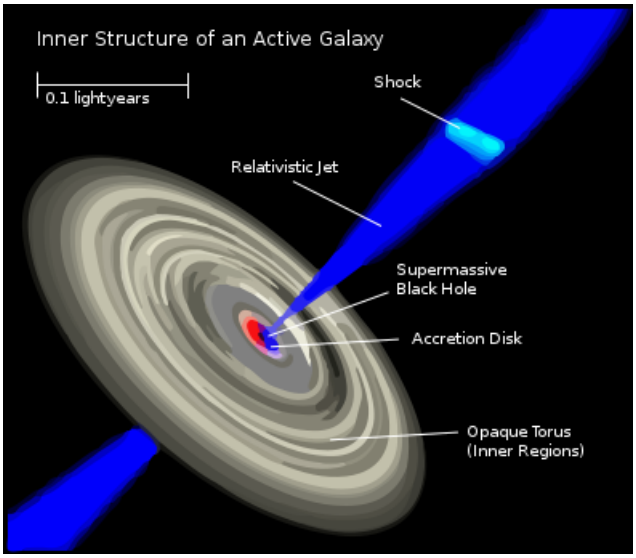

Figure 11: *Inner structure of a galaxy with an active galactic nucleus. Credit: Wikipedia*

2.2.3 Blazars

The blazars are AGNs with jets pointing toward the Earth and featureless optical spectra (i.e., lacking strong emission/absorption lines). The Fermi-LAT satellite proved that the blazars are the brightest extragalactic sources above 10 GeV. Many more of these blazars are not visible as point sources, being too faint and/or too far from us. They contribute to the unresolved γ-ray radiation, again observed by Fermi-LAT. The sum of resolved and unresolved blazars almost saturates the observed diffuse emission [83], with a margin of uncertainty of some ten percents, that should be attributed to other sources.

Blazars are good candidates to produce high energy neutrinos, as discussed in [84, 85, 86, 87, 88, 89]. They are broadly classified in BL Lac (namely BL Lacertae) and in flat spectrum radio quasars (FSRQ). BL Lac are characterized by featureless optical spectra (i.e., lacking strong emission/absorption lines) and they are believed to be the most promising source of high energy neutrinos after the papers of Tavecchio et al. [90, 91], whereas, in the past, FSRQ were believed to be a more promising source of high energy neutrinos.

Exploring the correlation between the arrival direction of neutrinos and the direction of γ-rays, with the condition that a neutrino event must have at least one γ-ray source as a counterpart, it is found that shower-like events[3] (with a typical angular resolution of $10^\circ - 15^\circ$) show connection with blazars [92, 93].

A recent analysis of the IceCube collaboration shows that the contribution of blazars to the diffuse flux of high energy neutrinos is about 25% [94]. However this kind of multi-messenger analysis strongly depends on the assumption on neutrino spectrum, as we will discuss in chapter 6 and 7. For example, assuming an E^{-2} spectrum for the extragalactic component of the neutrino spectrum, the contribution of blazars to this flux increases up to 50%.

On the other side in [9] the correlations between the track-like events above 200 TeV (with a typical angular resolution of 1°) and a sub-class of blazars, namely the BL Lacs, have been

[3] The event topology is discussed in chapter 4.

analyzed. No evidence of correlations has been found. Therefore the BL Lacs are not the main emitters of cosmic neutrinos above 200 TeV, with a significance of 3.7σ.

2.2.4 Starburst galaxy

The starburst galaxies are a subset of star forming galaxies (SFGs) that undergo an episode of vigorous star formation in their central regions. The gas density is much higher than what is observed in quiescent galaxies and for this reason the pp interaction is a plausible mechanism to produce high energy neutrinos [95, 96, 97]. Diffusion in starburst galaxies might also become weaker due to strong magnetic turbulence, while advective processes might be enhanced. Since the losses by inelastic collisions and advection are nearly independent of energy, the hadronic emission of starburst is expected to follow more closely the injected CR nucleon spectrum, $E^{-\alpha}$, with $\alpha \simeq 2.15$ [95].

The nearest starburst galaxies are M82 and NGC 253, both at a distance of 3.5 Mpc. These galaxies exhibit relatively hard γ-ray spectrum in the GeV to TeV energy range, with a spectral index between 2.1 and 2.3 [98]. Due to the harder emission spectrum and a higher pion production efficiency, the starburst subset is predicted to dominate the total diffuse γ-ray emission of SFGs beyond a few GeV [97]. On the other hand, the emission from starburst galaxies is sub-dominant with respect to the γ-rays emission from BL Lacs. Provided that the CR accelerators in starburst galaxies are capable of reaching energies exceeding 20-30 PeV per nucleon, the hadronic emission can also contribute significantly to the diffuse neutrino emission at PeV energies.

It has been noticed that the flux of neutrinos measured by IceCube is too high with respect to the flux of gamma around 100 GeV and above this energy [99]. However an important aspect is that the γ-rays, produced into the starburst galaxies, are easily re-processed to low energies; therefore it is easier to observe a starburst galaxy using the infrared radiation, for example. In any case it is important to remark that, as for BL Lacs, in this type of multi-messenger approach the assumptions on the neutrino spectrum play a crucial role. In Section 6.1.3 this aspect is discussed.

2.3 COSMOGENIC NEUTRINOS

The cosmogenic neutrinos are generated by the $p\gamma$ interaction, where the photon targets consist in the cosmic microwave background radiation (CMB) [100]. In this scenario, analyzed in [101, 102, 103, 104], protons must have a huge energy to produce the so called cosmogenic neutrinos, since the energy of the CMB is of the order of 10^{-3} eV.

According to the photo-hadron decay scheme, described in section 1.4, neutrinos are produced with $\sim$ 5% of energy with respect to the energy of the primary protons. The resulting ultra-high-energy neutrinos escape from the interaction zone. If the interaction happens between accelerated protons and the lowest energy part of the CMB spectrum, the corresponding neutrinos are very energetic, in the range of EeV, i.e. $10^{3 \div 4}$ PeV. The interaction can occur also between protons and the most energetic part of the cosmic background, i.e. the EBL; in this scenario the secondary neutrinos have energy in the PeV region. Generally,

the energy of a proton, required to create a pion plus a baryon (proton or neutron) in the $p\gamma$ interaction, is given by:

$$E_p^{\min} = \frac{m_\Delta^2 - m_p^2}{4E_\gamma} \tag{16}$$

where E_γ is the energy of the target photons, m_Δ and m_p are the masses of the baryon Δ and the proton, respectively.

The expected flux of cosmogenic neutrinos strongly depends on the cosmic-ray composition and cosmological source evolution; this is the reason because different models differ greatly in their neutrinos flux prediction. To have an estimation of the order of magnitude, a neutrino flux of

$$E^2 \frac{d\phi}{dE} \sim 5 \times 10^{-9} \text{ GeV cm}^{-2} \text{ s}^{-1} \text{ sr}^{-1}$$

is expected around EeV energy, as we can see in the Fig.10. Up to now the cosmogenic neutrinos have not been detected and this fact helps to constraint many theoretical models. The most stringent experimental limit has been placed by the ANITA experiment [105], although the IceCube and Auger experiments are more sensible than ANITA below 10 EeV. There are also other future neutrino telescopes, particularly the Askaryan Radio Array (ARA) [106], that have as a main goal the detection of these ultra high energy neutrinos.

It is important to clarify the meaning of the "non detection"of cosmogenic neutrinos, because IceCube has detected 3 events with deposited energy above 1 PeV, that could be cosmogenic neutrinos at a first glance. Indeed one could think that these events come from neutrinos produced by the interaction of accelerated protons with the EBL background. However, this is not so: the PeV events cannot be attributed to the cosmogenic neutrinos, because this would imply many more higher-energy neutrinos that should have been detected, but were not, as discussed in [107].

Summarizing this chapter, we can say that nowadays there are many ideas for the sources of high energy neutrinos, even if (as we will discuss in chapter 6 and 7) it is not clear whether any of them, alone, is sufficient to explain the entire signal detected by IceCube. There are, instead, several bounds for many sources described in this chapter. More data and experiments are necessary to clarify the situation.

3 PROPAGATION OF COSMIC NEUTRINOS

One of the most important properties of neutrinos is that they weakly interact with the matter. In this way they retain information on the source. This is a special property since other particles are re-processed during their path (γ-rays and protons for example). For this reason neutrinos can be used as "probe particles". On the other hand the small cross section of neutrinos makes their detection hard, as we will see in the following. In this chapter we discuss the neutrino propagation, describing neutrino oscillations and examining the neutrino decay scenario.

This chapter is based on two original works published during the Phd [1, 2].

3.1 NEUTRINO OSCILLATIONS

In 1957 Bruno Pontecorvo [108] hypothesized that mass eigenstates and flavor eigenstates do not coincide for neutrinos. Therefore, since a certain neutrino of flavor ℓ, that we denote as ν_ℓ, is a superposition of mass eigenstates, the oscillation between different flavor eigenstates occurs during the propagation. In 1962 Maki, Nakagawa and Sakata [109] introduced the matrix, that is known as PMNS matrix, to explain the neutrino oscillations predicted by Bruno Pontecorvo. An exhaustive treatment of this argument can be found in these two reviews on neutrino physics [110, 111].

The probability of oscillations of neutrinos in vacuum, from a ν_ℓ to a $\nu_{\ell'}$, is given by:

$$P_{\ell\ell'} = |\sum_{i=1}^{3} U_{\ell' i}\, e^{iE_i t}\, U^*_{\ell i}|^2 \quad \text{with } \ell = e, \mu, \tau \tag{17}$$

in which the $U_{\ell i}$ are the elements of the Pontecorvo matrix [112]. The phase term

$$\phi_{ij} = \Delta m^2_{ij} \frac{L}{4E}$$

that is obtained from the previous expression developing the calculation, is relevant for the oscillation of atmospheric neutrinos whereas for cosmic neutrinos, i.e. TeV neutrinos and distance greater than some parsec, the phase term is so high that only the average value makes sense. In order to have an idea of it, let us recall a useful numerical expression for the phase term:

$$\phi_{ij} = 1.27 \, \frac{\Delta m^2_{ij}}{\mathrm{eV}^2} \, \frac{\mathrm{L}}{\mathrm{m}} \, \frac{\mathrm{GeV}}{\mathrm{E}}$$

For neutrinos produced at a distance of 100 Mpc and with 1 TeV of energy the phase term is equal to 1 for $\Delta m^2 \sim 10^{-16}$ eV^2. On the contrary we know that the present values of Δm^2 are much greater, i.e.:

$$\Delta m^2_{21} \quad = \quad 7.5 \times 10^{-5} \text{ eV}^2$$

$$\Delta m^2_{3\ell} \quad = \quad 2.5 \times 10^{-3}\ \mathrm{eV}^2 \tag{18}$$

where $\Delta m^2_{3\ell} = \Delta m^2_{31} > 0$ for Normal Hierarchy (NH) and $\Delta m^2_{3\ell} = \Delta m^2_{32} < 0$ for Inverted Hierarchy (IH) [113].

Therefore the probability of oscillations of cosmic neutrinos in vacuum over large distances, from a ν_ℓ to a $\nu_{\ell'}$, is given by the following phase averaged expression:

$$P_{\ell\ell'} = \sum_{i=1}^{3} |U^2_{\ell i}||U^2_{\ell' i}| \text{ with } \ell = e, \mu, \tau \tag{19}$$

3.1.1 The natural parametrization

Since this work is focused on high energy cosmic neutrinos it is convenient to use a special description for neutrino oscillations. We will use the approach proposed in [1] that is specialized for our case. We refer to it as "natural parametrization". This is a method that has the advantage to permit the computation of neutrino oscillation probabilities and their uncertainties with analytical formulas, without a Montecarlo simulation. Moreover, it is sufficiently accurate for the present purposes, as largely discussed in [1].

We begin by counting the number of independent vacuum oscillation parameters [112]

$$P_{\ell\ell'} = \sum_{i=1}^{n} |U^2_{\ell i}||U^2_{\ell' i}| \text{ where } \ell = e, \mu, \tau \tag{20}$$

in the case of n light neutrinos.

The vacuum oscillation formula depends upon the squares of the leptonic mixing matrix $|U^2_{\ell i}|$. They correspond to $(n-1)^2$ independent parameters, as it is clear considering all $|U^2_{\ell i}|$ as independent (albeit constrained) parameters except the ones of the first row and column, that can be obtained from unitarity, e.g., $|U^2_{\mu 1}| = 1 - \sum_{i=2}^{n} |U^2_{\mu i}|$.

But the vacuum oscillation probabilities $P_{\ell\ell'}$ are also *symmetric* in the exchange of the flavor indices $\ell \leftrightarrow \ell'$, thus they require less parameters. Since we can again rely on similar unitarity relations when we sum on all flavors, namely $\sum_\ell P_{\ell\ell'} = 1$, this implies that the number of independent parameter is just $n(n-1)/2$. This means that when $n = 3$ we have 3 independent parameters, when $n = 4$ we have 6 of them, etc.

From here on and in view of the present experimental situation, we focus on the three flavor case ($n = 3$) where we have three parameters, as first remarked (to the best of our knowledge) in ref. [114].

Next, we motivate and introduce the choice of the three natural parameters. The parameters P_0, P_1, P_2 are defined as follow:

$$P_0 = \frac{P_{ee} - \frac{1}{3}}{2}\ ,\ P_1 = \frac{P_{e\mu} - P_{e\tau}}{2}\ ,\ P_2 = \frac{P_{\mu\mu} + P_{\tau\tau} - 2P_{\mu\tau}}{4} \tag{21}$$

We would like to give our reasons (that are largely based on the available experimental informations) why we consider that Eq. 21 is the optimal choice of parameters:

1. the oscillation probability that is singled out in P_0 is P_{ee}, that is well-known (being directly measured by low energy solar neutrino experiments and probed also by reactor and high energy solar neutrino experiments);

Table 4: *Table of present values and errors of the natural parameters [1].*

Parameter	Mean value	Standard deviation
P_0	0.109	0.005
P_1	0.000	0.029
P_2	0.010	0.007

2. the difference of $P_{e\mu} - P_{e\tau}$ contains most of the uncertainties;

3. the last combination of oscillations probabilities, P_2, is positive and very small;

4. a specific choice of the overall coefficients is adopted in order to have coefficients that are either zero or close to 1 in the expressions of all oscillation probabilities, Eq. 22;

5. setting $P_0 = P_1 = P_2 = 0$, all oscillation probabilities become $P_{\ell\ell'} = 1/3$, namely, any information on the original flavor is lost: the three parameters describe the potentially measurable information on flavor that survives cosmic neutrino oscillations.

The above argument clarifies that it is possible to introduce such a parameterization directly, without the need to associate it to a specific scheme of approximation of the mixing matrix, but rather, keeping it exact.

We can write in terms of P_0, P_1, P_2 the matrix that contains the probabilities of oscillations of cosmic neutrinos. This is the following symmetric matrix:

$$\mathcal{P} = \begin{pmatrix} \frac{1}{3} + 2P_0 & \frac{1}{3} - P_0 + P_1 & \frac{1}{3} - P_0 - P_1 \\ & \frac{1}{3} + \frac{P_0}{2} - P_1 + P_2 & \frac{1}{3} + \frac{P_0}{2} - P_2 \\ & & \frac{1}{3} + \frac{P_0}{2} + P_1 + P_2 \end{pmatrix} \tag{22}$$

It acts on the vector of fluxes before oscillations $\phi^0 = (\phi_e^0, \phi_\mu^0, \phi_\tau^0)$ just as

$$\phi = \mathcal{P}\, \phi^0 \tag{23}$$

giving the vector of fluxes observed after oscillations, $\phi = (\phi_e, \phi_\mu, \phi_\tau)$.

3.1.2 Connection with the standard parameters of neutrino mixing

Compact and useful expressions of the natural parameters in terms of four standard parameters [20], the mixing angles $\theta_{12}, \theta_{23}, \theta_{13}$ and CP violation phase δ, are as follows:

$$\begin{aligned} P_0 &= \frac{1}{2}\left\{(1-\epsilon)^2\left[1 - \frac{\sin^2 2\theta_{12}}{2}\right] + \epsilon^2 - \frac{1}{3}\right\} \\ P_1 &= \frac{1-\epsilon}{2}\left\{\gamma \cos 2\theta_{12} + \beta\frac{1-3\epsilon}{2}\right\} \\ P_2 &= \frac{1}{2}\left\{\gamma^2 + \frac{3}{4}\beta^2(1-\epsilon)^2\right\} \end{aligned} \tag{24}$$

where we introduce for convenience the following 4 small parameters:

$$\begin{aligned} \epsilon &= \sin^2\theta_{13} \quad & \alpha &= \sin\theta_{13}\cos\delta\sin 2\theta_{12}\sin 2\theta_{23} \\ \beta &= \cos 2\theta_{23} \quad & \gamma &= \alpha - \tfrac{\beta}{2}\cos 2\theta_{12}(1+\epsilon) \end{aligned} \tag{25}$$

These expressions are exact. Note property 3 listed in Sect. 3.1.1 of this parameterization.

The parameters α, β, γ are small and to date not known precisely, whereas ϵ is very small and precisely known. We can then order these parameters according to their (presumed) size, and consider $\sin^2 2\theta_{12}$ as zeroth order; $\sin\theta_{13}$, $\cos 2\theta_{23}$, α, β, γ of first order; ϵ of second order. In the same sense, P_0 is a zeroth-order parameter; P_1 is first order in α and β; P_2 is second order in α and β. Note that P_2 is bound to be positive.

Using the present knowledge of mixing angles and CP violating phase [113], we obtain the values and the errors of the natural parameters. We show the results in the Table 4, assuming normal mass hierarchy. It is easy to repeat the same steps with inverted hierarchy, but the differences are not large. From this Table we notice that with present data the average values obey $\langle P_0\rangle \gg \langle P_1\rangle \simeq \langle P_2\rangle$ whereas their variances obey $\delta P_1 \gg \delta P_0 \simeq \delta P_2$. P_0 is well known, because is related to survival probability of solar low energy neutrinos and θ_{13}, or ϵ, is well measured by reactor experiments. As we see from figure of [1], P_0 and P_1 are well represented by Gaussian functions; P_2 is not Gaussian but it is a very small parameter. For these reasons, as we argue from here on, we can use a Gaussian approximation without introducing severe inaccuracies in the numerical analysis of the oscillations. This is a new result, that allows one to obtain convenient analytical expressions for different examined quantities and to quantify easily the uncertainties.

The probabilities of oscillation given in Eq. 22 have a very simple form: they depend linearly upon the natural parameters. Moreover, in first approximation, they could be expressed only in terms of P_0, because P_1 and P_2 give small corrections. Using the value of Table 4 and the natural parameterization of oscillation matrix, we obtain the probabilities of oscillations:

$$\begin{aligned} P_{ee} &= 0.552 \pm 0.010, \quad & P_{e\mu} &= P_{e\tau} = 0.224 \pm 0.029 \\ P_{\mu\tau} &= 0.378 \pm 0.008, \quad & P_{\mu\mu} &= P_{\tau\tau} = 0.398 \pm 0.029 \end{aligned} \tag{26}$$

Two couples of probabilities have (almost) the same values, because with the present best fit value $\langle P_1\rangle = 0$ and the numerical differences between these expressions are small.

3.1.3 Flavor composition at Earth

We denote the fractions of ν_ℓ at source and the one at Earth (i.e., after oscillations) respectively as:

$$\xi^0_\ell = \phi^0_\ell / \sum_\ell \phi^0_\ell \text{ and } \xi_\ell = \phi_\ell / \sum_\ell \phi_\ell$$

where of course $\sum_\ell \phi^0_\ell = \sum_\ell \phi_\ell$.

In the first chapter we have seen that in the standard mechanisms of production of cosmic neutrinos no ν_τ are produced. Therefore we can write a general flavor composition at the source in this manner:

$$(\xi^0_e : \xi^0_\mu : \xi^0_\tau) = (1-g : g : 0) \quad \text{with } 0 \le g \le 1$$

Using Eq.23 we found that after propagation the flavor composition is modified as follows:

$$\xi_e = \frac{1}{3} + (2-3g)P_0 + g\ P_1 \quad (27)$$

$$\xi_\mu = \frac{1}{3} + \frac{1}{2}(-2+3g)P_0 + (1-2g)P_1 + g\ P_2 \quad (28)$$

$$\xi_\tau = \frac{1}{3} + \frac{1}{2}(-2+3g)P_0 + (-1+g)P_1 - g\ P_2 \quad (29)$$

These equations show the power of the natural parametrization. Indeed it is possible to directly compute the flavor composition after the oscillations and its uncertainty, with simple analytical expressions.

If we want to consider realistic scenario of neutrino production we can recall the Tab.3, in which different mechanisms are reported. They can be obtained from the previous equations using:

- $g = \frac{2}{3}$ for pions decay;
- $g = 1$ for damped muons;
- $g = 0$ for neutrons decay

The flavor fraction ξ_e, ξ_μ and ξ_τ relative to these mechanisms of production are illustrated in Fig.12, with pions decay in orange, damped muons in red and neutrons decay in green.

For precision, it is important to recall that these flavor compositions at the source are approximate. The correct flavor composition is always related to the assumption on the neutrino spectrum, as discussed in chapter 1. In the case of pp interaction and power law spectrum of the primary protons $E^{-\alpha}$, the flavor composition at the source is a function of the spectral index α. In the case of $p\gamma$ interaction the situation is more complicate and the spectrum of target photons is relevant. Anyway, in the well accepted standard scenario of cosmic neutrinos produced by pions decay and E^{-2} spectrum, the flavor composition after oscillation $(\xi_e : \xi_\mu : \xi_\tau) = (1/3 : 1/3 : 1/3)$ is a good approximation, as it can be noted in Fig.12 looking at the orange distributions.

3.1.4 The fraction of $\bar{\nu}_e$ at Earth

Another quantity that is interesting for cosmic neutrinos is the amount of $\bar{\nu}_e$ after the oscillations. This is due to the fact that a $\bar{\nu}_e$ of 6.3 PeV can interact with an electron producing a W^- boson,

$$\bar{\nu}_e\ e^- \rightarrow W^-$$

Table 5: *Flavor composition at Earth at 90% C.L. considering the natural parametrization and three standard mechanisms of production.*

	ξ_e	ξ_μ	ξ_τ
Pions decay	0.302 - 0.365	0.323 - 0.357	0.309 - 0.344
Damped muons	0.177 - 0.272	0.350 - 0.446	0.366 - 0.390
Neutrons decay	0.535 - 0.567	0.177 - 0.272	0.177 - 0.272

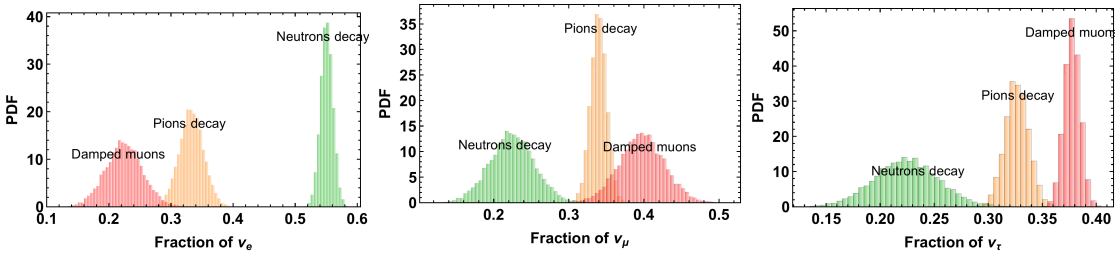

Figure 12: *Flavor fraction of ξ_e, ξ_μ and ξ_τ after oscillations, using pions decay, neutrons decay and damped muons as mechanisms of production.*

This process is called "Glashow resonance"[115] and it represents the typical signature for the $\bar{\nu}_e$. We will analyze in details this process in section 4.5.4; now we limit our analysis to the fraction of $\bar{\nu}_e$ expected in two extreme cases. Indeed, in the first chapter, we have seen that pp and $p\gamma$ mechanisms give different fractions of $\bar{\nu}_e$. Particularly, the amount of $\bar{\nu}_e$ in the pp mechanism at the source is $\sim 1/6$, whereas no $\bar{\nu}_e$ are produced in the $p\gamma$ mechanism considering the delta approximation, i.e. only the creation of the Δ^+ particle from the $p\gamma$ interaction (see Tab.3 and [1, 116, 3]).

In order to evaluate what is the amount of $\bar{\nu}_e$ after oscillations we need to know not only the fraction of $\bar{\nu}_e$ at the source but also the amount of $\bar{\nu}_\mu$. Recalling the Tab.3 we have in pp scenario:

$$\xi^0_\ell = \frac{1}{6}(1,2,0) \quad \xi^0_{\bar{\ell}} = \frac{1}{6}(1,2,0)$$

and in the delta approximation of $p\gamma$ scenario:

$$\xi^0_\ell = \frac{1}{6}(2,2,0) \quad \xi^0_{\bar{\ell}} = \frac{1}{6}(0,2,0)$$

Using the natural parametrization the fractions of electron antineutrinos at Earth are given by linear expression in the parameters P_0 and P_1:

$$\xi^{pp}_{\bar{\nu}_e} = \frac{1}{6} + \frac{1}{3}P_1 \tag{30}$$

$$\xi^{p\gamma}_{\bar{\nu}_e} = \frac{1-3\,P_0}{9} + \frac{1}{3}P_1 \tag{31}$$

The numerical values for these two scenarios at 3σ C.L. are:

$$\xi^{pp}_{\bar{\nu}_e} = 0.167 \pm 0.029$$
$$\xi^{p\gamma}_{\bar{\nu}_e} = 0.075 \pm 0.029$$

where the uncertainty is due to P_1. Note that we are using recent measurements of the oscillation parameters [113] and in particular we have included the effect of θ_{13}, which is now measured and known to be non-zero.

This result implies that, if we know the total flux of neutrinos, we expect about the double of Glashow resonance events in the case of pp interaction with respect to the $p\gamma$ scenario. Anyway in realistic scenarios the discrimination can be more difficult compared to this idealized case. In fact, as remarked in Sec.1.4.2, in the $p\gamma$ interaction it is possible to have a certain contribution of π^- and therefore of $\bar{\nu}_e$ [23, 25]. In some cases the differences between pp and $p\gamma$ scenarios is much less than a factor 2, making these scenarios not distinguishable from an experimental point of view [5].

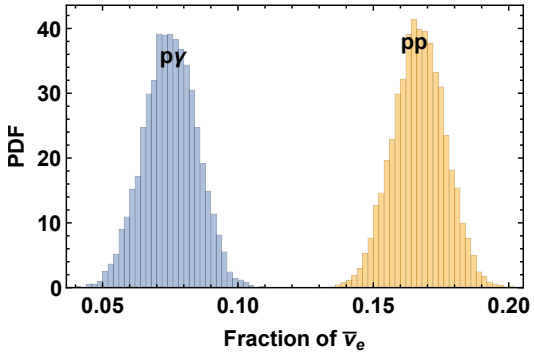

Figure 13: *Fraction of ν_e due to the pp or the $p\gamma$ interaction obtained using the natural parametrization, in an idealized situation [1].*

3.2 NEUTRINO DECAY

In this section we analyze an exotic scenario that could occur during the propagation of neutrinos into the universe, i.e. the neutrino decay. It was first discussed in [117, 118] in 1972.

We consider non-radiative decay processes of the kind $\nu_i \to \nu_j + X$, where ν_i and ν_j indicate neutrino (or antineutrino) mass eigenstates with masses $m_i \geq m_j$, while X represents one (or more) invisible particle in the final state. For a source of (relativistic) neutrinos at a distance L, the ν_i-component of the flux is depleted due to decay by the factor:

$$D_i\,(L,\,E) = \exp\left(-\frac{L}{E} \times \frac{m_i}{\tau_i}\right) \tag{32}$$

where E is the neutrino energy and τ_i is the i-th neutrino lifetime. As a consequence, the sensitivity to the unknown ratios τ_i/m_i is essentially determined by neutrino energy and baseline, being L/E the critical parameter.

The most favorable combination is provided by the SN1987A ($L = 50\,\text{kpc}$, $E \sim 20\,\text{MeV}$); the observation of electron antineutrinos in Kamiokande-II and IMB permits to exclude that the states ν_1 and ν_2 (which have a non negligible ν_e component) decay to ν_3 (or to a sterile state) yielding the lower limit $\tau/m \gtrsim 10^5\,\text{s/eV}$ [119, 120]. Note that, in the absence of sterile neutrinos, this limit only applies to scenarios in which both ν_1 and ν_2 decays to ν_3, thus requiring an inverted mass hierarchy $m_3 \leq m_1 \leq m_2$.

Other bounds are less stringent. As an example, the strongest model-independent limits on ν_2 non-radiative decay are obtained from solar neutrinos for which $E \sim$ few MeV and $L = 1.5 \times 10^8\,\text{km}$ and are at the level of $\tau_2/m_2 \gtrsim 10^{-4}\,\text{s/eV}$ [121, 122]. For decay modes involving the appearance of electron antineutrinos, a more stringent limit $\tau_2/m_2 > 1.1 \cdot 10^{-3}$ s/eV is given by the non-observation of solar $\overline{\nu}_e$ in Kamland [123]. The ν_3 lifetime can be bounded by atmospheric and long-baseline neutrino data, obtaining $\tau_3/m_3 \gtrsim 10^{-10}$ s/eV [124]. These different situations are reported in Tab.6.

As it was suggested, e.g. by [125], independent and highly competitive limits can be obtained by the observation of high energy cosmic neutrinos in neutrino telescopes. If we consider $E \sim 100\,\text{TeV}$ and $L \sim 1\,\text{Gpc}$ as representative values for the energy and the distance travelled by (extragalactic) cosmic neutrinos (see also Tab.6), we obtain $L/E \sim 10^3\,\text{s/eV}$. We thus understand that the present observations of solar, atmospheric and long baseline neutrinos

Table 6: *Table of τ/m that can be tested with different sources of neutrinos at different distances.*

	SN1987A	Cosmic	Sun	Atmospheric
L (cm)	1.5×10^{23}	3×10^{27}	1.5×10^{13}	6.4×10^{8}
E (eV)	2×10^{7}	10^{14}	5×10^{6}	10^{9}
τ/m (sec/eV)	$\geq 2 \times 10^{5}$	$\geq 10^{3}$	$\geq 10^{-4}$	$\gtrsim 10^{-10}$

do not exclude the possibility that cosmic neutrinos decay. Even the SN1987A bound, that numerically corresponds to larger values $\tau/m \gtrsim 10^5\,\mathrm{s/eV}$, only applies to specific scenarios in which both ν_1 and ν_2 decay into ν_3 or to an additional (mainly sterile) mass eigenstate. To maximize the effect of neutrino decay, we consider a *Complete Decay Scenario* for cosmic neutrinos.

The complete decay scenario can be investigated with cosmic neutrinos thanks to the flavor composition, because in the case of neutrino decay the flavor composition dramatically changes with respect to the standard scenarios analyzed before. In particular, in the assumption that only one stable state exists, the flavor ratios at Earth of decaying neutrinos are only determined by the neutrino mixing matrix and they does not depend upon the production mechanism and the decay kinematics. Indeed, only one mass eigenstate survives in the complete decay scenario, giving the following flavor composition:

$$\xi_\ell = |U_{\ell j}|^2 \,. \tag{33}$$

where $U_{\ell j}$ are the elements of the Pontecorvo mixing matrix.

If we assume normal mass hierarchy, the stable eigenstate is necessarily ν_1, namely $j = 1$, since $m_1 < m_2 < m_3$. In this case the expected flavor ratios at Earth are

$$(|U_{e1}|^2 : |U_{\mu 1}|^2 : |U_{\tau 1}|^2) \sim (0.68 : 0.21 : 0.11)$$

For inverted mass hierarchy, the lightest and stable state is ν_3, namely $j = 3$, and the final flavor ratios are expected to be

$$(|U_{e3}|^2 : |U_{\mu 3}|^2 : |U_{\tau 3}|^2) \sim (0.02 : 0.57 : 0.41)$$

In both cases, the central values of the predicted flavor fractions are outside the ranges expected for stable neutrinos, that are reported in Tab.5.

In order to understand the "state of the art" in chapter 5 we will show how to connect the expected flavor composition to an experimental observable quantity. Moreover we will compare these expectations with the new measurements provided by IceCube, referring to the recent papers [2, 126].

4 DETECTION

In this chapter we discuss the characteristics of the neutrino telescopes, focusing on IceCube, ANTARES and KM3NeT. We describe the deep inelastic scattering, that is the main process that makes possible the high energy neutrino detection. Moreover we discuss what is the response of the detector to each flavor of neutrino, focusing on the two main topologies of events: tracks and showers. We also discuss the response of the detector to the Glashow resonance (a process involving electron antineutrinos) and to the double pulses (a process involving tau neutrinos). The informations reported in this chapter are necessary to understand Chapter 5 and Chapter 6, where the interpretation of the observed data will be given.

Part of this chapter is based on an original work published during the Phd [3].

4.1 THE NEUTRINO TELESCOPES

The idea to observe high energy neutrinos was first discussed in 1961 by Markov and Zheleznykh [127]. The first neutrino telescopes were liquid or plastic scintillators, culminated in the modern Cherenkov telescopes. Although details vary from experiment to experiment, modern high-energy neutrino telescopes consist of strings of photo-multiplier tubes (PMT) distributed throughout a natural Cherenkov medium such as water or ice. Typical spacing of PMT is 10-20 meters along a string with string spacing of 30-100 meters [128]. Such experiments can observe neutrinos of different flavors, over a wide range of energies, by looking at the Cherenkov light produced by the secondary particles. These particles come from the deep inelastic scattering between high energy neutrinos and the nucleons contained into ice or water. We discuss the deep inelastic scattering in Section 4.3.

There are two methods to detect high energy neutrinos:

- historically the first one uses the so called throughgoing muons, i.e. the induced muons produced by the charge current interaction of a ν_μ outside the detector. This method provides us with a good angular resolution, corresponding to about 1° [129] in ice and about $[0.1^\circ - 0.3^\circ]$ in water [130, 131]. On the other side the energy is reconstructed with a large uncertainty of about a factor 2 [132], due to the fact that only a fraction of the muon's path can be detected;
- the second method, adopted by the IceCube experiment for the first discovery of a diffuse flux of high energy neutrinos [133], uses events with the vertex of interaction contained into the detector. For this reason these events are called High Energy Starting Events (HESE). This method is sensitive not only to ν_μ but also to ν_e and ν_τ, that produce showers (both electromagnetic and hadronic) into the detector. The showers provides worse angular resolution than tracks, of the order of $10^\circ - 15^\circ$ in ice [133] and some degrees in water [131]. On the contrary the energy is well reconstructed in this case, with an uncertainty of about 15% (see Appendix D.2).

Nowadays several Cherenkov neutrino telescopes are operating in the world:

1. IceCube, a km^3 detector located in the South Pole that uses the ice as target for high energy neutrinos [133];
2. ANTARES, with a volume of 0.03 km^3 located in France, that uses the water as target [134];
3. Baikal, a 1.5 km^3 neutrino detector conducting research in Lake Baikal (Russia) [135];
4. KM3NeT, that will have a volume of about 1 km^3 and it uses the water as target for high energy neutrinos. It is located in Sicily (Italy) but at the moment it is operating with few strings. It is expected to work with the full configuration in 2020 [131].

Why a km^3 detector is required to observe high energy neutrinos ? Let us consider the events contained into the detector. The expected number of events depends upon the fluence of high energy neutrinos F_ν, the number of target N and the cross section of deep inelastic scattering σ_{DIS}.

- Considering Waxman and Bahcall [12] (see Sec.6.1.3), the upper bound of the high energy neutrino flux (all flavor) was expected to be order of:

$$\frac{d\phi^{\text{WB}}}{dE} \simeq 5 \times 10^{-8} \frac{1}{\text{GeV cm}^2 \text{ sec sr}} \left(\frac{E}{1 \text{ GeV}} \right)^{-2}$$

  Therefore, the fluence in 1 year is obtained by the following integral:

$$\mathcal{F}_\nu \simeq \int_{E_{min}}^{E_{max}} 4\pi \times \frac{d\phi^{\text{WB}}}{dE} \times \pi \cdot 10^7 \, dE$$

  If we consider $E_{min} = 100$ TeV and $E_{max} = \infty$, the fluence is equal to:

$$\mathcal{F}_\nu \simeq 2 \times 10^{-4} \frac{\nu}{\text{cm}^2 \text{ year}}$$

- the cross section of deep inelastic scattering at 100 TeV is order of [136, 137]:

$$\sigma_{\text{DIS}} = 10^{-34} \text{cm}^2$$

- the number of target is given by

$$N(V) = \frac{\rho \, V}{m_N} = 6 \times 10^{38} \frac{V}{\text{km}^3}$$

  where ρ is the density of the detector's target; let us consider $\rho = 1$ g/cm^3 that is exact for water and it is a good approximation for ice. m_N is the nucleon's mass and it is equal to $\frac{1}{m_N} \simeq 6 \times 10^{23}$ g^{-1}. V is the volume of the detector and it is our free parameter.

Therefore the expected number of events above 100 TeV per year is expected to be:

$$\mathcal{F} \times \sigma_{\text{DIS}} \times N(V) \simeq 10 \, \frac{\text{events}}{\text{year}} \, \frac{\text{V}}{\text{km}^3}$$

This is a rough and optimistic calculation (let us remember that we are using an upper bound on the high energy neutrinos flux). It is useful to have an idea of the volume required to observe high energy neutrinos. In the following of this chapter we provide more precise elements to understand the physics involved in neutrino telescopes, in order to calculate the expected number of neutrino events accurately.

4.2 CHARACTERISTICS OF THE ICECUBE DETECTOR

In this section we describe the main characteristics of the IceCube detector, since Chapters 5 and 6 will be dedicated to the interpretation of the events detected by IceCube up to now.

As we have seen in the previous section, because of the small neutrino cross sections, a very large detector is required to observe astrophysical neutrinos [138]. At the same time the flavor identification is relevant, since the background from atmospheric neutrinos is much lower for ν_e and ν_τ than for ν_μ. Recall that the angular resolution is also very important for detecting point sources and energy resolution is important in determining neutrino energy spectra, which is important for identifying a diffuse flux of extraterrestrial neutrinos.

In this section we describe the main features of IceCube, a km^3 telescope placed in the South Pole. It detects neutrinos by observing the Cherenkov radiation from the charged particles produced by neutrino interactions.[1] The detector consists of 5160 digital optical modules (DOMs), 86 vertical strings, each containing 60 DOMs and it has a mass of 1 Gigaton.

ICECUBE: 80 strings, in the baseline IceCube, are placed on a 125 meter grid covering 1 km^2 on the surface. DOMs are attached to the strings every 17 m, at a depth between 1450 and 2450 m under the Antarctic ice (see Fig.14). Although the minimum energy is analysis dependent, the baseline allows to detect muon neutrinos down to energies of about 100 GeV.

DEEPCORE: Another 6 strings, called "DeepCore", are situated in a denser (72-meter) triangular grid. The DeepCore strings have 50 DOMs with 7-meter spacing at the bottom of the strings; 10 DOMs higher up serve as a veto. DeepCore extends IceCube sensitivity down by a factor of 10 in energy. The outer IceCube strings and top DOMs in DeepCore will serve to veto events originating outside of the central detector, greatly reducing the backgrounds for contained events. DeepCore uses newer PMTs, with higher quantum efficiency than the IceCube standard. The denser spacing and more efficient PMTs give DeepCore a lower threshold than IceCube, around 10 GeV.

ICETOP: In addition to the DOMs buried in ice, the IceCube Observatory includes a surface air shower array known as IceTop. IceTop consists of 160 ice filled tanks, each instrumented with two IceCube DOMs. The purpose of IceTop is to detect cosmic-ray air showers, with a threshold of about 300 TeV, in order to study the cosmic-ray flux and composition; the combination of air shower array data and TeV muon fluxes (observed by IceCube) provides significant handles on the cosmic ray composition. IceTop also serves several calibration functions for IceCube. IceTop can also be used to veto high-energy cosmic ray air showers in IceCube; conversely, one can search for muon free showers from PeV photons.

In the following of the work we will refer to IceCube, in its complete configuartion, as IC86.

4.3 DEEP INELASTIC SCATTERING

Neutrinos collide with nucleons contained into the ice or into the water mainly via deep inelastic scattering (DIS). This process happens with the exchange of a $W^\pm$ (Charge Current, CC) or a Z^0 boson (Neutral Current, NC). The cross section of this interactions is very small and a detailed

[1] We will investigate in detail the processes and the effective areas in the next section.

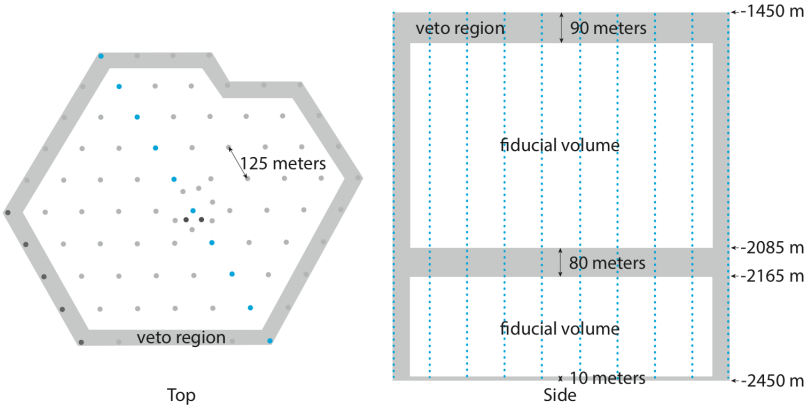

Figure 14: *Drawing of the IceCube array [133]. The side view (right) shows a cross-section of the detector indicated in the top view (left) in blue. Events producing first light in the veto region (shaded area) were discarded as entering tracks (usually from cosmic ray muons entering the detector). Most background events are nearly vertical, requiring a thick veto cap at the top of the detector. The shaded region in the middle contains ice of high dust concentration. Because of the high degree of light absorption in this region, near horizontal events could have entered here without being tagged at the sides of the detector without a dedicated tagging region.*

treatment of the processes can be found in [136, 137]. Here we provide a brief discussion of the deep inelastic scattering. Let us consider the charge current (CC) process:

$$\nu_\ell \, N \to \ell^- + \text{ anything}$$

where N is the nucleon. The differential cross section is written in terms of the Bjorken scaling variables

$$x = \frac{Q^2}{2m_N \nu} \tag{34}$$

$$y = \frac{\nu}{E_\nu} \tag{35}$$

as

$$\frac{d^2\sigma}{dxdy} = \frac{2G_F^2 m_N E_\nu}{\pi} \left(\frac{M_W^2}{Q^2 + M_W^2} \right)^2 \left[xq(x, Q^2) + x\bar{q}(x, Q^2)(1-y)^2 \right] \tag{36}$$

where $-Q^2$ is the invariant momentum transfer between the incident neutrino and outgoing muon, $\nu = E_\nu - E_\ell$ is the energy loss in the laboratory (target) frame, m_N and m_W are the nucleon and intermediate-boson masses and $G_F = 1.16632 \times 10^{-5}$ GeV^{-2} is the Fermi constant. The functions $q(x, Q^2)$ and $\bar{q}(x, Q^2)$ are the quark distribution functions (see [137] for the details). Let us define also the variable

$$S = (P_\nu + P_N)^2 \simeq 2E_\nu m_N$$

when $E_\nu \gg m_N$.

Table 7: *Charged-current and neutral-current cross sections and their sum for $\nu_\mu N$ interactions according to the CTEQ4DIS distributions [137].*

E_ν [eV]	$\sigma_{CC}[cm^2]$	$\sigma_{NC}[cm^2]$	$\sigma_{DIS}[cm^2]$
10^{12}	0.6399×10^{-35}	0.2039×10^{-35}	0.8438×10^{-35}
10^{13}	0.4617×10^{-34}	0.1575×10^{-34}	0.6192×10^{-34}
10^{14}	0.2022×10^{-33}	0.7667×10^{-34}	0.2789×10^{-33}
10^{15}	0.6342×10^{-33}	0.2600×10^{-33}	0.8942×10^{-33}
10^{16}	0.1749×10^{-32}	0.7482×10^{-33}	0.2497×10^{-32}

Table 8: *Charged-current and neutral-current cross sections and their sum for $\bar{\nu}_\mu N$ interactions according to the CTEQ4DIS distributions [137].*

E_ν [eV]	$\sigma_{CC}[cm^2]$	$\sigma_{NC}[cm^2]$	$\sigma_{DIS}[cm^2]$
10^{12}	0.3542×10^{-35}	0.1243×10^{-35}	0.4785×10^{-35}
10^{13}	0.3008×10^{-34}	0.1091×10^{-34}	0.4099×10^{-34}
10^{14}	0.1683×10^{-33}	0.6515×10^{-34}	0.2334×10^{-33}
10^{15}	0.6051×10^{-33}	0.2493×10^{-33}	0.8544×10^{-33}
10^{16}	0.1734×10^{-32}	0.7423×10^{-33}	0.2476×10^{-32}

From Eq.34 we have $Q^2 = 2m_N\ x\ \nu$, therefore (using Eq.35) it is possible to write Q as

$$Q^2 = S\ x\ y$$

In first approximation $x \simeq 1/3$, whereas $y \simeq 1/2$ at TeV energy [136, 137]. It is interesting to evaluate at which energy Q^2 becomes comparable with m_W^2. Using the previous approximations we found:

$$2m_N\ E_\nu \frac{1}{6} \simeq m_W^2 \rightarrow E_\nu \simeq 20\ \text{TeV}$$

This implies that in the region $E_\nu \ll 20$ TeV the cross section of deep inelastic scattering increases linearly with the energy. On the contrary, above some tens of TeV, the effect of the propagator becomes relevant and the behavior of the cross section changes.

A similar procedure can be used to calculate the cross section for neutral current (NC) interaction and the details are reported in [136, 137]. Therefore also the behavior of the NC cross section is similar, i.e. it increases linearly below tens of TeV and then the effect of the propagator becomes important. The NC cross section is about 3 times smaller than the CC cross section between 10 TeV and 10 PeV, that is the relevant energy window for high energy neutrinos, as it can be noticed in Tab.7 and Tab.8.

From the same tables we also notice that the difference between the CC cross sections of neutrino and antineutrino is small around 100 TeV (about 15%) and it becomes even smaller (few %) at PeV energies.

Therefore we can provide a useful parametrization of the total cross section of deep inelastic scattering (CC+NC) that works well for energies from 100 TeV to some PeV, where the difference

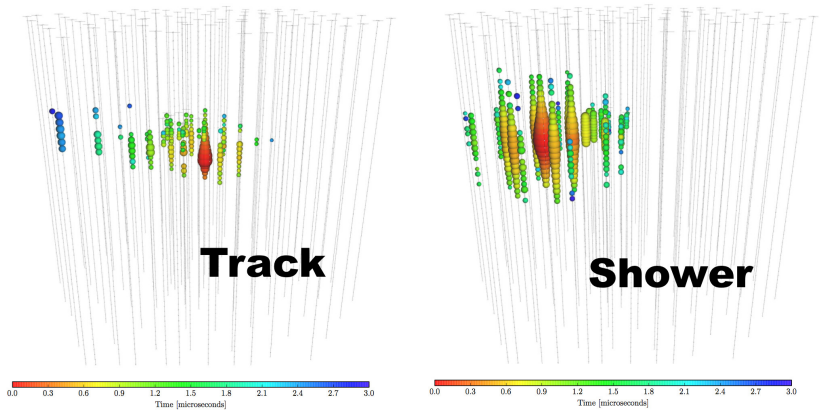

Figure 15: *Representation of a track (left panel) and of a shower (right panel) in IceCube. Figure from [133].*

between the cross section of ν and $\bar{\nu}$ is negligible. The approximation is given by the following formula:

$$\sigma_{\text{DIS}}(E_\nu) = 0.9 \left(\frac{E_\nu}{\text{PeV}}\right)^{0.45} \times 10^{-33}\ \text{cm}^2 \tag{37}$$

4.4 NEUTRAL CURRENT AND CHARGED CURRENT INTERACTIONS

Neutrinos interact via charged current (CC) and neutral current interaction (NC) with the nucleons contained into the ice (IceCube) or into the water (ANTARES and KM3NeT). Let us discuss these processes for each flavor of neutrino.

4.4.1 Neutral current interaction

In neutral current interaction a neutrino transfers a fraction of its energy to a nuclear target producing just a *hadronic shower*. All neutrinos show the same behavior when they interact via NC; therefore it is not possible to distinguish the flavor composition looking at this process. Moreover it is not possible to distinguish this shower from an electromagnetic shower that can be produced in charge current processes, as we will see in the following of this section. The average deposited energy in NC interactions is about $1/4$ of the primary neutrino's energy, whereas the other part of the energy is carried away by the outgoing neutrino and it is not detectable.

The shower like events, that occur in NC interaction, are characterized by a "blob" that extends for few strings (see the right panel of Fig. 15) and by a poor angular resolution, of the order of 10° in ice and about a factor 5 better in water.

4.4.2 Charged current interaction

ELECTRON NEUTRINOS:

$$\nu_e + N \to e^- + \text{hadrons}$$

In this CC interaction a charged lepton is produced, which carries about 3/4 of the incoming neutrino energy. The path of the electron is short (few meters) and the energy is released in the form of an *electromagnetic shower*. The other part of the energy is transferred to the nuclear target and it is released in the form of an hadronic shower. The two showers are not distinguishable from each others. When the vertex of interaction is contained into the detector, as it happens in IceCube for High Energy Starting Events (HESE), the charged current interaction of ν_e is a favorable case for the energy reconstruction, since almost all the energy of the primary ν_e is deposited into the detector [132].

MUON NEUTRINOS:

$$\nu_\mu \ + \ N \rightarrow \mu^- \ + \ \text{hadrons}$$

Also in this process the lepton takes about 3/4 of the neutrino's energy. Anyway the behavior of muon is different than the one of electron, because a muon with an energy of TeV can travel for some kilometers, producing a *track*. The energy loss of a muon can be described in terms of a linear function as follows:

$$\frac{dE}{dR} = -(\alpha + \beta E)$$

where the coefficient α denotes the continuous energy loss whereas the coefficient β denotes the catastrophic loss. Both α and β depend logarithmically on the energy. The path $R(E_i, E_f)$, as a function of the initial energy E_i and the final energy E_f, is obtained integrating this function:

$$R(E_i, E_f) = -\int_{E_i}^{E_f} dE \ \frac{1}{\alpha + \beta E}$$

It follows that a useful approximated expression for the muon range in water is the following one:

$$R(E_i, E_f) = \frac{1}{\beta} \times \log_{10}\left(\frac{1 + \frac{E_i}{\alpha/\beta}}{1 + \frac{E_f}{\alpha/\beta}}\right)$$

where $\frac{1}{\beta} \simeq 2.5$ km and $\alpha/\beta = 0.5$ TeV in our region of interest, i.e. between TeV and PeV energies. Therefore at PeV energies muon tracks can be up to 10 kilometers long, while, on the scale of a kilometer cube detector, showers are nearly point sources. For this reason it is not required that the vertex of interaction is contained inside the detector. On the contrary muons produced outside the detector, the so-called throughgoing muons, have been used as the first method to detect high energy neutrinos and they are still used in ANTARES and IceCube. The throughgoing muons come from the opposite hemisphere from the one where the detector is placed. As a consequence IceCube can only detect throughgoing muons that come from North.

Of course it is also possible to observe tracks generated by the interaction of a ν_μ with the vertex of interaction contained into the detector. These tracks are part of the HESE dataset, but they are less than the shower like events.

The muon tracks, above $\sim$ 100 TeV, are characterized by a good angular resolution of the order of 1° in the ice [129]. The angular resolution of tracks in water is even better and it can reach the sub-degree precision in the incoming neutrino telescope KM3NeT[131]. For this reason the track-like events are very useful for the point-source search.

TAU NEUTRINOS:

$$\nu_\tau \ + \ N \rightarrow \tau^- \ + \ \text{hadrons}$$

Also in this interaction the lepton takes about 3/4 of the neutrino's energy. Before decaying, the tau travels for

$$L = \gamma c t \simeq 50 \text{ m} \left(\frac{E_\tau}{1 \text{ PeV}} \right)$$

that is greater than the electron's path but much smaller than the muon's path. In CC interaction of ν_τ electromagnetic and hadronic showers are produced. Therefore the ν_τ CC interaction is associated to the *shower-like events*. In this case the energy deposited into the detector is a bit less with respect to the ν_e CC interaction. This is due to the fact that the τ lepton, in most cases, decays and produce neutrinos, that carry away part of the energy. In [139] it has been estimated that about 20% of the energy of τ is not detectable.

At low energy (below $\sim$ 0.5 PeV), it is impossible to distinguish showers produced by charged current (CC) interactions of ν_τ from those produced by CC interactions of ν_e and neutral current (NC) interactions of all neutrino flavors. The only way to distinguish a ν_τ is to observe a double vertex of interaction into the detector [140, 141, 142], which is produced by the CC interaction of ν_τ (1° vertex of interaction) when the τ has sufficient energy to reach another string before to decay (2° vertex of interaction). This process is called "Double bang", whereas if the double signal is seen in a single DOM, by the study of the time structure of the signal, it is called "Double pulse"[143]. We discuss these processes in detail in section 4.5.

For completeness let us notice that the decay of τ produces muons, with a branching ratio of 17% [20]. Therefore also the CC interaction of ν_τ can produce track-like events, but we have to take into account that these muons take about 1/4 of ν_τ energy whereas the muons from ν_μ CC interaction take about 3/4 of ν_μ energy. As a consequence the contribution of ν_τ to the track-like events is 5% or less, depending upon the spectrum of neutrinos, as discussed in [3].

4.5 EFFECTIVE AREAS

The response of the detector can be described by means of "effective area" that it is usually obtained with Montecarlo simulations. It is, however, important to understand the main properties of the effective area (A_{eff}) on physical basis, following physical considerations [3].

The effective areas A_ℓ allow to evaluate the expected number of events with the following general formula:

$$N_{ev} = 4\pi \ \text{T} \int_0^\infty \sum_\ell \frac{d\phi_\ell}{dE_\nu}(E_\nu) \ A_\ell(E_\nu) \ dE_\nu \tag{38}$$

where $\ell = e, \mu, \tau$ denotes the flavor, T is the exposure time, $\frac{d\phi_\ell}{dE_\nu}(E_\nu)$ is the differential flux of neutrinos with flavor ℓ usually given in units of $\text{GeV}^{-1}\text{cm}^{-2}\text{sec}^{-1}\text{sr}^{-1}$. The factor 4π is the result of the integration over the solid angle, in the assumption that the flux of neutrinos is isotropic, as expected for a population of high energy neutrinos with extragalactic origin. If we consider the total effective area the Eq.38 provides the expected total number of events. Otherwise, if we use the effective areas divided per flavors ℓ we find the expected number of events produced by neutrinos of a specific flavor ν_ℓ.

4.5.1 High Energy Starting Events

Let us discuss first the effective areas of High Energy Starting Events (HESE), i.e. the events with the vertex of interaction contained into the detector. This class of events is sensitive to all the interactions discussed in the previous section (NC and CC interactions of ν_ℓ, all flavor). We expect that the effective area is given by:

$$A_{\text{eff}} = \left[N_n \times \sigma(E_\nu) \times \frac{1 + h(E_\nu)}{2} \right] \times \epsilon(E_\nu) \tag{39}$$

where

- E_ν is the true energy of the incoming neutrinos;
- $N_n = \frac{\rho V}{m_N} = 5.5 \times 10^{38}$ is the number of nucleons in 1 km^3 of ice, with density of 0.92 g/cm^2. In water the number of target is equal to $N_n = \frac{\rho V}{m_N} = 6.0 \times 10^{38}$;
- $\sigma(E_\nu)$ is the cross section for neutrino-nucleon interaction. One considers CC and NC, namely charge current and neutral current interactions, discussed in Sec.4.3;
- the factor $h(E_\nu)$ describes neutrino absorption in the Earth, modeled using PREM [144] and averaged over the angle of arrival of neutrinos. For energies $E_\nu = 10,\ 100,\ 1000$ and 10000 TeV we find that $h = 0.91,\ 0.66,\ 0.37$ and 0.18, respectively. Above $\simeq$ 400 TeV half of neutrinos are absorbed into the Earth. The calculation are reported in the appendix B.1;
- the parameter $\epsilon(E_\nu)$ gives the effective volume of the detector with respect to an ideal detector. It also contains the information on the energy threshold chosen for the experiment. It is possible to find the function $\epsilon(E_\nu)$ comparing the theoretical effective area with the realistic one, usually provided by the experimental collaboration.

In the left panel of Fig.16 the effective areas of IceCube [26] for CC interactions (divided per flavors) and the effective area of NC interactions are represented. At high energy the total effective areas are well reproduced by using the analytical expression of Eq.39 with $\epsilon = 0.4$. It means that IceCube corresponds to an ideal detector of 0.4 km^3 above PeV energy.

4.5.2 Throughgoing muons

The throughgoing muons are produced by ν_μ that interact via CC interaction outside the detector. For this reason the effective volume of the detector is larger than its physical dimension. To be detected, a neutrino must produce a muon with sufficient range to reach the detector. The main ingredients of the effective area, discussed before, remain still valid but we have to consider also the probability of detection. It is given by the product of the interaction probability (or the inverse interaction length $\lambda^{-1} = n\sigma_\nu$) and the range of the muon R_μ

$$P_{\nu\to\mu} \simeq n\sigma_\nu R_\mu$$

where n is the number density of target nucleons discussed in the previous section, σ_ν is the charged current interaction cross section and the range is $R_\mu \simeq$ 5m per GeV for low energy muons. The muon range is determined by catastrophic energy loss (brehmsstrahlung, pair production and deep inelastic scattering) for muons with energies exceeding $\sim$ 500 GeV [128]. The effective areas of throughgoing muons, for ANTARES [145], IceCube [146] and KM3NeT (ARCA) [147] are reported in the right panel of Fig.16

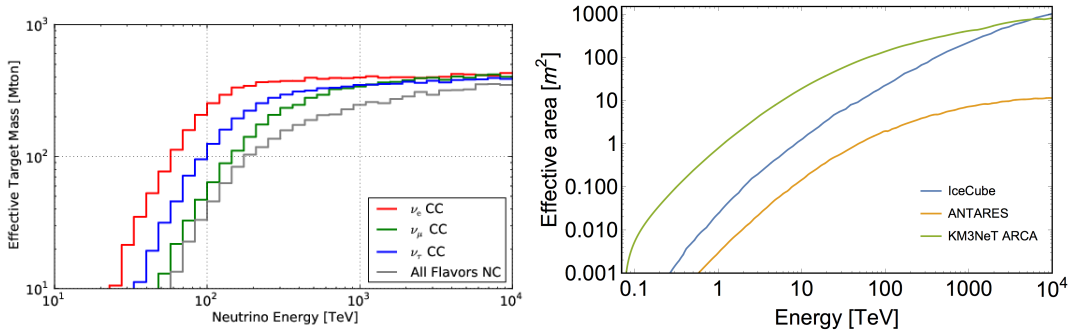

Figure 16: *In the left panel the effective areas relative to the high energy starting events (HESE) [133]. In the right panel muon neutrino effective areas for point-source search. The one adopted for ANTARES [145] is that in the declination band $-45^\circ < \delta < 0^\circ$, the one for IceCube [146] is for $-30^\circ < \delta < 0^\circ$, the one for ARCA [147] is an average value.*

4.5.3 Double bang and double pulse

As discussed in Sec.4.4.2, tau neutrinos of very high energy can be identified since they produce a typical signature into the detector, i.e. the double bang (two vertex of interaction in two different strings) or double pulses (two separated signals in a single DOM).

This class of events is very important because ν_τ are not expected to be produced in the atmosphere but they are predicted to be a non negligible component of the cosmic neutrino flux due to flavor oscillations, as we have seen in chapter 3 of this thesis. This represents a distinctive signature of a cosmic population and

the detection of a ν_τ would be the definitive proof that cosmic neutrinos have been observed.

The paper [143] is dedicated to the search of τ neutrinos in IceCube. In this work it is investigated the possibility to observe a "double pulse". The effective area of this process A_τ^{2P} is provided in that paper and its interpretation is given in [3]. Here we provide a short review of this process.

Considering that double pulse events are a *subset* of the events caused by CC tau neutrino interactions, we describe the effective area as,

$$A_\tau^{2P}(E_\nu) = \epsilon_{2P} \times \eta_{CC} \times A_\tau(E_\nu) \times P_{2P}(E_\nu, L_{min}) \tag{40}$$

where $A_\tau(E_\nu) \approx 13.4\ \mathrm{m}^2 (E_\nu/\mathrm{PeV})^{0.455}$ is the effective area for ν_τ calculated by IceCube in [133], the factor $\eta_{CC} = (1 + \sigma_{NC}/\sigma_{CC})^{-1} \approx 0.7$ gives the fraction of ν_τ interactions that are due to CC processes and the constant $\epsilon_{2P} < 1$ describes the effect of geometrical and quality cuts implemented by IceCube for the search of these events. The function $P_{2P}(E_\nu, L_{min})$ describes the probability that a neutrino with energy E_ν produces a tau traveling more than L_{min} before it decays, where L_{min} is the minimum distance[2] to give rise to an observable double pulse in the detector.

The taus produced in CC-DIS have an average energy equal to:

$$E_\tau = (1 - \langle y \rangle) E_\nu \simeq \frac{3}{4} E_\nu \tag{41}$$

[2] One can implement a condition for containment replacing $P_{2P}(E_\nu, L_{min}) \to P_{2P}(E_\nu, L_{min}) - P_{2P}(E_\nu, L_{max})$ with $L_{max} \sim 0.5$ km; we checked that the changes are not conspicuous in the range of energies of interest.

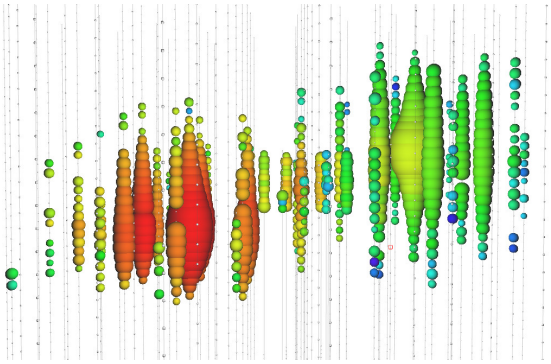

Figure 17: *Simulation of a double bang events. The two vertices of interaction are visibile (creation of ν_τ and its decay). Credit: IceCube website*

where $\langle y \rangle$ is the mean inelasticity which is nearly constant in the energy range that we are considering [136, 137] (see also Sec.4.3). If we neglect τ energy dispersion and assume the one-to-one relationship between E_τ and E_ν expressed by Eq.41, the probability $P_{2P}(E_\nu, L_{min})$ is given by:

$$P_{2P}(E_\nu, L_{min}) = \exp\left[- \frac{E_{min}(L_{min})}{E_\nu} \right] \tag{42}$$

where E_{min} represents the minimum neutrino energy which is necessary to produce a tau with decay length larger than L_{min}. This can be calculated as:

$$E_{min} = \frac{L_{min}}{c\, t_\tau} \times \frac{m_\tau c^2}{1 - \langle y \rangle} = 3.3 \text{ PeV} \left(\frac{L_{min}}{120 \text{ m}} \right) \tag{43}$$

with $m_\tau c^2 = 1.777$ GeV and $t_\tau = 0.29 \cdot 10^{-12}$ s.

Using the expression in Eq.40, we find that the effective area of IceCube, in the energy region from 0.1 to 10 PeV, is reasonably well described setting

$$\epsilon_{2P} = 0.25 \text{ and } E_{min} = 0.5 \text{ PeV} \tag{44}$$

that corresponds to

$$L_{min} = 18 \text{ m}$$

In other words the following parameterized expression for the effective area can be used:

$$A_\tau^{2P} = \bar{A}_{2P} \times \left(\frac{E_\nu}{\text{PeV}} \right)^\beta \exp\left(- \frac{E_{min}}{E_\nu} \right) \text{ with } \begin{cases} \bar{A}_{2P} = 2.33 \text{ m}^2 \\ \beta = 0.455 \\ E_{min} = 0.5 \text{ PeV} \end{cases} \tag{45}$$

as showed in Fig.18 for a direct comparison of the IceCube effective area. Let us notice that $\beta = 0.455$ is almost the same exponent of the cross section given in Eq.37.

Up to now no double pulses events have been observed. This is not surprising, since this topology of events is rare. Indeed the estimations of [3] and [143] say that the rate is expected to be lower than 0.2 events per year, with the present technology and the present knowledge of the cosmic neutrino flux. We will discuss in great detail the high energy neutrino flux and its interpretation in the next chapter.

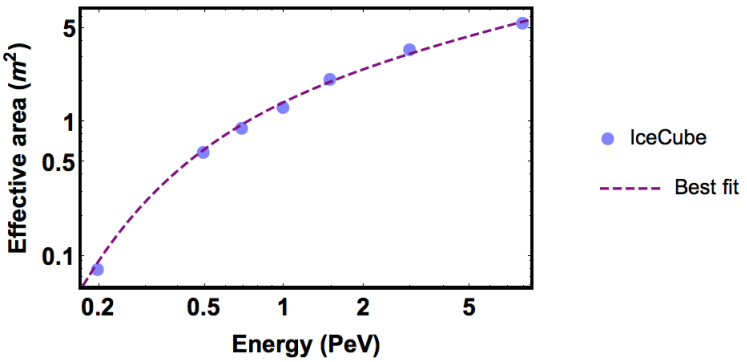

Figure 18: *Effective areas of double pulse. The points are the values given by IceCube [143] while the line is the parameterization described in [3] and in Eq.45.*

4.5.4 Glashow resonance

We have already discussed the Glashow resonance in section 3.1.4. We have seen that it is a typical signature of the $\bar{\nu}_e$, since only antineutrinos of this flavor can interact via Glashow resonance. Here we analyze this process from the point of view of the interaction and the effective area.

Let us recall that the process $\overline{\nu}_e + e^-$, mediated by an intermediate W boson, has a resonant character at:

$$E_{\rm G} = \frac{M_W^2}{2m_e} = 6.32 \text{ PeV} \tag{46}$$

The total cross section of this process can be found in [116]. Note that in the original work of Glashow [115] the cross section is wrong by a factor 2, because at that time the helicity states was ignored. The right cross section is given by:

$$\sigma_{\rm G}(E) = \frac{G_{\rm F}^2\ (\hbar c)^2\ M_{\rm W}^2}{3\pi} \frac{E}{E_{\rm G}\left[\left(\frac{E}{E_{\rm G}} - 1\right)^2 + \left(\frac{\Gamma_{\rm W}}{m_{\rm G}}\right)^2\right]} \frac{1}{B.R.(W^- \to \bar{\nu}_\mu\ \mu^-)} \tag{47}$$

where $G_{\rm F}$ is the Fermi constant, $M_{\rm W} \simeq 80$ GeV is the mass of the W^- boson and $\Gamma_{\rm W} = 2.085$ GeV is its FWHM, $E_{\rm G} = \frac{M_{\rm W}^2}{2\ m_e} \simeq 6.32$ PeV is the energy in which the cross section reaches its maximum value and $B.R.(W^- \to \bar{\nu}_\mu\ \mu^-)$ is the branching ratio of the leptonic channel, that is equal to $B.R.(W^- \to \bar{\nu}_\mu\ \mu^-) \simeq 0.105$ [20].

The cross section at $E \simeq E_{\rm G}$ is about 2 orders of magnitude larger than that of DIS and provides the dominant contribution to the $\bar{\nu}_e$ interaction rate at few PeVs. The properties of events produced by Glashow resonance depend on the final state of the interaction process, i.e. on the W^- decay mode. In 2/3 of cases the W^- decays in hadrons whereas in 1/3 of cases decays via leptonic channel.

Following Eq.39, the effective area for Glashow resonance can be parametrized as follows:

$$A_e^{\rm G}(E_\nu) = \left[N_{\rm e} \times \sigma_{\rm G}(E_\nu) \times \frac{1}{2} \times \frac{1}{2}\right] \times \epsilon(E_\nu) \tag{48}$$

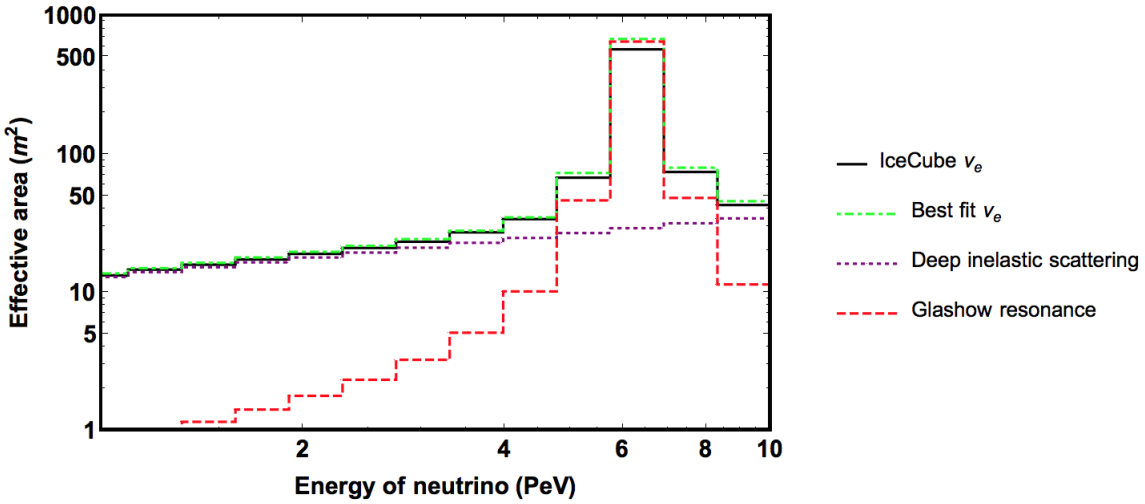

Figure 19: *Effective areas of ν_e and $\bar{\nu}_e$ at high energies. The effective area given by IceCube (continuous line) is reproduced within 10 % on average (15 % in the worst bin) by the sum of a contribution due to DIS (dotted line) and the contribution of Glashow resonance (dashed line). Figure from [3].*

where $\sigma_G(E_\nu)$ is the total $\overline{\nu}_e + e$ cross section [115] and

$$N_e = \frac{10}{18} \times N_n = 3.1 \times 10^{38}$$

is the total number of electrons in $1\,\mathrm{km}^3$ of ice. The first factor $1/2$ takes into account that only $\overline{\nu}_e$ interact through Glashow resonance and that IceCube calculations are obtained by considering an equal fraction of ν_e and $\bar{\nu}_e$ arriving at the Earth. The second factor $1/2$ is obtained by assuming complete absorption of antineutrinos crossing the Earth, that is a good approximation for neutrinos of 6.3 PeV.

In order to verify the adequacy of our interpretation, we compare in Fig.19 the IceCube effective area, $A_e(E_\nu)$, with the sum of the two contributions $\frac{1}{2}A_e^G(E_\nu) + A_e^{DIS}(E_\nu)$.[3] We are able to reproduce $A_e(E_\nu)$ within 10 % accuracy, showing that the main physical ingredients are correctly understood and implemented. The small difference between our parametrization and IceCube calculation near the Glashow resonance could be due to a slightly lower efficiency of IceCube to detect muons and tau produced by leptonic channels of the W^- boson.

Considering that the Glashow resonance cross section has a peak around 6.32 PeV, the cross section is well approximated by a Dirac Delta function:

$$\sigma_G(E_\nu) = K_G \times \delta(E_\nu - E_G)$$

where K_G is a constant. Therefore it is possible to use the same approximation also for the effective area, obtaining the following useful numerical expression:

$$A_e^G(E_\nu) \simeq 1630\ \mathrm{m}^2 \times \delta\left(\frac{E_\nu}{\mathrm{PeV}} - 6.32\right) \tag{49}$$

[3] The factor $1/2$ comes from the assumption $\phi_{\nu_e}=\phi_{\bar{\nu}_e}$, contained in the IceCube effective area [133].

5 NEUTRINO FLAVOR AND EVENT TOPOLOGY

This chapter is dedicated to the flavor composition of high energy neutrinos. We discuss the global flavor composition analyzing the events observed by IceCube and comparing the experimental results with the theoretical predictions. We also use the observed flavor composition to test the full neutrino decay scenario. Moreover we dedicate a section to specific flavors of neutrino, such as the electron antineutrinos, that can be tested by the Glashow resonance, and the tau neutrinos, that can be tested thanks to the double pulse events.

This chapter is based on five papers published during the Phd [1, 2, 3, 4, 5]. It is explicitly stated whenever an updated version of the results is presented and a comparison with the results of the papers is provided.

5.1 EVENT TOPOLOGY

There are two datasets available from the IceCube experiment in which neutrinos of astrophysical origin have been observed, as already discussed in Chapter 4. The first one refers to upward going muons induced by charged current (CC) interaction of $\nu_\mu + \overline{\nu}_\mu$ crossing the Earth. These neutrinos arriving in IceCube originate from the Northern hemisphere. In the following, we refer to this sample with the name of "throughgoing muons". The second dataset is characterized by neutrinos that interact into a fiducial volume of the detector, with a contained interaction vertex; we refer to this sample as "High Energy Starting Event"(HESE).

5.1.1 Throughgoing muons

The IceCube collaboration used data from 2009 to 2015 to measure CC upgoing muon neutrino events, with the field of view restricted to the Northern hemisphere [129]. The highest energy sample (with reconstructed energy above 190 TeV) corresponds to 29 events of this type, that are reported in Tab.18. The most energetic event corresponds to a reconstructed muon energy of about 4.5 PeV. A purely atmospheric origin of them is excluded at 5.6σ of significance. The corresponding cosmic muon flavor (neutrino+antineutrino) flux, estimated from these data, was obtained with a fit to the power-law[1]:

$$\frac{d\phi_\mu}{dE} = F_\mu \times \frac{10^{-18}}{\text{GeV cm}^2 \text{ s sr}} \left(\frac{E}{100 \text{ TeV}}\right)^{-\alpha} \tag{50}$$

The parameters are $F_\mu = 0.90^{+0.30}_{-0.27}$ and $\alpha = 2.13 \pm 0.13$.

[1] From here on, we always denote with $\frac{d\phi_\ell}{dE}$ the flux of neutrinos plus the flux of antineutrinos of flavor ℓ. When only the flux of neutrinos or antineutrinos is considered it is explicitly written.

5.1.2 High Energy Starting Events

In 4 years of data taking, 54 HESE have been detected[2]. They are classified in 14 tracks and 39 showers events (1 of them is not identified). Among them, 16 events come from the Northern hemisphere, 37 events come from the Southern hemisphere and 1 event was detected with declination equal to zero. These events are characterized by a deposited energy greater than 30 TeV and the most energetic HESE deposited an energy of 2 PeV into the detector.

The flux attributed to astrophysical neutrinos is described, in first approximation, by an isotropic distribution and a power-law spectrum. The all flavor flux is equal to:

$$\frac{d\phi}{dE} = F \times \frac{10^{-18}}{\text{GeV cm}^2 \text{ s sr}} \left(\frac{E}{100 \text{ TeV}}\right)^{-\alpha} \tag{51}$$

with $F = 6.7^{+1.1}_{-1.2}$ and $\alpha = 2.50 \pm 0.09$. We denote with F the normalization of the all flavor flux.

Although the bulk of HESE events seen from the Southern sky suggest a power-law spectrum with spectral index $\alpha \approx 2.5$, the subset of highest energy HESE, above 200 TeV, is in agreement with a much harder spectrum and more precisely, with the same distribution suggested by the throughgoing muons: see Fig. 6 of [6] and Fig. 5 of [129], and discussions therein. In other words, the flux of the highest energy HESE events observed from the Southern sky is compatible with the same hard spectrum, $\alpha \approx 2$, suggested by throughgoing muons.

5.1.3 The atmospheric background

An important fraction of events detected by IceCube are due to the atmospheric background. Let us briefly describe the different backgrounds and the veto technique, adopted in IceCube for HESE to reduce the effect of the background.

CONVENTIONAL BACKGROUND When primary cosmic ray protons and nuclei collide with the atmosphere their interactions produce secondary particles, among which a huge amount of pions is produced [148]. From the decay of pions, neutrinos are produced, as largely discussed in Sec.1.2. The spectrum of the secondary particles peaks in the GeV range but it extends up to high energy, with approximately a power-law behavior.

The muons produced from pions decay can travel for a distance:

$$d \simeq c \times \tau_\mu \times \gamma_\mu \simeq 1 \text{ km } \frac{E_\mu}{0.3 \text{ GeV}}$$

where c is the speed of light, $\tau_\mu = 2.2$ μs is the lifetime of muons and γ_μ is the Lorentz factor. After that distance the muons decay; therefore at the relevant energies for IceCube, i.e. some tens of TeV energy, the muons do not decay and only muon neutrinos from pions decay are produced, giving a flavor composition equal to

$$(\nu_e : \nu_\mu : \nu_\tau) = (0 : 1 : 0)$$

and an energy spectrum $E^{-3.7}$. A smaller contribution of about 10% is provided by neutrinos from kaons decay. The normalization of the conventional atmospheric background is known

[2] During the writing of this thesis the 6 years HESE dataset, containing 82 events, has been presented in the ICRC conference. Since this data are still not published, in the following of the thesis we will consider as most recent data the 6 years throughgoing muons dataset and the 4 years HESE.

with an uncertainty of 25% [149] and it is mainly given by the uncertainty on the cosmic rays flux and the uncertainty on the processes that occur in atmosphere.

ATMOSPHERIC MUONS In addition to conventional atmospheric neutrinos, there are also atmospheric muons produced in the pion decay, with an energy spectrum $E^{-3.7}$. For what concerns the HESE analysis in IceCube, the atmospheric muons (if correctly reconstructed) come only from the Southern hemisphere, because muons produced in the Northern hemisphere are absorbed passing through Earth. Moreover atmospheric muons are precious for the HESE analysis, since they always reach the detector together with conventional atmospheric muons. For this reason in IceCube there is a veto system that refuses an event characterized by a coincident signal, that is produced by the muons in the veto and by the atmospheric neutrinos into the detector.

PROMPT NEUTRINOS Prompt neutrinos are produced by the decay of heavy mesons, containing the quark charm. Also these neutrinos are expected to have a power-law spectrum, with spectral index $\alpha \approx 2.7$, because heavy mesons are highly unstable and decay before interacting. The flavor composition of prompt neutrinos in a neutrino telescope is $(\nu_e : \nu_\mu : \nu_\tau) \approx (1 : 1 : 0)$ and it is different from what is expected for cosmic neutrinos produced in pion decay, that have a flavor composition at Earth of $(\nu_e : \nu_\mu : \nu_\tau) \approx (1 : 1 : 1)$. The flux of prompt neutrinos has been calculated in [150] and we refer to this model as ERS in the following. The uncertainty on the theoretical normalization is about 30%-35%. We discuss the prompt neutrinos also in the following, in the context of a multi-component model to explain IceCube data (see Sec.6.3.1).

5.2 FLAVOR COMPOSITION: TRACK-TO-SHOWER RATIO

In this section we discuss the flavor composition of the events observed in IceCube, following Palladino et al. [4]. We present an updated analysis, that is obtained using the most recent available data.

The search for High Energy Starting Events (HESE) in IceCube detector provided the first evidence for a high-energy neutrino flux of extraterrestrial origin [133, 151, 152]. In three year of data taking [151], 37 events with deposited energies above 30 TeV were observed, whereas the expected background was 8.4 ± 4.2 events due to penetrating muons (i.e. muons generated by the interaction of cosmic rays with the atmosphere) and 6.6 ± 5.9 events due to atmospheric neutrinos. In the new dataset containing four years of HESE [149] 54 events have been observed. The significance of the excess, over the atmospheric background, is larger than 6σ.

The scientific debate about the origin of these events is extremely lively. It is commonly accepted that neutrinos have been seen, but their origin and propagation is not understood. The flavor composition is a useful tool to proceed in the discussion. The flavor discrimination is, in principle, possible by looking at the topology of the events. Most HESE have 'shower' topology, that is produced by neutral current (NC) interactions of all neutrino flavors and charged current (CC) interactions of ν_e and ν_τ (as we have seen in chapter 4), since the decay length of the τ lepton is too short to be resolved below ~ 1 PeV. On the other hand, events with 'track' topology are produced by CC interactions of ν_μ. Thus, the crucial observable quantity is the ratio between track and shower events at high energy. This can be used to confirm the cosmic origin of the events and/or to discriminate among different production scenarios.

In order to reduce the contamination from atmospheric neutrinos, we focus on the subset of events with deposited energy above 60 TeV, where the signal is expected to dominate. Also the throughgoing muons are included in this analysis. The advantage of the track-to-shower ratio representation is that the experimental likelihood, i.e. the observed track-to-shower ratio, does not depend upon the spectral index. On the other hand, the theoretical expectations slightly depend upon the spectral index and they vary by 15%-20% for $\alpha \in [2.0, 2.6]$.

5.2.1 Expectations

FROM NEUTRINOS TO HESE EVENTS. Let us consider HESE with energies between 60 TeV to 3 PeV, that are likely to be dominated by the signal due to cosmic neutrinos. The expected number of events produced by an isotropic flux ϕ_ℓ of neutrinos and antineutrinos of flavor ℓ is:

$$N_{ev,\ell} = 4\pi\, T \int \frac{d\phi_\ell}{dE}(E)\, A_\ell(E)\, dE \tag{52}$$

where $\ell = e,\ \mu,\ \tau$ and T is the observation time. The effective areas $A_\ell(E)$ are provided by the IceCube collaboration [133] and include the effects of neutrino cross sections, partial neutrino absorption in the earth, detector efficiency and specific cuts of the HESE analysis, as discussed in Sec.4.5.

In order to calculate the contribution given by a specific topology of events and to correctly compute the track-to-shower ratio, we separate the total effective area of ν_μ in the effective area of shower-like events and in the effective area of track-like events,

$$A_\mu(E) = A_\mu^{\mathrm{T}}(E) + A_\mu^{\mathrm{S}}(E) \tag{53}$$

where $A_\mu^{\mathrm{T}}(E) \equiv p_{\mathrm{T}}(E)\, A_\mu(E)$ is the effective area for ν_μ CC interactions that produce tracks in the detector, while $A_\mu^{\mathrm{S}}(E) \equiv (1 - p_{\mathrm{T}}(E))\, A_\mu(E)$ is the effective area for neutral current (NC) interactions that are instead observed as showers. The parameter $p_{\mathrm{T}}(E)$ is the probability that an *observed* event (i.e. passing all the cuts in the HESE analysis) produced by a muon neutrino with energy E is a track-like event. This quantity is given by,

$$p_{\mathrm{T}}(E) = \frac{\sigma_{\mathrm{CC}}(E)\, M_\mu^{\mathrm{CC}}(E)}{\sigma_{\mathrm{NC}}(E)\, M^{\mathrm{NC}}(E) + \sigma_{\mathrm{CC}}(E)\, M_\mu^{\mathrm{CC}}(E)}$$

where $\sigma_{\mathrm{CC}}(E)$ and $\sigma_{\mathrm{NC}}(E)$ are the cross section for CC and NC interactions of neutrinos [136, 137] while $M_\mu^{\mathrm{CC}}(E)$ and $M^{\mathrm{NC}}(E)$ are the effective detector mass for CC and NC interactions of ν_μ [133]. The probability p_{T} is mildly dependent on energy and approximately equals 0.8 [4].

The number of showers N_{S} and tracks N_{T} in the IceCube detector can be then calculated according to:

$$\begin{aligned} N_{\mathrm{S}} &= 4\pi\, T \int_0^{\overline{E}} dE \left\{ \frac{d\phi_e}{dE}(E)\, A_e(E) + \frac{d\phi_\tau}{dE}(E)\, A_\tau(E) + \right. \\ &+ \left. \frac{d\phi_\mu}{dE}(E)\ [1 - p_{\mathrm{T}}]\ A_\mu(E) \right\} \\ N_{\mathrm{T}} &= 4\pi\, T \int_0^{\overline{E}} dE\, \frac{d\phi_\mu}{dE}(E)\, p_{\mathrm{T}}\, A_\mu(E) \end{aligned} \tag{54}$$

In the above relation, we neglected the small fraction of ν_τ CC-events followed by taus decaying into muons which can be potentially observed as tracks for the reasons described in Sec.4.5.3. Moreover, we introduced an upper integration limit at $\overline{E} = 3\,\mathrm{PeV}$ since the HESE analysis includes only events with deposited energy below 3 PeV. In principle, the effects of the threshold at $E_{\mathrm{dep}} = 3\,\mathrm{PeV}$ should be implemented as a correction of the effective areas. Here, we assume that this can be mimicked by a sharp cut in the $A_\ell(E)$ at the neutrino energy $E = 3\,\mathrm{PeV}$. In the following we will relax this hypothesis, discussing the consequence of the non observation of resonant events.

The advantage of this approach is that, relying on the effective areas calculated by IceCube, it automatically implements the correct relation between the neutrino energy and the deposited energy in the detector. This relation is flavor-dependent and is the critical ingredient to correctly predict the track-to-shower ratio.[3]

Using Eqs.(54) we calculate the track-to-shower ratio, that is a function of the spectral index of the neutrino spectrum. We consider $\alpha = 2.5$ that is the best fit of the spectral index in the 4 years HESE dataset [149], obtaining:

$$\frac{N_{\mathrm{T}}}{N_{\mathrm{S}}} = \frac{\xi_\mu}{2.9 - 2.7\,\xi_\mu - 1.1\,\xi_\tau} \tag{55}$$

where ξ_ℓ is the flavor faction at Earth (see chapter 3) and we considered that $\xi_e = 1 - \xi_\mu - \xi_\tau$. The numerical coefficients of Eq. 55 depend mildly on the spectral index, as quantified in [4].

THE EFFECT OF NEUTRINO OSCILLATIONS. In chapter 3 we have discussed the effect of neutrino oscillations over cosmic distances. It is generally expected that a cosmic population is characterized by a flavor content $(\xi_e : \xi_\mu : \xi_\tau) \sim (1/3 : 1/3 : 1/3)$, assuming the standard scenario of neutrinos produced by pion decays. In this case the track to-shower ratio in IceCube, as can be calculated from Eq. 55, is equal to:

$$\frac{N_{\mathrm{T}}}{N_{\mathrm{S}}} = 0.20 \tag{56}$$

If we consider a spectral index $\alpha \neq 2.5$, this prediction is only marginally affected as discussed in [4], where the three years dataset and $\alpha = 2$ have been considered instead.

The equipartition of neutrino flavors at Earth is, however, only an approximation which can be tested using IceCube data: a certain imprint of the neutrino production mechanism does remain. It is important to exploit the track-to-shower ratio observed by IceCube to discriminate the neutrino origin. To realistically explore this possibility, it is necessary to quantify the relevance of uncertainties in oscillation parameters for the predictions of $N_{\mathrm{T}}/N_{\mathrm{S}}$. Let us recall the flavor composition described in the chapter 3. We consider
i) $(\xi_e : \xi_\mu : \xi_\tau) = (1/3 : 2/3 : 0)$ for π decay (orange);
ii) $(\xi_e : \xi_\mu : \xi_\tau) = (1 : 0 : 0)$ for β decay of *neutrons* (green);
iii) $(\xi_e : \xi_\mu : \xi_\tau) = (0 : 1 : 0)$ for π decay with *damped muons* (red),
where we made reference to the color code used in Fig. 20.

[3] We tested the validity of our calculations by comparing them with the expected numbers of events in Supp. Tab. IV of [151]. For the best fit astrophysical spectrum and an exposure of 988 days we obtain $N_{\mathrm{S}} = 14.8$ and $N_{\mathrm{T}} = 3.6$ to be compared with $N_{\mathrm{S}} = 14.4$ and $N_{\mathrm{T}} = 3.8$. Also, we reproduce the fraction of tracks produced by π/K and prompt atmospheric neutrinos within 3%. This shows that our approach is appropriate for the level of precision desired for this analysis.

These theoretical expectations are summarized in Fig. 20. The distributions of the flavor compositions are obtained with the natural parametrization described in chapter 3.

We see that N_T/N_S distributions are well separated when different neutrino production mechanisms are considered. This means that a precise determination of N_T/N_S could provide hints on the neutrino origin, even with the present knowledge of neutrino mixing parameters [1]. From the neutrino physics point of view, large contributions to N_T/N_S dispersions are provided by the δ and θ_{23} parameters.

For the purposes of our discussion, it is important to note that the track-to-shower ratio has a limited range of possible values, if neutrinos have cosmic origin. If we take the average values of the distributions and we assume the spectral index $\alpha = 2.5$, we obtain

$$0.11 < \frac{N_T}{N_S} < 0.27 \quad \text{[expected from cosmic origin]} \tag{57}$$

The minimal value is obtained for neutron-decay ($\xi^0_e : \xi^0_\mu : \xi^0_\tau = 1 : 0 : 0$) whereas the maximum value is obtained for damped muons scenario ($\xi^0_e : \xi^0_\mu : \xi^0_\tau = 0 : 1 : 0$). If we vary the spectral index, this interval shifts by $\sim \mp$ 10% and also the oscillation parameters affect slightly these expectations (see [4]).

5.2.2 Observations

In the 4 years HESE dataset [149], 32 events have been observed in the energy window $60\,\text{TeV} < E_{\text{dep}} < 3\,\text{PeV}$, consisting of $n_S = 24$ showers and $n_T = 8$ tracks events, against an expected background of ~ 4.5 events from atmospheric muons and neutrinos.

This information can be combined with the results of the independent analysis that comes from the throughgoing muons dataset. The flux has been already described in section 5.1. Using the best fit of the spectral index, with an uncertainty of 30% on the normalization (see Fig.6 of [129]), and using Eq.54, we found that the expected number of tracks is equal to $n^\mu_T = 4.0 \pm 1.2$.

From Fig.6 of [129] we observe that the spectral index and the normalization are anti-correlated and $F(\alpha)$, of Eq.50, is well approximated by

$$F_\mu(\alpha) = 0.9 + 1.54 \times (\alpha - 2.13) \tag{58}$$

Therefore, considering Eq.54 with $\alpha = 2$ and $F_\mu = 0.7$ we expect $n_T = 3.7$, while considering $\alpha = 2.26$ and $F_\mu = 1.1$ we expect $n_T = 4.2$.

THE TRACK-TO-SHOWER RATIO. Using the expected backgrounds reported in [151] and scaling them with the time of data taking, we found on average $b_T = 3.1$ and $b_S = 1.0$ background events expected from atmospheric neutrinos (2.5 tracks and 1.0 showers) and muons (0.6 tracks and no showers). In the above estimates, we assume that the prompt atmospheric neutrinos give a negligible contribution, as it is suggested by the spectral and the angular distributions of IceCube events. The number of signal events, associated to cosmic sources, can be estimated separately for track and shower events, as follows:

$$\begin{aligned} \mathcal{L}_T(s) &\propto (b_T + s)^{n_T} \times \exp(-s) \times \exp\left[-\frac{(s - n^\mu_T)^2}{2 \times (\Delta n^\mu_T)^2}\right] \\ \mathcal{L}_S(s) &\propto (b_S + s)^{n_S} \times \exp(-s) \end{aligned}$$

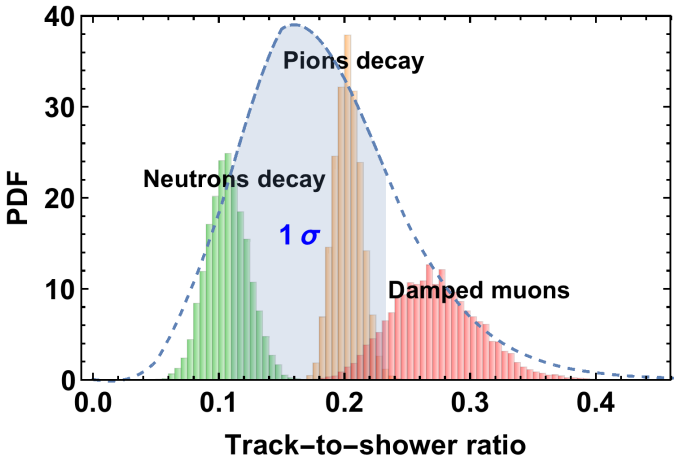

Figure 20: *Expected track-to-shower ratio of cosmic neutrinos for the four production mechanisms described in the text. The distributions show the effect of uncertainties in the neutrino oscillation parameters. The left (resp. right) panel is obtained for normal (resp. inverse) hierarchy. The shaded region is the likelihood corresponding to Eq. 59.*

Marginalizing over the total number of events as follows:

$$\mathcal{L}_{\text{obs}}(r) = \int_0^\infty \mathcal{L}_T(r \times s)\mathcal{L}_S(s)\; s\; ds$$

where

$$r = \frac{\text{track events}}{\text{shower events}},$$

we compute the track-to-shower ratio of cosmic neutrino. At 1σ C.L we obtain:

$$0.11 \leq r \leq 0.23 \tag{59}$$

The 1σ interval is obtained integrating the likelihood of the track-to-shower ratio $\mathcal{L}_{\text{obs}}(r)$ from r_1 to r_2, with r_1 and r_2 are such that $\mathcal{L}_{\text{obs}}(r_1) = \mathcal{L}_{\text{obs}}(r_2)$. The likelihood distribution of Eq.5.2.2 for the track-to-shower ratio of cosmic neutrinos is represented by the shaded region in Fig.20.

DISCUSSION AND SUMMARY The analysis proposed in this section is an updated version of that of Palladino et al.[4]. It has been done combining the most recent informations provided by HESE [149] and throughgoing muons [129].

Fig.20 shows clearly that: *i)* there is no tension between the present observational results and the assumption of a cosmic neutrino population, because the central observational value is in the middle of the expected region; *ii)* there is no clear preference for a specific neutrino production mechanism, being the observational error comparable to the difference between the various predictions.

This new result is in agreement with the result of Palladino et al.[4] and the other analyses on the flavor composition proposed in [149, 153, 154, 27]. Let us notice that considering the 4 years dataset of HESE and the 6 years dataset of throughgoing muons we have obtained a likelihood function with a smaller dispersion with respect to [4]. Anyway, it is not yet possible to exclude any mechanism of production of cosmic neutrinos.

5.3 FLAVOR COMPOSITION: TRIANGLE REPRESENTATION

An alternative way to explore the flavor composition is the "triangle of flavors", that has been used in several papers [1, 149, 153, 154, 27]. This representation is complementary to the track-to-shower ratio one, because in this case the theoretical expectations are fixed on the flavor triangle, whereas the regions, related to the observations, change with the assumed neutrino spectrum. See the appendix of Viviani's theorem A.1 for the details.

In this section we use both the natural parametrization discussed in chapter 3 and the Monte Carlo simulation, showing that there is good agreement between them. Moreover we compare our theoretical analysis with the three years IceCube HESE data + throughgoing muons.

As production mechanisms, which we will use to compute our expectations in the flavor triangle, we consider:
1. pions decay (blue);
2. neutrons decay (green);
3. damped muons (red);
4. charm mesons (orange).
The latter mechanism of production was not discussed in chapter 3. It is the same mechanism that produces atmospheric prompt neutrinos, i.e. the decay of heavy mesons, with an initial flavor ratio $(\xi_e : \xi_\mu : \xi_\tau) = (1/2 : 1/2 : 0)$.

Using the different flavor compositions at the source, we represent the expected regions by propagating the errors on the predictions with a Monte Carlo simulation; this gives rise to the 4 dotted regions in the flavor triangles in Fig. 21 and 22. The errors are given by the uncertainties on the mixing angles (especially θ_{23}) and the δ_{CP} [113]. In order to represent the points on the triangle we use the following formulas, discussed also in the appendix A.2.

$$\begin{aligned} x &= \frac{\xi_\mu - \xi_e}{\sqrt{3}} \\ y &= \xi_\tau \end{aligned}$$

These regions can be compared with those obtained with a Gaussian treatment of the errors on P_0, P_1 and P_2. Following the implementation of Appendix A.2, we obtain the 4 ellipses of Fig. 21 and 22 that enclose the 99% CL regions. As it is clear from the two figures, the differences between the Montecarlo and the Gaussian treatments are not important. Therefore the Gaussian approach seems to be better for the present needs, since it is significantly easier to implement.

Let us recall that the expected theoretical regions (the dotted areas obtained by Montecarlo and the elliptic curves corresponding to Gaussian approximation) depend only on the initial flavor ratio and are not affected by the energy spectrum of the neutrinos, that is assumed to have the same shape for all flavors. In other words, the four theoretical regions shown on the flavor triangles of Fig. 21 are just identical to those of Fig. 22. This is the main difference with the track-to-shower ratio discussed in the previous section, in which the theoretical track-to-shower ratio was a function of the spectrum.

On the contrary, the 1σ, 2σ and 3σ zones depend on the energy distribution of the neutrinos. The confidence levels, indicated in the flavor triangle, result from the data analysis of IceCube events (the high energy starting events, whose initial vertex is in the detector and the

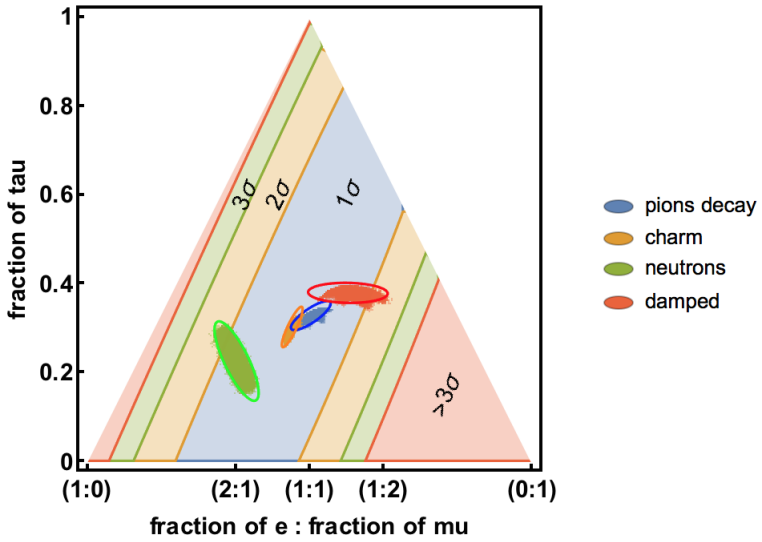

Figure 21: *Flavor triangle. The present observational information on the flavor composition of cosmic neutrinos at 1, 2 and 3σ analyzed assuming α = 2 [133] is compared with the expectations derived for four different hypotheses on the mechanism of production of the neutrinos. The ellipses derive from the gaussian parameters P_0, P_1, P_2 that characterize the natural parametrization. See Appendix A.2. Figure from [1].*

throughgoing muons) discussed in [153] and [4]. They have been obtained assuming a power law distribution given by:

$$\frac{d\phi}{dE} = \phi_0 E^{-\alpha} \tag{60}$$

Thus, the inferred flavor ratio is a function of spectral index α. In Fig. 21 we have used the value preferred by the simplest theoretical expectations, namely $\alpha = 2$ [133]. This value of the spectral index is not in agreement anymore with the present HESE dataset, that prefers $\alpha = 2.5 \pm 0.1$ [149]. On the other side, it is important to remark that $\alpha = 2$ is compatible within 1σ with the present throughgoing muons analysis [129] and with the very high energy part of HESE [149].

For comparison, we have shown also the case $\alpha = 2.3$ [151] in Fig. 22, namely the best fit value of the dataset of high energy starting events collected by IceCube in the first three years. The comparison with Fig. 21 shows that the true value of the spectral index plays some role in determining the allowed regions: the steeper spectrum $\alpha = 2.3$ enhances the role of electron neutrinos and diminishes the one of muon neutrinos (whose effective area is very small close to the threshold, as it can be noticed looking at the left panel of Fig.16) thus it requires to increase the content of muon neutrinos at the source ξ^0_μ in order to reproduce the observed track-to-shower ratio. For this reason, the agreement of the neutron decay scenario with the data worsens for $\alpha = 2.3$. However, this kind of effect is not yet crucial for the analysis and in particular the neutron decay scenario is not yet excluded. In fact, the most important conclusion is just that the small number of events presently available does not allow us to exclude any mechanism of production [4]. This remains true also using $\alpha = 2.5$, namely the best fit of 4 years HESE, in agreement with the track-to-shower ratio analysis proposed in the previous section.

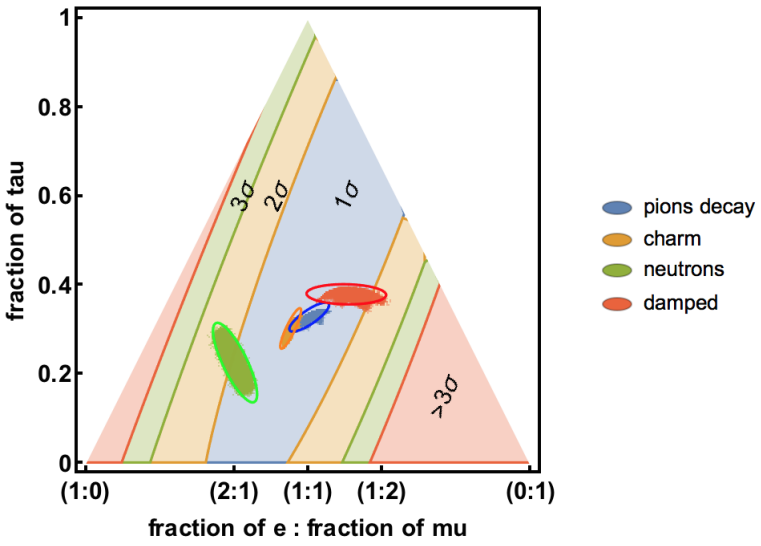

Figure 22: *Same as previous figure but using the spectral index $\alpha = 2.3$ in the analysis of the IceCube data. Figure from [1].*

The confidence levels are in reasonable agreement with those of IceCube data analysis [153, 149] (see again figure 21) and with those of [4]. The uncertainties due to the oscillation parameters have been presented in [4] in a different manner, but the results are in excellent agreement.

5.4 NEUTRINO DECAY

In section 3.2 the neutrino decay scenario has been discussed from the theoretical point of view. In this section we compare the theoretical expectation with the recent data observed by IceCube.

In the theoretical chapter dedicated to neutrino decay we have seen that, assuming complete neutrino decay, the flavor composition is given by

$$\xi_\ell = |U_{\ell j}|^2 \tag{61}$$

where $j = 1$ for Normal Hierarchy (NH) and $j = 3$ for Inverted Hierarchy. In section 5.2 we have seen how to transform the flavor composition into an observable quantity, i.e. the track-to-shower ratio.

5.4.1 The expected track-to-shower ratio

Combining the Eq.61 of neutrino decay scenarios and the Eq.55 of track-to-shower ratio, we have:

$$\frac{N_T}{N_S} = \frac{|U_{\mu j}|^2}{2.9 - 2.7\,|U_{\mu j}|^2 - 1.1\,|U_{\tau j}|^2}, \tag{62}$$

where the index j indicates the stable mass eigenstate. For normal mass hierarchy, the stable state is ν_1; using the best-fit values of the oscillation parameters, we obtain $(N_T/N_S)_{NH} = 0.10$. For inverted mass hierarchy, the stable state is ν_3 and the track-to-shower ratio becomes $(N_T/N_S)_{IH} = 0.58$. These predictions are only marginally dependent on the assumed spectral index. Indeed, if we consider an harder neutrino spectrum with $\alpha = 2$ [2], we obtain $(N_T/N_S)_{NH} = 0.12$ and $(N_T/N_S)_{IH} = 0.62$ that deviate from what obtained with $\alpha = 2.5$ by small amounts compared to theoretical and experimental uncertainties. Let us remark that in case of complete neutrino decay we loose all the information on the initial mechanism of production. Only the hierarchy is relevant for the evaluation of the flavor composition at Earth.

An important contribution to the uncertainties of the track-to-shower ratio is provided by the uncertainties of neutrino oscillation parameters. In this case we cannot use the natural parametrization therefore, in order to correctly account for these uncertainties, we construct likelihood distributions of $\sin^2\theta_{12}$, $\sin^2\theta_{13}$, $\sin^2\theta_{23}$ and δ from the $\Delta\chi^2$ profiles given by [113]. Namely, we assume that the probability distributions of each parameter are provided by $\mathcal{L} = \exp\left(-\Delta\chi^2/2\right)$. Then, we combine the various likelihood functions assuming negligible correlations and we determine the probability distributions of N_T/N_S by Montecarlo extraction of the oscillation parameters. The resulting Probability Density Function (PDF) distributions are reported in Fig.(23) in blue (red) for normal (inverted) mass hierarchy. These distributions are obtained by assuming the spectral index $\alpha = 2.5$ which, as discussed below, represents the best-fit value for the astrophysical component in the IceCube HESE data[149].

The predicted track-to-shower ratios fluctuate in rather large intervals. We refer to them using $\mathcal{L}_{th}(r)$. Namely, we obtain the ranges $(N_T/N_S)_{NH} = 0.04 - 0.10$ and $(N_T/N_S)_{IH} = 0.40 - 0.60$ by integrating out symmetrically $(1 - CL)/2$ on both sides of the distributions and by using a confidence level CL = 68.3%. The largest contributions to N_T/N_S statistical fluctuations come from δ and θ_{23} for normal and inverted mass hierarchy, respectively. Even if fluctuations are large, the predicted track-to-shower ratios for normal and inverted hierarchy are well separated, indicating that the two cases can be discriminated by a sufficiently accurate experimental determination of N_T/N_S. Moreover, by comparing it with the results of [4] and Sec.5.2, we see that the track-to-shower ratio for the neutrino decay scenarios, considered in this work, is different from that of stable neutrinos, even taking into account the uncertainty in the neutrino production mechanism. Indeed, there is only a partial overlap between the probability density function of decaying neutrinos in the normal hierarchy scenario and that of stable neutrinos produced by β decay of neutrons. This degeneracy can be resolved by improving the knowledge of δ and θ_{23} parameters.

5.4.2 Expectations vs Observations

Even if the error is large, the best fit value for the track-to-shower ratio falls in the region between theoretical expectations for neutrino decay with normal and inverted mass hierarchy disfavoring both scenarios. In order to quantify this statement, we have to take into account that both theoretical expectations and experimental determinations of the track-to-shower ratio are affected by uncertainties.

We use a general procedure to quantify the difference between the theoretical $\mathcal{L}_{th}$, i.e. the distribution for theoretical predictions in the two scenarios that we are testing, and the

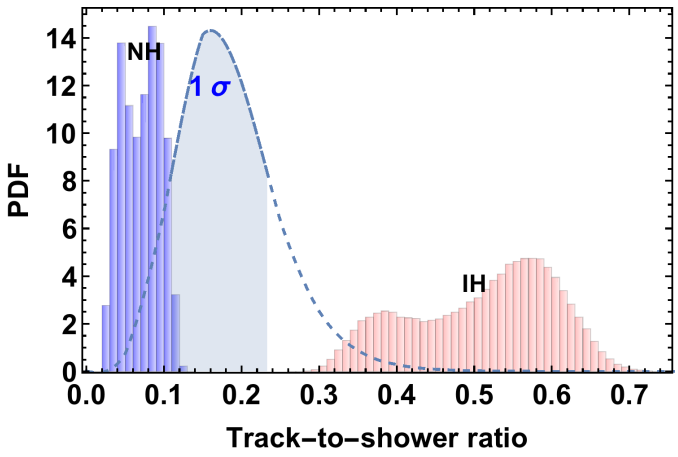

Figure 23: *The expected track-to-shower ratio for decaying cosmic neutrinos in the assumption of normal (blue) and inverse (red) mass hierarchy. The distributions show the effect of uncertainties in the neutrino oscillation parameters. The blue line is the normalized likelihood functions for the track-to-shower ratio obtained by combining the 4 years HESE dataset [149] and 6 years throughgoing muons dataset [129].*

experimental distribution $\mathcal{L}_{\text{obs}}$, i.e. the likelihood distribution obtained by using the recent IceCube data discussed in section 5.2. We define the following likelihood function:

$$\mathcal{L}(\Delta) = \int_0^\infty \mathcal{L}_{\text{obs}}(r+\Delta) \times \mathcal{L}_{\text{th}}(r)\, dr \tag{63}$$

In the assumption of normal mass hierarchy, the function $\mathcal{L}(\Delta)$ is peaked at a positive value for Δ and $\Delta = 0$ is excluded at 90% CL, corresponding to about 1.7σ.

In the assumption of inverted mass hierarchy the function $\mathcal{L}(\Delta)$ is peaked at a negative value for Δ and the value $\Delta = 0$ is excluded at 99.3% CL, corresponding at about 3σ. The above values of CL were obtained integrating the likelihood from 0 to r for NH and from $-r$ to 0 for IH. The value r respects the condition $\mathcal{L}(0) = \mathcal{L}(r)$ in both cases.

In conclusion, neutrino decay is excluded at about 2σ for normal hierarchy and about 3σ for inverted mass hierarchy. We remark that the inverted mass hierarchy scenario is also constrained by the observation of electron antineutrinos from SN1987A. The data from Kamiokande, IMB and Baksan, indeed, agree well with the hypotheses of a "standard emission", see e.g. [155, 156], in which the energy carried by $\overline{\nu}_e$ is about one sixth of $\mathcal{E} = 3 \times 10^{53}$ erg. In the inverted hierarchy scenario, the amount of electron antineutrinos expected in the detectors is suppressed by more than one order of magnitude, thus requiring implausible astrophysical scenarios, in which the radiated energy is increased by a large factor with respect to $\mathcal{E}$. On the contrary, in the assumption of normal hierarchy, the states ν_1 (which has a non negligible ν_e component) is stable and thus non-radiative decay cannot be excluded by SN1987A observations [157]. In this case, cosmic neutrinos provide the most stringent bounds on neutrino lifetimes.

CONCLUSIONS In this section an updated study of [2] has been performed. We have calculated the impact of the non-radiative neutrino decay scenario on the track-to-shower ratio expected in IceCube, including the uncertainties on the oscillation parameters and on the neutrino mass hierarchy. We have shown that, in scenarios with only one stable neutrino, the track-to-shower ratio is different from that predicted in the case of stable neutrinos, even taking into account

the uncertainty on the neutrino production mechanism. We have then used the information provided by the combination of HESE events above 60 TeV and the throughgoing muons observed by IceCube to constrain the neutrino decay hypothesis. We have shown that, despite the large observational uncertainties, the data already disfavor the possibility of neutrinos decay at about 2σ level for normal hierarchy and about 3σ for inverted mass hierarchy. We remark that this result is at present the most stringent limit on non-radiative neutrino decay for normal mass hierarchy and it is in agreement with the analysis proposed in [2, 126, 27].

5.5 DOUBLE PULSE AND GLASHOW RESONANCE

In section 4.5.3 and 4.5.4 we have studied the effective areas of double pulses and resonant events (events produced by the Glashow resonance). These events concern specific flavor of neutrino, namely the ν_τ for double pulses and the $\bar{\nu}_e$ for Glashow resonance. In other words, this topology of events provides other informations about the flavor, that are different with respect to the HESE analysis (all flavor) and the throughgoing muons analysis (ν_μ).

In this section we estimate the expected number of events for both processes. In order to do that we use the hard spectrum suggested by throughgoing muons (see Eq.50 and Eq.58), for the following reasons:

- double pulses and resonant events are produced by very energetic neutrinos, with energy of the order of PeV;
- the best fit of the throughgoing muon flux is obtained considering neutrinos with energy between 200 TeV and 8 PeV, whereas the high energy starting events have a much lower energy threshold, at 30 TeV;
- at high energy both HESE and throughgoing muon events are fitted well by the same hard spectrum.

We use Eq.58 to evaluate also the impact of the uncertainty due to the spectral index α on the expected number of events.

5.5.1 Double pulses-Tau neutrinos

Using the effective area of double pulses described in section 4.5.3 and assuming that the flux of neutrinos is a power law, it is possible to obtain an analytical expression for the expected number of double pulse events:

$$N_{2P}(\alpha) \simeq \frac{4\pi^2}{10^{1+\alpha}} \times \frac{\bar{A}_{2P}}{m^2} \times F_\tau(\alpha) \times \frac{T}{yr} \times \left(\frac{E_{min}}{PeV}\right)^{\beta-\alpha+1} \Gamma\left(\alpha-\beta-1, \frac{E_{min}}{E_{cut}}\right) \tag{64}$$

where Γ is the incomplete gamma function and the normalization F_τ is equal to the normalization F_μ of Eq.58, as it is expected for neutrinos produced by charged pions decay with few % uncertainty due to uncertainties in neutrino oscillation parameters (see Sec. 3.1.3 for details).

The above expression allows us to investigate the dependence of the expected number of double pulse events on the spectral index α and on the high energy cutoff E_{cut} of the neutrino spectrum. In particular, it makes possible to show that our knowledge of the neutrino spectrum

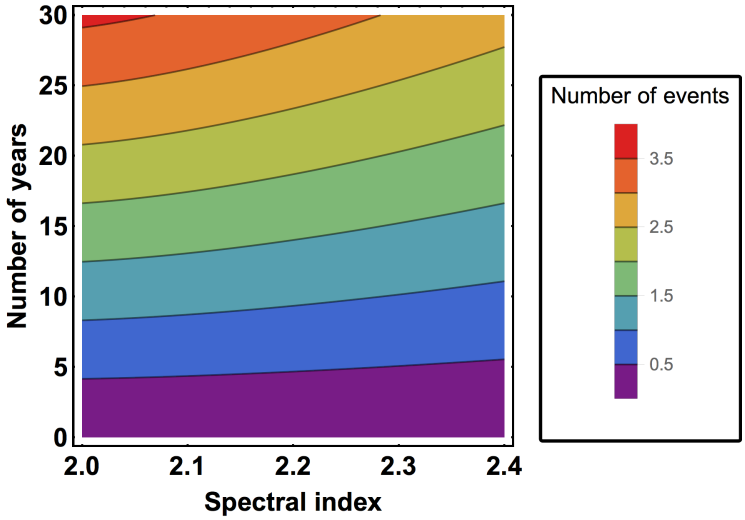

Figure 24: *Expected number of double pulse event as a function of the spectral index and the number of years of data taking.*

is already sufficient to make significative predictions. Let us remark that this expression is general and it can be updated in the future using the new value of the normalization at 100 TeV $F_\tau(\alpha)$, in the units of Eq.50.

The number of double pulse events expected in 4 years of data taking is 0.48, 0.43, 0.36 for $\alpha = 2.0, 2.2, 2.4$, so it is not surprising that IceCube has not detected any double pulse events so far. Our calculations are done by adopting the nominal cutoff energy $E_{cut} = 10$ PeV. However, the predicted values do not dependent strongly on the assumed high energy cutoff. For $\alpha = 2.0$, the counting rate varies indeed by only $\sim 25\%$ when the cutoff energy is varied within the decade $E_{cut} = 5 - 50$ PeV. For larger values of α, the dependence of $N_{2P}(\alpha)$ on E_{cut} is considerably weaker. Considering this aspect and that the normalization of the neutrino spectrum is known with an uncertainty of 30%, the most optimistic expectation for double pulse events after 4 years of data taking is

$$N_{2P} = 0.6 \pm 0.2$$

The dependence of $N_{2P}(\alpha)$ on the spectral index is mainly given by the normalization $F(\alpha)$ of the cosmic neutrino flux at 100 TeV, see Eq.64 . The residual dependence on α is relatively weak and affects the final results at level of few % when $\alpha \in [2.0 - 2.6]$. Considering the best fit to the spectrum of high energy starting events, with $\alpha = 2.5$ and $F = \frac{6.7}{3}$ (see Eq.51), we obtain 0.5 events expected in 4 years.[4] These results are slightly different with respect to what obtained in [3] since in this work we have used a more recent measurement of the neutrino spectrum. Anyway, the conclusions remain very similar, with a difference of few % in the expected number of events.

We show in Fig.24 the expected number of double pulse events as a function of the spectral index and the number of years of data taking. In order to observe a double pulse event in IceCube with a probability larger than 90 %, that corresponds to an expected number of events

[4] The softer spectrum is compensated by the greater normalization at 100 TeV; therefore the expectation is very similar to the expectation obtained in the case of $\alpha = 2$.

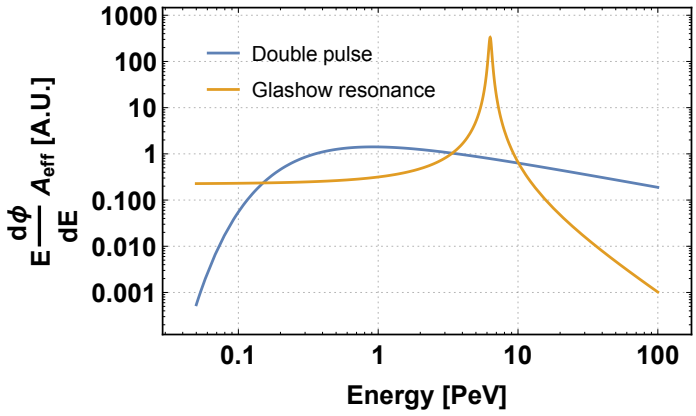

Figure 25: *Parental distribution for double pulse and resonant events, considering a hard spectrum with $\alpha = 2$. Figure from [3].*

equal to 2.3 using Poissonian statistics, we have to wait about 15 years in the most favorable case, i.e. a hard spectrum with $\alpha = 2$.

Fig.25 shows in blue the parental function $E \times \frac{d\phi_\tau}{dE} \times A_\tau^{\text{zp}}$ (in arbitrary units) for double pulses, calculated with $\alpha = 2$. This function is peaked around 0.5 PeV and approximately one half of the double pulse signal is due to neutrinos with initial energy below 2 PeV, i.e. to the energy region already probed by HESE observations in IceCube. In other words, as remarked in [143], the optimal neutrino energy window to see the double pulse events is between 0.1 to 10 PeV. It is important to remark the consequence of this fact:

> assuming cosmic origin, a large fraction of the double pulse events are generated by a parent neutrino spectrum which is already observed by IceCube;

conversely, the lack of observation of double pulse events would have dramatic implications, either on the origin of these events or on the nature of neutrino oscillations.

5.5.2 Glashow resonance-Electron antineutrinos

Using the effective area of the Glashow resonance described in section 4.5.4, we can compute the expected number of resonant events. We focus on the hadronic Glashow resonance, as it results in a signal around 6.3 PeV that can be distinguished from that of deep inelastic scattering (see [3, 5] for more details). For this purpose it is sufficient to multiply the effective area of the Glashow resonance calculated in 4.5.4 by the branching ratio of the hadronic channel, that is equal to $\sim 2/3$.

Using the δ approximation, for the effective area of the Glashow resonance, the expected number of events is given by the following analytic expression:

$$N_{\text{G}}(\alpha) \approx 3.27 \times F_e(\alpha) \times \frac{T}{\text{year}} \times \xi_{\bar{\nu}_e} \times \left(\frac{E_{\text{G}}}{100 \ \text{TeV}} \right)^{2-\alpha} \tag{65}$$

where the factor $F_e(\alpha)$ is equal to $F_\mu(\alpha)$ of Eq.58 (assuming the usual equipartition resulting from neutrinos produced by pion decays and neutrino oscillations), T is the exposure time and $E_{\text{G}} = 6.32$ PeV is the typical Glashow resonance energy.

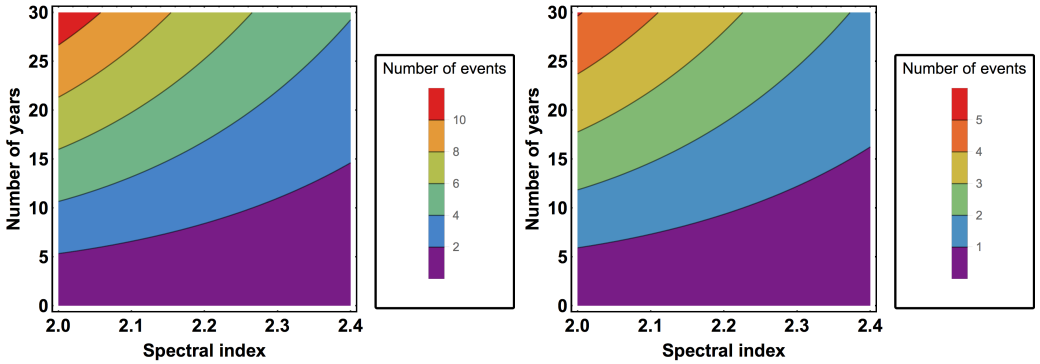

Figure 26: *Probability to observe at least one cascade above 2 PeV as a function of spectral index and number of years of exposure. On the left panel pp interaction at the source, on the right panel $p\gamma$ interaction at the source.*

The parameter $\xi_{\bar{\nu}_e}$ is the fraction of electron antineutrinos in the total flux of neutrinos. In the case of pp interactions, about an equal number of neutrinos and antineutrinos are produced at the source, with a flavor composition $(1:2:0)$. Therefore, after neutrino oscillations, the flavor composition becomes $(1:1:1)$ and the fraction of $\bar{\nu}_e$ is about $1/6$ of the total flux. On the other hand, if the production mechanism is $p\gamma$ and we consider the simplest scenario, only π^+ are produced and there are not $\bar{\nu}_e$ at the source. Taking into account neutrino oscillations and their uncertainties, the fraction of $\bar{\nu}_e$ arriving at Earth with respect to the total flux of neutrinos is given by:

$$\xi_{\bar{\nu}_e} = \begin{cases} \dfrac{1}{6} + \dfrac{P_1}{3} & = 0.17 \pm 0.01 \quad \text{if } pp \text{ source} \\ \dfrac{1-3P_0}{9} + \dfrac{P_1}{3} & = 0.07 \pm 0.01 \quad \text{if } p\gamma \text{ source} \end{cases} \tag{66}$$

where $\xi_{\bar{\nu}_e}$ as a function of P_i is obtained using the natural parametrization described in chapter 3. This extreme scenario maximizes the difference between the signals from pp and $p\gamma$ sources; when we take into account the possibility that some amount of $\bar{\nu}_e$ is also created by $p\gamma$ interactions at the source, the difference diminishes [5].

Anyway we have seen that the contamination of $\bar{\nu}_e$ at the source for $p\gamma$ interaction is dependent on the target photon spectrum, typically around 20-50 % with respect to the flux of ν_e, in the energy range between 1 TeV and 1 PeV (see [23, 25]). In our simplified scenario the two mechanisms give separate predictions for $\xi_{\bar{\nu}_e}$ even if uncertainties on oscillation parameters are included.

The expected number of events, as a function of the spectral index α and the number of years of data taking, is illustrated in Fig.26 for the pp (left panel) and the simplified $p\gamma$ mechanisms. In the assumption of pp interactions at the source, we obtain 1.53, 0.96, 0.55 expected events in 4 years with α =2.0, 2.2 and 2.4 respectively. These numbers are reduced by $\simeq 50\%$ for the simplified $p\gamma$ interactions (see Eq.65 and Eq.66).

The previous results are obtained by assuming an unbroken power law for the neutrino flux in the energy region below 10 PeV. The presence of an energy cutoff below E_G drastically decreases the number of events due to the Glashow resonance. In the opposite case in which the energy cutoff is much larger than 10 PeV the number of Glashow events is not affected, since the cross section is peaked at 6.32 PeV.

Table 9: *Number of double pulses and resonant events expected in 1 year for a power law spectrum, as a function of the spectral index α, using the normalization of the spectrum given in Eq.58. The cutoff of the spectrum is at 10 PeV.*

	Throughgoing muons			HESE
	$\alpha = 2$	$\alpha = 2.2$	$\alpha = 2.4$	$\alpha = 2.5$
Double pulses	0.12	0.11	0.09	0.13
Glashow resonance pp	0.38	0.24	0.14	0.15
Glashow resonance $p\gamma$	0.17	0.11	0.06	0.07

Up to now the resonant events have not been observed by IceCube. Anyway this is not surprising and it does not represent an issue, because, even if we consider a hard spectrum with $\alpha = 2$, the probability to observe zero events with an expectation of 1.53 events is equal to 22% that corresponds to 1.2σ of exclusion. Considering that, once we have fixed the spectral index α, the normalization of the neutrino spectrum is known with an uncertainty of about 30%, the most optimistic expectation for the number of resonant events after 4 years of data taking is

$$N_G \simeq 1.5 \pm 0.5$$

Therefore the non observation of events is disfavored at $1.2 \pm 0.3\sigma$. Considering the best fit spectrum of high energy starting events $\alpha = 2.5$ and $F_e = \frac{F}{3} \simeq 2.23$ (see Eq.51) the expectation worsens and only 0.6 events are expected in 4 years of data taking.

The possibility that the three events with energy above the PeV observed by IceCube are produced by the leptonic channel of the Glashow resonance has been analyzed in [3] and it is disfavored at 3σ, at least.

In order to clarify what is the relevant energy region of the parental neutrino flux contributing to the resonant events, we show in Fig.25, in orange line, the function $E \times \frac{d\phi}{dE} \times A_{\text{eff}}$ (in arbitrary units) using $\alpha = 2$, as was done for double pulse events.

5.5.3 Discussion

In Tab.9 we summarize the expected rate of double pulses and resonant events.

In this section we found that the non-observation of double pulse events does not contradict the hypothesis of a cosmic neutrino population. This conclusion is only marginally dependent on the assumed cosmic neutrino spectrum. In fact, we have shown that:
i) one half of the expected signal is due to neutrinos with energy below $E_\nu = 2$ PeV, i.e. *from a spectral region that is already observed in the HESE data* (see Fig. 25 and discussion in section 5.5.1)
ii) In the most favorable case, with spectral index $\alpha = 2$ *we need to wait about 15 more years to observe a double pulse with a probability greater than 90 %.*

Concerning the resonant events, the absence of events close to the Glashow resonance energy $E_G = 6.32$ PeV is not problematic under this hypothesis, since only ~ 1.6 events are expected due to Glashow resonance after 4 years in the most optimistic hypothesis of pp interaction and hard spectrum with $\alpha = 2$. An exposure time of few more years should be sufficient, in this optimistic case, to observe the first resonant event. Anyway let us remark that even if IceCube will not observe resonant events in the next years this would not necessarily be an issue, since

in the case of soft spectrum $\alpha = 2.4$ and $p\gamma$ mechanism of production more than 30 years are required to observe an event with a probability greater than 90%.

6 ICECUBE SPECTRAL ANOMALY AND GALACTIC NEUTRINOS

Before IceCube, the most popular expectation on high energy neutrinos, typically adopted in sensitivity studies, was that:

1. most of them have an extragalactic origin, as motivated by the existence of many extreme astrophysical objects and of extragalactic cosmic rays [11]. Therefore the spectrum is expected to be isotropically distributed, since many distant sources contribute to it;
2. their spectrum is distributed like E_ν^{-2}, as motivated by the expectations on cosmic rays at the sources and due to Fermi acceleration mechanism. A very well-known implementation was the one due to Waxman & Bahcall [12], where also an estimation of the normalization was calculated. The spectrum of cosmic neutrinos was expected to be above the atmospheric background at some tens of TeV.

After IceCube, these hypotheses has been minimally modified in order to take into account that the observed HESE spectrum does not agree well with E_ν^{-2}. The minimal modification amounts to use single power law $E^{-\alpha}$, isotropic and with $\alpha \sim 2.5$, a value obtained by fitting the observations of IceCube. In this chapter, pluses and the minuses of this position are summarized in Sec.6.1, motivating an alternative and more satisfactory hypothesis to account for the observations of IceCube and to forecast future findings (see Sec.6.2 and 6.3). If the alternative hypothesis is correct, it is premature to dismiss the position described just above, concerning the extragalactic ν signal. Moreover, as we will discuss below, there are a lot of interesting consequences for the astronomy of high energy neutrinos.

This chapter is based on two papers published during the Phd [6, 7].

6.1 CRITICAL DISCUSSION OF THE SINGLE POWER LAW MODEL

To begin with, let us clarify which are the goals of this section.
1) The aim of this section is not to prove wrong the assumption of a single power law $E^{-\alpha}$, isotropically distributed, that is the most commonly adopted one for the analyses of IceCube data. This is still viable at present, if one adopts very conservative criteria, i.e. if one discards some data set or information and/or if one accepts various discrepancies. Our aims are to motivate the reasons of interest toward another hypothesis capable to interpret the IceCube data, illustrating its advantages and its physical interest, deriving its implications, showing that it can be tested with future data.
2) Also the issue of minimality requires additional discussion. The "single power law" hypothesis has two free parameters, the normalization and the slope, that adds only one parameter to the previously adopted hypothesis (the normalization of the assumed E_ν^{-2} flux). However, in

view of the fact that, to date, we lack firm theoretical bases for the interpretation of IceCube observations, we should not exaggerate the heuristic power of mathematical criteria. Moreover, in the simplest version of our model, the spectrum has two components with fixed slopes: one of them behaves as E_ν^{-2}, the other one as $E_\nu^{-2.7}$. Thus the free parameters for the fit are again two, the normalizations of the fluxes.

Now we proceed to a critical assessment of the single power law model for high energy neutrino emission, that, in view of its popularity and of the almost general acceptance at present, can be considered as the *null hypothesis* adopted for the HESE analysis.

6.1.1 Angular anisotropy

The list of the candidate extragalactic sources of ultra-high-energy neutrinos comprises several disparate astrophysical objects, including various classes of active galactic nuclei (AGN) [158, 159] such as BL Lacertae objects [160, 91, 92]; of peculiar galaxies, such as starburst-galaxies [95, 96, 97]; of extreme stellar objects as Gamma ray bursters (GRB) [161, 162]; etc. They differ greatly in physical and observable characteristics. However, a common feature of these objects is an almost isotropic angular distribution in the sky, except for the brightest among them, which could stand out. This is the main reason why it is assumed that, in first approximation, the (supposedly extra-galactic) high energy neutrinos detected by IceCube should be isotropically distributed (we incidentally note that also certain hypothetical sources in the Galaxy, such as the halo, might lead to a similar distribution).

In reference [163] the angular distribution of the events observed by IceCube was analyzed, showing a significant excess of events on the galactic plane. The analysis is repeated with different angular bins and the significance is always larger than 3σ. A similar work is done in ref. [164], where the arrival directions of high-energy neutrinos are discussed, focusing on the possibility that neutrinos are not only extragalactic but they can be also produced in the halo or in the disk of our Galaxy. The result of ref. [164] is that the present data are compatible with a purely extragalactic component, but also a mixed flux (extragalactic plus galactic neutrinos) is well compatible with the data. On the contrary a purely galactic component is disfavored at about 2σ, as can be seen from Fig. 2 of that paper. In Sec.6.2.2, we perform a new independent analysis of the angular distribution, obtaining results which are consistent with those described here.

The angular anisotropy represents the first hint to reconsider the null hypothesis.

6.1.2 Spectral distribution

In this section we discuss the fact that different datasets collected by IceCube suggest different power law distributions. We begin with a brief review of the relevant datasets, pointing out their correspondence to the neutrino fluxes. Then, we will compare the power law distributions, obtained from the different datasets.

THE DIFFERENT DATASETS AND THEIR SUMMARIES AS POWER-LAW DISTRIBUTIONS IceCube has observed two main classes of events, as discussed in Sec.5.1 (see also Appendix D.1 and D.2 for details of the events.). The high energy starting events (HESE), whose vertex is contained in the detector, and the passing muons (aka throughgoing muons, aka tracks) that are the traditional signal of neutrinos. The HESE are divided in two classes: 1) *direction*: those from

the Northern sky and those from the Southern sky 2) *topology*: those of shower type and those of track type. The passing muons instead are all from the Northern sky and all of track type. Note that the experimental sample of HESE North events is not very large, and the subset of HESE North tracks is even smaller; the experimental sample of passing muon events, collected in IceCube, is much larger than the sample of HESE Northern muons. We discuss below and in details which are the specific datasets that we use in the analysis.

The above considerations concern the experimental classification of the data. Passing now to the physical interpretation of these data in terms of neutrino fluxes, it is essential to remark the following:

> the throughgoing muon events, measured in IceCube, give us information on the flux of muon neutrinos and antineutrinos coming from the Northern sky, just as the set of HESE Northern muon events.

Let us recall the well-known fact that neutrino oscillations connect tightly the electron, the muon and the tau neutrino fluxes, and in the particular and natural case of neutrinos coming from pion decay, these fluxes are approximately the same, as we have seen in Sec.3.1.3. Let us finally recall that the inclusion of passing muon data has been important to verify the consistency of the IceCube observations with three flavor neutrino oscillations in the recent past [4]. All these considerations point out the importance of including the passing muons in the analysis.

Comparison of the power law distributions obtained from different datasets

Let us begin recalling the HESE events, already described in Sec.5.1.2. The all-flavor extraterrestrial component of the HESE observed by IceCube, after 4 years of data taking, is fitted by a single power law spectrum, without an energy cutoff, obtaining:

$$\frac{d\phi}{dE} = F \times \frac{10^{-18}}{\text{GeV cm}^2 \text{ sec sr}} \left(\frac{E}{100 \text{ TeV}}\right)^{-\alpha} \tag{67}$$

with [149]

$$F = 6.7^{+1.1}_{-1.2} \quad \text{and} \quad \alpha = 2.50 \pm 0.09$$

However, a careful analysis of the most recent IceCube data reveal a difference between the flux that comes from the Southern sky and the one that comes from the Northern sky. These two subsets of data give the following best-fit fluxes:

$$F_N = 2.1^{+2.9}_{-1.6}, \quad \alpha_N = 2.0^{+0.3}_{-0.4},$$
$$F_S = 6.8^{+1.6}_{-1.5}, \quad \alpha_S = 2.56^{+0.11}_{-0.12}$$

In order to quantify the difference between North and South HESE power-law fluxes we analyze the distribution of their spectral indices, described approximately by two Gaussian functions $g_N(\alpha)$ and $g_S(\alpha)$. Following the procedure reported in the Appendix C.1, a mild tension of 1.3σ between the dataset of HESE North and HESE South, $\delta\alpha = 0.56 \pm 0.42$ is found.

Let us discuss now the passing muons. Since the IceCube experiment is located in the South pole, the passing muons give information on the muon neutrino flux coming from the Northern sky. This information must be consistent with the information from HESE North dataset, that are also generated by neutrinos that come from the Northern sky. Moreover, as already recalled, the passing muons dataset contains a larger number of events than the HESE North

dataset alone, which allows us to obtain stronger inferences. More precisely, comparing the flux obtained by fitting the passing muon data with the flux obtained fitting the HESE seen from the Southern sky results in a much greater tension. In [129] the flux of diffuse astrophysical muons is analyzed and it is found $\alpha_p = 2.13 \pm 0.13$ for the spectral index. This flux is obtained using events in the energy range between 191 TeV and 8.3 PeV but, if the single power law hypothesis were the true one, this flux would be the right one also at lower energies. On the other hand, the dataset of HESE South gives a preference for a softer spectrum, i.e. $\alpha_s \simeq 2.56 \pm 0.12$.

Using the procedure described in Appendix C.1, it is possible to compare the fluxes that describe the various datasets, just as we did above with the fluxes obtained only from HESE data. The results are:

- A discrepancy equal to 2.4σ when we compare the fluxes obtained from the passing muons with the one obtained from HESE-Southern sky, namely $\delta\alpha = 0.43 \pm 0.18$, where $\delta\alpha$ denotes the difference between the spectral indices;
- A similar tension of 2.3σ between the power-law distribution that describes the passing muons dataset and the global best fit of HESE, namely $\delta\alpha = 0.37 \pm 0.16$.
- Compatibility between HESE North and passing muons, namely, $\delta\alpha = 0.13 \pm 0.33$.

These results represent an update of those obtained in [6] with an old dataset of throughgoing muons.

Since the tracks are generated by muon neutrinos[1] and the showers by all flavor neutrinos, the discrepancy may be explained in two major ways,

1. The flux of ν_μ has a different behavior with respect to the flux of ν_e and ν_τ, but there are no theoretical reasons to sustain this point;
2. The Northern sky and the Southern sky are detecting two different population of neutrinos: an almost purely extragalactic component from the Northern sky and a mixed component (galactic plus extragalactic) from the Southern sky.

In conclusion, analyzing the spectral distribution of the fluxes derived by the different datasets it is possible to conclude that there is a difference in the shape of the neutrino flux observed in the Southern sky and of the one observed in the Northern sky, with a significance of at least 2.7σ. Indeed, combining the 1.3σ (HESE North - HESE South) and 2.4σ (Passing muons - HESE South) hints, the overall significance becomes 2.7σ, which means a p-value smaller than 0.7%.

This significance represents the second hint to go beyond the single power law model.

6.1.3 Extragalactic power law neutrinos, protons and γ-rays

In this section we analyze the connections between cosmic neutrino and other radiations, i.e. cosmic rays and gamma. Let us consider a source transparent to protons, as it happens in the model proposed by Waxman and Bahcall [12]. This model predicts an upper bound for the cosmic neutrino flux, connected to the amount of energy of ultra high energy cosmic rays, in the energy interval between $10^{19} - 10^{21}$ eV. Their argument goes as follows: high energy protons, produced by the extra galactic sources, lose a fraction ϵ of their energy through photo-meson

[1] We neglect the contribution of the tracks coming from ν_τ that is of the order of 5% or less, as explained in chapter 4.

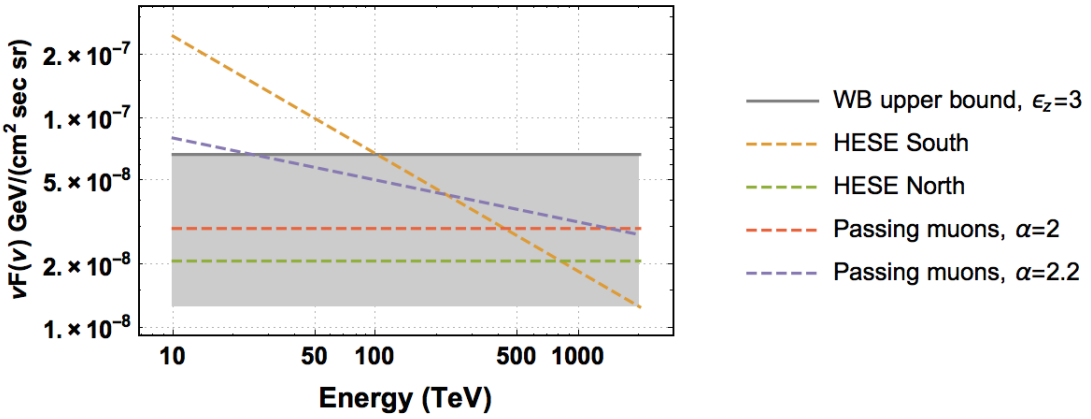

Figure 27: *Comparison between the limit given by a source transparent to ultra-high energy cosmic rays and the power law fluxes that describe the present IceCube data [6].*

production of pions before escaping the source, so that the resulting present day energy density of all-flavor neutrinos will be given by,

$$E_\nu^2 \frac{d\phi}{dE_\nu} \simeq \frac{3}{2}\, \epsilon\, I_{\max} \tag{68}$$

where $I_{\max}$ is given by:

$$I_{\max} = 0.25 \xi_Z t_H \frac{c}{4\pi} E_{CR}^2 \frac{d\dot{N}_{CR}}{dE_{CR}} \simeq 1.5 \times 10^{-8} \xi_Z \text{ GeVcm}^{-2}\text{s}^{-1}\text{sr}^{-1} \tag{69}$$

where ξ_Z is connected with cosmology and takes into account the energy loss of neutrinos at redshift different from 0 and the upper bound is obtained for $\epsilon = 1$, i.e. when all the energy of protons is transferred to pions. The numerical value of $I_{\max}$ is obtained using $E_{CR}^2 \frac{d\dot{N}_{CR}}{dE_{CR}} = 10^{44}\text{ergMpc}^{-3}\text{yr}^{-1}$. The comparison of this model to the fluxes, that have been derived by IceCube using the 4 years dataset, is illustrated in Fig. 27. The bands related to the fluxes are due to the uncertainties on the normalization and on the slope. The upper limit is given by,

$$\phi + \Delta\phi = \phi + \sqrt{[\phi(F,\alpha) - \phi(F^+,\alpha)]^2 + [\phi(F,\alpha) - \phi(F,\alpha^+)]^2} \tag{70}$$

where ϕ is the flux at best fit, $F^+ = F + \Delta F$ and $\alpha^+ = \alpha + \Delta\alpha$ if $E_\nu < 100$ TeV or $\alpha^+ = \alpha - \Delta\alpha$ if $E_\nu > 100$ TeV. With the same procedure, the lower limit $\phi - \Delta\phi$ is obtained. The values of F, α and their uncertainties are reported in section 6.1.2.

The two fluxes derived from the HESE-Northern sky and from the passing muons dataset are compatible with the Waxman-Bahcall model. On the other hand, the HESE-Southern sky data begin to show some critical behavior below 60-70 TeV, because they exceed this limit. Note that in this region, a lot of events were already observed, so it cannot be a problem attributed to the low statistic. To have a more precise idea, let us use the flux derived by the IceCube collaboration in [149], which includes events above 10 TeV. The energy flux of HESE from the Southern sky at 25 TeV is equal to:

$$E^2 \frac{d\phi_s}{dE}(25\text{ TeV}) = 1.5 \pm 0.4 \times 10^{-7}\, \frac{\text{GeV}}{\text{cm}^2\text{ s sr}} \tag{71}$$

This means that the Waxman and Bahcall limit is violated at 2σ at that energy and the violation is even larger at lower energies: in fact, the same spectral shape should extend also at lower energies, if the hypothesis of single power law holds true. Once again, these considerations suggest to reconsider some of the assumptions. Recent analyses on the connections between high energy neutrinos and cosmic rays have been performed in [165, 166].

Another connected remark emerges comparing the flux of neutrinos with the IGRB (isotropic gamma-ray background). The first step in this direction was done by Murase et al. [167][168], using the two years dataset of IceCube events. In this work the pp scenario is considered and the neutrino flux is compared to the diffuse γ-ray background flux measured by Fermi. A strong upper limit on the spectral index of the source of neutrinos it is obtained, i.e. $\alpha \leq 2.2$. A softer spectrum would give an excess of neutrinos with respect to the γ-ray in the 100 GeV region, contradicting the theory. In Bechtol et al.[99] this kind of analysis is performed using more recent data. The extrapolated flux of neutrinos exceeds the flux of gamma around 0.1 TeV, even in the most conservative hypothesis in which the extrapolated flux follows an E^{-2} spectrum. This excess represents a problem in the scenario of star-forming galaxy, where the pp interaction is the dominant mechanism for the neutrino production. Moreover the γ-rays are not absorbed in that energy region, even if they come from distance of some Gigaparsec.

The above remarks are our last hint that the null hypothesis requires some critical consideration. The previous issues, concerning the comparison of power law distributed neutrinos with protons and γ-rays, can indicate some of the following possibilities:
i) an exotic source of neutrinos (e.g. exotic dark matter);
ii) absorption of protons and/or gammas in the source[2];
iii) a galactic component of neutrinos on top of the extragalactic one.
In this chapter we will explore the last option. It should be stressed that the limit on the neutrino flux, given by the comparison with cosmic rays and IGRB, applies only on the extragalactic component.

6.2 THE νgal1 MODEL

Considering the hints of the previous sections, we explore the hypothesis that from the Northern sky comes an almost purely extragalactic flux of neutrinos, whereas from the Southern sky come both extragalactic and galactic neutrinos. This hypothesis can justify the spectral differences in the IceCube dataset *and* the angular anisotropy of the observed events. Moreover this hypothesis "recovers" the upper limit of Waxman and Bahcall [12], that is in strong disagreement with the IceCube global fit already at $\simeq 100$ TeV. At the same time, it solves the problems arising from the comparison with the IGRB, discussed just before. Let us refer to the two component model with the term νgal1. Later in this chapter we introduce a variant of this model, called νgal2.

6.2.1 General motivations

The hypothesis of a Galactic component is motivated by the position of the Earth in the Galaxy and by the location of IceCube detector. Let us begin with a standard model for the Galaxy, i.e.

[2] It could happen especially in the $p\gamma$ mechanism of production, because the γ-rays produced by the decay of π^0 can interact with the target photons contained into the source and can be trapped into the source. In this kind of opaque source the connection with neutrinos can be difficult, as discussed in [22].

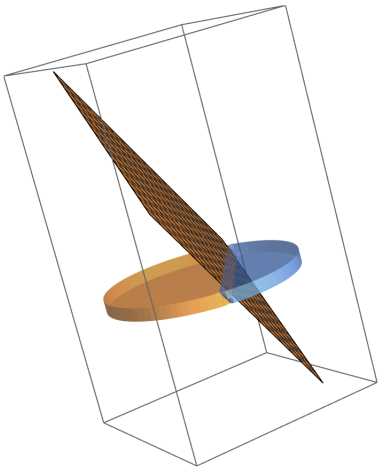

Figure 28: *A simplified cylindrical model of the Galaxy. The relative orientation of Earth's equatorial plane (orthogonal to rotation axis) is also shown, being blue the Northern sky and orange the Northern sky [6].*

a cylinder of radius 15 kpc and a variable height of some kpc. The axis of rotation of the Earth forms an angle of 30° with respect to the galactic plane, so that the equator of the Earth makes an angle of 60° with it. The equator is represented by a plane, perpendicular to the normalized vector $(u_x, u_y, u_z) = (0.484, 0.747, 0.456)$. Imposing the condition that the plane includes Earth, that is at 8.5 kpc from the center of the Milky Way, the equation of the plane is obtained. At this point it is easy to evaluate the volume of the Galaxy seen by the Northern sky and the one seen by the Southern sky; the result is about 70% from the South and 30% from the North (see Fig.29.)

In addition to this, one can take into account that matter is not distributed uniformly, as it can be seen, e.g., from Fig. 2 of [36]. This is another good reason to believe that the Southern sky contains also a galactic component of neutrinos, that is on the contrary negligible from the Northern sky.

However, the above modeling is good only for a cursory exploration and to obtain a first idea. The region where the Galactic neutrino emission is more intense is not known a priori and should be eventually measured by neutrino observatories. E.g. it is natural to modify and extend the above model of the region where neutrino emission is more intense, by adding two parameters: the radius of the cylinder and its galactic height.[3] Of course if the radius of such region is much smaller than the distance between Earth and Galactic center, $R \sim 8.5$ kpc, all the emitting region will lie in the Southern hemisphere. The values of these parameters have to be obtained from the analysis of high energy neutrino data.

Note incidentally that the Fermi satellite detects an intense, diffuse galactic emission up to 100 GeV (see Fig.7). At higher energies, closer to those explored by neutrino telescopes, HESS has proved that the galactic γ-rays emission due to point like sources is quite intense; a diffuse galactic component at high energy, unfortunately, is not yet probed and hard to be probed. In short, the existing gamma ray data indicate the existence of a significant component of the high energy radiation that can be attributed to the Galaxy, and this consideration does not contradict

[3] An alternative parameterizations uses two exponential distributions $n_\nu \propto \exp(-r/\delta r)\exp(-|h|/\delta h)$ where r is the distance from the Galactic center and h is the Galactic height; δr and δh are model parameters.

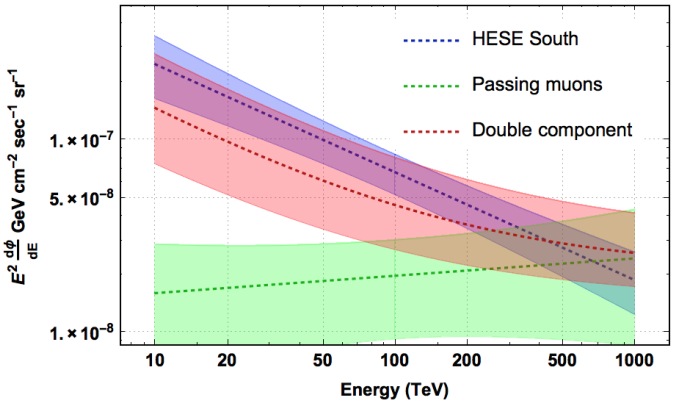

Figure 29: *Comparison between the fluxes measured by IceCube from the Northern sky [169] and Southern sky [149] with the* νgal1 *model [6].*

(but rather supports) the hypothesis that something similar happens for high energy neutrinos. We will come back on these considerations later on.

6.2.2 The Galactic component

Spectrum and intensity of the galactic component

Let us assume that IceCube is observing two populations of neutrinos. It seems natural to describe the neutrinos coming from the Northern sky, that are likely to be extragalactic, with an unbroken power law, distributed isotropically over the sky. Moreover, it becomes natural to describe the observations of IceCube by adding a new power law flux in the Southern sky, in which the galactic population of neutrinos gives an important contribution.

The specific choice of spectra, discussed below, defines the specific model called νgal1. For the extragalactic component, the spectral index $\alpha = 2$ is adopted, since it coincides with the best-fit value obtained for the Northern sky HESE flux. For the galactic component, the spectral index $\alpha = 2.7$ is adopted, i.e. the spectral index of the galactic cosmic rays flux. It follows that:

$$\begin{aligned} \frac{d\phi_{\rm N}}{dE_\nu} &= \frac{d\phi_{\rm EG}}{dE_\nu} \\ \frac{d\phi_{\rm S}}{dE_\nu} &= \frac{d\phi_{\rm G}}{dE_\nu} + \frac{d\phi_{\rm EG}}{dE_\nu} \end{aligned}$$

or more explicitly:

$$\frac{d\phi_{\rm N}}{dE} = F_{\rm EG} \left(\frac{E}{100\ \text{TeV}}\right)^{-2} \times \frac{10^{-18}}{\text{GeV cm}^2\ \text{sec sr}} \tag{72}$$

$$\frac{d\phi_{\rm S}}{dE} = \left[F_{\rm G} \left(\frac{E}{100\ \text{TeV}}\right)^{-2.7} + F_{\rm EG} \left(\frac{E}{100\ \text{TeV}}\right)^{-2}\right] \times \frac{10^{-18}}{\text{GeV cm}^2\ \text{sec sr}} \tag{73}$$

Considering the events with deposited energy above 60 TeV,[4] IceCube has detected 32 events in 4 years, 9 from the Northern sky, 22 from the Southern sky and one at latitude zero. Using the

[4] Following [4] we limit the analysis to this subset of data, where the atmospheric background gives a small contribution.

Table 10: *Comparison between the νgal1 model and the events from the Southern sky with deposited energy above 60 TeV of the 4 years dataset of IceCube. For the galactic and the extragalactic components the best-fit value are used, see Eq. 76. For the prompt neutrinos the number of events is quoted at 90% C.L. and the best-fit value is 0. Table from [6].*

	Gal. $E^{-2.7}$	Extragal. E^{-2}	Backg.	Prompt	Expected	Observed
Tracks	1.2	2.5	1.5	<0.8	5.2	4.5
Showers	6.5	10.1	0.5	<3.1	17.2	18
Total	7.7	12.6	2.0	<3.9	22.3	22.5
Fraction	34.5%	56.5%	9%			

effective areas for each hemispheres, which recently became available on the IceCube website [5], the likelihood functions for the extragalactic and the galactic normalizations (F_{EG}, F_G) can be obtained. The likelihood for the normalization at 100 TeV of the flux from the Northern sky, is defined as:

$$\mathcal{L}_{EG}(s) \propto (b + 3.6s)^{9.5} \cdot \exp[-(b + 3.6s)] \tag{74}$$

where $b = 2.1$ is the background due to conventional atmospheric neutrinos, considering the best-fit value[6]. The coefficient 3.6, instead, is the number of events expected in the case of normalization equal to one at 100 TeV. The result is $F_{EG} = 2.1^{+1.1}_{-0.6}$ at 68% of confidence level. This extragalactic component is perfectly compatible with the upper limit given by the IGRB observed by Fermi (see [99]). Let us remark that we are using the HESE both for the North and South hemisphere, because for this dataset the effective areas are available and we can perform our calculation using $\alpha = 2$ for the extragalactic component.

Taking into account the uncertainties given by the supposed extragalactic component, the likelihood for the normalization at 100 TeV of the galactic component, seen from the Southern sky, is given by:

$$\mathcal{L}_G(s) \propto \int_0^\infty (b + 6.0 s_{EG} + 3.1 s)^{22.5} \cdot \exp[-(b + 6.0 s_{EG} + 3.1 s)] \cdot \mathcal{L}_{EG}(s_{EG}) ds_{EG} \tag{75}$$

where the background is the same as before and the coefficients 6.0 and 3.1 are the expected number of events from the Southern sky in the case of normalization equal to one at 100 TeV, respectively for spectral index $\alpha = 2$ and $\alpha = 2.7$. The result is $F_G = 2.5^{+2.4}_{-1.3}$ at 68% confidence level. Summarizing, with the present informations, the best fit flux obtained using the νgal1 model is:

$$\frac{d\phi_S}{dE} = \left[2.5 \left(\frac{E}{100\ \text{TeV}}\right)^{-2.7} + 2.1 \left(\frac{E}{100\ \text{TeV}}\right)^{-2}\right] \cdot 10^{-18} \frac{1}{\text{GeV cm}^2 \text{ sec sr}} \tag{76}$$

In Fig. 29 this flux is compared to the fluxes from Northern and Southern sky measured by IceCube. We show in Fig.29 only the flux that describes the passing muons that, as discussed above, has a much smaller uncertainty than the flux that describes the HESE from Northern sky, and it is perfectly compatible with the latter. In that figure we have used the flux of

[5] `https://icecube.wisc.edu/science/datalanding`

[6] We scaled with time the expectation for the backgrounds contained in [151]. We are not considering the component produced by atmospheric prompt neutrinos in the νgal1 model, because it is zero at the best fit. Anyway, this will be considered in the νgal2 model.

throughgoing muons contained in [169] that is a bit harder than the most recent measurements of [129]; however the result remains unchanged.

The red band is simply obtained propagating the uncertainties on the normalization, since the shape is fixed. From this figure, the following two features are evident: at low energies, there is good agreement between the two-component flux and the flux measured from the Southern sky. At high energy, instead, there is a good agreement between the two-component flux and the flux measured from the Northern sky.

Using the best fit values, the number of events from the Southern sky due to the extragalactic component is 12.6 (56.5%), whereas the number of events due to the galactic component is 7.7 (34.5%). The sum of these two quantities is different from 100% due to the atmospheric background, that is small but present. The expected number of events are calculated using Eq.52 and the IceCube effective areas A^s_ℓ of the Southern sky, and the fluxes found in this section, separating the contribution of the extragalactic and galactic component as follows:

$$N_{\rm EG,G} = 2\pi\ {\rm T} \int_0^\infty \frac{1}{3} \frac{d\phi_{\rm EG,G}}{dE} [A^s_e(E) + A^s_\mu(E) + A^s_\tau(E)] dE \tag{77}$$

where T=4 years is the exposure time of HESE dataset that we are considering. Let us notice that we are using a factor 2π instead of the factor 4π used in Eq.52, because here we calculate only the expectation for Southern hemisphere. We assume that the flux of each flavor is $1/3$ of the total flux, as expected to a good approximation for a production mechanism due to pion decay and for the subsequent neutrino oscillations.

Due to the large uncertainties on the extragalactic component, i.e. the flux from the Northern sky, the normalization of the galactic component (at 100 TeV) can fluctuate in the interval 1.2 - 4.9, giving a contribution between 17% and 67% to the number of events observed from the Southern sky. In table 10 the number of events from the Southern sky observed by IceCube in 4 years is compared with theoretical prediction of the two-components neutrino flux.

Angular distribution of IceCube events

In our hypothesis, a large fraction of the low energy events seen by IceCube have to come from a region close to the Galactic disk. As a primary test we study the angular distribution of the HESE events detected by IceCube in the Southern sky, that is the region where galactic events are supposed to lie.

We begin by describing the model for the angular distribution. We use the galactic coordinates b (latitude) and ℓ (longitude) to identify the events, and consider the distribution in the variable

$$x = \sin(b) \tag{78}$$

First of all, we are interested in considering one population of galactic neutrino events characterized by a small galactic latitude and localized mostly in the Southern sky. We assume the (normalized) differential distribution,

$$\lambda(x) = \frac{e^{-\frac{x^2}{2\delta x^2}}}{\sqrt{2\pi}\ \delta x} \text{ with } \delta x = \sin 10^\circ \tag{79}$$

where we have fixed the value of angular extent of this population, δx, due to the angular resolution for shower events in IceCube. For isotropic events instead, we expect a flat distribution in x but localized in the Southern sky. So we have, $dN/d\Omega = \Theta(\mathbf{su})/(2\pi)$, where $d\Omega =$

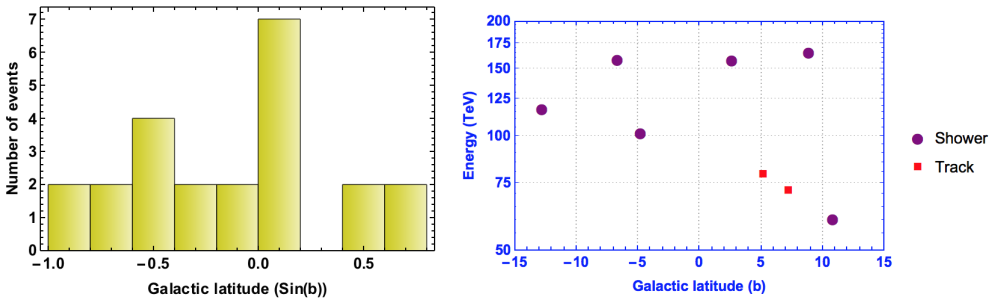

Figure 30: *Two presentations of events seen by IceCube in the Southern sky and with deposited energy above 60 TeV. In the left panel we show the galactic latitude of all events. In the right panel we show those with energy below 200 TeV and in the region close to the Galactic plane. Figure from [6].*

$d\ell\ d\sin(b)$, Θ is the Heaviside function, $\mathbf{u} = (\cos b \cos \ell, \cos b \sin \ell, \sin b)$ is the direction of the event in galactic coordinates, $\mathbf{s}$ is the direction of the celestial South pole.[7] Integrating $dN/d\Omega$ over ℓ we get

$$\mu(x) = \frac{1}{\pi} \mathrm{Re}\left[\arccos\left(-\frac{x}{\sqrt{1-x^2}} \times \tan(b_{\mathrm{CS}})\right)\right] \text{ with } \tan(b_{\mathrm{CS}}) = -0.512 \tag{80}$$

We can use the normalized angular distribution

$$\rho(x, f) = f\ \lambda(x) + (1-f)\ \mu(x) \text{ with } 0 \leq f \leq 1 \tag{81}$$

to model the cases in which one or both components are present, depending on the value of the fraction of events due to the galactic component, f.

The data of IceCube (of which we present some graphical summaries in Fig. 30) can be compared with this model. Hereafter we report our results: a) fitting the data, using the χ^2 described in the Appendix C.2, we find $f = 0.26 \pm 0.15$. This is consistent with the previous independent result, obtained using the spectral information, that gave $f = 0.35^{+0.32}_{-0.18}$. Note that with the angular analysis the uncertainty decreases;
b) we have tested the goodness of fit (see Appendix C.3) for the three hypothesized angular distributions: 1) the extragalactic (isotropic) distribution 2) the purely galactic (low latitude distribution) 3) the mixed model (with both components). It should be noted that the model with mixed composition is not the result of a fit to the angular data, but it is determined independently from the fit of the energy spectrum. We find that all statistical tests in Fig. 31 give very similar results. A purely galactic component can be excluded. On the other side, *both the isotropic and the mixed model are compatible with the data, although the model with two components fares better*. The results of the hypothesis tests are reported in the table of Fig. 31, as well as a plot of the different cumulative distributions, which are compared with the experimental one;
c) Finally, we note that our hypothesis implies a correlated angle-energy distribution in IceCube, namely a large fraction of the low energy events seen by IceCube in the Southern sky have to come from a region close to the Galactic disk. The distribution of the data, given in Fig. 30, shows that this is indeed the case. In fact, there are 8 events below 200 TeV *and* with $|b| < 15°$. This is not so far to the expectation of 7.7 events, that one reads from Tab. 10.

[7] Its galactic latitude b_{CS} equals the declination of galactic South (in equatorial coordinates) $b_{\mathrm{CS}} = \delta_{\mathrm{GS}} = -27.13°$.

Isotropic	Statistic	P-Value
Anderson-Darling	0.900633	0.411712
Cramér-von Mises	0.179197	0.311676
Kolmogorov-Smirnov	0.164302	0.51163
Kuiper	0.205025	0.452628
Pearson χ^2	8.65217	0.278602
Watson U^2	0.10093	0.276265

Galactic	Statistic	P-Value
Anderson-Darling	18.8361	0.0000260885
Cramér-von Mises	0.657672	0.0161494
Kolmogorov-Smirnov	0.364958	0.00297431
Kuiper	0.489583	0.0000275405
Pearson χ^2	24.6522	0.000874378
Watson U^2	0.513828	0.0000619517

Mixed	Statistic	P-Value
Anderson-Darling	0.218436	0.984587
Cramér-von Mises	0.0293979	0.978104
Kolmogorov-Smirnov	0.0876799	0.987639
Kuiper	0.116734	0.968333
Pearson χ^2	2.3913	0.935057
Watson U^2	0.0266726	0.975217

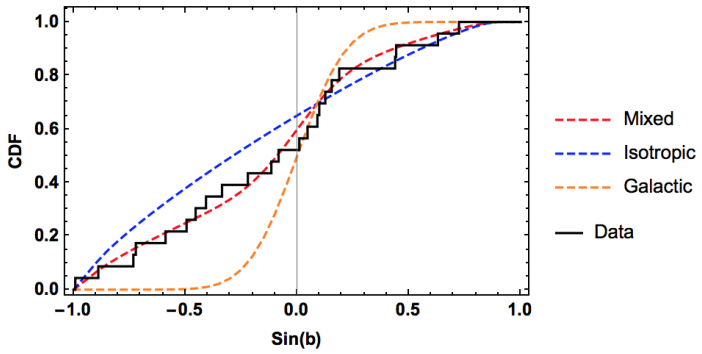

Figure 31: *Results of different hypothesis tests for isotropic, galactic and mixed model. In the bottom of the panel, the comparison between cumulative density function of the three models and data of Southern sky above 60 TeV. Figure from [6].*

Summarizing, we have performed various independent tests and analyses of the angular distribution of the events observed by IceCube. Our results are slightly more conservative but consistent with those obtained by [164] and do not contradict the ones of [163], see Sect. 6.1.1. The main findings are three:

- the angular distribution of the Southern sky (HESE) events is in excellent agreement with the hypothesis of a two-component distribution, formulated previously;
- a purely extragalactic (isotropic) distribution cannot be excluded by the existing observations of the angular distribution;
- the fraction of galactic neutrino events can be independently determined using only the energy spectra or using only the angular distribution: the two determinations are in agreement, and the second method gives a better estimation of the galactic contribution, because the uncertainty is smaller.

The interest to significantly increase the present statistics is quite evident.

6.3 THE νgal2 MODEL

The main aim of this section is to generalize the model described in the previous section (that we called νgal1). We motivate and introduce a new model, denoted as νgal2. This model still assumes that the main component of the IceCube cosmic neutrinos is of extragalactic origin, with the presence of an important Galactic contribution. The model νgal2 tries to address the following important questions:

1. How crucial is the choice of the spectral index of the Galactic component? What happens if it is closer to the one indicated by observations of γ-rays and some models of cosmic ray propagation, i.e. $\alpha \approx 2.4 - 2.6$?
2. What happens changing the normalization of the Galactic component?
3. What is the effect of atmospheric prompt neutrinos from charm decay?

We derived the νgal2 model after exploring these questions, quantifying the expectations and considering constraints, and assessing the stability of its predictions. Moreover we also provide theoretical considerations to support our choices in the multi-component model. This section is mainly based on [7].

6.3.1 Considerations on the high energy neutrino spectrum

The spectral index of extragalactic neutrinos. Theoretical inference

A hard energy spectrum $\approx E^{-\alpha}$ for extragalactic neutrinos, with $\alpha \approx 2.0$, is motivated by models of cosmic rays production at the source in the framework of the Fermi acceleration mechanism. A very well-known case is the generic model developed in Waxman & Bahcall [12], where the neutrino spectrum is assumed to have $\alpha = 2.0$. Note that this assumption was used in the first IceCube fits [133].

Similar results have been obtained in other specific models. E.g., the shape of the extragalactic component in the starburst galaxies model of [95] is

$$\frac{d\phi}{dE} \propto E^{-2.15\pm0.1} \tag{82}$$

and this extends up to 0.3 PeV at least. A generic bound, $\alpha < 2.1 - 2.2$, was derived by the authors of [167], assuming hadro-nuclear (pp) scenarios for neutrino production. Also in very different models, as [92, 89], based on the hypothesis that the neutrino sources are (some types of) BL Lac/blazars, the power spectrum of the extragalactic neutrino component has a very hard spectral index, close to $\alpha \approx 2$. The latter kind of models is apparently motivated by the Fermi-LAT measurements obtained at much lower energies and extrapolating the Fermi measurements by several orders of magnitude. See [170] for a principled discussion of the expectations from $p\gamma$ sources, in which different target photon distributions are considered.

According to the previous theoretical and experimental arguments, the spectral index of the extragalactic component is reasonably expected in the conservative (wide) range

$$\alpha_{\rm EG} \in [1.9\ ,\ 2.3] \tag{83}$$

The information on the flux normalization coming from theoretical models is more uncertain; simple models for neutrino production, e.g., in inner jets of AGN [171] or in collimated jets inside progenitors of gamma-ray bursts and supernovae [172] seem to be not able to explain the IC signal. We use the IC data themselves to constrain the normalization of the extragalactic flux, as it will be explained in Sect.6.3.2.

Expectation on the Galactic component

Here we discuss the core of the νgal2 model, namely the component attributed to Galactic neutrinos, defined by its spectral index and its normalization.

THE SPECTRAL INDEX OF THE GALACTIC COMPONENT Cosmic rays up to few PeV arrive at Earth with a power-law distribution with $\alpha \approx 2.7$. This is thought to be the result of a harder injection spectrum, modified after the propagation inside the Galaxy. However, neutrinos are plausibly produced in collisions close to their cosmic sources and, in this case, they should reflect the injection spectrum. According to this physical picture, neutrinos should have a spectrum harder (i.e. flatter) than $\alpha \approx 2.7$.

There are several attempts to estimate the Galactic neutrino flux. Two theoretical estimations [173, 174] find an interesting level of the diffuse neutrino flux from the Galactic plane: in both cases the power-law approximation of this flux, $\phi \propto E^{-\alpha}$ has a spectral index $\alpha = 2.5 - 2.6$ in the region from some 10 of TeV up to several hunderds of TeV.

A phenomenological model characterized by radially dependent cosmic-ray transport properties has been recently used to compute the γ-ray and neutrino diffuse emission of the Galaxy [175]. The model, designed to reproduce both Fermi-LAT γ-ray data and local cosmic ray observables, naturally reproduces the anomalous TeV diffuse emission observed by Milagro in the inner Galactic plane. Above 100 TeV it predicts a neutrino flux with a spectral index $\alpha \approx 2.4 \div 2.5$ that is about two to five times larger than the neutrino flux obtained with conventional models in the Galactic Center region. This neutrino flux explains up to 25% the flux measured by IceCube.

Moreover, the spectral index of the γ-ray emission, observed at lower energies from the Milky Way, resembles $\alpha \approx 2.4 - 2.6$ more than $\alpha \approx 2.7$. This can be seen from the right panel of Fig. 36, where we compare a neutrino spectrum with spectral index $\alpha = 2.4$ with the gamma rays seen by *Fermi*-LAT.

According to the above arguments, the spectral index of the Galactic component can be assumed to be in the range:

$$\alpha_{G} \in [2.4\ ,\ 2.7] \tag{84}$$

that does not overlap with the corresponding range for the extragalactic neutrinos. Moreover, in order to maximize the difference with the assumptions of νgal1 model, but keeping in mind the above theoretical and observational indications, we will assume the extremal value $\alpha_{G} = 2.4$.

THE NORMALIZATION OF THE GALACTIC COMPONENT The normalization factor of the Galactic neutrino flux is poorly constrained by theoretical models, although experimental indications of a non zero value exist. Apart from the mentioned IceCube spectral anomaly, the first hint arises from the intense flux of γ-rays observed by *Fermi*-LAT and Agile, coming from the Galactic plane and its surroundings. Assuming that a fraction of the signal is due to hadronic processes, a comparable flux of high-energy neutrinos is foreseen. Second, the angular distribution of HESE is compatible with the isotropy, but the assumption of a certain degree of anisotropy near to the Galactic plane improves the agreement with the observations [164, 6].

Fig.32 shows the position on the sky (Galactic coordinates) of HESE. To reduce the atmospheric background, only events with deposited energy > 60 TeV are used. The angular precision of shower events is $\sim 15^{\circ}$. Events with $|b| \leq 15^{\circ}$ are compatible to be originated in the Galactic plane.

Referring to Fig.32, there are 18 events in the region $|b| > 15^{\circ}$. The solid angle covered by this region is approximatively three times larger than the corresponding region with $|b| \leq 15^{\circ}$. Thus, roughly six events are expected in the low longitude region assuming an isotropic detector response. The 14 observed events represents a $\sim 2\sigma$ excess with respect to this hypothesis.

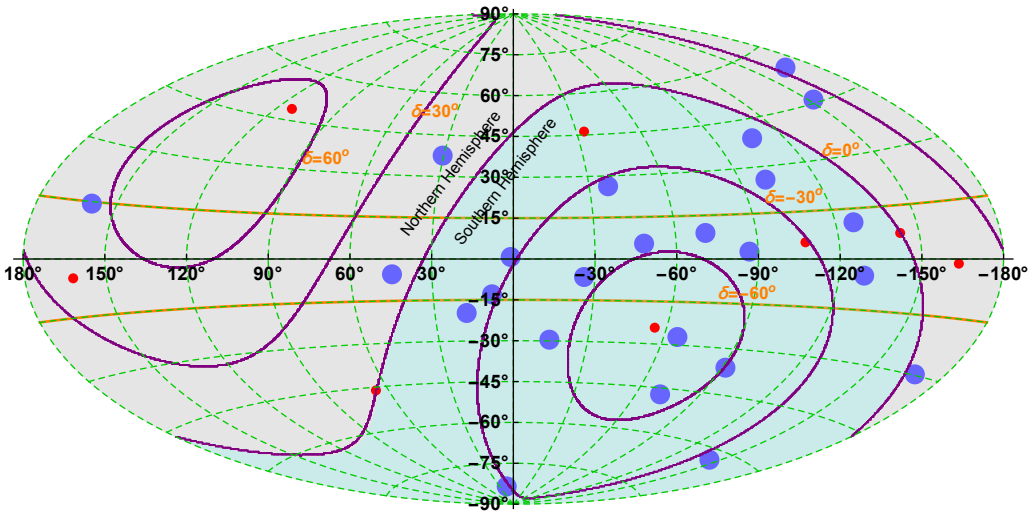

Figure 32: *Distribution of the position of HESE (blue: shower events; red: tracks) with deposited energy* > 60 *TeV represented in Galactic coordinates. The angular uncertainties are not represented; the shower-like events have an angular uncertainty of* $10^\circ - 15^\circ$*, whereas the track-like events have an angular uncertainty of about* 1°*. Figure from [7].*

These experimental hints supporting the existence of a Galactic component are discussed in different ways in several works [176, 163, 6, 173, 177]. E.g., the paper [177] finds that it is theoretically possible to have similar signals in IceCube. Their model called *Case C* predicts 1 event per year, using using the assumption that the diffusion coefficient of Galactic cosmic rays is not uniform into the Galaxy but it changes as a function of the distance from Galactic center.

Thus, we will explore the hypothesis that the Galactic neutrino emission yields an observable signal, namely, few HESE events per year in IceCube. As for the case of the extragalactic flux, we extrapolate the normalization of the Galactic component from the data itself.

THE SPATIAL EXTENSION OF THE GALACTIC COMPONENT The Galactic flux has been considered isotropic and has been seen only from the Southern hemisphere in the νgal1 model. This is a minimal hypothesis, useful to evaluate the total number of HESE of Galactic origin. Models explaining the IceCube excess in the 10-100 TeV range in the Southern sky in term of decaying or annihilating dark matter candidates [178] can yield different signatures and are not considered in the following.

A more detailed scenario considers also the spatial extension of the Galactic component, taking into account observational constraints derived from the ANTARES [134] neutrino telescope. In particular, as discussed in Sec.6.3.3, the Galactic neutrino flux is assumed to be isotropic within a region (in Galactic coordinates) of latitude $|b| \leq b^*$ and longitude $|\ell| \leq \ell^*$. The values b^* and l^* will be discussed later in Sec.6.4.2.

Prompt neutrinos

Even if a component in the atmospheric neutrino originating from the prompt decay of very heavy mesons (typically containing a charm quark) is expected from standard cosmic ray interactions with atmospheric nuclei, this flux of *prompt neutrinos* is not yet measured. Let us recall that the spectrum of prompt neutrinos is expected to be $E^{-2.7}$ and the flavor composition is expected to be $(\nu_e : \nu_\mu : \nu_\tau) \approx (1 : 1 : 0)$ (see Sec.5.1.3) for the discussion on the atmospheric backgrounds.

IceCube has recently investigated the existence of a prompt component in the measured ν_μ [129] in the region of energy below few 100 of TeV. From the absence of evidence, 90% C.L. upper limit on the normalization predicted by the reference calculation [150] (denoted as ERS) is set to $0.50\times$ ERS. More recent calculations predict smaller fluxes [179, 180, 181], that are not yet significantly probed instead.

Differently from the νgal1 model, here we assume the existence of a prompt neutrino component in addition to cosmic neutrinos. In order to maximize the effect of the contribution from prompt neutrinos without exceeding severely the constraints from theory and observations, we will assume as normalization term the 90% c.l. upper limit $0.50\times$ ERS set by IceCube.

6.3.2 The recipes

Here we summarize the result of the discussion of the previous sections to define the νgal2 model. Besides the conventional atmospheric neutrinos, we consider three other components: the isotropic extragalactic component, the diffuse Galactic component (presumably enhanced near the Galactic plane) and the prompt (atmospheric) neutrinos. In addition:

1. We use the IceCube measurement of the flux of passing muons to describe the extragalactic component $\phi_{\rm EG}$. The flux is assumed to be isotropic, with a normalization known within 30% and the spectral index within $\approx 6\%$. We assume that the total extragalactic neutrino flux is given by the spectrum of throughgoing muons reported in section 5.1 multiplied by a factor of three, in order to account for the three neutrino flavors. At the highest energies, this component is the dominant one;

2. We assume the existence of a diffuse Galactic component $\phi_{\rm G}$, mainly originating from the Southern hemisphere. This Galactic component produces the observed asymmetry between HESE South and HESE North, and between HESE and the passing muons, softening the spectrum of Southern sky below $\approx$ 100 TeV. We assume (Sect. 6.3.1) that its spectral index is $\alpha_{\rm G} = 2.4$.

   We estimate the normalization factor for the Galactic component considering the *angular distribution* of the HESE events arising from the Southern sky, and more precisely, the distribution in the Galactic latitude (see the νgal1 model and Sect. 6.3.1). From that analysis we found that a fraction 0.26 ± 0.15 of the 23 HESE observed from the Southern hemisphere, with deposited energy above 60 TeV, can be of Galactic origin. It follows that our normalization is chosen to reproduce the expected number of Galactic HESE, i.e.

   $$N_{\rm G} = 6.0 \pm 3.5 \text{ in } 4 \text{ years} \tag{85}$$

   This assumption is compatible within errors with that used for the νgal1 model and it does not exceed the diffuse flux limit derived from the ANTARES neutrino telescope

Table 11: *Summary of the number of HESE events expected for each component in four years. The μ background and the conventional background are taken from [151] and scaled with the exposure time. The other predictions are obtained using the fluxes derived here in Eq. 87 (νgal2 model) and the published effective areas of HESE [133]. Table from [7].*

Component	North	South	Sum
Extragalactic [129]	8.8 ± 1.7	$16.1^{+1.5}_{-1.9}$	$24.9^{+3.2}_{-3.6}$
Galactic [6]	≈ 0	6.0 ± 3.5	6.0 ± 3.5
Prompt [129, 150]	1.5 ± 0.8	2 ± 1	3.5 ± 1.8
Atmospheric μ [151]	0	12.4 ± 6.2	12.4 ± 6.2
Conventional π/K [151]	6.2 ± 1.9	3.6 ± 1.2	9.8 ± 3.1
Total [7]	16.5 ± 2.7	40.1 ± 7.5	56.6 ± 8.7
Observed [149]	16.5	37.5	54

for neutrinos originating in the Southern sky [182]. In addition, this does not contradict the theoretical expectation of 1 event per year [177] within 1σ and even less in view of theoretical uncertainties.

3. We assume the presence of a prompt atmospheric neutrino component ϕ_{prompt}. This is isotropic and with a power-law energy spectrum, with spectral index $\alpha = 2.7$ and with normalization equal to the 90% c.l. IceCube upper limit, i.e. $0.50\times$ ERS.

Following these considerations, the all-flavor flux in the νgal2 model is given by,

$$\frac{d\phi}{dE} = \sum_i \frac{F_{0,i} \times 10^{-18}}{\text{GeV cm}^2 \text{ s sr}} \left(\frac{E}{100 \text{ TeV}}\right)^{-\alpha_i} \tag{86}$$

where the coefficients of normalizations and the spectral indexes are,

$$\begin{aligned} F_{0,\text{EG}} &= 3 \times 0.90^{+0.30}_{-0.27} & \alpha_{\text{EG}} &= 2.13 \pm 0.13 \\ F_{0,\nu\text{prompt}} &= 0.6 \pm 0.3 & \alpha_{\text{prompt}} &= 2.7 \\ F_{0,\text{G}} &= 1.5 \pm 0.8 & \alpha_{\text{G}} &= 2.4 \end{aligned} \tag{87}$$

It is important to remark that adding the third component (i.e. the prompt neutrinos) is not necessary to improve the agreement with data and the minimal model νgal1 is already sufficient to explain the IceCube observation. On the other hand, we know that prompt neutrinos must be present in the range of energy between TeV and PeV; therefore, in order to build a general model, we take into account also this component in the νgal2. In a sense, we can say that the νgal1 is a phenomenological model, whereas the νgal2 is obtained from more reliable theoretical assumptions.

6.3.3 Results

Using the fluxes and the total HESE effective areas described in section 4.5, we compute the total number of expected events, with the standard formula introduced by Eq.52, summing on the different flavors ℓ:

$$N_{ev} = 4\pi \, T \int_0^\infty \sum_\ell \frac{d\phi_\ell}{dE}(E) \; A_\ell(E) dE \tag{88}$$

Table 12: Fraction of Galactic flux, as a function of its extension in longitude ℓ, that can be seen in different intervals of declination. The hypothesis is that the flux is isotropic in the region of Galactic latitude $|b| \leq 4^\circ$ and Galactic longitude $|\ell| \leq 30^\circ, 50^\circ$ or 70°. Table from [7].

Extension δ	$[60, 90)$	$[30, 60)$	$[0, 30)$	$[-30, 0)$	$[-60, -30)$	$[-90, -60)$
$\|b\|^* = 4^\circ, \|\ell\|^* = 30^\circ$	0%	0%	0%	52%	48%	0%
$\|b\|^* = 4^\circ, \|\ell\|^* = 50^\circ$	0%	0%	17%	34%	43%	6%
$\|b\|^* = 4^\circ, \|\ell\|^* = 70^\circ$	0%	2%	25%	24%	34%	15%

where we sum over the flavors $\ell = e, \mu, \tau$. The cosmic components are equipartitioned in the three flavors while the prompt neutrinos are equipartitioned among electron and muon neutrinos. The effective areas for events arising from the South and North sky differ, in particular because of the absorption of very high-energy neutrino in the Earth. When the events are separated for each hemisphere, the solid angle factor in Eq. 88 is 2π. The time exposure for HESE data is assumed to be $T = 4$ yr.

In Table 11 the contributions from the different components are reported. In the case of prompt and Galactic neutrinos, the uncertainty is simply given by the uncertainty on the flux normalization. The Galactic component is obtained using the HESE effective areas for the Southern sky. For extragalactic neutrinos the uncertainty is obtained comparing the expected number of events obtained at best fit with the highest (lowest) normalization and the highest (lowest) shape. This procedure is justified by the strong correlation between the normalization and the spectral index, that can be noticed in Fig.6 of [129]. The expected background (atmospheric μ; conventional neutrinos from charged π, K decays) is estimated using the values reported in [151] and scaled with the considered exposure time T. The uncertainty δ on the total number of events is obtained combining the various uncertainties δ_i in quadrature, $\delta = \sqrt{\sum_i \delta_i^2}$.

The expected spectra for the different components are reported in Fig. 33, separated for the Northern and for the Southern hemisphere. The bands are due to the uncertainties on the normalization and on the spectral index. More precisely, the upper limit of the bands is obtained with the following formula for the increment,

$$\sqrt{[\phi(F, \alpha) - \phi(F^+, \alpha)]^2 + [\phi(F, \alpha) - \phi(F, \alpha^+)]^2} \tag{89}$$

where ϕ is the flux at best fit, $F^+ = F + \Delta F$ and $\alpha^+ = \alpha + \Delta\alpha$ if $E_\nu < 100$ TeV or $\alpha^+ = \alpha - \Delta\alpha$ if $E_\nu > 100$ TeV. The lower limit of the bands is obtained with the same procedure.

In Table 11 8.8 extragalactic events are expected from the Northern hemisphere and 16.1 extragalactic events from the Southern hemisphere. Since the solid angle covered by the region with $|b| \geq 15^\circ$ is about $3/4$ of 4π, under the hypothesis of isotropic flux we expect to see ~ 6.5 events from North and ~ 12 events from South, coming outside the Galactic plane. Observing the map in Fig.32 we found 12.5 events in Southern sky and 5.5 events in the Northern sky (1 event is at declination $\delta = 0^\circ$), in good agreement with the expectations.

Remarks and discussion

The agreement of the νgal2 with the observations is good, both for the Northern and for the Southern hemisphere. Indeed the total number of HESE observed by IceCube is compatible with

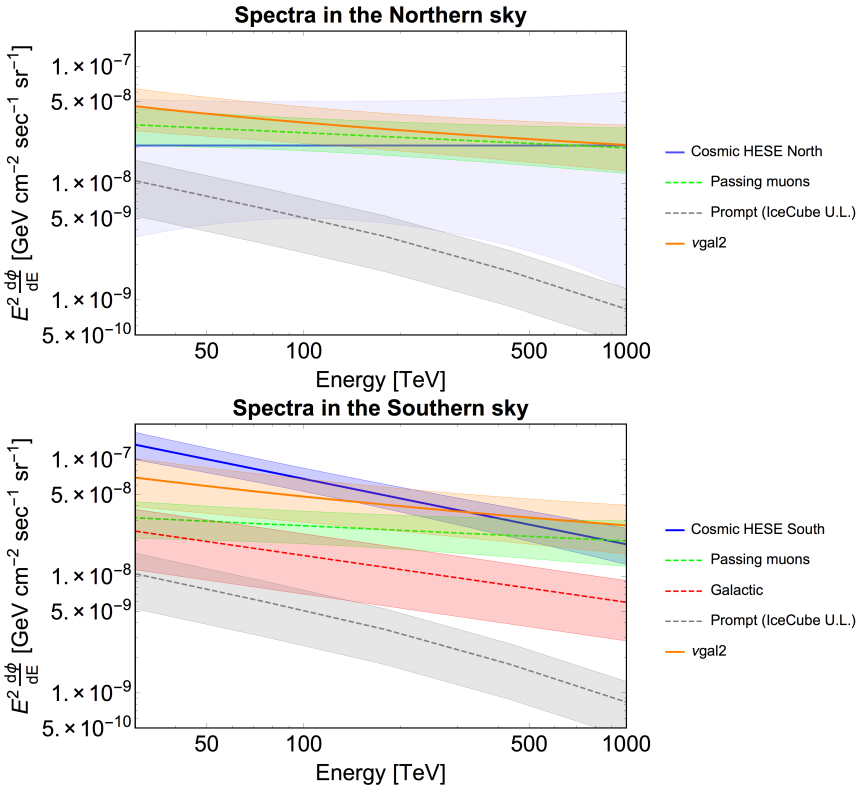

Figure 33: *The different components of the high-energy neutrino flux in the νgal2 model. For comparison, the single power-law fits obtained by the IceCube collaboration are also given (light blue). Figure from [7].*

our predictions (Table 11) within 1σ. Moreover we can notice that the extragalactic contribution is the larger component of the HESE events seen from the Southern sky, but it amount to about half of the total number of events. The remaining part is attributed to conventional neutrinos, atmospheric muons, prompt neutrinos and Galactic neutrinos. Even assuming the maximum allowed flux, prompt neutrinos cannot explain the difference between the spectra derived from the passing muons and HESE in the Southern sky.

In Fig. 33 the fluxes predicted by our model are compared with the fluxes observed by IceCube in Northern and Southern hemisphere. A good agreement can be noticed below $\approx$ 100 TeV; it means that not only the $E^{-2.7}$ of νgal1 [6] but also an $E^{-2.4}$ can adequately explain the low energy data [7]. We conclude that the detailed shape of the Galactic spectrum is not crucial for the argument, whereas the presence of a significant Galactic component (i.e. of a normalization sufficiently large) is instead necessary to explain the North-South asymmetry and to soften the spectrum of the Southern hemisphere at low energy.

Finally, Fig.34 shows the contribution of the Galactic component ϕ_G to the signal ($\phi_G + \phi_{EG} + \phi_{prompt}$ or only $\phi_G + \phi_{EG}$ in νgal1) in the Southern sky; we can notice that the prediction of νgal2 model differs from νgal1 model by about a factor 2 at low energy, due to the fact that here a prompt neutrino component is taken into account and the spectrum of Galactic neutrinos is harder.

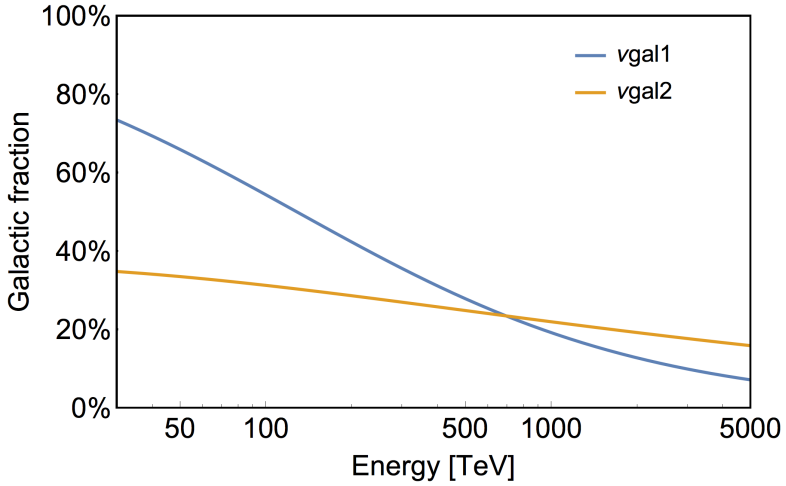

Figure 34: *Fraction of the neutrino emission in the Southern sky (after removing the conventional background and the muons) due to a Galactic emission, as function of neutrino energy. Figure from [7].*

6.4 EXPECTATION FROM νgal1 AND νgal2 MODEL

6.4.1 Test with IceCube

Before going further, we summarize our hypothesis. The high energy neutrinos are distributed according to a double component, with a softer spectrum below some 100 TeV, where the galactic component dominates, and an harder spectrum above $\simeq 0.5$ PeV, where the extragalactic component gives the main contribution. The first is distributed as E^{-2} in the νgal1 model and as $E^{-2.13}$ in the νgal2 model, whereas the second is distributed as $E^{-2.7}$ in the νgal1 model and as $E^{-2.4}$ in the νgal2 model. For what concerns the angular distribution, the extragalactic component is distributed isotropically whereas the galactic component is distributed around the Milky Way center and plane; the precise distribution (or, in first approximation, the extension of this component in galactic latitude and longitude) will be matter of observational investigations.

There are many interesting consequences of this hypothesis, that are common for both models. For instance:
1) in the next years at least an event at the Glashow resonance due to the extragalactic component must be observed;
2) the observation of double pulse events will be the definitive proof of the cosmic origin of the high energy neutrinos. Evidently, this will be very important, even if not a specific test of our hypothesis;
3) the difference of the track-to-shower ratio of the two-components can be measured in IceCube;
4) there must be also high energy gammas associated to the galactic neutrinos;
5) in order to measure precisely the galactic component at low energy, an important contribution could come from telescopes located in the Northern Hemisphere, as they can measure the neutrinos from the Southern sky by means of passing muons, namely in a cleaner way than the high energy starting events, that are instead the observational tool exploited by IceCube.
Let us discuss these tests of validation in the following section.

GLASHOW RESONANCE AND DOUBLE PULSES Using our estimation of the extragalactic flux described in the νgal1 and νgal2 models we are able to calculate the expected number of resonant and double pulse events.

The expected number of resonant events after 4 years is equal to ~ 1.5 with an uncertainty of about 30%. This prediction is obtained in the context of pp interaction and it is valid for both our model within the uncertainty. Up to now the resonant events have been not observed. The probability to not observe resonant events is given by the Poissonian statistics and it is equal to $e^{-1.5} \simeq 0.22$. This means, in a Gaussian treatment, that it is disfavored at 1.2σ; therefore, the non observation of resonant events does not represent a critical issue for our model nowadays. In order to accept or discard our hypothesis with a significance of 3σ more than 10 years, with the present exposure, are required. The contribution of the galactic component to this class of events is negligible, due to the its softer spectrum. Indeed we have seen in section 5.5.2 that the expected number of resonant events is highly sensitive to the shape of the spectrum.

The same argument can be discussed for the double pulses events. In this case the expected number of events after 4 years is equal to ~ 0.5 with an uncertainty of about 20%. The rate is much lower than what expected for resonant events. Therefore it is perfectly compatible with the non observation of events, within 0.5σ. In order to observe a double pulse event with a probability of 90% and 99% with the present exposure we have to wait ~ 15 and ~ 35 years respectively. Let us recall that the double pulse is less sensitive to the slope of the neutrino spectrum with respect to the Glashow resonance events, because about half of the signal is given by the already observed neutrinos, with energy between 100 TeV and 1 PeV [3]. Note that the galactic component gives a small contribution to the double pulse events, i.e. $\simeq 0.03$ expected events per year.

THE TRACK-TO-SHOWER RATIO It is important to notice that the track-to-shower ratio for the galactic and the extragalactic components are different, even if the mechanism of production is the same (we refer to the standard case of pion decay). This remains true despite the uncertainties on the oscillation parameters, as can be seen in Fig.35, where we have chosen the spectrum assumed in νgal1 model, i.e. E^{-2} for the extragalactic component and $E^{-2.7}$ for the Galactic one. The difference in the track-to-shower ratio is due to the different spectral shape, since the larger spectral index (namely the case of galactic ν) penalizes track events. This aspect is not surprising if we look at the effective areas of section 4.5 and we remember that the track-to-shower ratio is a function of the shape (see the discussion of section 5.2). The difference is reduced for the νgal2 model, where there is a less difference between the spectral shapes of the two components. Anyway, a certain imprint remains also in this second scenario.

IMPLICATION FOR γ ASTRONOMY The galactic component of neutrino implies the existence of a galactic component of very high energy γ-rays. These gamma rays can be observed, because their path in the Galaxy is shorter than their mean free path. The same consideration is not true for the extragalactic gamma rays associated to neutrinos, because when the energy is above 10 TeV they are absorbed after about 100 Mpc, due to the interaction with the extragalactic background light (EBL). It is possible to give a lower limit on the flux of gammas, that corresponds to the case of pp interaction at the source. Recalling the discussion of section 1.3.3, the ratio between the flux of gamma and the flux of neutrinos is given by the following formula:

$$\frac{\phi_\gamma}{\phi_\nu} = 1.009 + 0.622(\alpha - 2.3) + 0.140(\alpha - 2.3)^2 + 0.009(\alpha - 2.3)^3 \tag{90}$$

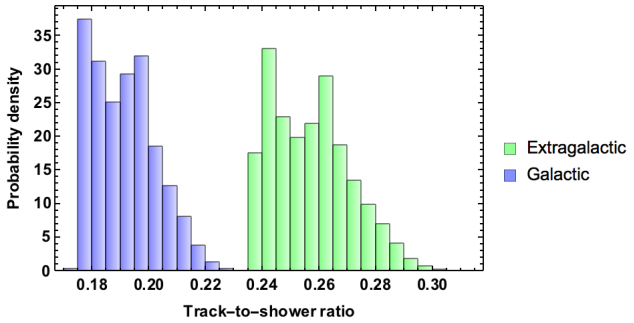

Figure 35: *Comparison between the track-to-shower ratio of galactic (blue) and extragalactic (green) components, assuming the same mechanism of production, i.e. pion decay. Figure from [6].*

Therefore the ratio is equal to 1 within the 30%, for a power law spectrum $E^{-\alpha}$ with $2 \leq \alpha \leq 2.7$ and the flux of galactic gamma must be of the same order of the neutrino flux:

$$\phi_\gamma(E) \simeq \phi_G(E) \tag{91}$$

Let us notice that the cutoff on ϕ_γ is at higher energy with respect to the cutoff on the galactic neutrino spectrum. In fact the energy of γ is typically $E_\pi/2$, whereas the energy of neutrinos is $\simeq E_\pi/4$ (see 1 for a complete description of the secondary neutrinos spectrum). The relationship between galactic HE neutrinos and HE γ-rays is also discussed in [183], focusing on SNRs, PWN and binary systems. Recall also that in the case of binary system if the γ-rays are produced from protons, the flux of HE neutrinos can significantly exceed the one of γ-rays (by a factor of e^τ where τ is the optical depth) considering that they escape from the region without absorption, unlike γ-rays.

In the other case, the flux of gamma must be larger than the flux of neutrinos to have a consistent theory. At present there are no measurements of gamma rays in the same energy range of neutrinos (above 30 TeV), so a direct comparison is not possible. Fig. 36 shows the diffuse flux of galactic gamma rays (see [184],[185]) and the estimated flux of galactic neutrinos (νgal1 model in the left panel and νgal2 model in the right panel) in the energy range in which they are already measured. No firm conclusion can be derived nowadays from these results, although it seems that the νgal2 is better in agreement with the γ-rays flux when it is extrapolated at low energy, using the same power law spectrum $E^{-2.4}$ at low energies.

FUTURE KM^3-CLASS TELESCOPES IN THE NORTHERN HEMISPHERE Our hypothesis requires that in the vicinity of the galactic disk there is a population of high energy neutrinos, with energies below few 100 of TeV. The present data are compatible with a large fraction of events with this origin. In our reference hypothesis, this fraction is about 30%, with a great uncertainties, since the 1σ interval includes values that differ by a factor of two (above or below). This means that the existence of a galactic component is reasonable even if nowadays it is hard to quantify it precisely; future experiments in the Northern hemisphere will be necessary to prove its existence and to measure this component precisely.

Let us remark that the 30% refers to the fraction of supposed galactic events with respect to the total number of events observed from the Southern sky. If all the events (both from South and North) are considered, the galactic contribution becomes 24% at best fit. However let us remark that the precise extension of this signal (in angle and in energy) is not known and this

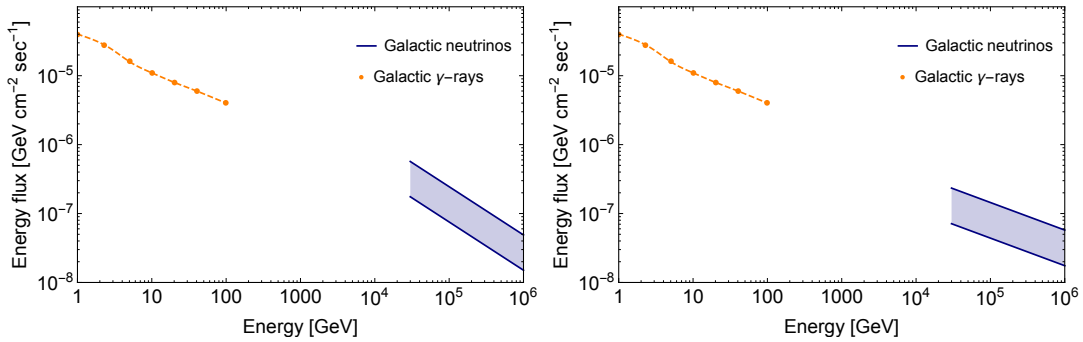

Figure 36: *In orange, spectrum of diffuse gamma-ray emission from the inner Galaxy ($-80^o \leq l \leq 80^o$, $-8^o \leq b \leq 8^o$, measured by Fermi-LAT. In blue, spectra of galactic neutrinos $E^{-2.7}$ (left panel) and $E^{-2.4}$ (right panel) with their uncertainties. Figures from [6] and [7].*

requires further experimental investigations. In order to validate this assumption, neutrino telescopes of sufficient volume and located in the Northern hemisphere are needed.

The KM3NeT [131] and the BAIKAL-GVD [135] are such kind of experiments; the first will be in the Mediterranean Sea, the second one in Baikal Lake. They will be in the right geographical position to validate the presence of a diffuse galactic neutrino component, thanks to the possibility to use passing muons of relatively low energies. Note that in water the angular resolution is much better than in ice and it attains sub-degree [131]. In this manner, the precise angular extension will be investigated. Moreover, also 'high energy starting events' below few 100 TeV will be useful for the same purpose.

Also the extragalactic component can be measured with a similar precision to that of the IceCube experiment, using the high energy starting events in the energy range above some 100 TeV, where the background due to atmospheric neutrinos is negligible.

6.4.2 Constraints from the ANTARES telescope

A Galactic neutrino component is likely not isotropically distributed over the 2π sr of the Southern sky. In the following, we will assume that Galactic neutrinos are produced in a rectangular region symmetrically extended with respect to the Galactic center up to Galactic latitude $|b|^*$ and longitude $|\ell|^*$. The solid angle covered by this region corresponds to

$$\Delta\Omega^* = 4 \sin |b|^* \cdot |\ell|^* \,. \tag{92}$$

Under this assumption, the normalization factor $F_{0,G}$ given in (87) is null outside this rectangular region and inside becomes

$$F^*_{0,G} = F_{0,G} \cdot \frac{2\pi}{\Delta\Omega^*} \tag{93}$$

The ANTARES neutrino telescope [145] searched for an excess of events with respect to the background of atmospheric neutrinos in a region with $|b|^* = 3°$ and $|\ell|^* = 40°$, corresponding to $\Delta\Omega^* = 0.145$ sr. From the null observation, and assuming a spectral index $\alpha_g = 2.4$, a 90% C.L. upper limit on the normalization for one-flavor neutrino of $\Phi^{1f}_{Antares} = 2.0 \times 10^{-17}$ (GeV cm^2 s sr)$^{-1}$ was derived. Assuming a 1:1:1 flavor ratio, this value must be multiplied by a factor of three to give the 90% c.l. upper limit on all neutrino flavors, $\Phi^{3f}_{Antares}$. When compared

with eq. 93 for $\Delta\Omega^* = 0.145$ sr, the predicted flux $F^*_{0,G} = 6.5 \times 10^{-17}$ (GeV cm^2 s sr)$^{-1}$, is above $\Phi^{3f}_{Antares}$. Thus, at 90% C.L. it is excluded that the region originating Galactic neutrinos has dimensions smaller than $|b|^* < 3^\circ$ and $|\ell|^* < 40^\circ$. Larger production regions are still compatible with the ANTARES limits.

In Tab.12 we considered three rectangular regions with latitude $|b|^* = 4^\circ$ and different values of Galactic longitude $|\ell|^*$. Here, we evaluated the fraction of the Galactic neutrino flux seen in different intervals of declination δ. For the IceCube geographical location in the South Pole, remember that the elevation corresponds to the declination: $\delta > 0$ (< 0) correspond to upgoing (downgoing) events.

We can notice that the minimal hypothesis in which the Galactic flux is only seen from the Southern hemisphere ($\delta < 0$) is valid for $|\ell|^* \leq 30^\circ$. IceCube can observe this sky region only using the contained events (HESE) that have a poor angular resolution. If the Galactic flux extends at larger longitudes, IceCube has the possibility to detect the signal also using upgoing muons. For instance, if $|\ell|^* = 70^\circ$, about $1/4$ of the flux would come from the Northern hemisphere. However, since the flux measured by IceCube from the Northern hemisphere, both with passing muons and HESE, seems to have spectral index very close to $\alpha = 2$, it is plausible that the Galactic flux has a longitudinal extension not exceeding 50°.

In addition to tracks, ANTARES is studying the Galactic center region also using cascade events, mainly induced by CC ν_e and neutral current interactions. The angular resolution of upgoing showering events in ANTARES is about $3^\circ - 4^\circ$, thus comparable with the considered minimal extension of the rectangular region in Galactic longitude. This will allow to test in a short timescale our scenario of Galactic neutrino production. Finally, the incoming experiment KM3NeT [131] has the chance to give the final answer to the existence of such Galactic neutrino flux, since it can observe most of the Galactic plane using passing muons and cascade events with an even better angular resolution than ANTARES.

During the writing of the thesis a new upper limit of the ANTARES collaboration has been published. Based on this last work [186] the Galactic component cannot produced more than 5.6 of the 54 HESE detected by IceCube, at 90% confidence level. Let us recall that this upper limit is still in agreement with both our models, in which we predict a Galactic contribution of 6.0 ± 3.0 events.

A new upper limit on the Galactic flux has been published also by the IceCube collaboration [187]. The result is that the Galactic contribution is smaller than 14% at 90% C.L.. It means that 7.5 of the 54 HESE, detected in 4 years, can have a Galactic origin. Therefore our models are consistent also with this limit.

Moreover it is important to remark that this number of events can appear negligible. On the contrary, comparing it with the events that come from the Southern hemisphere and deposit more than 60 TeV into the detector, we find that the contribution of Galactic events is of the order of 25%-30% and it is still sufficient to soften the spectrum below 100 TeV. Adding the small contribution expected from prompt neutrinos, the contribution of "non extragalactic"events increases up to 40%, when the analysis is limited to the subset of events from South above 60 TeV.

6.4.3 Summary and conclusions

The main goal of IceCube has been to show the existence of a new component of high-energy neutrinos, on top of atmospheric neutrinos. A simple assumption proved to be reasonably

appropriate to summarize the data and the present understanding. This is the assumption of a single new population, distributed isotropically and with a power law spectrum with slope significantly different from $\alpha = 2$. This is a minimal modification of the hypothesis suggested by the scenario of extragalactic origin but it leads to a certain number of issues, examined and discussed in Sect. 6.1.

However, there is no strong theoretical reason to omit the galactic contribution to the observed high-energy neutrinos; on the contrary, astronomical data, gamma rays included, suggest including it. In Sec.6.2 we have introduced and discussed the model νgal1 model. We have shown that the inclusion of another significant component of the high energy neutrino flux, with the slope of the observed galactic cosmic rays spectrum, and with an extension till few 100 TeV, is consistent with the known IceCube data.

The angular distribution of the total galactic contribution (including point sources and diffuse component) is not precisely known but the galactic latitude should be within $|b| < (5-20)^\circ$ and the galactic longitude extends from $|l| < 40^\circ$ or an even wider region. Although we would like to observe point sources eventually, the high energy neutrino astronomy is in a similar position as the ordinary one more than 200 years ago, at the times of T. Wright, I. Kant, W. Herschel, when the shape of the Milky Way was understood. It should be stressed, however, that neutrinos will give unique information on galactic and extragalactic cosmic rays.

We have shown that the dominant extragalactic component predicts observable events of new type in IceCube, those from Glashow resonance and those of double-pulse type. We have emphasized that the galactic component is more important at comparably low energies (below few 100 TeV) and can be observed by exploiting through-going muons from the Northern Hemisphere. It leads to a peculiar flavor ratio and should be accompanied by a (diffuse) emission of very high energy gamma rays, calculable from the neutrinos, and extended till some few 100 TeV.

In the near future, a combined analysis of the data of IceCube and ANTARES will permit us to obtain more precise inferences on the parameters of the two component model. It is important to emphasize that within this model, the angular features and those of the energy spectrum are closely entangled and should be analyzed together.

In Sec.6.3 we have generalized the νgal1 model into the νgal2 model, that is based on more accurate theoretical considerations. This second model includes the contribution of prompt neutrinos and an harder galactic component, according to the galactic γ-rays already measured. Moreover we have considered the effect of the spatial distribution of the Galactic neutrinos, the impact of the new observations of the passing muons above few 100 TeV and from the Northern sky, which we assume to derive from an extragalactic component and the constraints arising from the ANTARES neutrino telescope on neutrinos from the Southern hemisphere.

Different results arise from the discussion of the νgal2 model.

1) A Galactic component, assumed with energy distribution $E^{-2.4}$ (as motivated in Sect. 6.3.1) and with a smaller normalization coefficient than the one assumed in νgal1 (as discussed in Sect. 6.3.2) is also compatible with the existing observations. It explains the distribution of the HESE from the Southern sky, receiving both Galactic and extragalactic contributions. In the model, HESE from the North are induced only by extragalactic neutrinos, whose flux is measured from the passing muon sample.

2) Assuming a spectral index of 2.4 instead of 2.7 as in the νgal1 case the fraction of Galactic neutrino events at lower energies diminishes, whereas we have a relatively large amount of

Galactic neutrinos at higher energies, as emphasized in Fig. 34 [8] . This increases the probability that an excess of events with respect atmospheric neutrinos can be seen by the ANTARES detector.

3) The Milky Way is mostly visible from the Southern sky (Table 12). This means that the Galactic component could be measured in IceCube using HESE only, while is accessible as upgoing muons and cascades in neutrino telescopes located in the Northern hemisphere.

4) The prompt neutrino flux cannot produce a North-South asymmetry, but it could modify the shape of the spectrum, making it softer at low energies. However, after the recent bounds obtained by IceCube, its presence is too small to modify significantly the HESE spectrum, thereby accounting for the discrepancy between the HESE South data and the passing muon data. This conclusion becomes even stronger if the most recent calculations of prompt neutrinos [179, 180, 181] are considered.

A crucial dataset used to test this model–in any of its variant, νgal1, νgal2, or others–is the IceCube HESE from the Southern sky and below few 100 of TeV. Moreover, a common feature of all the νgal models is that most of the cosmic neutrino events at high Galactic latitude are of extragalactic origin. Therefore, the subset of the HESE North and South that come from a Galactic latitude $|b| \geq 10^\circ - 15^\circ$ (the angular resolution of the showers) should be consistent between them. It is important that, in the future, the IceCube collaboration perform similar tests. Referring to Table 11, a potential problem arises if some background process, caused or connected to atmospheric muons, is not fully under control as currently expected: in this case, the reliability of the conclusions should be reassessed. In any case, the existing statistics is still insufficient to be certain of a significant Galactic neutrino emission, and a firmer conclusion can be obtained with more HESE data (still on IceCube disks) and with data collected from the direction of the Galactic plane by Mediterranean neutrino telescopes (ANTARES and KM3NeT in the near future).

As a last remark, during writing the thesis two new upper limits on the Galactic component have been published by ANTARES [188] and IceCube [189]. The multi-component models proposed in [6] and [7] and described in this chapter, that predicts a Galactic contribution between 10% and 20%, are still compatible with these recent experimental constraints, concerning the Galactic flux.

[8] Note incidentally that if the knee of the cosmic ray spectrum (observed at the Earth) is due to a feature of the accelerators, we would expect to have a corresponding feature in the Galactic neutrinos at energies of $\epsilon_\nu \times E_{\rm knee} \approx 1/20 \times 3$ PeV $= 150$ TeV: this makes it evident how important is a detailed study of the Galactic neutrinos emission.

7 MULTI-MESSENGER ASTRONOMY: NEUTRINOS AND γ-RAYS

The last chapter of the thesis is dedicated to the multi-messenger analysis, i.e. the search of spatial and/or spectral correlations between high energy neutrinos and other known radiations. This kind of analysis is crucial to determine the source of high energy neutrinos and will become even more important in the future, with the increase of the data. In this chapter we focus on the possibility to detect high energy neutrinos produced in the Galactic center, where the HESS collaboration has recently detected a possible PeVatron, i.e. a region that could be able to accelerate protons till PeV energies. Then we focus on two promising extragalactic classes of sources of high energy neutrinos, namely blazars and star forming galaxies. Blazars are the brightest objects in the γ-rays sky above 100 GeV, therefore it is natural to consider them as a promising source of high energy neutrinos. On the other hand, also the star forming galaxies could provide the ideal condition to produce high energy neutrinos, thanks to the high density of matter (with respect to normal galaxies) that offer a natural target for the pp interactions.

This chapter is based on three papers published during the PhD. Namely the section 7.2 is based on [8], whereas the section 7.3 is based on [9, 10]. Section 7.4 contains original results.

7.1 INTRODUCTION

In this chapter we discuss the potential of a "multi-messenger" investigation. In fact, the neutrinos from cosmic ray collisions are accompanied by γ-rays, as we have seen in Sec.1.3.3; therefore, the hypothetical sources of neutrinos must also be sources of γ-rays.

However the γ-rays can be absorbed during their path and/or into the source. The absorption of γ-rays is significantly different for Galactic and extragalactic γ-rays. The probability of absorption can be evaluated with the analytical expression suggested in [8]:

$$P(E_\gamma) = \exp[-\sum_i \tau_i(E_\gamma)]$$

where

$$\tau_i(E_\gamma) = 1.315 \times \frac{L_i}{L_0} \times \frac{n_{\gamma,i}}{n_{\gamma,\mathrm{CMB}}} \times f\left(\frac{E_i}{E_\gamma}\right) \tag{94}$$

where the quantities chosen for the normalization are L_0=10 kpc (a typical galactic distance) and $n_{\gamma,\mathrm{CMB}} = 410.7\ \mathrm{cm}^{-3}$. The function $f(x)$ is given by:

$$f(x) \simeq -a \cdot x \cdot \log[1 - \exp(-b\ x^c)], \quad \begin{cases} a = 3.68 \\ b = 1.52 \\ c = 0.89 \end{cases} \tag{95}$$

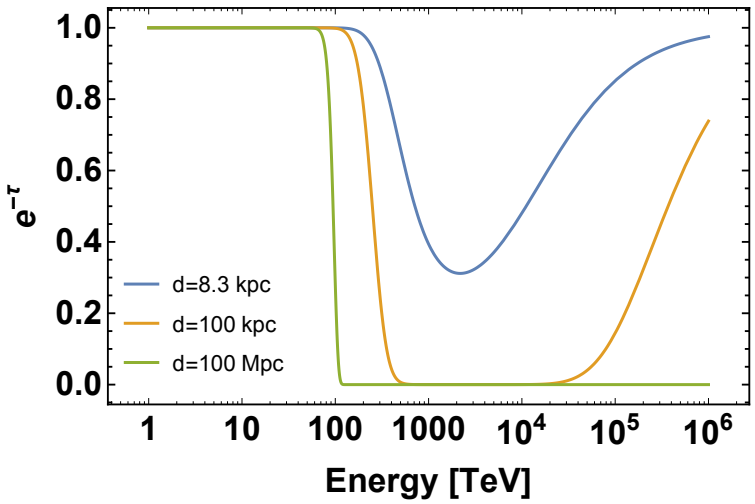

Figure 37: *Absorption of γ-rays due to the CMB considering different distances from the source to Earth.*

with $x = \frac{E_i}{E_\gamma}$. The details to derive $f(x)$ are reported in Appendix B.2.

Considering only the absorption due to the interaction of γ-rays with the CMB, the parameter of Eq.94 are $n_{\gamma,i} = 410.7$ cm^{-3}, $E_i = 1111$ TeV and we obtain the three lines represented in Fig.37, for distances of $L = 8.3$ kpc, 100 kpc, 100 Mpc . We notice that the absorption of γ-rays from the Galactic center becomes important around some hundreds TeV (blue line) whereas the absorption of γ-rays from extragalactic sources is relevant already at 100 GeV (green line). At the present Galactic γ-rays are measured until 10-20 TeV whereas γ-rays with energy around 100 TeV could be measured by the future experiments.

Therefore the possibility of observing the γ-rays from extragalactic sources is by no means guaranteed. Moreover, the γ-rays could have a different distribution from those of the neutrinos (e.g., if the neutrinos are emitted isotropically near the nuclear region of an active galactic nucleus (AGN), whereas the γ rays emerge as a collimated beam of one jet instead) or could, possibly, be absorbed and/or strongly reprocessed at the source.

However we see from Fig.37 that, even in case of γ-rays from distant sources, the intergalactic medium does not absorb γ-rays with energies below 100 GeV or so. Thus, through the use of results from astrophysical modeling, there is hope for revealing a correlation between these γ-rays and the observed neutrinos.

7.2 NEUTRINOS FROM THE GALACTIC CENTER

The supermassive black-hole in the center of the Milky Way, located in the radio source Sgr A*, is one of the most interesting astronomical objects: see Ref. [190] for an extensive review. It is now in a state of relative inactivity [191] but there is no good reason for it to be stationary. E.g., there are interesting hints for a much stronger emission few 100 years ago [192]; on the time scale of 40,000 years, major variability episodes are expected [193]; Fermi bubbles [194] could be visible manifestations [195] of its intense activity. Therefore, it is reasonable to expect that a

past emission from the Galactic Center leads to observable effects. Such scenario was recently considered in Ref. [196].

The latest observations by the H.E.S.S. observatory [47], that various regions around Sgr A* emit γ-rays till many tens of TeV, are offering us new occasions to investigate this object. These γ-rays obey non-thermal distributions, which are moreover different in the closest vicinity of Sgr A* and in its outskirts. In the latter case, the γ-rays seem to extend till very high energies ($\sim$ 35 TeV) without a perceivable cut-off.

The γ-rays seen by H.E.S.S. can be attributed to cosmic ray collisions [47]. This is a likely hypothesis, but the proof of its correctness requires neutrino telescopes. In this connection, it is essential to derive reliable predictions for the search of a neutrino signal from Sgr A* and its surroundings, and H.E.S.S. observations are very valuable in this respect. Remarkably, the possibility that the Galactic Centre is a significant neutrino source is discussed since the first works [197] and it is largely within expectations: indeed Sgr A* is one of the main point source targets, already for the IceCube observatory [198].

In this section we discuss the implications of the findings of H.E.S.S., briefly reviewed in Sect. 7.2.1, where we also explain our assumptions on the γ-ray spectra at the source. The expected signal in neutrino telescopes, evaluated at the best of the present knowledge, is shown in Sect. 7.2.2 and it is quantified in Sect. 7.2.3. We argue that the PeVatron hypothesis makes the case for a cubic kilometer class neutrino telescope, located in the Northern hemisphere, more compelling than ever.

7.2.1 The γ-ray spectra from the Galactic Center Region

The excess of VHE γ-rays reported by the H.E.S.S. collaboration [47] comes from two regions around the Galactic Center: a Point Source (HESS J1745-290), identified by a circular region centered on the radio source Sgr A* with a radius of 0.1°, and a Diffuse emission, coming from an annulus with inner and outer radii of 0.15° and 0.45° respectively. The observed spectrum from the Point Source is described by a cut-off power law distribution, as

$$\frac{d\phi_\gamma}{dE}(E) = \phi_0 \left(\frac{E}{1\,\text{TeV}}\right)^{-\Gamma} \exp\left(-\frac{E}{E^\gamma_{\text{cut}}}\right) \tag{96}$$

while in the case of Diffuse emission an unbroken power law is preferred; in the last case, however, also cut-off power law fits are presented, as expected from standard mechanisms of particle acceleration into the Galaxy.

The H.E.S.S. collaboration has summarized its observations by means of the following parameter sets:

- Best fit of the Point Source (PS) region:
  $\Gamma = 2.14 \pm 0.10$,
  $\phi_0 = (2.55 \pm 0.37) \times 10^{-12}$ TeV^{-1} cm^{-2} s^{-1},
  $E^\gamma_{\text{cut}} = 10.7 \pm 2.9$ TeV;
- Best fit of the Diffuse (D) region:
  $\Gamma = 2.32 \pm 0.12$,
  $\phi_0 = (1.92 \pm 0.29) \times 10^{-12}$ TeV^{-1} cm^{-2} s^{-1};

However, in order to predict the neutrino spectrum, the γ-ray spectrum at the source–i.e. the emission spectrum–is needed. We will discuss the implication of the assumption that the

emitted spectra coincide with the observed spectra as described by the previous functional forms and furthermore we will discuss the assumption that the γ-ray emission at the source is described by different model parameters, namely:

- Diffuse emission as a cut-off (DC) power law with:
  $\Gamma = 2.32$,
  $\phi_0 = 1.92 \times 10^{-12}$ TeV^{-1} cm^{-2} s^{-1},
  $E^{\gamma}_{\rm cut} = 0.4$ PeV, 0.6 PeV or 2.9 PeV.

The inclusion of a cut-off for the emission from the Diffuse region agrees with the observations of H.E.S.S. and is motivated simply by the expectation of a maximum energy available for particle acceleration.

Note that the γ-ray observations extend till 20-40 TeV. This is an important region of energy but it covers only the lower region that is relevant for neutrinos: the latter one extends till 100 TeV, as clear e.g., from Fig.2 and 3 of [39] and Fig.1 of [36]. In other words, it should be kept in mind that until γ-ray observations till few 100 TeV will become available–thanks to future measurements by HAWC [199] and CTA [200]–the expectations for neutrinos will rely in part on extrapolation and/or on theoretical modeling. In this section, unless stated otherwise, we rely on a 'minimal extrapolation', assuming that the above functional descriptions of the γ-ray spectrum are valid descriptions of the emission spectrum.

A precise upper limit on the expected neutrino flux can be determined from the H.E.S.S. measurement, assuming a hadronic origin of the observed γ-rays. The presence of a significant leptonic component of the γ-rays would imply a smaller neutrino flux. In principle, however, also other regions close the the Galactic Center, but not probed by H.E.S.S., could emit high-energy γ-rays and neutrino radiation, leading to an interesting signal. One reason is that the annulus, chosen by H.E.S.S. for the analysis, resembles more a region selected for observational purposes rather than an object with an evident physical meaning;[1] another reason is that the ice-based neutrino telescope IceCube integrates on an angular extension of about 1°, which is 5 times larger than the angular region covered in [47]. In view of these reasons, the theoretical upper limit on the neutrino flux that we will derive is the *minimum* that is justified by the current γ-ray data.

7.2.2 High-energy neutrinos from the Galactic Center Region

Neutrinos could be produced in hadronic interactions of PeV protons with the ambient gas: since each neutrino carries about 5% of the energy of the parent proton (as explained in section 1.3) we expect to see neutrinos in the multi-TeV range, in angular correlation with the high-energy γ-rays emitted from the Galactic Center Region. This scenario is supported by the observed correlation between the γ-ray emission and molecular clouds reported in [47].

In this section we do not consider the absorption of γ-rays from the Galactic center to the Earth. This is largely discussed in [8]. It is only important to recall that the effect of the conventional photons background is negligible for γ-rays below 100 TeV, whereas the presence of a speculative infrared field, close to the Galactic center, could produce the energy cut-off observed by the HESS collaboration in the diffuse flux. Therefore we compute the flux of neutrinos starting from the observed flux of γ-rays in the following of the section.

[1] Again because of this consideration, and also in view of the fact that the angular resolution of the neutrino telescopes operated in water matches the physical size of the two regions, we will present the predictions for the Point Source and the Diffuse region separately.

PRESENT UPPER LIMIT ON NEUTRINOS FROM SGR A* To date, IceCube has set the best 90% C.L. upper limit on the $\nu_\mu + \bar{\nu}_\mu$ flux assuming an unbroken E^{-2} spectrum from Sgr A* at [198],

$$\frac{d\phi_\mu}{dE} = 7.6 \times 10^{-12} \left(\frac{E}{\text{TeV}}\right)^{-2} \text{ TeV}^{-1} \text{ cm}^{-2} \text{ s}^{-1} \tag{97}$$

Such a limit corresponds to the absence of a significant event excess over the known background, that in the analysis of IceCube [201] amounts to 25.2 background events in a circle of 1°. This limit has been obtained by means of downward-going track-type events, as discussed in the next section.

Presumably, this is the safest information we have on the neutrino emission from Sgr A*, even if it does not correspond to a realistic assumption on the emitted neutrino spectrum. In principle, the assumption of a differential neutrino spectrum in the form of an E^{-2} dependence would be a consequence of the first order Fermi acceleration mechanism, but there is no observational evidence that this is a reliable assumption, and moreover, this is not supported by the observed γ-ray spectrum.

MODEL PREDICTION / THEORETICAL UPPER BOUND The model prediction that we are going to derive is based instead on the current γ-ray observations and on the assumption that such emission is fully hadronic. The expectation that we obtain is well compatible with the IceCube non-detection. Indeed, the flux of Eq. 97 is much larger and has a distribution harder than the upper limit on the neutrino flux derived from the γ-ray observations. This is evident from Fig. 38, discussed in details just below.

Keeping in mind the crucial hypothesis, that the γ-rays observed by H.E.S.S. are fully hadronic, our model prediction can be regarded also as a theoretical upper bound. It is very important however to distinguish clearly the experimental upper limit of Eq. 97 from this theoretical upper limit on the expected neutrino signal, derived through γ-rays. The latter is more realistic and also much more stringent, but, just as the former, it depends upon various theoretical assumptions.

In order to illustrate this point, we remark that the γ-ray data collected by H.E.S.S. cannot exclude that the $\nu_\mu + \bar{\nu}_\mu$ spectrum hardens to E^{-2} above 20-40 TeV; however, the normalization of this component has to be some 5 times smaller than Eq. 97, if the spectrum is a smooth distribution (a continuous function) linked to the observed γ-rays spectrum. This kind of (very speculative) scenario, along with other scenarios mentioned in Sect. 7.2.1, might increase the expected neutrino signal.

However we prefer to focus conservatively on the minimal scenario that was defined in Sect. 7.2.1 as it is motivated by H.E.S.S. measurements. We will show that the theoretical limit on the neutrino flux, corresponding to the γ-ray flux observed by H.E.S.S., is below the capabilities of the detectors currently in data-taking, whereas it could be within the reach of the future detectors.

METHOD TO CALCULATE THE MUON NEUTRINO FLUX Assuming a purely hadronic origin of the emission γ-ray spectrum $\phi_\gamma(E)$, we can calculate the muon neutrino and antineutrino

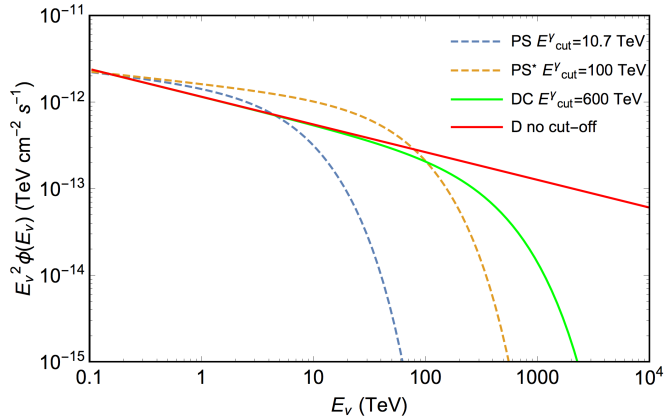

Figure 38: *Predicted muon neutrino and antineutrino fluxes (summed) for the Point Source best fit with a cut-off at $E^{\gamma}_{cut} = 10.7$ TeV and for an arbitrary cut-off at $E^{\gamma}_{cut} = 100$ TeV. Also shown the fluxes for the Diffuse best fit without cut-off and with a cut-off at $E^{\gamma}_{cut} = 600$ TeV. Figure from [8].*

spectrum through the precise relations based on the assumption of cosmic ray-gas collisions [21],

$$\begin{aligned}\phi_{\overset{(-)}{\nu_\mu}}(E) &= \alpha_\pi\, \phi_\gamma\left(\frac{E}{1-r_\pi}\right) + \alpha_K\, \phi_\gamma\left(\frac{E}{1-r_K}\right) + \\ &+ \int_0^1 \frac{dx}{x}\, K_{\overset{(-)}{\nu_\mu}}(x)\, \phi_\gamma\left(\frac{E}{x}\right)\end{aligned} \tag{98}$$

where $\alpha_\pi = 0.380\ (0.278)$ and $\alpha_K = 0.013\ (0.009)$ for ν_μ and $\bar{\nu}_\mu$ respectively and where $r_x = (m_\mu/m_x)^2$ with $x = \pi, K$. In each expression, the first two contributions describe neutrinos from the two-body decay by pions and kaons, while the third term accounts for neutrinos from muon decay. The kernels for muon neutrinos $K_{\nu_\mu}(x)$ and for muon antineutrinos $K_{\bar{\nu}_\mu}(x)$, which also account for oscillations from the source to the Earth, are

$$K_{\nu_\mu}(x) = \begin{cases} x^2(15.34 - 28.93x) & 0 < x \leq r_K \\ 0.0165 + 0.1193x + 3.747x^2 - 3.981x^3 & r_K < x < r_\pi \\ (1-x)^2(-0.6698 + 6.588x) & r_\pi \leq x < 1 \end{cases}$$

$$K_{\bar{\nu}_\mu}(x) = \begin{cases} x^2(18.48 - 25.33x) & 0 < x \leq r_K \\ 0.0251 + 0.0826x + 3.697x^2 - 3.548x^3 & r_K < x < r_\pi \\ (1-x)^2(0.0351 + 5.864x) & r_\pi \leq x < 1 \end{cases}$$

Applying such procedure, the expected (upper limits on the) neutrino spectra are obtained from the γ-ray spectrum. This is the closest we can go to a model-independent approach. This procedure is much more precise than the one described in section 1.3.3, where we only considered the neutrinos produced by pions decay. On the other side, using the procedure of [21], also contribution from kaons and η particles are taken into account. Moreover the procedure of [21] is completely general and it is valid for each spectrum, not only for a power law spectrum.

RESULTS FOR THE $\nu_\mu + \bar{\nu}_\mu$ FLUXES We show in Fig. 38 the sum of the muon neutrino and antineutrino fluxes, derived using for $\phi_\gamma(E)$ the four models introduced in Sect. 7.2.1, namely: 1) the best fit flux of the Point Source region (with 10.7 TeV cut-off), 2) the same one assuming that the cut-off is at 100 TeV, 3) the best fit flux of the Diffuse region (without cut-off), 4) the

same one including a cut-off at 600 TeV.

Our results compare reasonably well with the fluxes given in the Extended Data Figure 3 of ref. [47], that however concern the total flux of neutrinos (i.e. all three flavors). The conclusion stated in Ref. [47], based on the observed γ-ray fluxes and on the criterion stated in [36], is that these fluxes are potentially observable.

Here, we would like to proceed in the discussion further, clarifying the condition for observability in the existing detectors and quantifying the expected number of signal events that can be detected. We will discuss how the conclusion depends upon the features of the detector.

7.2.3 Expected signal in neutrino telescopes

Current neutrino telescopes, like ANTARES [134], IceCube [149] and those under construction as KM3NeT [131] and Baikal-GVD [135], could be able to detect the neutrinos from the Galactic Center Region by looking for track-like events from the direction of this source.

TRACK-LIKE SIGNAL EVENTS As discussed in Sec. 4.4 the use of track-like events for the search of point sources is desirable because of the relatively good angular resolution, of the order of 1° in ice and several times better in water. This allows the detectors to operate with a manageable rate of background events, due to atmospheric muons and neutrinos. A detailed discussion of the effect of the atmospheric background on this type of measurement is proposed in [8].

In principle, IceCube can also look at the Southern sky by exploiting the HESE sample [149], namely events of high energy with a vertex contained in the detector. The HESE are mainly composed of shower-type events above 30 TeV, that have an angular uncertainty of about 10°, much worse than that of track-like events, as we have seen in Sec.4.4 and Sec.4.5.1. However, in the case of Sgr A* we are interested in a point-source and to lower energy, so a high angular precision on the reconstructed event direction and an energy threshold much lower than 30 TeV are needed. We will show the importance of these considerations by a direct quantitative evaluation of the HESE event rate.

EFFECTIVE AREAS The angular resolution for current neutrino telescopes is such that both the PS and the D regions are seen as point-like regions. Thus, the effective areas of ANTARES [145] and IceCube [146] are those used for the search of point-like sources in the declination range relevant for the observation of the Galactic Center. Likewise, the effective area of KM3NeT-ARCA [147] refers to the point source search: it is applied to the next configuration including two building blocks, each with 115 detection units. These effective areas, that we use for the calculation of the rates, are shown in the right panel of Fig. 16.

The rate of track-like events R (number of events per year) that a detector is able to measure, assuming a certain angular search region, is given by the convolution of the expected flux from the source, $\phi_{\nu_\mu}(E) + \phi_{\bar{\nu}_\mu}(E)$, and the detector effective area, $A^i_{\rm eff}(E)$, through the relation,

$$\mathrm{R}^i = \int_0^\infty \frac{d\phi_\mu}{dE}\, A^i_\mu(E)\, dE \tag{99}$$

where the apex i denotes which experiment we are considering, i.e. ANTARES, KM3NeT (ARCA) or IceCube. The last formula is very similar to Eq.38, although we notice that the factor

Table 13: First 4 columns: *Spectral parameters assumed for the γ-ray fluxes, consistent with the H.E.S.S. observations as explained in the text: the search region (PS=Point Source or D=Diffuse), the spectral index Γ, the flux normalization ϕ_0 in units of 10^{-12} TeV^{-1} cm^{-2} s^{-1} and the energy cut-off E_{cut} in TeV (see Eq. 96). For the PS and the D models, we show also the maximum and minimum expected values.* Last 3 columns: *Expected number of $\nu_\mu + \bar{\nu}_\mu$ events per year: downward-going tracks and HESE events in IceCube, upward-going tracks in ANTARES and ARCA. Table from [8].*

	γ-rays			$\nu_\mu + \bar{\nu}_\mu$		
	Γ	ϕ_0	E_{cut}	$R^{ANTARES}$	R^{ARCA}	R^{IC}
PS	2.14	2.55	10.7	$6.2 \cdot 10^{-3}$	1.1	$5.2 \cdot 10^{-2}$
"	2.04	2.92	13.6	$9.5 \cdot 10^{-3}$	1.5	$8.2 \cdot 10^{-2}$
"	2.24	2.18	7.8	$3.9 \cdot 10^{-3}$	0.7	$3.2 \cdot 10^{-2}$
D	2.32	1.92	-	$1.2 \cdot 10^{-2}$	1.4	$1.3 \cdot 10^{-1}$
"	2.20	2.21	-	$2.1 \cdot 10^{-2}$	2.2	$2.6 \cdot 10^{-1}$
"	2.44	1.63	-	$7.5 \cdot 10^{-3}$	1.0	$7.4 \cdot 10^{-2}$
DC	2.32	1.92	400	$1.0 \cdot 10^{-2}$	1.3	$9.7 \cdot 10^{-2}$
DC	2.32	1.92	600	$1.1 \cdot 10^{-2}$	1.3	$1.0 \cdot 10^{-1}$
DC	2.32	1.92	2900	$1.2 \cdot 10^{-2}$	1.4	$1.2 \cdot 10^{-1}$

4π is not present, because here we are considering a flux from a point source and not a diffuse flux that extends over the full solid angle. Also the exposure time T is not present, since it is fixed to 1 year. Moreover in Eq.99 we use only the flux of muon neutrinos and antineutrinos because we are interested in events with a good angular resolution, that can point the source.

As discussed above, KM3NeT and ANTARES can look at the Galactic Center using upward-going muons, while IceCube has to use downward-going muons further subject to the condition that their vertex is contained in the detector; moreover, the first type of telescopes has a much better angular resolution, which allows them to reduce the background considered in the analysis, thus increasing the signal to noise ratio. Despite the fact that the dimensions of KM3NeT and IceCube are comparable, the effective areas differ significantly *at low energies*, as can be ascertained from Fig. 16. Note however that the two effective areas become very similar around PeV energies, as expected because of the similar physical sizes of these two neutrino telescopes. The different effective areas lead to the difference in the number of events expected in IceCube and KM3NeT, which amounts to about an order of magnitude.

EXPECTED SIGNAL RATES The rates of events for ANTARES, KM3NeT-ARCA and IceCube are given in Tab. 13 with the names $R^{ANTARES}$, R^{ARCA}, R^{IC}, considering the different spectral model of γ-ray data presented above, and accounting for both contributions from muon neutrinos and antineutrinos, as expressed in Eq. 98. Baikal-GVD will have a threshold of few TeV and a volume similar to KM3NeT-ARCA, so the results are expected to be similar, but we cannot provide a precise evaluation of the signal since we do not have the effective area.

For comparison, we calculated that the expected rate corresponding to Eq. 97 (namely assuming a E^{-2} distribution) in IceCube is 3.8 per year, namely, more than one order of magnitude above the values of Tab. 13. This illustrates the great importance of investigating the γ-ray distribution at higher energies than currently observed.

As can be seen from Tab. 13, the detectors located in the Northern hemisphere are better suited for neutrino searches from Sgr A*. In fact, when the source is below the horizon, they can observe the Galactic Center Region through upward-going track events, that are not polluted by the atmospheric muons. Such detectors are ANTARES, Baikal-GVD and KM3NeT. We find that the expected rates in ANTARES are just one order of magnitude smaller than those expected in IceCube with downward-going events: this result is well in agreement with the ones in [176].

DISCUSSION Among the γ-ray models presented in this table, the most plausible ones are, presumably, those described by a power law *with* a cut-off.

In the Diffuse case, even considering the less favorable case (the one with lowest energy cut-off, which implies a cut off in the primary spectrum of protons at about 4 PeV, where the *knee* of the Earth-observed CR spectrum is located) predictions are such that the incoming km^3 class detectors in the Northern hemisphere as KM3NeT-ARCA could measure these neutrinos with a rate of few events per year: several years of data-taking will be in any case needed in order to establish the presence of a proton galactic accelerator up to PeV energies and address the origin of very-high-energy cosmic rays. In case of non-detection, however, strong constraints will be derived concerning the proton acceleration efficiency of this poorly-understood source.

Unfortunately, with the current neutrino telescopes, these predictions cannot be probed yet. Anyway, since most of the signal is expected in the 1-100 TeV energy band, the Northern hemisphere telescopes cannot escape from the issue of atmospheric neutrino background events.

7.3 NEUTRINOS FROM BL LACS

In this connection, Fermi-LAT, that has obtained a relatively complete survey of the γ-ray sky below a few 100 GeV, has produced results that are of special interest. In the region $E_\gamma > 10$ GeV, the brightest objects are the blazars (we refer to e.g., [202] for a review), radio-loud AGN whose relativistic jet is closely aligned with the line of sight. They are broadly classified as BL Lacs (namely BL Lacertae) and as flat spectrum radio quasars (FSRQ). BL Lacs are characterized by featureless optical spectra (i.e. lacking strong emission/absorption lines). A finer classification of BL Lacs is considered below.

Blazars have been described in Sec.2.2.3, in the chapter dedicated to the description of different plausible sources of high energy neutrinos. They are widely considered to be promising candidates for high-energy neutrino emission ([84, 85, 86, 171, 203, 204, 205, 93, 206, 207, 94, 208, 209]). Moreover, certain analyses of IceCube data (we refer to [206] for a very recent and comprehensive work) suggest that a fraction of the events seen by IceCube could be attributed to blazars.

In recent works ([91, 160, 90, 89]) focus was put on the subclass of blazars called BL Lacs; the present study also concentrates on this hypothesis. In the models of Tavecchio et al., (we refer to in particular [91, 90, 89]), the secondary high-energy particles (neutrinos and γ-rays) are to a good extent produced in alignment with the direction of the jet (spine-layer model) and therefore one expects a tight correlation of the signals. This highly definite astrophysical setup adds motivations to the present investigation.

At this point we can formulate the question that we examine and discuss:

Are the highest energy extragalactic neutrinos seen by IceCube fully attributable to BL Lacs?

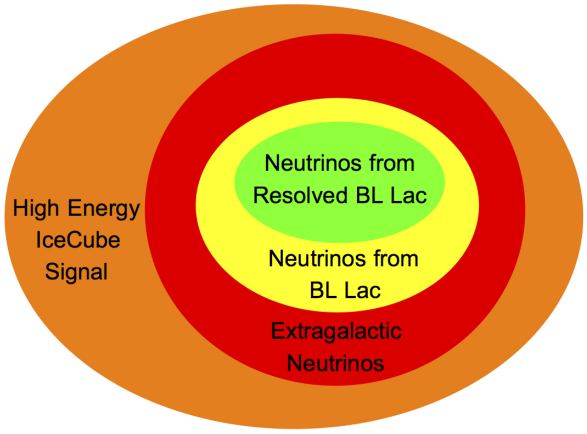

Figure 39: *Scheme of the present investigation: We assume that* a part of the high energy neutrino signal *seen by IceCube includes extragalactic neutrinos. We investigate whether the extragalactic emission can be attributed largely or fully to BL Lac emission, relying on the fact that a large fraction of BL Lacs, as discussed in Sect. 7.3.1, is observed by Fermi-LAT. Figure from[9].*

This hypothesis, presented in a slightly more general form in Fig. 39, is investigated in this section. We note that neutrinos and the γ-rays are observed at rather different energies in IceCube and Fermi-LAT, respectively, and that the details of the connections greatly depend upon on uncertain theoretical modeling. Thus, the investigation is bound to proceed on phenomenological grounds. We refer to [94] for a similar and complementary study of blazars and neutrinos.

The outline of this section is as follows. In Sect. 7.3.1 we define the context of the discussion; we discuss under which conditions the above hypothesis is viable. Then we perform the crucial test, by searching for correlations between extragalactic neutrinos and the subclass of high-energy emitting BL Lacs that are identified astronomically. We argue in Sect. 7.3.4 that the number of observed correlations is too small and that the hypothesis is not supported. We also derive the expectation on multiplets of neutrino events and compare this with the observations (Sect. 7.3.5). We discuss, in Sect. 7.3.6, the results and the possible ways out from the conclusion that the observed neutrinos with energy above 200 TeV receive only a minor contribution from BL Lacs.

7.3.1 Extragalactic neutrinos and BL Lacs

Before examining the connection, we need to discuss a few important questions: 1) Which set of neutrino data gives us the best chance of extracting and identifying the extragalactic part of the signal; 2) What is the fraction of the extragalactic neutrinos of IceCube that should correlate with BL Lacs; 3) How do we compare with the limit on neutrino emission from blazars obtained by IceCube in [94]?

Importance of the high-energy through-going events

In Sec.5.1 we have discussed that there are two main classes of signals detected in IceCube: 1) The *through-going events*, that are muons (or antimuons) due to neutrinos interacting outside the detector; and 2) the *high-energy starting events* (HESE), whose vertex is instead contained inside the instrumented volume. Among HESE, one distinguishes those events where there is a track, associated to charged-current muon neutrino interactions, and those where the track is absent and the energy is deposited in a small region, that are associated to the other types of flavor and interactions.

Recently IceCube has published a relatively large set of 29 through-going events, collected over six years ([129]) and with very high energy; all of them have energy ≥ 0.2 PeV and the highest energy event seen to date corresponds to a neutrino with more than 4.5 PeV and belongs to only this dataset. These through-going events provide strong support for the observation of a signal of cosmic neutrinos previously claimed by IceCube with the HESE dataset. When comparison is possible, the two datasets are consistent with a common, simple interpretation. In this paragraph we discuss the three main reasons why we consider that this specific dataset is particularly important for the investigation of the BL Lac hypothesis.

ENERGY DISTRIBUTION The neutrino signal corresponding to the through-going event dataset is compatible with a single power-law distribution with a spectral index $\gamma = 2.13 \pm 0.13$ ([129]). It is remarkable that this distribution agrees well with the high-energy part of the HESE dataset, as argued in [7] and eventually proved in [129] (see also Sec.5.1).[2] The bulk of the HESE data, that includes the events collected at lower energies, indicates a different spectral index instead, closer to $\gamma = 2.5$. This feature of the HESE data can be attributed to the onset of another component of the signal with lower energy that is plausibly not entirely of extragalactic origin, as discussed in Chapter 6, dedicated to the interpretation of the IceCube neutrino events. We note that a relatively hard distribution of extragalactic neutrinos can be extrapolated at lower energies without particular difficulty, whereas, if the extragalactic neutrinos were distributed as $E_\nu^{-2.5}$ at low energies, this would imply an excessive amount of γ-rays ([10]), or too many low-energy track events, similar to those expected from prompt atmospheric neutrinos and for which we have no evidence ([7]). Thus, in order to remain cautious for what concerns the interpretation of the extragalactic neutrino distribution (i.e. the population of neutrinos that is relevant to assess the BL Lacs contribution) we deem that it is preferable to focus the discussion on the high-energy part of the spectrum. This is consistent with our model that we have presented in Chapter 6, where the extragalactic component is distributed as E^{-2} in the νgal1 model of Sec.6.2 and as $E^{-2.13}$ in the νgal2 of Sec.6.3.

NORTHERN HEMISPHERE The through-going events originate from muon neutrinos/antineutrinos that are converted into muons/antimuons near the detector. For this class of signal events, the Earth works, at once, as a neutrino converter and as a screen for the atmospheric muons. Thus, most of the events come from below the horizon; in the case of IceCube this means the Northern hemisphere. In this hemisphere, it is expected that the contribution of the signal due to galactic sources is small or absent, as described in Sec.6.3 (see particularly Tab.12). This statement

[2] A featureless and hard power-law spectrum would suggest a pp production mechanism for neutrino production, rather than the usually expected $p\gamma$ mechanism. However, it is not possible to say that the $p\gamma$ mechanism is unavoidable for BL Lacs. Moreover, the spectrum is measured only in a small range of energy between 200 TeV and some PeV. The high energy part of the spectrum is not yet sensitive to the mechanism of production, and this is not a critical aspect of the BL Lac hypothesis. We refer to [170, 23] for a detailed discussion of the photohadronic interaction.

is even more true for the specific dataset used in [129], which satisfies also the high-energy criterion discussed immediately above. We refer to [176, 6, 7] for further discussion.

POINTING OF THROUGH-GOING EVENTS The last and most important characteristic of through-going events is that their arrival directions are known relatively well. This is a general feature of events of the track type, although in some cases the precision is bad, similar to the one of the HESE, shower events. In Table 4 of [129], reported in Appendix D.1 for completeness, the declinations δ and the right ascension α are given along with their asymmetric errors $\delta_{\pm}$ and $\alpha_{\pm}$, at the 50% CL and at 90% CL. We have checked that the errors in the two cases scale roughly according to a Gaussian distribution but we use, as a rule, the more conservative case (90% CL) in our analysis. The angular span of these two angular coordinates is given by the sum of the upper and lower ranges, that are, in general, different: $\Delta\delta(i) = \Delta\delta_{+}(i) + \Delta\delta_{-}(i)$ and likewise $\Delta\alpha(i) = \Delta\alpha_{+}(i) + \Delta\alpha_{-}(i)$ where $i = 1, 2, 3....29$. Each event subtends a solid angle of $\Omega(i) = \Delta\delta(i) \times \Delta\alpha(i)$, that, according to the quoted confidence levels, is expected to include the true direction with a confidence level of $0.9^2 = 81\%$. We note that the total angular size spanned by the neutrino events is small

$$\sum_{i=1}^{29} \Omega(i) = 3.5\% \times (2\pi), \tag{100}$$

where we compare with the solid angle subtended by Northern sky. It is also convenient to define a single (linear) angle that quantifies the region around the individual event as follows,

$$\theta(i) \equiv \sqrt{\frac{\Omega(i)}{\pi}}. \tag{101}$$

We refer to this angle as the "average angular resolution". A histogram of values based on the 29 events is shown in Fig. 40. We note the presence of two outlying events, whose direction is identified only poorly. These are event number 6 and event number 14 in Table 4 of [129]. In order to be more quantitative, we note that 1) the event number 6 alone covers 61% of the solid angle spanned by neutrinos given in Eq. 100; and that 2) if we exclude the two outliers, and consider the angle spanned by the remaining 27 events, $3.5\% \rightarrow 0.9\%$. Considering the angular resolutions shown in Fig.40 and excluding the two outliers, we have the average angular resolution $\bar{\theta} = 1.2^{\circ} \pm 0.9^{\circ}$, in agreement with the expected angular resolution in the ice for track-like events (see Sec.4.4.2).

INVESTIGATION OF THE ORIGIN OF THE EXTRAGALACTIC COMPONENT The first reason why the 29 through-going events, the largest sample of high-energy events collected by IceCube, are so important to us is that they are compatible with an extragalactic origin. The fact that these events come from the Northern hemisphere gives us further confidence supporting the hypothesis that the cosmic neutrino signal that contributes to this dataset has an extragalactic origin. The latter feature (i.e. pointing) offers us the chance to use these data to identify the sources of the events; we use it in Sect. 7.3.4 to test our assumption on the high-energy neutrino emission from BL Lac.

7.3.2 Fraction of correlated neutrino events

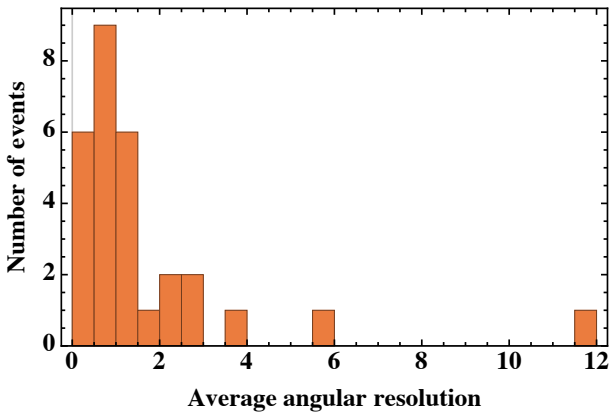

Figure 40: *Values for the 29 through-going events of the average angular resolution, defined as described in Eq. 101. We note the two outliers, discussed in the text [9]. Figure from [9].*

MODELING OF BL LAC The γ-rays telescopes and in particular Fermi-LAT can see individually only a fraction of the BL Lacs. The rest corresponds to objects that are too dim (i.e. too far and/or too under-luminous) to be observed; we refers to these as un-resolved BL Lacs. This fraction is of the order of one and it is widely believed that the class of BL Lacs that are un-resolved gives an important contribution to the "diffuse" γ ray emission at the highest energies.

It is possible to be more precise thanks to the model of [83]. In that paper, a detailed parameterization of the luminosity function of the BL Lacs distribution, differential in $0.1 - 100$ GeV luminosity (L_γ), redshift (z) and photon index (Γ),

$$\frac{\partial^3 N}{\partial L_\gamma \partial z \partial \Gamma}, \tag{102}$$

is studied. The parameters are obtained, within errors, thanks to the observational data. The result depends on modeling and in the following we adopt the result from the two best models of [83], there referred to as LDDE (luminosity-dependent density evolution) and PLE (pure luminosity evolution).

Exploiting the results of this analysis it is not difficult to calculate the total flux of γ-rays due to BL Lacs,

$$\phi^\gamma_{\rm tot} = \int dL_\gamma dz d\Gamma \, \frac{\partial^3 N}{\partial L_\gamma \partial z \partial \Gamma} \, \frac{dF}{dE_\gamma}(L_\gamma, z, \Gamma; E_\gamma), \tag{103}$$

where dF/dE is the differential flux of the single power-law source, that integrated over the energies gives,

$$F(L_\gamma, z, \Gamma) = \frac{\mathcal{N}_\gamma}{4\pi D_c^2(z)} (1+z)^{-\Gamma} \text{ with } \mathcal{N}_\gamma = \frac{L_\gamma}{\langle E_\gamma \rangle}, \tag{104}$$

where $D_c(z)$ is the comoving distance and the factor $(1+z)^{-\Gamma}$ accounts for the redshift. For a sample plot of the total flux in the case of LDDE model, obtained using Eq. 103, see Fig. 3 of [10].

The result of the calculations of the quantities relevant for the present analysis, namely the γ-ray fluxes from resolved and un-resolved BL Lacs, are given in [10], which is fully based on the work of [83]. The flux of γ-rays due to the resolved BL Lacs is, $\phi^{\gamma}_{\rm res} = 8.5 \times 10^{-7}$ ph/(cm^2 s sr), with a small uncertainty. The flux of the un-resolved BL Lacs is given by $\phi^{\gamma}_{\rm unres} = \phi^{\gamma}_{\rm tot} - \phi^{\gamma}_{\rm res}$, thus, its value depends on theoretical modeling. Table 2 of [10] gives the result for the two models mentioned above: $\phi^{\gamma}_{\rm unres}({\rm LDDE}) = 8^{+2}_{-1.3} \times 10^{-7}$ ph/(cm^2 s sr) and $\phi^{\gamma}_{\rm unres}({\rm PLE}) = 10^{+2.1}_{-1.7} \times 10^{-7}$ ph/(cm^2 s sr). We use conservatively the upper range of the largest prediction (PLE), $\phi^{\gamma}_{\rm tot} < 20.6 \times 10^{-7}$ ph/(cm^2 s sr) and the lower range of the smallest prediction (LDDE), $\phi^{\gamma}_{\rm tot} > 15.2 \times 10^{-7}$ ph/(cm^2 s sr), thereby finding the fraction of the γ ray flux due to resolved BL Lacs,

$$f_{\gamma} = \frac{\phi^{\gamma}_{\rm res}}{\phi^{\gamma}_{\rm tot}} = 0.5 \pm 0.1. \tag{105}$$

Therefore, this fraction is relatively well-known, the uncertainty being about 20% (we note incidentally that the un-resolved flux can account for a large part of the diffuse flux observed above 10 GeV as argued in [83]).

An important remark is as follows. On the one hand, we would like to have information on γ ray emission at the highest energy, but on the other hand, the Universe becomes opaque to γ rays above 100 GeV, and this limits the useful observational window. From this point of view, the subset of BL Lacs characterized by an intense emission above 50 GeV, collected in the catalog 2FHL, [210], is particularly interesting for us and we use it in the following. A complete model of the cosmological evolution of these objects is not yet available; however, the BL Lacs of the 2FHL catalog belong mostly to the subclass of the high-frequency synchrotron peak (HSP) that were studied in [83]. We note that the HSP have a negative cosmological evolution, that is, they are more abundant at low redshift (we refer in particular to Fig. 11 of [83]). From this consideration, it is expected that the visible fraction of the BL Lacs included in [210] is possibly even higher than 0.5. This conclusion is very important in view of the subsequent analysis.

HYPOTHESIS ON NEUTRINO EMISSION In most theoretical models, the neutrino luminosity is proportional to the γ ray luminosity; we refer to [211]; [84, 85, 86, 203, 171, 204, 205, 89]. Therefore, we assume that the fraction of the extragalactic neutrino flux f_{ν} that corresponds to resolved BL Lacs (i.e. the tagged fraction) equates the fraction determined immediately above[3],

$$f_{\nu} = f_{\gamma}, \tag{106}$$

and we assume that this is true in particular for what concerns the BL Lacs that emit the very-high-energy events observed by means of through-going muons.

Since we use the integrated quantities, this inference should be relatively stable and not crucially dependent upon the detailed connection between neutrinos and gamma rays. We argued that the fraction of neutrinos due to the BL Lacs that emits γ-rays at the highest observed energies (in particular those included in 2FHL catalog) is not underestimated by f_{γ}. In other words, when we use Eq. 105 along with the high-energy neutrino signal, we obtain the minimum number of expected correlations with the BL Lacs in the 2FHL catalog.

[3] We note that we do not need to introduce a proportionality coefficient between the flux of γ-rays and the flux of neutrinos, since we are only interested in the fraction of visible flux with respect to the theoretical (expected) total flux. E.g., in [89] the almost constant coefficient $\phi_{\nu} = 0.46\phi_{\gamma}$ is obtained in a BL Lac scenario, but it disappears from the ratio of Eq. 105.

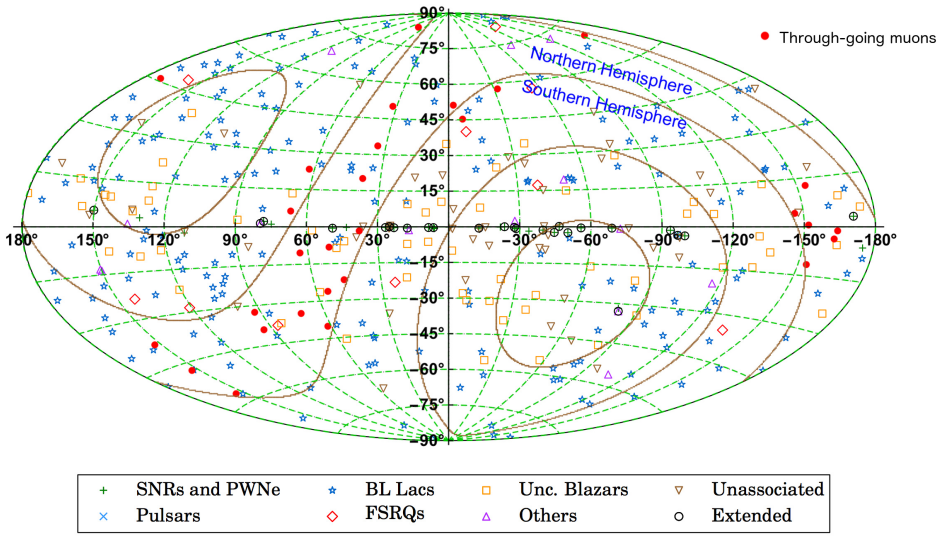

Figure 41: *Map, in Galactic coordinates, of the γ-ray sky observed by Fermi-LAT, from [210]. The red points indicate the 29 through-going muons, with a deposited energy above 200 TeV, observed by IceCube over 6 years; their angular uncertainties are not represented in this figure, but are taken into account in the calculations. The brown lines represent intervals of declination of* $30°$ *[9].*

7.3.3 Comparison with the bound on neutrinos obtained by IceCube

Recently IceCube has published a study ([94]) concerning neutrinos from blazars where a limit on the fraction of the signal neutrino events observed and attributable to these astrophysical objects was obtained. This study is relatively similar in spirit to the present work, namely, it is a search for correlations between certain classes of astronomical objects and the observed neutrinos, hypothesized to originate from these objects. Thus, it is especially important to highlight the differences between our approaches and theirs:

1. IceCube collaboration focusses on the study of blazars whereas we prefer to be more specific and emphasize the comparison with the BL Lacs instead, following Tavecchio et al. [91, 90, 89];

2. the result of IceCube is based on data of energy above 10 TeV, that is, well below the lowest energy of the through-going muon dataset that we use, 200 TeV;

3. finally and most importantly, we consider the total set of BL Lacs, not only those that are resolved, since it is presumable that also the ones that are not resolved emit high energy neutrinos.

Therefore, we examine here the bound of IceCube from a different perspective.

We consider the simplest description of the neutrino signal that explains the through-going muons flux. This is a power law with $\alpha = 2$, a value admitted within 1σ, as illustrated in Fig. 6 of [129]. From the same figure we find that the normalization of flux of ν_μ and $\bar{\nu}_\mu$ is equal to

$$\frac{d\phi_\mu}{dE}(\text{through-going}) = (6 \pm 2)\left(\frac{E}{1\ \text{GeV}}\right)^{-2} \frac{10^{-9}\ \text{GeV}}{\text{cm}^2\ \text{s sr}}, \tag{107}$$

with an uncertainty of about 30% on the normalization. This describes the extragalactic neutrino flux that we assume to be fully explained by BL Lac emission. In order to calculate the fraction of the neutrino flux due to resolved BL Lacs, we simply have to multiply it by the fraction given in Eq. 105, obtaining

$$\frac{d\phi_\mu^{\rm res}}{dE}(\text{theo.}) = (3 \pm 1.2) \left(\frac{E}{1\ \text{GeV}}\right)^{-2} \frac{10^{-9}\ \text{GeV}}{\text{cm}^2\ \text{s sr}}, \tag{108}$$

where we summed the uncertainties in quadrature. The bound obtained by IceCube is reported in Table 3 of [94] for the case where $\alpha = 2$, "All 2LAC Blazars" and "equal weighting". The bound is

$$\frac{d\phi_\mu^{\rm res}}{dE}(\text{obs.}) < (4.7 \pm 0.5) \left(\frac{E}{1\ \text{GeV}}\right)^{-2} \frac{10^{-9}\ \text{GeV}}{\text{cm}^2\ \text{s sr}}, \tag{109}$$

where we use the 1σ uncertainty instead of the 90% confidence level (C.L) quoted in the table. This bound is not incompatible with the hypothesis that BL Lacs produce all the extragalactic neutrino flux. We note that the second reason why we have chosen to discuss the spectral index $\alpha = 2$ for the through-going muons flux is that this value permits a direct comparison between the measured fluxes and the bound. The bound of IceCube becomes tighter by increasing α and for $\alpha = 2.2$ excludes that the blazars of [210] emit more that 50% of the neutrinos ([94]). However, in view of Eq. 105, this is not incompatible with the hypothesis that the BL Lacs (those resolved and unresolved) account for the full extragalactic neutrino emission. Similar analyses, using a wider set of catalogs for the γ-ray sources, are presented in [206]; the results are slightly tighter but comparable with those of IceCube.

7.3.4 Spatial connection between BL Lacs and high-energy neutrinos

Here we investigate whether the counterparts of high-energy neutrino events contained in [129] are the BL Lacs.

The number of expected correlations

Cosmic rays that hit the terrestrial atmosphere yield secondary particles that act as background events, that is, they contaminate the observational sample: These are (1) muons that come mostly from the sky above the detector and affect the interpretation of the HESE dataset but not much the through-going muons and (2) neutrinos and antineutrinos that have a different (softer) energy spectrum than the signal and are mostly muon neutrinos and antineutrinos at relatively low energies. The role of neutrinos in the decay of charmed mesons is not known precisely and this creates uncertainty in the inferences at a few 100 TeV, as we have seen in Sec.5.1.3 dedicated to the atmospheric backgrounds; however it is possible to use the data themselves to obtain a bound on this component that is not far from the current theoretical predictions as shown in [129].

Therefore in order to calculate the number of expected correlations, the first step is the evaluation of the number of tracks that can be attributed to the signal, i.e. to astrophysical neutrinos (or equivalently what can be attributed to the atmospheric background). This can be done using Table 4 of [129], where the "signalness" s_i for each event $i = 1, 2...29$ is given. This quantity is defined as the ratio of the astrophysical expectation over the sum of the atmospheric and astrophysical expectations for a given energy proxy and the best-fit spectrum. We use these

values of s_i to build a likelihood function that estimates the total number of events that can be attributed to the signal, or equivalently, the number of events that have to be attributed to the background. This is obtained expanding the polynomial $\mathcal{P}(x)$,

$$\mathcal{P}(x) = \prod_{i=1}^{29}[s_i x + (1 - s_i)] = \sum_{n=0}^{29} p_n x^n, \tag{110}$$

where the coefficient $p_n \leq 1$ represents the probability that there are exactly $N_{\rm signal} = n$ signal events; the consistency condition $\sum_{n=0}^{29} p_n = 1$ holds true. In this manner, we found that the through-going event dataset contains a number of signal events equal to

$$N_{\rm signal} = 20.4 \pm 2.4, \tag{111}$$

where we quote the uncertainty at 1σ. When we combine this information with that provided by Eq. 105, we find that the number of neutrino events, which should show a spatial correlation with BL Lacs, is simply

$$N_{\rm corr} = f_\nu \times N_{\rm signal}. \tag{112}$$

The contribution to its uncertainty is given both by the uncertainty on the experimental data N_s and by the uncertainty on f, as follows:

$$\Delta N_{\rm corr} = N_{\rm corr} \sqrt{\left(\frac{\Delta N_{\rm signal}}{N_{\rm signal}}\right)^2 + \left(\frac{\Delta f_\nu}{f_\nu}\right)^2}. \tag{113}$$

This results in

$$N_{\rm corr} = 10.2 \pm 2.4, \tag{114}$$

that has an uncertainty of 25%. Therefore, we assume that the likelihood $\mathcal{L}_{th}(n)$ that gives the expected number of correlations is a Gaussian function, with mean value $\mu = 10.2$ and standard deviation $\sigma = 2.4$.

Number of observed correlations estimated adopting IceCube uncertainties

In order to search for the counterparts of the high-energy neutrinos, we use the coordinates of the through-going muons and also the uncertainties[4] listed in Table 4 of [129] along with the 2FHL catalog of the γ-ray sources of the Fermi-LAT collaboration ([210]). These data are shown in Fig. 41. We note that most of the neutrino events come from the region between $0^\circ \leq \delta \leq 30^\circ$; this is consistent with the fact that other neutrinos in this sample are largely absorbed in the Earth, since they have high declinations and high energies (namely, a reconstructed energy of muons above 200 TeV): [129].

When we compare them with the positions of the BL Lacs in [210], we find that there is only one correlation within the 81% C.L. More precisely, the neutrino event number 6 of Table 4 of [129] can be associated with the BL Lac *J1725.1+1154* or the BL Lac *J1555.7+1111*. (As already discussed, we used the confidence level interval reported in Table 4 of [129]. This corresponds to 90% C.L. for declination and right ascension, and therefore the two dimensional confidence level is slightly less, i.e. $0.9 \times 0.9 = 81\%$.)

[4] In the table, only statistical uncertainties are reported. We assume here that the systematic uncertainties give a sub-dominant contribution to the total uncertainties and discuss this point in the following.

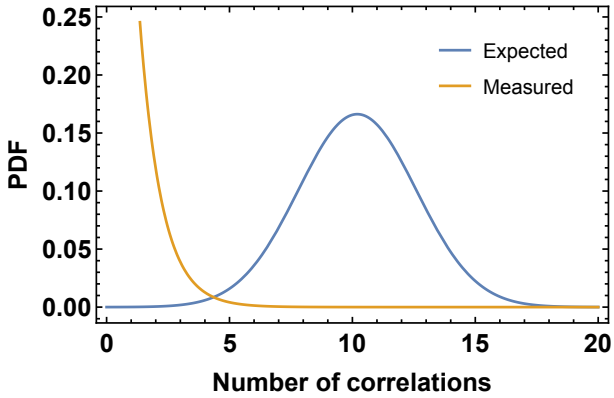

Figure 42: *The orange line is the PDF of the observed number of correlations. In blue line we show the expected number of correlations, assuming that the BL Lacs are the main emitters of high-energy neutrinos, discussed after Eq. 114. Figure from [9].*

It is important to underline that the direction of the neutrino event number 6 is not well reconstructed. In fact this event is one of the two outliers illustrated in Fig.40 and its angular uncertainty is of the order of 10°, much larger than the typical value of about $\sim 1^\circ$. Therefore this correlation could be attributed to the poor angular uncertainty of the events. However, in order to be conservative, we do not rule out this correlation in the rest of this analysis.

In order to generalize the procedure, we scale the uncertainties given in Table 4 of [129] by a coefficient k, in the following manner:

$$\Delta(k) = \frac{k}{1.65} \times \Delta_{90\%}, \tag{115}$$

where $\Delta_{90\%}$ are the uncertainties on the declination and on the right ascension quoted in the table at 90% C.L., $\Delta(k)$ are the new uncertainties of α and δ, and k denotes the number of (one dimensional) σ of our interval. The value of the two-dimensional confidence level is given simply by the square of the integral of the standard normal distribution between $-k$ and k,

$$\text{C.L.}(2\ \text{d.o.f}, k) = \left[\int_{-k}^{k} \frac{1}{\sqrt{2\pi}} e^{-\frac{x^2}{2}}\, dx\right]^2. \tag{116}$$

Table 14: *Number of correlations as a function of k and the corresponding confidence level (C.L.). Table from [9].*

k	C.L.	N. of correlations
1	0.466	0
1.5	0.751	1
2	0.911	1
2.5	0.975	2
3	0.995	4
3.5	0.999	6
4	> 0.999	6

Some values of k, the corresponding confidence levels and the number of correlations observed within a certain C.L. are reported in Table 14. The number of correlations within a certain C.L. (see Table 14) is reasonably well fitted by a probability density function with an exponential shape. Therefore the Probability Distribution Function (PDF) of the observed number of correlations is given by the derivative of

$$\mathcal{L}_{obs}(n) = 1 - \exp\left(\frac{n}{n^*}\right) \text{ with } n^* = 0.90 \pm 0.05. \tag{117}$$

In Fig. 42 we show how many correlations are present within a certain confidence level. The PDF is shown in Fig. 42 by an orange line. The average number of correlations is 0.9 whereas the median value is 0.6. In the same figure the distribution of the expected number of correlations from theoretical considerations is also illustrated (blue line).

In order to compare two different distributions, that is, the expected theoretical correlations $\mathcal{L}_{th}(n)$ and the observed correlations $\mathcal{L}_{exp}(n)$, we use the same procedure described in [6], adopting the following formula to evaluate the "distance" between the distributions:

$$\mathcal{L}(\delta) = \int_0^\infty \mathcal{L}_{exp}(n) \times \mathcal{L}_{th}(n+\delta)\, dn. \tag{118}$$

We found that $\mathcal{L}(\delta)$ is in good approximation and normally distributed, with a mean value of $\mu = 9.4$ and a standard deviation of $\sigma = 2.5$. The null value is excluded at 3.7σ and this represents the difference between these two distributions. Taking into account the uncertainty in the fit of $\mathcal{L}_{th}(n)$ we found a similar result, since the two distributions are different with a significance of $3.7 \pm 0.1\sigma$. Excluding the outliers, that is, the neutrino event numbers 6 and 14, the difference between the two distributions has a significance of 4.1σ. These considerations are true under the hypothesis that neutrinos are produced in the BL Lacs, associated to the γ-rays that we observe from those sources. We refer to [212] for an alternative scenario in which high-energy neutrinos are not produced directly in the source but are given by the interaction of cosmic rays produced in a generic AGN and the EBL.

Combining the information provided by the theoretical likelihood and the experimental likelihood, it is also possible to find the contribution of the BL Lacs to the IceCube neutrinos above 0.2 PeV. We can estimate the fraction ξ of the events, that can be attributed to the BL Lacs, by means of the following likelihood function:

$$\mathcal{L}_{frac}(\xi) \sim \int_0^\infty \mathcal{L}_{exp}(\xi \times n)\mathcal{L}_{th}(n)\, dn \tag{119}$$

In this way, we find that the fraction is $\xi = 0.11$ at 67% C.L. and $\xi = 0.23$ at 90% C.L. Considering the present data, the probability that the BL Lacs contribute more than 50% to the through-going muons above 0.2 PeV is less than 1%.

Number of observed correlations estimated varying the angular intervals

An alternative procedure is the following one. If we disregard the angular resolution quoted by the IceCube collaboration, and we vary it instead, it is interesting to ask how many events have a counterpart within a certain angular distance. Considering a neutrino event with coordinates (α_1, δ_1) and a BL Lac with coordinates (α_2, δ_2), the angular distance d is given by the spherical distance, defined as follows:

$$d \equiv \sqrt{(\delta_2 - \delta_1)^2 + (\alpha_2 - \alpha_1)^2 \cos(\delta_1)\cos(\delta_2)}. \tag{120}$$

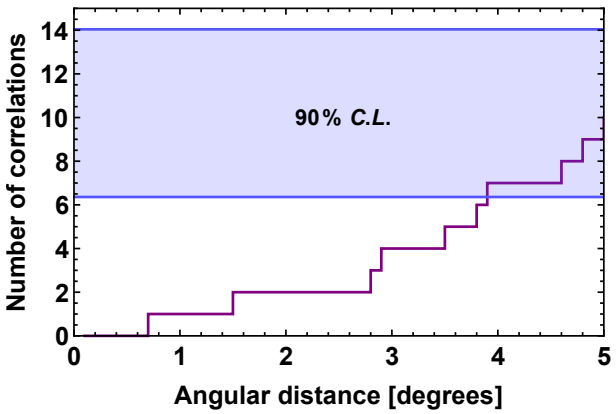

Figure 43: *Number of correlations found as a function of the angular distance between the position of the neutrino events and the position of the BL Lac. Within 1 degree, only 1 correlation has been observed. The horizontal band shows the expectations given in Eq. 114. Figure from [9].*

This expression can be obtained by expanding for $\delta_1 \approx \delta_2$ and $\alpha_1 \approx \alpha_2$, the scalar product of the two unit vectors in the given directions, $\cos(d) \equiv (n_1, n_2)$. Therefore, d subtends the region of solid angle

$$\Omega = \pi d^2, \tag{121}$$

and it is directly comparable with the average angular resolution θ defined in Eq. 101.

Using this procedure we find that only one event has a counterpart at distance $d \leq 1^\circ$; it is the through-going event number 23 of Table 4 of [129] that can be correlated with the BL Lac *J0211.2+1050*. We have tested that within $d \leq 2^\circ$ there are two possible counterparts. Finally, for completeness, we report in Tables 15 the 4 events[5] that show at least one correlation with a BL Lac within $\sim 3^\circ$.

In Fig. 43 we present a generalization of this analysis. Assuming that the BL Lacs are the counterpart of the IceCube neutrino events, we wonder how much the angular resolution of the tracks should be worsened, in order to observe a certain number of correlations.

If we want to recover the agreement with the expectation at 90% C.L., we need an average angular distance of $d \simeq 4^\circ$, namely, $\Omega = 50$ square degrees (Eq.121). This value is very different from the angular resolution declared for the tracks, typically close to 1° and more precisely equal to $\bar{\theta} = 1.2^\circ \pm 0.9^\circ$ for the present through-going muons dataset, as discussed after Eq. 101. Therefore the required angular resolution of 4° is in tension with the declared angular resolution with a significance of 3σ and could only be justified invoking a very large value of the systematic uncertainty.

7.3.5 Multiplets

Here, we discuss a more refined test of the hypothesis that BL Lacs are the main emitters of high-energy neutrinos: We evaluate the probability of observing at least one multiplet, that

[5] We note that the two correlations between the through-going muon number 6 and the BL Lacs are not present in this table, since the angular distance between them is larger than 3°, using the best fit coordinates of the neutrino directions. However, the very large uncertainties would not permit us to rule out the correlations between them.

is, two or more events from the same source. In this analysis we refer to identified BL Lacs contained in the second Fermi-Lat catalog ([210]).

As is clear from Fig. 41, most through-going muons come from the region $0^\circ \leq \delta \leq 30^\circ$. This is expected for the high-energy neutrino signal, due to the absorption in the Earth; this conclusion is consistent with the discussion given in [129]. Therefore we limit our analysis to the cleaner subset of BL Lacs that are contained in this part of the Northern sky. Repeating the same calculation of Sec. 7.3.4, for the subset of 23 events included in the interval of declination $0^\circ \leq \delta \leq 30^\circ$, we find that the number of events that can be attributed to cosmic neutrinos is equal to, $N_{\rm signal}(0^\circ \leq \delta \leq 30^\circ) = 16.9 \pm 2.1$ at 1σ. Using Eq. 112 we find that the number of signal events, expected to show a correlation due to their common origin, is equal to

$$N_{\rm corr}(0^\circ \leq \delta \leq 30^\circ) = 8.5 \pm 2.0, \tag{122}$$

at a C.L. of 1σ , which becomes 8.5 ± 3.2 at 90% C.L.

In this angular region, 43 BL Lacs are present in the Fermi-LAT catalog ([210]). Assuming that the probability of emitting a neutrino is proportional to the luminosity of the sources, as argued in [89], we define a weight w_i as follows:

$$w_i = \frac{L_i}{L_{tot}}, \tag{123}$$

where L_i and L_{tot}, taken from [210], are the luminosity of a single source and the sum of luminosity of the 43 sources, respectively. In order to evaluate the expected number of multiplets, as a function of the number of individual correlations, we perform several cycles of random extractions of 43 numbers, each one with a probability of extraction equal to w_i. Each one of these extractions can be thought of as a simulated experiment. Then, we count the frequency of occurrence of a multiplet with at least two or three events from the same source.[6]

The outcome is illustrated in Fig. 44. With the expected number of individual correlations, shown as a vertical band in the figure, the probability of non observation of a multiplet from a single source is between 25-75%. Thus, the fact that we do not observe any multiplet is not yet an issue. The lack of such an observation would become significant if the expected number of events was instead of the order of about 15-20. Therefore, this test will become important when the current 6-year statistics are doubled, or when we have 2-3 years of data from IceCube-Gen2, due to the bigger effective area of the incoming detector described in [213].

This analysis strongly depends on the class of objects considered and the absence of multiplets is not (yet) a problem assuming that high-energy cosmic neutrinos, above 0.2 PeV,

[6] In order to test the stability of our procedure, we also repeated the same calculation using a uniform extraction of the numbers, finding a very similar result.

Table 15: *Four events are reported here that show correlation with BL Lacs within 3°. The angular distance is defined in Eq. 120. Table from [9].*

ID μ event	BL Lac	d
23	J0211.2+1050	$< 1^\circ$
1	J0152.8+0146	$< 2^\circ$
2	J1942.8+1033	$< 3^\circ$
18	J2153.1-0041	$< 3^\circ$

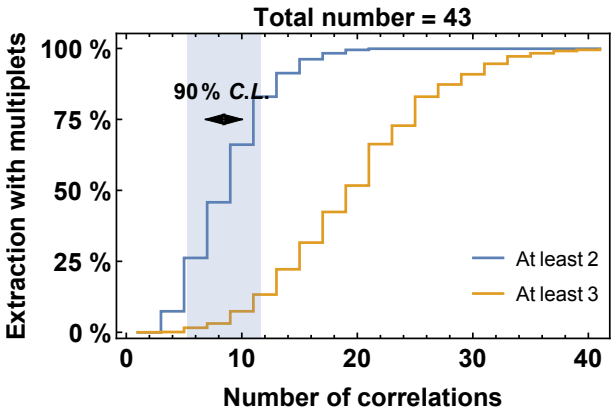

Figure 44: *Probability of observing one multiplet as a function of the number of correlations. We consider the 43 BL Lacs contained in the 2FHL Fermi-LAT catalog in the region $0° \leq \delta \leq 30°$. The luminosities of BL Lacs are taken into account in the calculation of the expectations. The expected number of correlations, assuming that the BL Lacs are the main emitters of high-energy neutrinos (Eq. 122), is indicated by the vertical band. Figure from [9].*

are fully produced by BL Lacs. We refer to [204] for a scenario in which, on the contrary, the absence of multiplets represents an issue even with the present IceCube data.

7.3.6 Summary and discussion

The BL Lacs are potentially good candidates for emitters of high-energy neutrinos. The existing upper bound on neutrino flux emitted from the resolved blazars, obtained by the IceCube collaboration ([94]), is not incompatible with the assumption that the BL Lacs account for the full high-energy part of the spectrum, measured by means of the through-going muons above 0.2 PeV, described in [129].

We have performed a refined test of this hypothesis. Among the through-going muon dataset, approximately two thirds of the events should be attributed to the astrophysical neutrinos. Assuming that these are produced in BL Lacs, we find that half of them, that is, approximately one third of the complete dataset, should be correlated with a BL Lac of the second Fermi-LAT catalog (2FHL). This leads us to expect some ten correlations with an uncertainty of about 25%. However we found that only the event number 6 has a BL Lac counterpart at 81% C.L. Even enlarging the search window, in order to reach 99% C.L., we find only three possible correlations. Generalizing, the average number of tracks that can be correlated with known BL Lacs is well below expectations.

This represents a serious issue for the hypothesis that the BL Lacs are the main sources of neutrinos above 0.2 PeV. Assuming that the systematic uncertainty (quoted in [129] only for the most energetic event) is smaller than the statistical uncertainty, this hypothesis turns out to be disfavored at about 3.7σ. Moreover, the direction of event number 6, that shows a correlation within 81% C.L., is not well reconstructed, since the uncertainty on its direction is of the order of 10°. Therefore the correlation with the BL Lac could simply be a coincidence due to poor angular resolution. If the result discussed above is not due to a statistical fluctuation and there

are no unaccounted systematic effects, the most plausible inference is that the BL Lacs are not the main emitters of the high-energy neutrinos above 0.2 PeV.

In view of the significance of this conclusion, it is important to discuss possible ways-out from the strong bound on the possible high-energy neutrino emission that we have obtained, that implies the conclusion that the observed neutrinos with energy above 200 TeV receive only a minor contribution from BL Lacs. We have shown that this hypothesis could be reconciled with the observations if the angular resolution of the tracks in IceCube was not as good as is quoted. The angular resolution of track-like events should be of $\sim 4^\circ$ to reconcile the expectations with the observations. The required departure is quite large and this makes this interpretation less plausible. For this reason, we are inclined to believe that this result argues in favor of the hypothesis that the high-energy neutrinos come from a population of faint neutrino emitters, meaning that most of the neutrino-emitting sources are not resolved with the present instrument; from a truly diffuse source (e.g., the halo of our Galaxy as argued in [214]); or from a type of source where γ-rays are heavily reprocessed and the radiation shifted at much lower energies. We note that it is also not possible to exclude the theory that BL Lacs themselves, as identified by γ-ray astronomy, are the sources of the highest-energy neutrinos seen by IceCube, if the neutrinos are emitted in a significantly wider angular range; this would imply a drastic departure from the spine-layer model of [91, 90, 89]. Finally, we remark that we cannot even exclude the possibility that BL Lacs are good emitters of neutrinos below 0.2 PeV, since this energy region has not been investigated in the present work.

In this section, we have also tested the probability of observing at least two events from the same source, assuming that BL Lacs are the high-energy neutrino emitters. Our result is that the non observation of multiplets does not represent an issue for the BL Lac hypothesis nowadays, but will become crucial in the future, especially after IceCube-Gen2 begins collecting data.

To conclude, some important remarks are in order: First, we highlight that our result complements and strengthens the recent upper bound on the blazar emission derived by IceCube in [94]. Second, we have argued that a correct understanding of the true spectrum of the extragalactic neutrinos is of utmost importance for multi-messenger astronomy. Third, we note that multi-messenger adopted in this section has great scientific potential and will allow us to proceed in the study of the origin of astrophysical neutrinos observed by IceCube, also for other types of astrophysical sources.

7.4 NEUTRINOS FROM STAR FORMING GALAXIES

In Sec.2.2.4 we provided a brief discussion of a specific class of Star Forming Galaxies (SFGs), namely the starburst galaxies (SBG), as promising source of high energy neutrinos. Let us recall some interesting aspects, that are relevant to proceed in the discussion.

A SBG is a special kind of galaxy that presents an extremely high star formation rate, of the order of $10 - 100\ M_\odot$/year, while normal galaxies have $1 - 5\ M_\odot$/year [215]. This very intense star forming activity is so high that makes the time-scale of exhausting the gas much shorter than the typical dynamical time-scale of the galaxy itself. Thanks to its activity a SBG is full of young stars, thus supernova events are likely to be present with a rate of the order of $0.03 - 0.3$ per year; moreover a SBG must have a large amount of gas available to inject the star forming processes. The simultaneous presence of cosmic rays, accelerated in shock waves created by the

exploding core-collapse SNe, and targets, i.e. a large amount of gas (moreover a high density dust can be present in some subclasses of SBG), makes this kind of galaxies a promising source of ultra high energy cosmic neutrinos, produced by the pp mechanism described in Sec.1.3. This kind of galaxies is mainly observed in infrared so far, because the bulk of its emission (UV emitted by young stars) is absorbed and re-emitted in this band. For this reason it is not useful to search correlations between high energy neutrinos and γ-rays from SBG, as done for BL Lacs in the previous section. Anyway it is always possible to search correlations with radiations in other energy band.

In this section we generalize the discussion, including also the contribution of Star Forming Galaxies with obscured or low-luminosity AGNs (SF-AGN). The contribution of these sources is relevant at low redshift, as we will see in Sec.7.4.1, and it should be included in the computation of the expected flux of high energy neutrinos.

From here on, we do not distinguish between SBG and SF-AGN and we will consider both sources, referring to them with the generic name of Star Forming Galaxies (SFG).

THE FLUX OF EXTRAGALACTIC NEUTRINOS As already done for the BL Lacs scenario, we focus on the throughgoing muons flux, since there are reasons to believe that it is the true extragalactic component of high energy neutrinos, as largely explained in the thesis and especially in Sec.6.2 and 6.3.

Let us recall that after 6 years of observation the $\nu_\mu + \bar{\nu}_\mu$ spectrum from the Northern hemisphere is well interpreted by an unbroken power law with a spectral index $\alpha = 2.13 \pm 0.13$, as described in Sec.5.1. Assuming that high energy neutrinos are produced by pion decays, the all flavor flux can be estimated multiplying it for a factor 3, as expected from neutrino oscillations (see Sec.3.1.3). Using these hypotheses the all flavor flux of extragalactic neutrinos is given by:

$$\frac{d\phi^{\text{EG}}}{dE_\nu} = \phi_0 \times \frac{10^{-18}}{\text{GeV cm}^2 \text{ sec sr}} \left(\frac{E}{100 \text{ TeV}} \right)^{-\alpha} \tag{124}$$

with $\phi_0 = 2.7^{+0.9}_{-0.8}$ and $\alpha = 2.13 \pm 0.13$ [129].

Using this flux and the effective area reported in Sec.4.5.1 it is possible to evaluate the expected number of HESE, as done in Tab.11. Here we evaluate also the uncertainties given by the spectral shape and the Poisson uncertainty. Therefore, the expected number of HESE, that can be attributed to the extragalactic component of high energy neutrinos, is equal to:

$$N^{\text{EG}}_{\text{HESE}} = 25 \pm 6$$

The total number of HESE observed in 4 years are 54 (see Appendix D.2). Therefore we expect that the extragalactic component contribute for about the 50% of these events, as remarked in Sec.6.3.

7.4.1 SFG only: unbroken power law

In the simplest scenario we assume that the Star Forming Galaxies (SFG) are the only emitters of high energy neutrinos. We consider both starburst galaxies (SBG) and star forming AGN (SF-AGN). Let us remark that SFGs produce neutrinos with a power law spectrum, since the dominant mechanism in this astrophysical environment is the pp mechanism, described in Sec.1.3.

Table 16: *Normalization at 1 TeV of the γ-rays flux expected from SFG, in units of* $\frac{10^{-14}}{\text{GeV cm}^2 \text{ sec sr}}$

α_{SFG}	$\phi_0^{1\text{ TeV}}$
2.00	10.3
2.15	5.3
2.30	2.0

THE FLUX OF γ-RAYS FROM SFG We consider the theoretical prediction of the flux of γ-rays expected from SFGs that are given in [97]. More specifically, we consider the flux of γ-rays produced at the source (not absorbed).

The extragalactic gamma rays background (EGRB), expected from Star Forming Galaxies, has been computed in [97] adopting the Herschel PEP/HerMES IR luminosity function up to $z \simeq 4$ [216] and the relation connecting the IR luminosity to the γ-ray luminosity presented by the Fermi Collaboration [217]. The luminosity function provides a fundamental tool to probe the distribution of galaxies over cosmological time, since it allows us to access the statistical nature of galaxy formation and evolution. It is computed at different redshifts and constitutes the most direct method for exploring the evolution of a galaxy population, describing the relative number of sources of different luminosities counted in representative volumes of the universe. At $z < 0.5$ the EGRB is dominated by normal galaxies (60%) and SF-AGN (40%). The abundance of normal galaxies steeply decreases for $z \geq 0.5$ and they are practically negligible at $z \geq 1.5$, while SF-AGN become the 80% of the total EGRB (at GeV energies and below, since at higher energy the contribution given by blazars is the dominant one, as we have seen in the previous section) and starburst galaxies contribute to the remaining 20%. In agreement with previous estimations, the SBG contribution increases with the redshift, becoming about 20%30% of the total at $z > 2$. This approach is quite similar to the one used in Sec.7.3.2 for the BL Lacs.

We use the normalization at 1 TeV for different spectral indices, taking them from Fig.5 of [97]. The uncertainty on these normalizations is order of 30%-40%. The best-fit values of the normalizations at 1 TeV, as a function of the spectral index α, are reported in Tab.16 in units of

$$\frac{10^{-14}}{\text{GeV cm}^2 \text{ sec sr}}$$

These units are different from the units of Eq.124, that are the typical units used by the IceCube collaboration, where the normalization of the flux is given at 100 TeV (see also Sec.5.1 for IceCube dataset).

THE FLUX OF NEUTRINOS FROM SFG Assuming pp mechanism of production and hadronic origin of γ-rays (i.e. from the decay of π^0), the flux of neutrinos, expected from the theoretical γ-rays flux emitted by SFG, is given by:

$$\phi_\nu(E) = r^K_{\nu\gamma} \times \phi^{\text{hadr}}_\gamma(E)$$

where $r^K_{\nu\gamma}$ has been derived from [21] and it is given in Eq.11:

$$r^K_{\nu\gamma} = 1.20 - 0.79(\alpha - 2) + 0.26(\alpha - 2)^2$$

This function is equal to 1 with an uncertainty of 25% in the range $2.0 \leq \alpha \leq 2.5$. Let us recall that the shape of the neutrino spectrum is the same of the primary protons in proton-proton

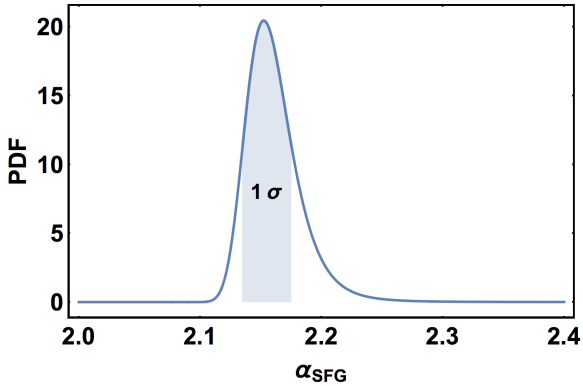

Figure 45: *Likelihood of the spectral index α_{SFG} assuming that extragalactic neutrinos are fully produced by SFG with an unbroken power law spectrum.*

interaction. Moreover we are assuming, in first approximation, an hadronic efficiency of 100% for the SFG, that seems to be adequate above the TeV.

The flux of neutrinos expected from SFG is given by:

$$\frac{d\phi_\nu^{SFG}}{dE_\nu}(\alpha_{SFG}) = r_{\nu\gamma}^K \; \phi_0^{1\ TeV}(\alpha_{SFG}) \times \frac{10^{-14}}{GeV\ cm^2\ sec\ sr} \left(\frac{E}{1\ TeV}\right)^{-\alpha_{SFG}}$$

and it is a function of the spectral index α_{SFG}, due to the correlation between the normalization and the spectral index. We evaluate the agreement between this flux and the flux measured by IceCube of Eq.124 building a likelihood function for the spectral index α_{SFG}. In order to do that we use the effective areas of Sec.4.5.1, by means of which it is possible to evaluate the number of HESE expected by star forming galaxies and to compare it with the measured one. We obtain a useful analytical approximation for the expected number of events, that is valid in the scenario of unbroken power law:

$$N_{HESE}^{SFG}(\alpha_{SFG}) = \frac{T}{1\ year} \times r_{\nu\gamma}^K \; \phi_0^{1\ TeV}(\alpha_{SFG}) \times \Gamma(\alpha_{SFG})$$

where $T = 4$ years is the present exposure time for the last available HESE dataset [149] and

$$\Gamma(\alpha_{SFG}) = 1.12 \left(\frac{\alpha_{SFG}}{2.15}\right)^{-12.8}$$

where the previous expression has been obtained using the HESE effective areas. Let us notice that in this simple model the expected number of neutrinos from SFG is only a function of the spectral index α, due to the correlation between $\phi_0^{1\ TeV}$ and α, as reported in Tab.16.

Likelihood

Using the previous equation it is possible to build a likelihood function with only 1 free parameter, i.e. the spectral index α_{SFG}, requiring the agreement between the number of HESE expected from the extragalactic component ($N_{HESE}^{EG} \pm \delta N_{HESE}^{EG} = 25 \pm 6$) and the number of HESE produced by SFG with a certain α_{SFG}. Therefore the likelihood function is simply given by a Gaussian expression:

$$\mathcal{L}_1(\alpha) \propto \exp\left\{-\frac{[N_{HESE}^{EG} - N_{HESE}^{SFG}(\alpha_{SFG})]^2}{2 \times (\delta N_{HESE}^{EG})^2}\right\}$$

The result is illustrated in Fig.45. We obtain a strong constraint on the spectral index α that should be between $2.135 \leq \alpha \leq 2.175$ (within 1σ) in order to reproduce the number of HESE that are likely to be of extragalactic origin. The best fit is given by

$$\alpha = 2.152$$

that is very close to $\alpha = 2.15$ predicted by Waxman and Loeb starting from theoretical assumption [95].

In this simple scenario, fully hadronic, we have found that SFG have the potential to explain the HESE observations, on the bases of spectral considerations.

7.5 GENERAL CONSIDERATIONS ON THE CORRELATION

We conclude the chapter with a general consideration on the correlation between cosmic neutrinos and sources. Assuming that there is an astrophysical source that emits high energy neutrinos, a certain number of correlations between the source (observed in γ-rays or other energy bands) and the IceCube neutrinos must be present. The number of correlations depends upon the fraction of visible (i.e. identified) sources with respect to the expected total number of sources. In the case of BL Lacs we have estimated that this fraction is equal to 0.5 ± 0.1 (see Sec.7.3.2). Here we describe a general procedure that can be applied to any source, not only BL Lacs or SFG.

Let us define the variabile ϵ as the fraction of identified sources (in a certain energy band) with respect to the total one. We expect that the number of correlations would correspond to

$$N_{\rm corr} = \epsilon \times (N^{\rm EG}_{\rm HESE} \pm \delta N^{\rm EG}_{\rm HESE})$$

The probability to observe no correlations is given by the *i)* Poissonian probability to observe zero events multiplied by *ii)* the Gaussian distribution of the expected number of events with extragalactic origin, as follows:

$$P_0(\epsilon) = \int_0^\infty \exp[-\epsilon \times n] \frac{1}{\sqrt{2\pi\ (\delta N^{\rm EG}_{\rm HESE})^2}} \exp\left[-\frac{(n - N^{\rm EG}_{\rm HESE})^2}{2 \times (\delta N^{\rm EG}_{\rm HESE})^2}\right] dn \tag{125}$$

using a Poissonian approach and taking into account the uncertainty on the "extragalactic" events. Therefore it is possible to define the equivalent Gaussian treatment as:

$$Erf\left(\frac{N_\sigma}{\sqrt{2}}\right) = 1 - P_0(\epsilon) \tag{126}$$

where Erf is the error function, defined as:

$$Erf(z) = \frac{2}{\sqrt{\pi}} \int_0^z e^{-t^2}\, dt$$

The Eq.126 gives directly the number of sigma at which a certain value of ϵ is excluded. The function $N_\sigma(\epsilon)$ is represented in Fig.46. We notice that $\epsilon < 0.1$ at 90% confidence level. This means that, if no correlation is seen, we need to have a class of emitters such that most of them ($\sim 90\%$) is unidentified.

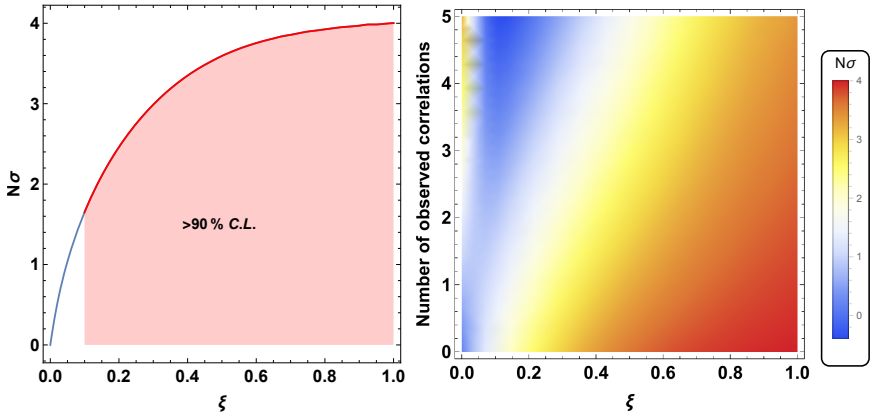

Figure 46: *Plot of the function $N_\sigma(\epsilon)$ (using Eq.126 and Eq.125) on the left panel, assuming that no correlations have been observed. On the left panel it is represented the $N_\sigma(\epsilon)$ as a function of the observed number of correlations k, using Eq.127. The numbers of σ of exclusion are reported in the legend.*

This procedure can be generalized considering what happens if the number of observed correlations is different from zero because this could occur in the near future. Using the Poissonian statistic the probability to observe k correlations, given $\epsilon \times n$ expected correlations, is equal to:

$$P(k|\epsilon \times n) = \frac{e^{-\epsilon \times n}(\epsilon \times n)^k}{k!}$$

Therefore Eq.125 becomes the following:

$$P_0(\epsilon, k) = \int_0^\infty \frac{e^{-\epsilon \times n}(\epsilon \times n)^k}{k!} \times \frac{1}{\sqrt{2\pi\ (\delta N_{\rm HESE}^{\rm EG})^2}} \exp\left[-\frac{(n - N_{\rm HESE}^{\rm EG})^2}{2 \times (\delta N_{\rm HESE}^{\rm EG})^2}\right] dn \qquad (127)$$

The results are represented in the right panel of Fig.46, combining Eq.127 and Eq.126.

Nowadays there is no evidence of correlations between high energy neutrinos and known astrophysical sources, although there are promising candidates to produce the neutrinos observed by IceCube. This scenario seems to favor a class of astrophysical objects in which most of the sources are unseen with ordinary radiation. This statement is true, within 2σ (blue region of right panel of Fig.46), even if few correlations between high energy neutrinos and known sources would be observed. Indeed, also in this case, it would be a preference for small values of ϵ, namely $\epsilon \leq 0.30$.

A REPRESENTATION OF DATA

A.1 VIVIANI'S THEOREM

The sum of the distances from any interior point to the sides of an equilateral triangle equals the length of the triangle's altitude.

The proof of Viviani's theorem is quite direct. Consider an equilateral triangle whose side has length a; its area is $ah/2 = \sqrt{3}/4a^2$. If we consider a point internal to the triangle, and we join it to the three vertices, we form 3 triangles with height s, t, u, whose areas sum to $a(s+t+u)/2$. Since this equates the $\sqrt{3}/4a^2$, the sum of the height is a constant. Similarly for the case of a point external to the triangle, considering heights with sign.

Viviani's theorem is largely used in particle physics to visualize various quantities. One can display the allowed regions of Mandelstam's variables (with signs) in a $2 \to 2$ body reaction or in a $1 \to 3$ decay, that satisfy

$$s + t + u = \sum_{i=1}^{4} m_i^2$$

possibly studying the density of the plan, i.e. the Dalitz plot[1] [218]. This theorem is largely used also in neutrino physics. E.g., this was used to display the regions allowed by unitarity constraints on the mixing elements of the electron neutrino ν_e or of the mass state that leads atmospheric neutrino oscillations ν_3,

$$\sum_{i=1,2,3} |U_{ei}^2| = 1 \text{ or } \sum_{\ell=e,\mu,\tau} |U_{\ell 3}^2| = 1$$

that are compatible with the observations [219]. It is also possible to depict the minimum value of the parameter $m_{\beta\beta}$ probed in neutrino-less double beta decay [220]. The probabilities of cosmic neutrino oscillations, that in the Gribov-Pontecorvo regime are just constants, satisfy a similar relation,

$$\sum_{\ell'=e,\mu,\tau} P_{\ell\ell'} = 1$$

Also flux fractions of cosmic neutrinos, either in the source (production point) or after oscillations, can be shown in similar manner, [221]

$$\sum_{\ell=e,\mu,\tau} {\xi_\ell}^0 = 1 \text{ or } \sum_{\ell=e,\mu,\tau} \xi_\ell = 1 \text{ where, e.g., } \xi_\ell = \frac{\Phi_\ell(E_\nu)}{\Phi_e(E_\nu) + \Phi_\mu(E_\nu) + \Phi_\tau(E_\nu)}$$

even if we need to assume the hypothesis that all fluxes Φ_ℓ, given by the sum of neutrinos and antineutrinos, have all the same energy distribution (e.g. power law) up to a normalization factor.

[1] Recall the relations with the energies in a $1 \to 3$ decay, $s = (p - p_1)^2 = M^2 + m_1^2 - 2ME_1$ and $t = (p - p_2)^2 = M^2 + m_2^2 - 2ME_2$ and the fact that the invariant phase space satisfies $dF \propto dE_1 dE_2 \propto dsdt$.

A.2 ALLOWED REGIONS IN THE GAUSSIAN APPROXIMATION

This procedure is useful to represent the allowed regions in the triangle of flavor [1]. Let us consider the two dimensional Gaussian likelihood,

$$\mathcal{L} = \frac{\exp\left[-\frac{1}{2}(\vec{v}-\langle\vec{v}\rangle)^t\ \Sigma^{-2}\ (\vec{v}-\langle\vec{v}\rangle)\right]}{2\pi\sqrt{\det(\Sigma^2)}} \text{ where } \vec{v} = \begin{pmatrix} x \\ y \end{pmatrix},\ \Sigma^2 = \begin{pmatrix} \sigma_x^2 & \sigma^2 \\ \sigma^2 & \sigma_y^2 \end{pmatrix}$$

A confidence level ($0 < C.L. < 1$) defines the allowed region $\mathcal{L} > \mathcal{L}_{\max}\ (1 - C.L.)$. Its contour is an ellipse that can be obtained from the following parametric expression,

$$\begin{pmatrix} x(\varphi) \\ y(\varphi) \end{pmatrix} = \begin{pmatrix} \langle x\rangle \\ \langle y\rangle \end{pmatrix} + \sqrt{-2\log(1-C.L.)} \begin{pmatrix} \cos\theta & \sin\theta \\ -\sin\theta & \cos\theta \end{pmatrix} \begin{pmatrix} \sigma_+\cos\varphi \\ \sigma_-\sin\varphi \end{pmatrix}$$

where $\varphi = [0, 2\pi]$ and where we defined,

$$\theta = \frac{1}{2}\arctan\left[\frac{2\sigma^2}{\sigma_y^2-\sigma_x^2}\right],\ \sigma_\pm^2 = \frac{2(\sigma_x^2\sigma_y^2-\sigma^4)}{\sigma_x^2+\sigma_y^2 \pm (\sigma_y^2-\sigma_x^2)\sqrt{1+\tan^2 2\theta}}$$

In the flavor triangle, we have known linear combinations of P_0, P_1, P_2,

$$x = (\xi_\mu - \xi_e)/\sqrt{3} \equiv x_0 + x_i P_i \text{ and } y = \xi_\tau \equiv y_0 + y_i P_i$$

A.3 GALACTIC AND EQUATORIAL COORDINATES

In order to study the correlations between the direction of neutrino events and the position of possible astrophysical sources, it is important to know the celestial coordinate systems, in particular the equatorial coordinates and the galactic coordinates.

EQUATORIAL COORDINATES In the equatorial coordinate system, in spherical coordinates, the fundamental plane is formed by projection of the Earth's equator onto the celestial sphere, forming the celestial equator. The primary direction is established by projecting the Earth's orbit onto the celestial sphere, forming the ecliptic, and setting up the ascending node of the ecliptic on the celestial equator, the vernal equinox. Right ascensions (α) are measured eastward along the celestial equator from the equinox, and declinations (δ) are measured positive northward from the celestial equator. Projections of the Earth's north and south geographic poles form the north and south celestial poles, respectively. The origin at the center of the Earth means the coordinates are geocentric. The fundamental plane and the primary direction mean that the coordinate system, while aligned with the Earth's equator and pole, does not rotate with the Earth, but remains relatively fixed against the background stars. A right-handed convention means that coordinates are positive toward the north and toward the east in the fundamental plane.

GALACTIC COORDINATES The galactic coordinate system is a celestial coordinate system in spherical coordinates, with the Sun as its center, the primary direction aligned with the approximate center of the Milky Way galaxy, and the fundamental plane parallel to an approximation

of the galactic plane but offset to its north. It uses the right-handed convention, meaning that coordinates are positive toward the north and toward the east in the fundamental plane. The galactic coordinates use the Sun as the origin. Galactic longitude (ℓ) is measured with primary direction from the Sun to the center of the galaxy in the galactic plane, while the galactic latitude (b) measures the angle of the object above the galactic plane. It is positive to the north, negative to the south. For example, the north galactic pole has a latitude of $+90^\circ$.

CHANGE OF COORDINATES Given equatorial coordinates δ (declination) and α (right ascension) the galactic coordinates (b and ℓ) can be computed from the formulas:

$$\begin{aligned}
\cos b \cos(l - 33^\circ) &= \cos\delta \cos(\alpha - 282.25^\circ) \\
\cos b \cos(l - 33^\circ) &= \sin\delta \sin 62.6^\circ + \cos\delta \sin(\alpha - 282.25^\circ) \cos 62.6^\circ \\
\sin b &= \sin\delta \cos 62.6^\circ - \cos\delta \sin(\alpha - 282.25^\circ) \sin 62.6^\circ
\end{aligned}$$

Here we report a useful code written for Mathematica. Using the equatorial coordinates `asc` for the right ascension and `dec` for the declination, the code calculates the galactic longitude `coordl` and the galactic latitude `coordb`.

```
coordb = 180/Pi* ArcSin[Sin[dec]*Cos[62.6*Pi/180] -
- Cos[dec]*Sin[(asc - 282.25*Pi/180)]*Sin[62.6*Pi/180]];

coordl1 = (Sin[dec]*Sin[62.6*Pi/180] +
+ Cos[dec]*Sin[asc - 282.25*Pi/180]*Cos[62.6*Pi/180])/ Cos[coordb*Pi/180];

coordl2 = Cos[dec]*Cos[asc - 282.25*Pi/180]/Cos[coordb*Pi/180];

coordl = Array[0 &, Length[coordb]];

For[j = 1, j <= Length[coordb], j++,
If[coordl1[[j]] >= 0, coordl[[j]] = ArcCos[coordl2[[j]]]*180/Pi + 33,
coordl[[j]] = -ArcCos[coordl2[[j]]]*180/Pi + 33]]
For[j = 1, j <= Length[coordb], j++, If[coordl[[j]] >= 180, coordl[[j]] = -360 + coordl[[j]],
Null]]
```

In Fig.47 it is reported a representation of IceCube neutrino events in equatorial coordinates (top panel) and galactic coordinates (bottom panel).

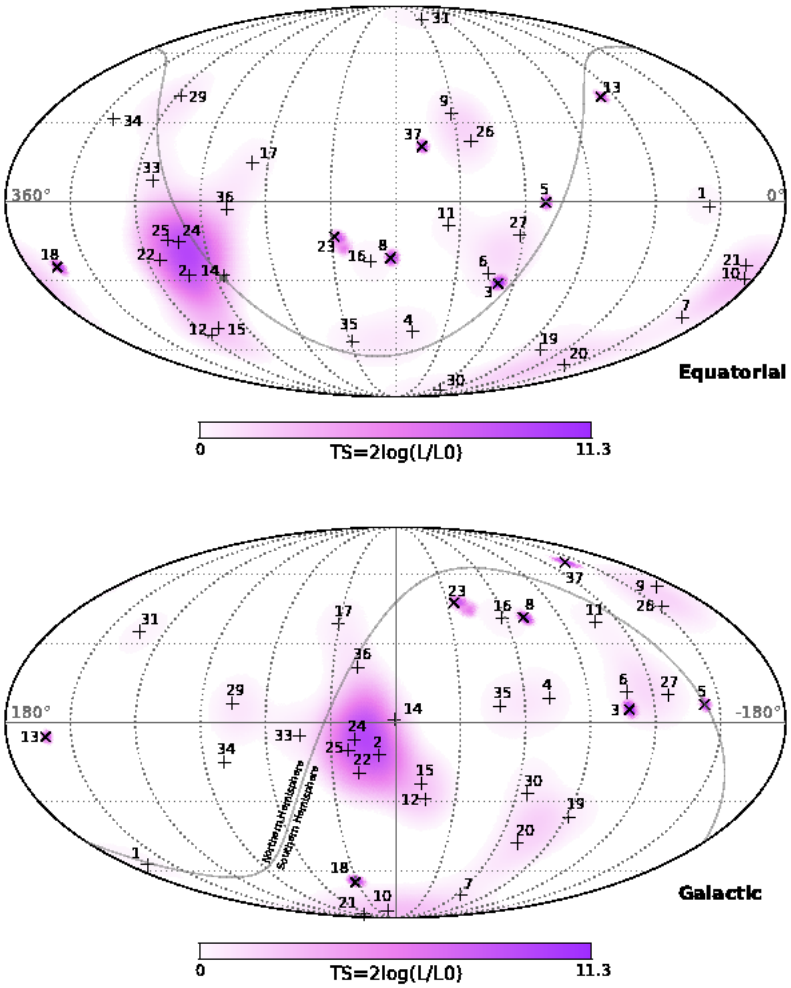

Figure 47: Representation of IceCube neutrino events in equatorial coordinates (top) and galactic coordinates (bottom). Figures from [151].

B ABSORPTION OF NEUTRINOS AND γ-RAYS

B.1 ABSORPTION OF NEUTRINOS IN EARTH

In order to evaluate the absorption of neutrinos crossing the Earth, the density profile of the Earth $\rho(r)$ is required, where r is the distance from the center of Earth. This is necessary to calculate the column density $L(\theta)$, where θ is the zenith angle, that has the dimensions of ℓ^{-2} (ℓ = length), as follows:

$$L(\theta) = 2\int_0^{R\sin\theta} \rho[|\vec{r}(\theta,z)|]\frac{1}{m_N}dz$$

where m_N is the mass of a nucleon, R is the radius of the Earth and r the distance from the center of the Earth, that depends by θ and the path z in the following manner:

$$|\vec{r}| = \sqrt{R^2 + 2Rz\cos\theta + z^2} \tag{128}$$

Using the column density $L(\theta)$ the absorption is simply given by:

$$P(E_\nu,\theta) = \mathrm{Exp}\{-L(\theta)\cdot[\sigma_{CC}(E_\nu) + \sigma_{NC}(E_\nu)]\}$$

where $\sigma_{CC}(E_\nu)$ and $\sigma_{NC}(E_\nu)$ are the cross section of deep inelastic scattering. In the case of an isotropic flux of neutrinos, such as the cosmic neutrinos, it is also interesting to evaluate a mean probability of absorption that depends only by energy, performing an integration on the angle:

$$P(E_\nu) = \int_0^1 P(E_\nu,\theta)\; d\cos(\theta)$$

Using the PREM model for the density profile of the Earth [144] (see the Fig.49), the survival probability of neutrinos is 0.91 at 10 TeV, 0.66 at 100 TeV, 0.37 at 1 PeV and 0.18 at 10 PeV [3]. The function $P(E_\nu)$ can be approximated by a power law into the energy range 50 TeV $\leq$ E$_\circ$ $\leq$ 5 PeV, giving the function:

$$P(E_\nu) = \frac{2}{3}\left(\frac{E_\nu}{100\ \mathrm{TeV}}\right)^{-0.27}$$

Let us notice that for electron antineutrinos with energy of $\sim$ 6.3 PeV the Glashow resonance channel is opened, besides the deep inelastic scattering channel. In this case the Earth becomes, in good approximation, opaque to neutrinos.

B.2 ABSORPTION OF γ-RAYS: STUDY OF THE FUNCTION $f(x)$

The evaluation of the effects of absorption via Eq. 94 rests on the estimation of the properties of the background radiation field and on the calculation of a single universal function. Note in passing that, even if we are interested to use these results to γ-rays emitted from the Galactic

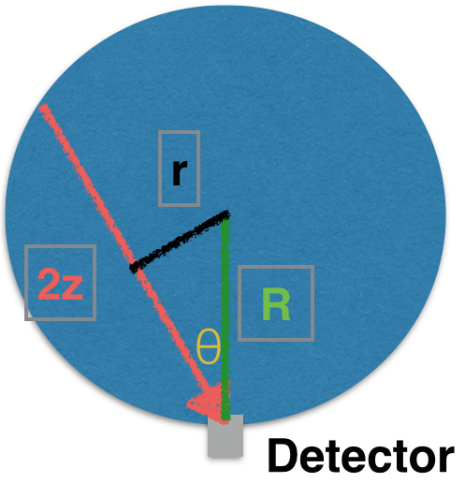

Figure 48: *Schematic representation of the quantities of Eq.128, namely r, R, z and θ.*

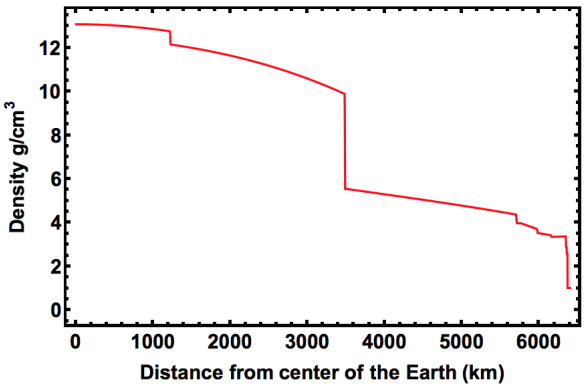

Figure 49: *Density profile of the Earth as a function of the distance from the center.*

Center, the results concerning γ-ray absorption can be applied to a very large variety of cases and situations.

In this appendix, we study $f(x)$ in details, providing a table of (virtually exact) numerical values for this function and discussing the bases of the approximation given in Eq. 95. The following material is useful to verify our results and to compare with other results in the literature, but has been confined in this appendix, so that it can be skipped by the uninterested Reader.

The pair creation process [222]

$$\gamma + \gamma_{\text{bkg}} \longrightarrow e^+ + e^-$$

Table 17: *Table of values of the function $f(x)$ as given in Eq. 129. In bold, the value of x in which the function reaches the maximum and half of the maximum.*

x	$f(x)$	x	$f(x)$
10^{-10}	7.32×10^{-9}	10^{-1}	6.32×10^{-1}
10^{-9}	6.57×10^{-8}	**0.503**	**1.076**
10^{-8}	5.81×10^{-7}	1	9.07×10^{-1}
10^{-7}	5.05×10^{-6}	**1.77**	**0.538**
10^{-6}	4.29×10^{-5}	5	3.27×10^{-2}
10^{-5}	3.54×10^{-4}	10	2.92×10^{-4}
10^{-4}	2.78×10^{-3}	20	1.78×10^{-8}
10^{-3}	2.04×10^{-2}	30	9.65×10^{-13}
10^{-2}	1.31×10^{-1}	50	$\simeq 0$
0.0756	**0.538**		

in the background of thermal photons with temperature T_i gives the opacity factor [223],

$$\tau_i = \frac{1}{\pi} \times r_e^2 L_i \times T_i^3 \times f\left(\frac{m_e^2}{T_i\, E_\gamma}\right)$$

that can be rewritten introducing the thermal photon density $n_{\gamma,i} = 2\zeta(3)T_i^3/\pi^2$. The function $f(x)$ is defined as,

$$f(x) = x^2 \int_0^1 d\beta\; R(\beta)\; \psi\left(\frac{x}{1-\beta^2}\right) \tag{129}$$

Here β is the velocity of the outgoing electron in the center of mass frame, and the two auxiliary functions are,

$$R(\beta) = \frac{2\beta}{(1-\beta^2)^2}\left[(3-\beta^4)\log\left(\frac{1+\beta}{1-\beta}\right) - 2\beta(2-\beta^2)\right]$$
$$\psi(z) = -\log\left(1-e^{-z}\right)$$

with $z = x/(1-\beta^2)$. Solving numerically the integral in Eq. 129 we found the values reported in Tab. 17.

First, we examine the behaviour of the integrand in β. The function $R(\beta) \sim 4\beta^2$ if $\beta \to 0$; on the contrary, when $\beta \to 1$, it diverges like $R(\beta) \sim -\frac{\log(1-\beta)}{(1-\beta^2)^2}$. The divergence is compensated by the behavior of the function $\psi(\frac{x}{1-\beta^2})$, that follows from $\psi(\frac{x}{1-\beta^2}) = \sum_{n=1}^{\infty} \frac{e^{-n\frac{x}{1-\beta^2}}}{n}$ at high values of $\frac{x}{1-\beta^2}$. Finally, $\psi(\frac{x}{1-\beta^2}) \approx -\log\frac{x}{1-\beta^2}$ at small values of $\frac{x}{1-\beta^2}$.

At this point, we study the behaviour of $f(x)$ in x:
For high x we can consider only the first term of the expansion of $\psi(\frac{x}{1-\beta^2})$, so the function $f(x)$ is well approximated by: $f(x) \approx x^2 \times \int_0^1 d\beta\; R(\beta) \exp\left(-\frac{x}{1-\beta^2}\right)$ within an accuracy of 1% for $x > 3$.
For small x the most important contribution to the integral is given when the $R(\beta)$ diverges and the $\psi(\frac{x}{1-\beta^2})$ is not exponentially suppressed. This condition is realized when $\beta < \sqrt{1-x} \approx 1 - x/2$ and in this region $\psi(\frac{x}{1-\beta^2}) \approx -\log\frac{x}{1-\beta^2}$; for $R(\beta)$ we can use the asymptotic expression, i.e. $R(\beta) \simeq 4\frac{\log\left(\frac{2}{1-\beta}\right)}{(1-\beta^2)^2}$. The approximation of the function $f(x)$ is given by: $f(x) \approx -4x^2 \int_0^{1-x/2}$

$d\beta \frac{\log\left(\frac{2}{1-\beta}\right)\log\left(\frac{x}{1-\beta^2}\right)}{(1-\beta^2)^2}$. This implies the behavior, $f(x) \approx -3.076\ x\ \log(x)$ to within an accuracy of about 3% in the interval $10^{-10} \leq x \leq 10^{-5}$.

A global analytical approximation of the $f(x)$, that respects the behavior for small and large values of x, is given by Eq. 95. Its accuracy is $\sim 3\%$ into the interval $10^{-10} \leq x \leq 10$. When $x > 10$ the function rapidly decreases, as we can see also from Tab. 17, where the values are obtained by numerically integrations without any approximation.

C STATISTICS

C.1 COMPATIBILITY OF TWO MEASUREMENTS

We have two measurements of one quantity x that are summarized by two likelihood functions $\ell_1(x)$ and $\ell_2(x)$. We want to test whether the two measurements are compatible or not. So, we introduce the variable that quantifies the difference of values δx and associate to this variable a new likelihood function by mean of the following overalap integral,

$$\ell\,(\,\delta x\,) = \int_{-\infty}^{+\infty} dx\; \ell_1(x)\,\ell_2(x-\delta x) \tag{130}$$

where the integrals are taken over the range of variation of the variable x that we assume to be the whole real axis. In the common case when the two likelihoods are approximated by Gaussian functions, $\ell_i(x) = g(x,\mu_i,\sigma_i)$, where,

$$g(x,\mu,\sigma) = \frac{e^{-\frac{(x-\mu)^2}{2\sigma^2}}}{\sqrt{2\pi}\sigma} \tag{131}$$

it is straightforward to show that,

$$\ell\,(\,\delta x\,) = g\left(\delta x\;,\;\mu_1-\mu_2\;,\;\sqrt{\sigma_1^2+\sigma_2^2}\right) \tag{132}$$

This result is very reasonable and admits the following interpretation: The value $\delta x = 0$, that can be considered as the case when there is no difference between the two likelihoods, deviates from the best fit value by the following 'numbers of sigma',

$$N_\sigma = \frac{|\mu_1-\mu_2|}{\sqrt{\sigma_1^2+\sigma_2^2}} \tag{133}$$

Supposing $\mu_1 > \mu_2$ (and quite similarly if $\mu_1 < \mu_2$) we can use the tail of the likelihood ℓ to estimate the statistical significance of a similar (or stronger) discrepancy,

$$\text{p-value} = 2\int_{-\infty}^{0} dy\;\ell(y) \tag{134}$$

that corresponds to N_σ if the Gaussian case applies and of course should be used only when the outcome is less than 1. This quantifies the significance of null hypothesis, that the two measurements are compatible. If the function ℓ does not deviate strongly from a Gaussian distribution, we can generalize the procedure and use the above p-value to quantify the difference between two likelihood functions with different medians $\mu_1 > \mu_2$.

C.2 EXTRACTION OF A PARAMETER IN A TWO COMPONENT MODEL

Suppose that we have a set of measurements of a certain observable quantity x, with values $x = x_1, x_2, x_3...$, and to know that they come from two different populations, with known distributions $\lambda(x)$ and $\mu(x)$, normalized to 1. We ask which is the optimal combination of these distributions that reproduces the set of measurements. This can be answered introducing the fraction of events of the first type $0 \leq f \leq 1$, corresponding to a fraction of $1 - f$ events of the second type, and using the following χ^2,

$$\exp\left(-\frac{\chi^2(f)}{2}\right) = \prod_i \left[f\lambda_i + (1-f)\mu_i \right] \text{ where } \lambda_i = \lambda(x_i) \text{ and } \mu_i = \mu(x_i) \tag{135}$$

This χ^2 can be used to estimate the fraction f. Suppose there is a minimum for some value $f = \bar{f}$ internal to the physical interval $0 < \bar{f} < 1$ and such that

$$\chi^2(f) = \frac{(f-\bar{f})^2}{\delta f^2} + o((f-\bar{f})^2) \tag{136}$$

it is easy to obtain the following analytical expressions,

$$\sum_i \xi_i(\bar{f}) = 0 \text{ and } \delta f^2 = \frac{1}{\sum_i \xi_i(\bar{f})^2} \text{ where } \xi_i(f) = \frac{\lambda_i - \mu_i}{\mu_i + f(\lambda_i - \mu_i)} \tag{137}$$

The two quantities $\bar{f}$ and δf characterize which is the optimal combination of the two populations that resembles more closely the given set of measurements, and they are usually quoted as $f = \bar{f} \pm \delta f$.

C.3 HYPOTHESIS TEST

The hypothesis tests are used to verify if a certain dataset is compatible with a theoretical cumulative distribution $f_{\text{th}}(x)$. Given a dataset of N measurements, $x_1, ..., x_N$, the experimental cumulative distribution $f_{\text{exp}}(x)$ is a step function, that increases by $1/N$ at each x_i as follows:

$$f_{\text{exp}}(x) = \begin{cases} 0 & \text{if} \quad x < x_1 \\ \frac{i}{N} & \text{if} \quad x_i \leq x < x_{i+1} \\ \dots & \\ 1 & \text{if} \quad x \geq x_N \end{cases}$$

There are different ways to compare the experimental and the theoretical cumulative. One of this is the Kolmogorov-Smirnov test, that measures the maximum distance between the two function:

$$d_{\text{max}} = \text{Max } |f_{\text{exp}}(x) - f_{\text{th}}(x)| \tag{138}$$

An illustration of this test is reported in Fig.50. The p-values of the Kolmogorov-Smirnov test are tabulated, as a function of d_{max} and N.

With the software Mathematica it is possible to compute the Kolmogorov-Smirnov test using the command:

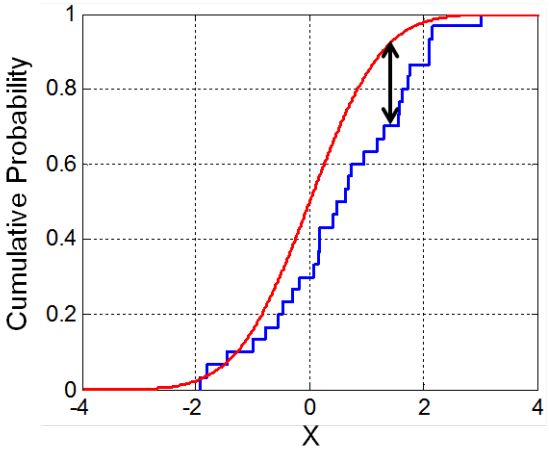

Figure 50: Illustration of the KolmogorovSmirnov statistic. Red line is the cumulative distribution function ($f_{\text{th}}(x)$), blue line is an experimental cumulative distribution function ($f_{\text{exp}}(x)$). The black represents the maximum distance between the two lines, i.e. the $d_{\max}$ of Eq.138. Credit: Wikipedia

```
KolmogorovSmirnovTest[dataset, pdfth, "TestDataTable"]
```

where `dataset` is the experimental dataset and `pdfth` is generated by the command:

```
pdfth=ProbabilityDistribution[fth[x],{x,a,b}]
```

where `fth[x]` represents the distribution that you want to test. Mathematica automatically calculates the cumulative functions, that are necessaries for the hypothesis test. This procedure is completely general and it can be used for each hypothesis test (Cramer Von Mises, Anderson Darling, Pearson χ^2 etc...).

D DATASET

D.1 THROUGHGOING MUONS DATASET

Table 18: *Summary of highest energy events above* 200 TeV *in 6 years of data taking. The "signalness"(given in the third column) is defined as the ratio of the astrophysical expectation over the sum of the atmospheric and astrophysical expectations for a given energy proxy (the reconstructed energy of the muons) and the best-fit spectrum. The "signalness"decreases up to about 10% when taking into account a prompt flux at the conservative upper limit of* $1.06\times ERS$ *(cf. Sec. 5.1.3). The angular errors (given in the* $6^{th}-7^{th}$ *and* $9^{th}-10^{th}$ *columns) are statistical errors only and do not include systematics. Table from [129].*

ID	MJD	Sign.	En.(TeV)	Decl.(deg)			R.A.(deg)		
					50%C.L.	90 % C.L.		50%C.L.	90 % C.L.
1	55056.70	0.78	480	1.23	$^{+0.08}_{-0.08}$	$^{+0.18}_{-0.22}$	29.51	$^{+0.15}_{-0.17}$	$^{+0.40}_{-0.38}$
2	55141.13	0.52	250	11.74	$^{+0.10}_{-0.18}$	$^{+0.32}_{-0.38}$	298.21	$^{+0.17}_{-0.22}$	$^{+0.53}_{-0.57}$
3	55355.49	0.65	340	23.58	$^{+0.91}_{-1.18}$	$^{+2.31}_{-4.13}$	344.93	$^{+1.14}_{-1.04}$	$^{+3.39}_{-2.90}$
4	55370.74	0.54	260	47.80	$^{+0.25}_{-0.22}$	$^{+0.56}_{-0.48}$	141.25	$^{+0.23}_{-0.16}$	$^{+0.46}_{-0.45}$
5	55387.54	0.49	230	21.00	$^{+0.57}_{-0.59}$	$^{+2.25}_{-1.56}$	306.96	$^{+0.94}_{-1.12}$	$^{+2.70}_{-2.28}$
6	55421.51	0.89	770	15.21	$^{+3.02}_{-3.10}$	$^{+9.35}_{-7.41}$	252.00	$^{+4.63}_{-6.48}$	$^{+9.56}_{-16.65}$
7	55464.90	0.77	460	13.40	$^{+0.24}_{-0.15}$	$^{+0.52}_{-0.45}$	266.29	$^{+0.22}_{-0.23}$	$^{+0.58}_{-0.62}$
8	55478.38	0.86	660	11.09	$^{+0.18}_{-0.19}$	$^{+0.41}_{-0.49}$	331.08	$^{+0.18}_{-0.35}$	$^{+0.49}_{-0.80}$
9	55497.30	0.92	950	0.50	$^{+0.10}_{-0.10}$	$^{+0.25}_{-0.21}$	88.95	$^{+0.18}_{-0.25}$	$^{+0.48}_{-0.53}$
10	55513.60	0.80	520	3.15	$^{+0.33}_{-0.25}$	$^{+0.70}_{-0.63}$	285.95	$^{+0.58}_{-0.42}$	$^{+1.29}_{-1.50}$
11	55589.56	0.52	240	1.03	$^{+0.07}_{-0.08}$	$^{+0.19}_{-0.21}$	307.71	$^{+0.08}_{-0.08}$	$^{+0.52}_{-0.44}$
12	55702.77	0.60	300	20.30	$^{+0.44}_{-0.62}$	$^{+1.00}_{-1.43}$	235.13	$^{+0.89}_{-0.55}$	$^{+2.70}_{-1.76}$
13	55722.43	0.47	210	35.55	$^{+0.28}_{-0.29}$	$^{+0.69}_{-0.69}$	272.22	$^{+0.50}_{-0.38}$	$^{+1.23}_{-1.19}$
14	55764.22	0.46	210	5.29	$^{+1.87}_{-1.96}$	$^{+4.85}_{-4.72}$	315.66	$^{+2.37}_{-1.39}$	$^{+5.91}_{-5.35}$
15	55896.86	0.59	300	1.87	$^{+0.57}_{-0.37}$	$^{+1.25}_{-1.18}$	222.87	$^{+0.90}_{-1.14}$	$^{+1.95}_{-7.73}$
16	55911.28	0.86	660	19.10	$^{+0.54}_{-0.77}$	$^{+2.21}_{-2.21}$	36.65	$^{+0.61}_{-0.56}$	$^{+1.85}_{-1.71}$
17	56062.96	0.45	200	31.96	$^{+0.30}_{-0.37}$	$^{+0.81}_{-0.85}$	198.74	$^{+0.49}_{-0.18}$	$^{+1.44}_{-1.09}$
18	56146.21	0.55	260	1.57	$^{+0.22}_{-0.18}$	$^{+0.46}_{-0.42}$	330.10	$^{+0.24}_{-0.36}$	$^{+0.65}_{-0.82}$
19	56211.77	0.46	210	-2.39	$^{+0.18}_{-0.19}$	$^{+0.42}_{-0.51}$	205.11	$^{+0.17}_{-0.24}$	$^{+0.54}_{-0.66}$
20	56226.60	0.88	750	28.04	$^{+0.31}_{-0.23}$	$^{+0.67}_{-0.66}$	169.61	$^{+0.45}_{-0.48}$	$^{+1.16}_{-1.11}$
21	56470.11	0.87	670	14.46	$^{+0.40}_{-0.39}$	$^{+0.86}_{-0.94}$	93.38	$^{+0.33}_{-0.34}$	$^{+0.83}_{-0.90}$
22	56521.83	0.71	400	-4.44	$^{+0.42}_{-0.39}$	$^{+1.21}_{-0.94}$	224.89	$^{+0.33}_{-0.32}$	$^{+0.87}_{-1.19}$
23	56579.91	0.49	390	10.20	$^{+0.15}_{-0.15}$	$^{+0.34}_{-0.49}$	32.94	$^{+0.20}_{-0.27}$	$^{+0.63}_{-0.62}$
24	56666.50	0.90	850	32.82	$^{+0.16}_{-0.14}$	$^{+0.39}_{-0.41}$	293.29	$^{+0.18}_{-0.40}$	$^{+0.55}_{-1.08}$
25	56799.96	0.73	400	18.05	$^{+0.75}_{-0.63}$	$^{+1.94}_{-1.80}$	349.39	$^{+1.13}_{-1.75}$	$^{+2.89}_{-4.12}$
26	56817.64	0.66	340	1.29	$^{+0.33}_{-0.29}$	$^{+0.83}_{-0.74}$	106.26	$^{+0.86}_{-0.74}$	$^{+2.27}_{-1.90}$
27	56819.20	0.995	4450	11.42	$^{+0.07}_{-0.08}$	$^{+0.17}_{-0.17}$	110.63	$^{+0.16}_{-0.28}$	$^{+0.46}_{-0.55}$
28	57049.48	0.46	210	4.56	$^{+0.19}_{-0.12}$	$^{+0.68}_{-0.50}$	100.48	$^{+0.23}_{-0.34}$	$^{+0.95}_{-1.87}$
29	57157.94	0.52	240	12.18	$^{+0.19}_{-0.18}$	$^{+0.37}_{-0.35}$	91.60	$^{+0.10}_{-0.37}$	$^{+0.16}_{-0.74}$

D.2 HESE

Table 19: Summary of contained events, above 30 TeV, in 4 years of data taking. The equatorial coordinates are reported in the 4th and 5th column, with a median uncertainty on the angular resolution in the 6th columns. The topology of the events (track or shower) is reported in the 7th column. Table from [149].

ID	Energy(TeV)	MJD	Dec. (deg.)	RA (deg.)	Med. Ang. Res. (deg.)	Topology
1	$47.6^{+6.5}_{-5.4}$	55351.32	-1.8	35.2	16.3	Shower
2	$117.0^{+15.4}_{-14.6}$	55351.47	-28.0	282.6	25.4	Shower
3	$78.7^{+10.8}_{-8.7}$	55451.07	-31.2	127.9	< 1.4	Track
4	$165.4^{+19.8}_{-14.9}$	55477.39	-51.2	169.5	7.1	Shower
5	$71.4^{+9.0}_{-9.0}$	55512.55	-0.4	110.6	< 1.2	Track
6	$28.4^{+2.7}_{-2.5}$	55567.64	-27.2	133.9	9.8	Shower
7	$34.3^{+3.5}_{-4.3}$	55571.26	-45.1	15.6	24.1	Shower
8	$32.6^{10.3}_{-11.1}$	55608.82	-21.2	182.4	< 1.3	Track
9	$63.2^{+7.1}_{-8.0}$	55685.66	33.6	151.3	16.5	Shower
10	$97.2^{+10.4}_{-12.4}$	55695.27	-29.4	5.0	8.1	Shower
11	$88.4^{+12.5}_{-10.7}$	55714.59	-8.9	155.3	16.7	Shower
12	$104.1^{+12.5}_{-13.2}$	55739.44	-52.8	296.1	9.8	Shower
13	$252.7^{+25.9}_{-21.6}$	55756.11	40.3	67.9	< 1.2	Track
14	$1040.7^{+131.6}_{-131.6}$	55782.52	-27.9	265.6	13.2	Shower
15	$57.5^{+8.3}_{-7.8}$	55783.19	-49.7	287.3	19.7	Shower
16	$30.6^{+3.6}_{-3.6}$	55798.63	-22.6	192.1	19.4	Shower
17	$199.7^{+27.2}_{-26.8}$	55800.38	14.5	247.4	11.6	Shower
18	$31.5^{+4.6}_{-3.3}$	55923.53	-24.8	345.6	< 1.3	Track
19	$71.5^{+7.0}_{-7.2}$	55925.80	-59.7	76.9	9.7	Shower
20	$1140.8^{+142.8}_{-132.8}$	55929.40	-67.2	38.3	10.7	Shower
21	$30.2^{+3.5}_{-3.3}$	55936.54	-24.0	9.0	20.9	Shower
22	$219.5^{+21.2}_{-24.4}$	55941.98	-22.1	293.7	12.1	Shower
23	$82.2^{+8.6}_{-8.4}$	55949.57	-13.2	208.7	< 1.9	Track
24	$30.5^{+3.2}_{-2.6}$	55950.85	-15.1	282.2	15.5	Shower
25	$33.5^{+4.9}_{-5.0}$	55966.74	-14.5	286.0	46.3	Shower
26	$210.0^{+29.0}_{-25.8}$	55979.26	22.7	143.4	11.8	Shower
27	$60.2^{+5.6}_{-5.6}$	56008.68	-12.6	121.7	6.6	Shower
28	$46.1^{+5.7}_{-4.4}$	56048.57	-71.5	164.8	< 1.3	Track
29	$32.7^{+3.7}_{-2.9}$	56108.26	41.0	298.1	7.4	Shower
30	$128.7^{+13.8}_{-12.5}$	56115.73	-82.7	103.2	8.0	Shower
31	$42.5^{+5.4}_{-5.7}$	56176.39	78.3	146.1	26.0	Shower
32	—	56211.74	—	—	—	Coincident
33	$384.7^{+46.4}_{-48.6}$	56221.34	7.8	292.5	13.5	Shower
34	$42.1^{+6.5}_{-6.3}$	56228.61	31.3	323.4	42.7	Shower
35	$2003.7^{+236.2}_{-261.5}$	56265.13	-55.8	208.4	15.9	Shower
36	$28.9^{+3.0}_{-2.6}$	56308.16	-3.0	257.7	11.7	Shower
37	$30.8^{+3.3}_{-3.5}$	56390.19	20.7	167.3	< 1.2	Track
38	$200.5^{16-4}_{-16.4}$	56470.11	14.0	93.3	< 1.2	Track
39	$101.3^{+13.3}_{-11.6}$	56480.66	-17.9	106.2	14.2	Shower
40	$157.3^{+15.9}_{-16.7}$	56501.16	-48.5	143.9	11.7	Shower
41	$87.6^{+8.4}_{-10.0}$	56603.11	3.3	66.1	11.1	Shower
42	$76.3^{+10.3}_{-11.6}$	56613.26	-25.3	42.5	20.7	Shower
43	$46.5^{+5.9}_{-4.5}$	56628.57	-22.0	206.6	< 1.3	Track
44	$84.6^{+7.4}_{-7.9}$	56671.88	0.0	336.7	< 1.2	Track
45	$429.9^{+57.4}_{-49.1}$	56679.20	-86.3	219.0	< 1.2	Track
46	$158.0^{+15.3}_{-16.6}$	56688.07	-22.3	150.5	7.6	Shower
47	$74.3^{+8.3}_{-7.2}$	56704.60	67.4	209.4	< 1.2	Track
48	$104.7^{+13.5}_{-10.2}$	56705.94	-33.2	213.0	8.1	Shower
49	$59.9^{+8.3}_{-7.9}$	56722.41	-26.3	203.2	21.8	Shower
50	$22.2^{+2.3}_{-2.0}$	56737.20	59.3	168.6	8.2	Shower
51	$66.2^{+6.7}_{-6.1}$	56759.22	54.0	88.6	6.5	Shower
52	$158.1^{+16.3}_{-18.4}$	56763.54	-54.0	252.8	7.8	Shower
53	$27.6^{+2.6}_{-2.2}$	56767.07	-37.7	239.0	< 1.2	Track
54	$54.5^{+5.1}_{-6.3}$	56769.03	6.0	170.5	11.6	Shower

BIBLIOGRAPHY

[1] A. Palladino and F. Vissani, "The natural parameterization of cosmic neutrino oscillations," *Eur. Phys. J.*, vol. C75, p. 433, 2015.

[2] G. Pagliaroli, A. Palladino, F. L. Villante, and F. Vissani, "Testing nonradiative neutrino decay scenarios with IceCube data," *Phys. Rev.*, vol. D92, no. 11, p. 113008, 2015.

[3] A. Palladino, G. Pagliaroli, F. L. Villante, and F. Vissani, "Double pulses and cascades above 2 PeV in IceCube," *Eur. Phys. J.*, vol. C76, no. 2, p. 52, 2016.

[4] A. Palladino, G. Pagliaroli, F. L. Villante, and F. Vissani, "What is the Flavor of the Cosmic Neutrinos Seen by IceCube?," *Phys. Rev. Lett.*, vol. 114, no. 17, p. 171101, 2015.

[5] D. Biehl, A. Fedynitch, A. Palladino, T. J. Weiler, and W. Winter, "Astrophysical Neutrino Production Diagnostics with the Glashow Resonance," 2016.

[6] A. Palladino and F. Vissani, "Extragalactic plus Galactic model for IceCube neutrino events," *Astrophys. J.*, vol. 826, no. 2, p. 185, 2016.

[7] A. Palladino, M. Spurio, and F. Vissani, "On the IceCube spectral anomaly," *JCAP*, vol. 1612, no. 12, p. 045, 2016.

[8] S. Celli, A. Palladino, and F. Vissani, "Neutrinos and γ-rays from the Galactic Center Region after H.E.S.S. multi-TeV measurements," *Eur. Phys. J.*, vol. C77, no. 2, p. 66, 2017.

[9] A. Palladino and F. Vissani, "Can BL Lac emission explain the neutrinos above 0.2 PeV?," 2017.

[10] A. Esmaili, A. Palladino, and F. Vissani, "A discussion of IceCube neutrino events, circa 2015," *EPJ Web Conf.*, vol. 116, p. 11002, 2016.

[11] T. K. Gaisser, F. Halzen, and T. Stanev, "Particle astrophysics with high-energy neutrinos," *Phys. Rept.*, vol. 258, pp. 173–236, 1995. [Erratum: Phys. Rept.271,355(1996)].

[12] E. Waxman and J. N. Bahcall, "High-energy neutrinos from astrophysical sources: An Upper bound," *Phys. Rev.*, vol. D59, p. 023002, 1999.

[13] L. V. Volkova, "Energy Spectra and Angular Distributions of Atmospheric Neutrinos," *Sov. J. Nucl. Phys.*, vol. 31, pp. 784–790, 1980. [Yad. Fiz.31,1510(1980)].

[14] P. Lipari, "Lepton spectra in the earth's atmosphere," *Astropart. Phys.*, vol. 1, pp. 195–227, 1993.

[15] S. R. Kelner, F. A. Aharonian, and V. V. Bugayov, "Energy spectra of gamma-rays, electrons and neutrinos produced at proton-proton interactions in the very high energy regime," *Phys. Rev.*, vol. D74, p. 034018, 2006. [Erratum: Phys. Rev.D79,039901(2009)].

[16] T. Sjostrand, L. Lonnblad, and S. Mrenna, "PYTHIA 6.2: Physics and manual," 2001.

[17] R. S. Fletcher, T. K. Gaisser, P. Lipari, and T. Stanev, "SIBYLL: An Event generator for simulation of high-energy cosmic ray cascades," *Phys. Rev.*, vol. D50, pp. 5710–5731, 1994.

[18] N. N. Kalmykov, S. S. Ostapchenko, and A. I. Pavlov, "Quark-Gluon String Model and EAS Simulation Problems at Ultra-High Energies," *Nucl. Phys. Proc. Suppl.*, vol. 52, pp. 17–28, 1997.

[19] J. Knapp, D. Heck, S. J. Sciutto, M. T. Dova, and M. Risse, "Extensive air shower simulations at the highest energies," *Astropart. Phys.*, vol. 19, pp. 77–99, 2003.

[20] C. Patrignani *et al.*, "Review of Particle Physics," *Chin. Phys.*, vol. C40, no. 10, p. 100001, 2016.

[21] F. L. Villante and F. Vissani, "How precisely neutrino emission from supernova remnants can be constrained by gamma ray observations?," *Phys. Rev.*, vol. D78, p. 103007, 2008.

[22] K. Murase, D. Guetta, and M. Ahlers, "Hidden Cosmic-Ray Accelerators as an Origin of TeV-PeV Cosmic Neutrinos," *Phys. Rev. Lett.*, vol. 116, no. 7, p. 071101, 2016.

[23] S. Hummer, M. Ruger, F. Spanier, and W. Winter, "Simplified models for photohadronic interactions in cosmic accelerators," *Astrophys. J.*, vol. 721, pp. 630–652, 2010.

[24] S. R. Kelner and F. A. Aharonian, "Energy spectra of gamma-rays, electrons and neutrinos produced at interactions of relativistic protons with low energy radiation," *Phys. Rev.*, vol. D78, p. 034013, 2008. [Erratum: Phys. Rev.D82,099901(2010)].

[25] S. Hummer, M. Maltoni, W. Winter, and C. Yaguna, "Energy dependent neutrino flavor ratios from cosmic accelerators on the Hillas plot," *Astropart. Phys.*, vol. 34, pp. 205–224, 2010.

[26] M. G. Aartsen *et al.*, "Evidence for Astrophysical Muon Neutrinos from the Northern Sky with IceCube," *Phys. Rev. Lett.*, vol. 115, no. 8, p. 081102, 2015.

[27] M. Bustamante, J. F. Beacom, and W. Winter, "Theoretically palatable flavor combinations of astrophysical neutrinos," *Phys. Rev. Lett.*, vol. 115, no. 16, p. 161302, 2015.

[28] W. Bednarek, "High energy neutrinos produced in the accretion disks by neutrons from nuclei disintegrated in the AGN jets," *Astrophys. J.*, vol. 833, no. 2, p. 279, 2016.

[29] T. C. Licquia and J. A. Newman, "Improved Estimates of the Milky Ways Stellar Mass and Star Formation Rate From Hierarchical Bayesian Meta-analysis," *Astrophys. J.*, vol. 806, no. 1, p. 96, 2015.

[30] O. Y. Gnedin, W. R. Brown, M. J. Geller, and S. J. Kenyon, "The Mass Profile of the Galaxy to 80 kpc," *Astrophys. J.*, vol. 720, p. L108, 2010.

[31] JAXA, "http://global.jaxa.jp/article/special/experiment/matsuoka01e.html,"

[32] "3FHL: The Third Catalog of Hard Fermi-LAT Sources," 2017.

[33] W. Baade and F. Zwicky, "On Super-novae," *Proceedings of the National Academy of Science*, vol. 20, pp. 254–259, May 1934.

[34] V. Ginzburg and S. Syrovatskii, "The origin of cosmic rays," 1964.

[35] S. Gabici, F. A. Aharonian, and S. Casanova, "Broad-band nonthermal emission from molecular clouds illuminated by cosmic rays from nearby supernova remnants," *Mon. Not. Roy. Astron. Soc.*, vol. 396, p. 1629, 2009.

[36] F. Vissani, F. Aharonian, and N. Sahakyan, "On the Detectability of High-Energy Galactic Neutrino Sources," *Astropart. Phys.*, vol. 34, pp. 778–783, 2011.

[37] M. L. Costantini, A. Ianni, and F. Vissani, "The interest in neutrinos from core collapse supernovae," *Nucl. Phys. Proc. Suppl.*, vol. 139, pp. 27–32, 2005. [,27(2005)].

[38] J. Alvarez-Muniz and F. Halzen, "Possible high-energy neutrinos from the cosmic accelerator RX J1713.7-3946," *Astrophys. J.*, vol. 576, pp. L33–L36, 2002.

[39] M. L. Costantini and F. Vissani, "Expected neutrino signal from supernova remnant RX J1713.7-3946 and flavor oscillations," *Astropart. Phys.*, vol. 23, pp. 477–485, 2005.

[40] G. Morlino, P. Blasi, and E. Amato, "Gamma Rays and Neutrinos from SNR RX J1713.7-3946," *Astropart. Phys.*, vol. 31, pp. 376–382, 2009.

[41] K. W. Weiler and N. Panagia, "Are Crab-type Supernova Remnants (Plerions) Short-lived?," *aap*, vol. 70, p. 419, nov 1978.

[42] S. Safi-Harb, "Plerionic Supernova Remnants," *AIP Conf. Proc.*, vol. 1505, pp. 13–20, 2012.

[43] D. Guetta and J. Granot, "Observational implications of a plerionic environment for GRBS," *Mon. Not. Roy. Astron. Soc.*, vol. 340, pp. 115–138, 2003.

[44] S. Nagataki, "High-energy neutrinos produced by interactions of relativistic protons in shocked pulsar winds," *Astrophys. J.*, vol. 600, pp. 883–904, 2004.

[45] W. Bednarek and R. J. Protheroe, "Gamma-rays and neutrinos from the Crab Nebula produced by pulsar accelerated nuclei," *Phys. Rev. Lett.*, vol. 79, pp. 2616–2619, 1997.

[46] L. Zhang and X. C. Yang, "TeV gamma-ray emission from Vela X: Leptonic or hadronic?," *Astrophys. J.*, vol. 699, pp. L153–L156, 2009.

[47] A. Abramowski *et al.*, "Acceleration of petaelectronvolt protons in the Galactic Centre," *Nature*, vol. 531, p. 476, 2016.

[48] T. Hayakawa, K. Torii, R. Enokiya, T. Amano, and Y. Fukui, "Molecular and Atomic Gas toward HESS J1745-303 in the Galactic Center: Further Support for the Hadronic Scenario," *Publ. Astron. Soc. Jap.*, vol. 64, p. 8, 2012.

[49] S. Razzaque, "The Galactic Center Origin of a Subset of IceCube Neutrino Events," *Phys. Rev.*, vol. D88, p. 081302, 2013.

[50] M. Su, T. R. Slatyer, and D. P. Finkbeiner, "Giant Gamma-ray Bubbles from Fermi-LAT: AGN Activity or Bipolar Galactic Wind?," *Astrophys. J.*, vol. 724, pp. 1044–1082, 2010.

[51] R. M. Crocker and F. Aharonian, "The Fermi Bubbles: Giant, Multi-Billion-Year-Old Reservoirs of Galactic Center Cosmic Rays," *Phys. Rev. Lett.*, vol. 106, p. 101102, 2011.

[52] W. de Boer, I. Gebauer, S. Kunz, and A. Neumann, "Evidence for a hadronic origin of the Fermi Bubbles and the Galactic Excess," 2015.

[53] R. M. Crocker, G. V. Bicknell, E. Carretti, A. S. Hill, and R. S. Sutherland, "Steady-State Hadronic Gamma-Ray Emission from 100-Myr-Old Fermi Bubbles," *Astrophys. J.*, vol. 791, p. L20, 2014.

[54] K. S. Cheng, D. O. Chernyshov, V. A. Dogiel, and C. M. Ko, "Multi-wavelength Emission from the Fermi Bubble II. Secondary Electrons and the Hadronic Model of the Bubble," *Astrophys. J.*, vol. 799, no. 1, p. 112, 2015.

[55] Y. Fujita, Y. Ohira, and R. Yamazaki, "A Hadronic-Leptonic Model for the Fermi Bubbles: Cosmic-Rays in the Galactic Halo and Radio Emission," *Astrophys. J.*, vol. 789, no. 1, p. 67, 2014.

[56] D. Hooper and T. R. Slatyer, "Two Emission Mechanisms in the Fermi Bubbles: A Possible Signal of Annihilating Dark Matter," *Phys. Dark Univ.*, vol. 2, pp. 118–138, 2013.

[57] M. Ackermann *et al.*, "The Spectrum and Morphology of the *Fermi* Bubbles," *Astrophys. J.*, vol. 793, no. 1, p. 64, 2014.

[58] S. Adrian-Martinez *et al.*, "A Search for Neutrino Emission from the Fermi Bubbles with the ANTARES Telescope," *Eur. Phys. J.*, vol. C74, no. 2, p. 2701, 2014.

[59] D. F. Torres, G. E. Romero, and F. Mirabel, "Neutrinos from microquasars," *Chin. J. Astron. Astrophys.*, vol. 5, pp. S133–S138, 2005.

[60] M. D. Trigo, J. C. A. Miller-Jones, S. Migliari, J. W. Broderick, and T. Tzioumis, "Baryons in the relativistic jets of the stellar-mass black hole candidate 4U 1630-47," *Nature*, vol. 504, p. 260, 2013.

[61] A. Levinson and E. Waxman, "Probing microquasars with TeV neutrinos," *Phys. Rev. Lett.*, vol. 87, p. 171101, 2001.

[62] C. Distefano, D. Guetta, E. Waxman, and A. Levinson, "Neutrino flux predictions for known galactic microquasars," *Astrophys. J.*, vol. 575, pp. 378–383, 2002.

[63] S. Adrian-Martinez *et al.*, "A Search for Time Dependent Neutrino Emission from Microquasars with the ANTARES Telescope," *JHEAp*, vol. 3-4, pp. 9–17, 2014.

[64] D. Eichler, M. Livio, T. Piran, and D. N. Schramm, "Nucleosynthesis, Neutrino Bursts and Gamma-Rays from Coalescing Neutron Stars," *Nature*, vol. 340, pp. 126–128, 1989.

[65] E. Waxman and J. N. Bahcall, "High-energy neutrinos from cosmological gamma-ray burst fireballs," *Phys. Rev. Lett.*, vol. 78, pp. 2292–2295, 1997.

[66] D. Guetta, D. Hooper, J. Alvarez-Muniz, F. Halzen, and E. Reuveni, "Neutrinos from individual gamma-ray bursts in the BATSE catalog," *Astropart. Phys.*, vol. 20, pp. 429–455, 2004.

[67] S. Ando and J. F. Beacom, "Revealing the supernova-gamma-ray burst connection with TeV neutrinos," *Phys. Rev. Lett.*, vol. 95, p. 061103, 2005.

[68] K. Murase, K. Ioka, S. Nagataki, and T. Nakamura, "High Energy Neutrinos and Cosmic-Rays from Low-Luminosity Gamma-Ray Bursts?," *Astrophys. J.*, vol. 651, pp. L5–L8, 2006.

[69] M. Spurio, "Particles and Astrophysics," *Springer book*, 2015.

[70] R. Abbasi *et al.*, "Limits on Neutrino Emission from Gamma-Ray Bursts with the 40 String IceCube Detector," *Phys. Rev. Lett.*, vol. 106, p. 141101, 2011.

[71] S. Adrian-Martinez *et al.*, "Search for muon neutrinos from gamma-ray bursts with the ANTARES neutrino telescope using 2008 to 2011 data," *Astron. Astrophys.*, vol. 559, p. A9, 2013.

[72] A. Albert *et al.*, "Search for high-energy neutrinos from bright GRBs with ANTARES," 2016. [Mon. Not. Roy. Astron. Soc.469,906(2017)].

[73] M. G. Aartsen *et al.*, "An All-Sky Search for Three Flavors of Neutrinos from Gamma-Ray Bursts with the IceCube Neutrino Observatory," *Astrophys. J.*, vol. 824, no. 2, p. 115, 2016.

[74] R. Antonucci, "Unified models for active galactic nuclei and quasars," *Ann. Rev. Astron. Astrophys.*, vol. 31, pp. 473–521, 1993.

[75] C. M. Urry and P. Padovani, "Unified schemes for radio-loud active galactic nuclei," *Publ. Astron. Soc. Pac.*, vol. 107, p. 803, 1995.

[76] G. Kauffmann *et al.*, "The host galaxies of AGN," *Mon. Not. Roy. Astron. Soc.*, vol. 346, p. 1055, 2003.

[77] F. W. Stecker, C. Done, M. H. Salamon, and P. Sommers, "High-energy neutrinos from active galactic nuclei," *Phys. Rev. Lett.*, vol. 66, pp. 2697–2700, 1991. [Erratum: Phys. Rev. Lett.69,2738(1992)].

[78] L. Nellen, K. Mannheim, and P. L. Biermann, "Neutrino production through hadronic cascades in AGN accretion disks," *Phys. Rev.*, vol. D47, pp. 5270–5274, 1993.

[79] A. P. Szabo and R. J. Protheroe, "Implications of particle acceleration in active galactic nuclei for cosmic rays and high-energy neutrino astronomy," *Astropart. Phys.*, vol. 2, pp. 375–392, 1994.

[80] F. W. Stecker, "A note on high energy neutrinos from agn cores," *Phys. Rev.*, vol. D72, p. 107301, 2005.

[81] F. W. Stecker, "PeV neutrinos observed by IceCube from cores of active galactic nuclei," *Phys. Rev.*, vol. D88, no. 4, p. 047301, 2013.

[82] O. Kalashev, D. Semikoz, and I. Tkachev, "Neutrinos in IceCube from active galactic nuclei," *J. Exp. Theor. Phys.*, vol. 120, no. 3, pp. 541–548, 2015.

[83] M. Ajello *et al.*, "The Cosmic Evolution of Fermi BL Lacertae Objects," *Astrophys. J.*, vol. 780, p. 73, 2014.

[84] R. J. Protheroe, "High-energy neutrinos from blazars," *ASP Conf. Ser.*, vol. 121, p. 585, 1997.

[85] A. Atoyan and C. D. Dermer, "High-energy neutrinos from photomeson processes in blazars," *Phys. Rev. Lett.*, vol. 87, p. 221102, 2001.

[86] W. Essey, O. E. Kalashev, A. Kusenko, and J. F. Beacom, "Secondary photons and neutrinos from cosmic rays produced by distant blazars," *Phys. Rev. Lett.*, vol. 104, p. 141102, 2010.

[87] W. Essey, O. Kalashev, A. Kusenko, and J. F. Beacom, "Role of line-of-sight cosmic ray interactions in forming the spectra of distant blazars in TeV gamma rays and high-energy neutrinos," *Astrophys. J.*, vol. 731, p. 51, 2011.

[88] K. Murase, Y. Inoue, and C. D. Dermer, "Diffuse Neutrino Intensity from the Inner Jets of Active Galactic Nuclei: Impacts of External Photon Fields and the Blazar Sequence," *Phys. Rev.*, vol. D90, no. 2, p. 023007, 2014.

[89] C. Righi, F. Tavecchio, and D. Guetta, "High-energy emitting BL Lacs and high-energy neutrinos - Prospects for the direct association with IceCube and KM3NeT," *Astron. Astrophys.*, vol. 598, p. A36, 2017.

[90] F. Tavecchio and G. Ghisellini, "High-energy cosmic neutrinos from spine-sheath BL Lac jets," *Mon. Not. Roy. Astron. Soc.*, vol. 451, no. 2, pp. 1502–1510, 2015.

[91] F. Tavecchio, G. Ghisellini, and D. Guetta, "Structured jets in BL Lac objects: efficient PeV neutrino factories?," *Astrophys. J.*, vol. 793, p. L18, 2014.

[92] P. Padovani, E. Resconi, P. Giommi, B. Arsioli, and Y. L. Chang, "Extreme blazars as counterparts of IceCube astrophysical neutrinos," *Mon. Not. Roy. Astron. Soc.*, vol. 457, no. 4, pp. 3582–3592, 2016.

[93] E. Resconi, S. Coenders, P. Padovani, P. Giommi, and L. Caccianiga, "Connecting blazars with ultra high energy cosmic rays and astrophysical neutrinos," 2016.

[94] M. G. Aartsen *et al.*, "The contribution of Fermi-2LAC blazars to the diffuse TeV-PeV neutrino flux," *Astrophys. J.*, vol. 835, no. 1, p. 45, 2017.

[95] A. Loeb and E. Waxman, "The Cumulative background of high energy neutrinos from starburst galaxies," *JCAP*, vol. 0605, p. 003, 2006.

[96] F. W. Stecker, "Are Diffuse High Energy Neutrinos from Starburst Galaxies Observable?," *Astropart. Phys.*, vol. 26, pp. 398–401, 2007.

[97] I. Tamborra, S. Ando, and K. Murase, "Star-forming galaxies as the origin of diffuse high-energy backgrounds: Gamma-ray and neutrino connections, and implications for starburst history," *JCAP*, vol. 1409, p. 043, 2014.

[98] B. C. Lacki, T. A. Thompson, E. Quataert, A. Loeb, and E. Waxman, "On The GeV & TeV Detections of the Starburst Galaxies M82 & NGC 253," *Astrophys. J.*, vol. 734, p. 107, 2011.

[99] K. Bechtol, M. Ahlers, M. Di Mauro, M. Ajello, and J. Vandenbroucke, "Evidence against star-forming galaxies as the dominant source of IceCube neutrinos," *Astrophys. J.*, vol. 836, no. 1, p. 47, 2017.

[100] V. S. Berezinsky and G. T. Zatsepin, "Cosmic rays at ultrahigh-energies (neutrino?)," *Phys. Lett.*, vol. 28B, pp. 423–424, 1969.

[101] M. Ave, N. Busca, A. V. Olinto, A. A. Watson, and T. Yamamoto, "Cosmogenic neutrinos from ultra-high energy nuclei," *Astropart. Phys.*, vol. 23, pp. 19–29, 2005.

[102] V. Berezinsky, A. Gazizov, M. Kachelriess, and S. Ostapchenko, "Restricting UHECRs and cosmogenic neutrinos with Fermi-LAT," *Phys. Lett.*, vol. B695, pp. 13–18, 2011.

[103] K. Kotera, D. Allard, and A. V. Olinto, "Cosmogenic Neutrinos: parameter space and detectabilty from PeV to ZeV," *JCAP*, vol. 1010, p. 013, 2010.

[104] R. Aloisio, D. Boncioli, A. di Matteo, A. F. Grillo, S. Petrera, and F. Salamida, "Cosmogenic neutrinos and ultra-high energy cosmic ray models," *JCAP*, vol. 1510, no. 10, p. 006, 2015.

[105] P. W. Gorham *et al.*, "New Limits on the Ultra-high Energy Cosmic Neutrino Flux from the ANITA Experiment," *Phys. Rev. Lett.*, vol. 103, p. 051103, 2009.

[106] K. Hanson, "The Askar'yan Radio Array," *J. Phys. Conf. Ser.*, vol. 375, p. 052037, 2012.

[107] L. Yacobi, D. Guetta, and E. Behar, "Implication of the Non-detection of gzk Neutrinos," *Astrophys. J.*, vol. 823, no. 2, p. 89, 2016.

[108] B. Pontecorvo, "Inverse beta processes and nonconservation of lepton charge," *Sov. Phys. JETP*, vol. 7, pp. 172–173, 1958. [Zh. Eksp. Teor. Fiz.34,247(1957)].

[109] Z. Maki, M. Nakagawa, and S. Sakata, "Remarks on the unified model of elementary particles," *Prog. Theor. Phys.*, vol. 28, pp. 870–880, 1962.

[110] A. Strumia and F. Vissani, "Neutrino masses and mixings and...," 2006.

[111] E. K. Akhmedov, "Neutrino physics," in *Proceedings, Summer School in Particle Physics: Trieste, Italy, June 21-July 9, 1999*, pp. 103–164, 1999.

[112] S. M. Bilenky and B. Pontecorvo, "Lepton Mixing and Neutrino Oscillations," *Phys. Rept.*, vol. 41, pp. 225–261, 1978.

[113] M. C. Gonzalez-Garcia, M. Maltoni, and T. Schwetz, "Updated fit to three neutrino mixing: status of leptonic CP violation," *JHEP*, vol. 11, p. 052, 2014.

[114] S. Pakvasa, W. Rodejohann, and T. J. Weiler, "Unitary parametrization of perturbations to tribimaximal neutrino mixing," *Phys. Rev. Lett.*, vol. 100, p. 111801, 2008.

[115] S. L. Glashow, "Resonant Scattering of Antineutrinos," *Phys. Rev.*, vol. 118, pp. 316–317, 1960.

[116] V. Barger, L. Fu, J. G. Learned, D. Marfatia, S. Pakvasa, and T. J. Weiler, "Glashow resonance as a window into cosmic neutrino sources," *Phys. Rev.*, vol. D90, p. 121301, 2014.

[117] J. N. Bahcall, N. Cabibbo, and A. Yahil, "Are neutrinos stable particles?," *Phys. Rev. Lett.*, vol. 28, pp. 316–318, 1972.

[118] S. Pakvasa and K. Tennakone, "Neutrinos of Non-zero Rest Mass," *Phys. Rev. Lett.*, vol. 28, p. 1415, 1972.

[119] J. A. Frieman, H. E. Haber, and K. Freese, "Neutrino Mixing, Decays and Supernova Sn1987a," *Phys. Lett.*, vol. B200, pp. 115–121, 1988.

[120] P. Baerwald, M. Bustamante, and W. Winter, "Neutrino Decays over Cosmological Distances and the Implications for Neutrino Telescopes," *JCAP*, vol. 1210, p. 020, 2012.

[121] A. S. Joshipura, E. Masso, and S. Mohanty, "Constraints on decay plus oscillation solutions of the solar neutrino problem," *Phys. Rev.*, vol. D66, p. 113008, 2002.

[122] A. Bandyopadhyay, S. Choubey, R. Gandhi, S. Goswami, and D. P. Roy, "The Solar neutrino problem after the first results from KamLAND," *Phys. Lett.*, vol. B559, pp. 121–130, 2003.

[123] K. Eguchi *et al.*, "A High sensitivity search for anti-nu(e)'s from the sun and other sources at KamLAND," *Phys. Rev. Lett.*, vol. 92, p. 071301, 2004.

[124] M. C. Gonzalez-Garcia and M. Maltoni, "Status of Oscillation plus Decay of Atmospheric and Long-Baseline Neutrinos," *Phys. Lett.*, vol. B663, pp. 405–409, 2008.

[125] J. F. Beacom, N. F. Bell, D. Hooper, S. Pakvasa, and T. J. Weiler, "Decay of high-energy astrophysical neutrinos," *Phys. Rev. Lett.*, vol. 90, p. 181301, 2003.

[126] M. Bustamante, J. F. Beacom, and K. Murase, "Testing decay of astrophysical neutrinos with incomplete information," 2016.

[127] M. A. Markov and I. M. Zheleznykh, "On high energy neutrino physics in cosmic rays," *Nucl. Phys.*, vol. 27, pp. 385–394, 1961.

[128] F. Halzen and D. Hooper, "High-energy neutrino astronomy: The Cosmic ray connection," *Rept. Prog. Phys.*, vol. 65, pp. 1025–1078, 2002.

[129] M. G. Aartsen *et al.*, "Observation and Characterization of a Cosmic Muon Neutrino Flux from the Northern Hemisphere using six years of IceCube data," *Astrophys. J.*, vol. 833, no. 1, p. 3, 2016.

[130] J. Schnabel, "Muon energy reconstruction in the ANTARES detector," *Nucl. Instrum. Meth.*, vol. A725, pp. 106–109, 2013.

[131] S. Adrian-Martinez *et al.*, "Letter of intent for KM3NeT 2.0," *J. Phys.*, vol. G43, no. 8, p. 084001, 2016.

[132] M. G. Aartsen *et al.*, "Energy Reconstruction Methods in the IceCube Neutrino Telescope," *JINST*, vol. 9, p. P03009, 2014.

[133] M. G. Aartsen *et al.*, "Evidence for High-Energy Extraterrestrial Neutrinos at the IceCube Detector," *Science*, vol. 342, p. 1242856, 2013.

[134] M. Ageron *et al.*, "ANTARES: the first undersea neutrino telescope," *Nucl. Instrum. Meth.*, vol. A656, pp. 11–38, 2011.

[135] A. D. Avrorin *et al.*, "Status of the Baikal-GVD Project," in *Proceedings, 16th Lomonosov Conference on Elementary Particle Physics: Particle Physics at the Year of Centenary of Bruno Pontecorvo: Moscow, Russia, August 22-28, 2013*, pp. 98–101, 2015.

[136] R. Gandhi, C. Quigg, M. H. Reno, and I. Sarcevic, "Ultrahigh-energy neutrino interactions," *Astropart. Phys.*, vol. 5, pp. 81–110, 1996.

[137] R. Gandhi, C. Quigg, M. H. Reno, and I. Sarcevic, "Neutrino interactions at ultrahigh-energies," *Phys. Rev.*, vol. D58, p. 093009, 1998.

[138] F. Halzen and S. R. Klein, "IceCube: An Instrument for Neutrino Astronomy," *Rev. Sci. Instrum.*, vol. 81, p. 081101, 2010.

[139] F. Vissani, G. Pagliaroli, and F. L. Villante, "The fraction of muon tracks in cosmic neutrinos," *JCAP*, vol. 1309, p. 017, 2013.

[140] J. G. Learned and S. Pakvasa, "Detecting tau-neutrino oscillations at PeV energies," *Astropart. Phys.*, vol. 3, pp. 267–274, 1995.

[141] D. F. Cowen, "Tau neutrinos in IceCube," *J. Phys. Conf. Ser.*, vol. 60, pp. 227–230, 2007.

[142] R. Abbasi *et al.*, "A Search for UHE Tau Neutrinos with IceCube," *Phys. Rev.*, vol. D86, p. 022005, 2012.

[143] M. G. Aartsen *et al.*, "Search for Astrophysical Tau Neutrinos in Three Years of IceCube Data," *Phys. Rev.*, vol. D93, no. 2, p. 022001, 2016.

[144] A. M. Dziewonski and D. L. Anderson, "Preliminary reference earth model," *Phys. Earth Planet. Interiors*, vol. 25, pp. 297–356, 1981.

[145] S. Adrian-Martinez *et al.*, "Constraints on the neutrino emission from the Galactic Ridge with the ANTARES telescope," *Phys. Lett.*, vol. B760, pp. 143–148, 2016.

[146] M. G. Aartsen *et al.*, "Searches for Extended and Point-like Neutrino Sources with Four Years of IceCube Data," *Astrophys. J.*, vol. 796, no. 2, p. 109, 2014.

[147] J. Schmid, "http://www.ecap.nat.uni-erlangen.de/members/schmid/Doktorarbeit/ JuliaSchmidDissertation.pdf,"

[148] T. K. Gaisser, T. Stanev, S. A. Bludman, and H.-s. Lee, "The Flux of Atmospheric Neutrinos," *Phys. Rev. Lett.*, vol. 51, pp. 223–226, 1983.

[149] M. G. Aartsen *et al.*, "A combined maximum-likelihood analysis of the high-energy astrophysical neutrino flux measured with IceCube," *Astrophys. J.*, vol. 809, no. 1, p. 98, 2015.

[150] R. Enberg, M. H. Reno, and I. Sarcevic, "Prompt neutrino fluxes from atmospheric charm," *Phys. Rev.*, vol. D78, p. 043005, 2008.

[151] M. G. Aartsen *et al.*, "Observation of High-Energy Astrophysical Neutrinos in Three Years of IceCube Data," *Phys. Rev. Lett.*, vol. 113, p. 101101, 2014.

[152] M. G. Aartsen *et al.*, "Atmospheric and astrophysical neutrinos above 1 TeV interacting in IceCube," *Phys. Rev.*, vol. D91, no. 2, p. 022001, 2015.

[153] M. G. Aartsen *et al.*, "Flavor Ratio of Astrophysical Neutrinos above 35 TeV in IceCube," *Phys. Rev. Lett.*, vol. 114, no. 17, p. 171102, 2015.

[154] C. A. Argelles, T. Katori, and J. Salvado, "New Physics in Astrophysical Neutrino Flavor," *Phys. Rev. Lett.*, vol. 115, p. 161303, 2015.

[155] G. Pagliaroli, F. Vissani, M. L. Costantini, and A. Ianni, "Improved analysis of SN1987A antineutrino events," *Astropart. Phys.*, vol. 31, pp. 163–176, 2009.

[156] F. Vissani, "Comparative analysis of SN1987A antineutrino fluence," *J. Phys.*, vol. G42, p. 013001, 2015.

[157] P. Baerwald, M. Bustamante, and W. Winter, "Neutrino Decays over Cosmological Distances and the Implications for Neutrino Telescopes," *JCAP*, vol. 1210, p. 020, 2012.

[158] F. W. Stecker, "A note on high energy neutrinos from agn cores," *Phys. Rev.*, vol. D72, p. 107301, 2005.

[159] F. W. Stecker, "PeV neutrinos observed by IceCube from cores of active galactic nuclei," *Phys. Rev.*, vol. D88, no. 4, p. 047301, 2013.

[160] P. Padovani and E. Resconi, "Are both BL Lacs and pulsar wind nebulae the astrophysical counterparts of IceCube neutrino events?," *Mon. Not. Roy. Astron. Soc.*, vol. 443, no. 1, pp. 474–484, 2014.

[161] J. K. Becker, M. Stamatikos, F. Halzen, and W. Rhode, "Coincident grb neutrino flux predictions: implications for experimental uhe neutrino physics," *Astropart. Phys.*, vol. 25, pp. 118–128, 2006.

[162] K. Asano and P. Mszros, "Neutrino and Cosmic-Ray Release from Gamma-Ray Bursts: Time-Dependent Simulations," *Astrophys. J.*, vol. 785, p. 54, 2014.

[163] A. Neronov and D. V. Semikoz, "Evidence the Galactic contribution to the IceCube astrophysical neutrino flux," *Astropart. Phys.*, vol. 75, pp. 60–63, 2016.

[164] S. Troitsky, "Search for Galactic disk and halo components in the arrival directions of high-energy astrophysical neutrinos," *JETP Lett.*, vol. 102, no. 12, pp. 785–788, 2015. [Pisma Zh. Eksp. Teor. Fiz.102,no.12,899(2015)].

[165] E. Roulet, G. Sigl, A. van Vliet, and S. Mollerach, "PeV neutrinos from the propagation of ultra-high energy cosmic rays," *JCAP*, vol. 1301, p. 028, 2013.

[166] A. Aab *et al.*, "Improved limit to the diffuse flux of ultrahigh energy neutrinos from the Pierre Auger Observatory," *Phys. Rev.*, vol. D91, no. 9, p. 092008, 2015.

[167] K. Murase, M. Ahlers, and B. C. Lacki, "Testing the Hadronuclear Origin of PeV Neutrinos Observed with IceCube," *Phys. Rev.*, vol. D88, no. 12, p. 121301, 2013.

[168] K. Murase, "On the Origin of High-Energy Cosmic Neutrinos," *AIP Conf. Proc.*, vol. 1666, p. 040006, 2015.

[169] M. G. Aartsen *et al.*, "The IceCube Neutrino Observatory - Contributions to ICRC 2015 Part II: Atmospheric and Astrophysical Diffuse Neutrino Searches of All Flavors," in *Proceedings, 34th International Cosmic Ray Conference (ICRC 2015): The Hague, The Netherlands, July 30-August 6, 2015*, 2015.

[170] W. Winter, "Photohadronic Origin of the TeV-PeV Neutrinos Observed in IceCube," *Phys. Rev.*, vol. D88, p. 083007, 2013.

[171] K. Murase, Y. Inoue, and C. D. Dermer, "Diffuse Neutrino Intensity from the Inner Jets of Active Galactic Nuclei: Impacts of External Photon Fields and the Blazar Sequence," *Phys. Rev.*, vol. D90, no. 2, p. 023007, 2014.

[172] K. Murase and K. Ioka, "TeVPeV Neutrinos from Low-Power Gamma-Ray Burst Jets inside Stars," *Phys. Rev. Lett.*, vol. 111, no. 12, p. 121102, 2013.

[173] J. Candia, "Detectable neutrino fluxes due to enhanced cosmic ray densities in the Galactic Center region," *JCAP*, vol. 0511, p. 002, 2005.

[174] Y. Q. Guo, H. B. Hu, Q. Yuan, Z. Tian, and X. J. Gao, "Pinpointing the knee of cosmic rays with diffuse PeV gamma-rays and neutrinos," *Astrophys. J.*, vol. 795, no. 1, p. 100, 2014.

[175] D. Gaggero, D. Grasso, A. Marinelli, A. Urbano, and M. Valli, "The gamma-ray and neutrino sky: A consistent picture of Fermi-LAT, Milagro, and IceCube results," *Astrophys. J.*, vol. 815, no. 2, p. L25, 2015.

[176] M. Spurio, "Constraints to a Galactic Component of the Ice Cube cosmic neutrino flux from ANTARES," *Phys. Rev.*, vol. D90, no. 10, p. 103004, 2014.

[177] G. Pagliaroli, C. Evoli, and F. L. Villante, "Expectations for high energy diffuse galactic neutrinos for different cosmic ray distributions," *JCAP*, vol. 1611, no. 11, p. 004, 2016.

[178] M. Chianese, G. Miele, and S. Morisi, "Dark Matter interpretation of low energy IceCube MESE excess," *JCAP*, vol. 1701, no. 01, p. 007, 2017.

[179] A. Bhattacharya, R. Enberg, M. H. Reno, I. Sarcevic, and A. Stasto, "Perturbative charm production and the prompt atmospheric neutrino flux in light of RHIC and LHC," *JHEP*, vol. 06, p. 110, 2015.

[180] M. V. Garzelli, S. Moch, and G. Sigl, "Lepton fluxes from atmospheric charm revisited," *JHEP*, vol. 10, p. 115, 2015.

[181] R. Gauld, J. Rojo, L. Rottoli, S. Sarkar, and J. Talbert, "The prompt atmospheric neutrino flux in the light of LHCb," *JHEP*, vol. 02, p. 130, 2016.

[182] J. A. Aguilar *et al.*, "Search for a diffuse flux of high-energy ν_μ with the ANTARES neutrino telescope," *Phys. Lett.*, vol. B696, pp. 16–22, 2011.

[183] N. Sahakyan, "Galactic sources of high energy neutrinos: Expectation from gamma-ray data," *EPJ Web Conf.*, vol. 121, p. 05005, 2016.

[184] A. A. Abdo *et al.*, "Fermi Large Area Telescope Measurements of the Diffuse Gamma-Ray Emission at Intermediate Galactic Latitudes," *Phys. Rev. Lett.*, vol. 103, p. 251101, 2009.

[185] P. Huntemeyer, "Galactic TeV gamma ray sources and diffuse emission: Results from Milagro," *PoS*, vol. TEXAS2010, p. 165, 2010.

[186] A. Albert *et al.*, "New Constraints on all flavour Galactic diffuse neutrino emission with the ANTARES telescope," 2017.

[187] M. G. Aartsen *et al.*, "Constraints on Galactic Neutrino Emission with Seven Years of IceCube Data," 2017.

[188] A. Albert *et al.*, "New Constraints on all flavour Galactic diffuse neutrino emission with the ANTARES telescope," 2017.

[189] M. G. Aartsen *et al.*, "Constraints on Galactic Neutrino Emission with Seven Years of IceCube Data," 2017.

[190] R. Genzel, F. Eisenhauer, and S. Gillessen, "The Galactic Center Massive Black Hole and Nuclear Star Cluster," *Rev. Mod. Phys.*, vol. 82, pp. 3121–3195, 2010.

[191] G. Ponti, M. R. Morris, R. Terrier, and A. Goldwurm, "Traces of past activity in the Galactic Centre," *Astrophys. Space Sci. Proc.*, vol. 34, pp. 331–369, 2013.

[192] K. Koyama, T. Inui, H. Matsumoto, and T. G. Tsuru, "A Time-Variable X-Ray Echo: Indications of a Past Flare of the Galactic-Center Black Hole," *Publ. Astron. Soc. Jap.*, vol. 60, p. 201, 2008.

[193] M. Freitag, P. Amaro-Seoane, and V. Kalogera, "Stellar remnants in galactic nuclei: mass segregation," *Astrophys. J.*, vol. 649, pp. 91–117, 2006.

[194] M. Su, T. R. Slatyer, and D. P. Finkbeiner, "Giant Gamma-ray Bubbles from Fermi-LAT: AGN Activity or Bipolar Galactic Wind?," *Astrophys. J.*, vol. 724, pp. 1044–1082, 2010.

[195] R. M. Crocker and F. Aharonian, "The Fermi Bubbles: Giant, Multi-Billion-Year-Old Reservoirs of Galactic Center Cosmic Rays," *Phys. Rev. Lett.*, vol. 106, p. 101102, 2011.

[196] Y. Fujita, S. S. Kimura, and K. Murase, "Hadronic origin of multi-TeV gamma rays and neutrinos from low-luminosity active galactic nuclei: Implications of past activities of the Galactic center," *Phys. Rev.*, vol. D92, no. 2, p. 023001, 2015.

[197] I. Zheleznykh, "Early years of high-energy neutrino physics in cosmic rays and neutrino astronomy (1957-1962)," *Int. J. Mod. Phys.*, vol. A21S1, pp. 1–11, 2006. [,1(2006)].

[198] M. G. Aartsen *et al.*, "Lowering IceCube's Energy Threshold for Point Source Searches in the Southern Sky," *Astrophys. J.*, vol. 824, no. 2, p. L28, 2016.

[199] R. W. Springer, "The High Altitude water Cherenkov (HAWC) Observatory," *Nucl. Part. Phys. Proc.*, vol. 279-281, pp. 87–94, 2016.

[200] S. Vercellone, "The next generation Cherenkov Telescope Array observatory: CTA," *Nucl. Instrum. Meth.*, vol. A766, pp. 73–77, 2014.

[201] M. G. Aartsen *et al.*, "Search for Time-independent Neutrino Emission from Astrophysical Sources with 3 yr of IceCube Data," *Astrophys. J.*, vol. 779, p. 132, 2013.

[202] P. Padovani, "The Blazar Sequence: Validity and Predictions," *Astrophys. Space Sci.*, vol. 309, pp. 63–71, 2007.

[203] F. Halzen and A. Kheirandish, "High Energy Neutrinos from Recent Blazar Flares," *Astrophys. J.*, vol. 831, no. 1, p. 12, 2016.

[204] K. Murase and E. Waxman, "Constraining High-Energy Cosmic Neutrino Sources: Implications and Prospects," *Phys. Rev.*, vol. D94, no. 10, p. 103006, 2016.

[205] C. F. Turley *et al.*, "Search for Blazar Flux-Correlated TeV Neutrinos in IceCube 40-String Data," 2016.

[206] P. Padovani, E. Resconi, P. Giommi, B. Arsioli, and Y. L. Chang, "Extreme blazars as counterparts of IceCube astrophysical neutrinos," *Mon. Not. Roy. Astron. Soc.*, vol. 457, no. 4, pp. 3582–3592, 2016.

[207] L. S. Miranda, A. R. de Len, and S. Sahu, "Blazar origin of some IceCube events," *Eur. Phys. J.*, vol. C76, no. 7, p. 402, 2016.

[208] T. Glsenkamp, "Analysis of the cumulative neutrino flux from Fermi-LAT blazar populations using 3 years of IceCube data," *EPJ Web Conf.*, vol. 121, p. 05006, 2016.

[209] S. Gao, M. Pohl, and W. Winter, "On the direct correlation between gamma-rays and PeV neutrinos from blazars," 2016.

[210] M. Ackermann *et al.*, "2FHL: The Second Catalog of Hard Fermi-LAT Sources," *Astrophys. J. Suppl.*, vol. 222, no. 1, p. 5, 2016.

[211] F. W. Stecker, "Diffuse Fluxes of Cosmic High-Energy Neutrinos," *Astrophys. J.*, vol. 228, pp. 919–927, 1979.

[212] O. E. Kalashev, A. Kusenko, and W. Essey, "PeV neutrinos from intergalactic interactions of cosmic rays emitted by active galactic nuclei," *Phys. Rev. Lett.*, vol. 111, no. 4, p. 041103, 2013.

[213] M. G. Aartsen *et al.*, "IceCube-Gen2: A Vision for the Future of Neutrino Astronomy in Antarctica," 2014.

[214] A. M. Taylor, S. Gabici, and F. Aharonian, "Galactic halo origin of the neutrinos detected by IceCube," *Phys. Rev.*, vol. D89, no. 10, p. 103003, 2014.

[215] L. J. Kewley, M. A. Dopita, R. S. Sutherland, C. A. Heisler, and J. Trevena, "Theoretical modeling of starburst galaxies," *Astrophys. J.*, vol. 556, pp. 121–140, 2001.

[216] C. Gruppioni *et al.*, "The Herschel PEP/HerMES Luminosity Function. I: Probing the Evolution of PACS selected Galaxies to z 4," *Mon. Not. Roy. Astron. Soc.*, vol. 432, p. 23, 2013.

[217] M. Ackermann *et al.*, "GeV Observations of Star-forming Galaxies with *Fermi* LAT," *Astrophys. J.*, vol. 755, p. 164, 2012.

[218] R. H. Dalitz, "Decay of tau mesons of known charge," *Phys. Rev.*, vol. 94, pp. 1046–1051, 1954.

[219] G. L. Fogli, E. Lisi, and G. Scioscia, "Accelerator and reactor neutrino oscillation experiments in a simple three generation framework," *Phys. Rev.*, vol. D52, pp. 5334–5351, 1995.

[220] F. Vissani, "Signal of neutrinoless double beta decay, neutrino spectrum and oscillation scenarios," *JHEP*, vol. 06, p. 022, 1999.

[221] G. Barenboim and C. Quigg, "Neutrino observatories can characterize cosmic sources and neutrino properties," *Phys. Rev.*, vol. D67, p. 073024, 2003.

[222] G. Breit and J. A. Wheeler, "Collision of Two Light Quanta," *Phys. Rev.*, vol. 46, pp. 1087–1091, 1934.

[223] I. V. Moskalenko, T. A. Porter, and A. W. Strong, "Attenuation of vhe gamma rays by the milky way interstellar radiation field," *Astrophys. J.*, vol. 640, pp. L155–L158, 2006.

ACKNOWLEDGEMENT

I am grateful to Francesco Vissani for all we did during the three years of PhD, and especially for offering me the chance to collaborate with him as a young scientist and not as an old student.
I owe a special thank to Francesco Villante, Giulia Pagliaroli, Silvia Celli, Maurizio Spurio, Daniel Biehl, Anatoli Fedynitch, Walter Winter and Tom J. Weiler for the precious collaborations in several works, that I have prepared during my PhD.
I am grateful also to Maurizio Spurio, Fabrizio Tavecchio, Walter Winter, Elisa Resconi and Antonio Capone for invitations, and above all for the pleasant and useful scientific discussions.
I would also like to thank Esteban Roulet, who has accurately reviewed my PhD thesis and sent me a detailed list of corrections.
Finally, I would like to express my gratitude toward the Gran Sasso Science Institute and in particular:
– to Eugenio Coccia, who succeeded to create an atmosphere conducive to research;
– to Felix Aharonian, Paolo Lipari and Marco Tavani for the useful scientific discussion;
– to all my friends and colleagues and markedly to Benedetta Belfatto, Carlo Mascaretti, Enrico Peretti, Chiara Righi and Vanessa Zema for the useful feedback in the final stage of revision of my opus;
– all the members of the administration, who helped me innumerable times and most of all, so effectively.